

**STUDIES ON SALT-RELATED PHENOMENA IN THE KHORAT BASIN USING
REMOTE SENSING, GEOPHYSICS, AND FIELD MAPPING**

Mr. Kitsana Malila

**A Thesis Submitted in Partial Fulfillment of the Requirements
for the Degree of Master of Engineering in Geotechnology
Suranaree University of Technology**

Academic Year 2001

ISBN 974-533-069-8

การศึกษาปรากฏการณ์ที่เกี่ยวข้องกับเกลือหินในแอ่งโคราชโดยใช้
การรับรู้ระยะไกล การสำรวจธรณีฟิสิกส์ และการสำรวจภาคสนาม

นายกฤษณะ มลิตา

วิทยานิพนธ์นี้เป็นส่วนหนึ่งของการศึกษาตามหลักสูตรปริญญาวิศวกรรมศาสตรมหาบัณฑิต

สาขาวิชาเทคโนโลยีธรณี

มหาวิทยาลัยเทคโนโลยีสุรนารี

ปีการศึกษา 2544

ISBN 974-533-069-8

Thesis title

**STUDIES ON SALT-RELATED PHENOMENA IN THE KHORAT BASIN
USING REMOTE SENSING, GEOPHYSICS AND FIELD MAPPING.**

Suranaree University of Technology Council has approved this thesis submitted in partial fulfillment of the requirement for a Master's Degree

Thesis Examining Committee

.....
(Dr. Chongpan Chonglakmani)
Chairman and Thesis Advisor

.....
(Assoc. Prof. Kittitep Fuenkajorn, Ph.D.)
Member

.....
(Dr. Friedrich Kuehn)
Member

.....
(Assoc. Prof. Tawit Chitsomboon, Ph.D.)
Vice Rector for Academic Affairs

.....
(Assoc. Prof. Vorapot Khompis, Ph.D.)
Dean of Institute of Engineering

กิจขณะ มลิตา: การศึกษาปรากฏการณ์ที่เกี่ยวข้องกับเกลือหินในแอ่งโคราชโดยใช้การรับรู้ระยะไกล การสำรวจธรณีฟิสิกส์และการสำรวจภาคสนาม

(STUDIES ON SALT-RELATED PHENOMENA IN THE KHORAT BASIN USING REMOTE SENSING, GEOPHYSICS AND FIELD MAPPING)

อ.ที่ปรึกษา: ดร.จงพันธ์ จงลักษณ์, 153 หน้า. ISBN 974-533-069-8

ปัญหาดินเค็ม การปนเปื้อนของสารละลายเกลือในชั้นน้ำบาดาล และการทรุดตัวของแผ่นดิน ในภาคตะวันออกเฉียงเหนือของประเทศไทย เป็นปัญหาที่นับวันจะทวีความรุนแรง สืบเนื่องมาจาก พื้นที่มากกว่า 33,000 ตารางกิโลเมตรของแอ่งโคราช ถูกรองรับด้วยชั้นตะกอนและเกลือหิน วัตถุประสงค์ของการศึกษาเพื่อหาความสัมพันธ์ของลักษณะทางธรณีวิทยาที่เกี่ยวข้องกับชั้นเกลือหิน โดยใช้การรับรู้ระยะไกล การสำรวจธรณีฟิสิกส์ และการสำรวจภาคสนาม

ผลของการศึกษาพบว่าภาพถ่ายดาวเทียมสามารถแสดงลักษณะทางปรากฏทางธรณีวิทยาที่มีความสัมพันธ์กับดินเค็มและการวางตัวของชั้นเกลือหิน ในพื้นที่ที่ทำการสำรวจธรณีฟิสิกส์ โครงสร้างของชั้นเกลือหิน มีลักษณะคดโค้งแบบอสมมาตร วางตัวในแนวแกนตะวันออกเฉียงเหนือและตะวันตกเฉียงใต้ บริเวณที่ราบลุ่มชั้นเกลือหินวางตัวอยู่ในระดับตื้น โดยมีลักษณะ โครงสร้างทางธรณีวิทยาที่เห็นเป็นเส้นตรง (lineament) จากภาพถ่ายดาวเทียมพาดผ่านในแนวขนานกับโครงสร้างของชั้นเกลือหินและยังพบวาระดับคุณภาพของน้ำบาดาลและน้ำพื้นผิวมีคุณภาพต่ำซึ่งตรงกันข้ามกับบริเวณเนินสูง โครงสร้างของชั้นเกลือหินวางตัวอยู่ในระดับลึกปราศจาก โครงสร้างทางธรณีวิทยาเป็นเส้นตรง และคุณภาพของน้ำบาดาลอยู่ในเกณฑ์ดี จากการศึกษาสรุปได้ว่าสภาพ โครงสร้างทางธรณีวิทยาเป็นเส้นตรงมีความสัมพันธ์กับโครงสร้างของชั้นเกลือหินรอยแยกรอยแตกและรอยเลื่อนของชั้นหิน

จากผลการศึกษาสามารถสร้างรูปแบบจำลองของวิวัฒนาการ การละลายของชั้นเกลือหินและการทรุดตัวได้ ดังนี้ (1) หมวดหินมหาสารคาม(เกลือหิน) และหมวดหินภูทอก ตกตะกอนในช่วงอายุ ตอนปลายครีเทเชียส ตามลำดับ (2) เทือกเขาภูพานยกตัว ให้ตะกอนตกทับถมแก่แอ่งโคราช โครงสร้างเกลือหินเริ่มคดโค้งแบบประทุนคว่ำ และประทุนหงาย (3) น้ำหนักตะกอนที่กดทับทำให้ชั้น เกลือหินเกิดการเคลื่อนตัวมากยิ่งขึ้นก่อให้เกิดโดมเกลือ (4) รอยแยกและรอยแตกเกิดขึ้นในชั้นเกลือหินและตะกอนชั้นบน น้ำจะละลายชั้นเกลือในระดับตื้น ผ่านทางรอยแยกและรอยแตก (5) หลุมยุบเกิดขึ้นจากการละลายชั้นเกลือหิน ประกอบกับการเพิ่มและลดของชั้นน้ำบาดาล (6) หลุมยุบปรากฏในบริเวณที่ราบลุ่ม บางแห่งถูกตะกอนปิดทับในสภาพภูมิประเทศปัจจุบัน

สาขาวิชาเทคโนโลยีธรณี

ปีการศึกษา 2544

ลายมือชื่อนักศึกษา.....

ลายมือชื่ออาจารย์ที่ปรึกษา.....

KITSANA MALILA: STUDIES ON SALT-RELATED PHENOMENA IN THE KHORAT BASIN USING REMOTE SENSING, GEOPHYSICS AND FIELD MAPPING THESIS ADVISOR: CHONGPAN CHONGLAKMANI, Ph.D. 153 PP. ISBN 974-533-069-8

LINEAMENT/ MAHA SARAKHAM FORMATION/ LAND SUBSIDENCE/ SEISMIC/ELECTRICAL RESISTIVITY/ MICROGRAVITY/KHORAT BASIN

The Khorat Basin contains a large evaporite basin of Cretaceous age which covers an area of about 33,000 square kilometer. The groundwater contamination, the distribution of saline soil, and the land subsidence in northeastern Thailand pose severe environmental problems. The objectives of research are to investigate and to clarify the geologic features related to salt phenomena in the Khorat Basin. To clarify the cause and associated relationship of the problems, remote sensing methodology, geophysical exploration and field mapping are applied to solve the problem.

The results of the study show that the satellite images show typical features that correlate with the distribution of the saline soil, structural setting and depth of the rock salt layers. In the geophysical survey area, the image feature from satellite shows parallel lineament trends. Salt structure in the areas shows asymmetrical anticline. The axes of salt structure are inferred in NE-SW trend parallel with prominent lineament direction. The salt structure represents shallow feature (100-130 m.). The surface topography of underlying shallow salt shows swamp, natural reservoir and high salinity. On the other hand, salt structure is deeper at high topography with light brown to dark tone. The groundwater in this area is good quality. It can be concluded that subsurface structure in the study area is closely related with linear feature such as fractures and faults.

The conceptual model for land subsidence and salt dissolution can be summarized as follow: (1) The Maha Sarakham Formation and the Phu Thok Formation were deposited in the Late Cretaceous respectively. (2) The Phu Phan uplift was formed. In the uplifted area, the sediment was supplied to the Khorat Basin. The salt layers were generally folded with broad and shallow anticlinal and synclinal structure. (3) Salt flowage was developed probably driven by sediment loading and gravity glide folding. (4) Fracture development and dissolution process continued to take place at shallow salt layer. (5) Natural sinkhole was initiated by salt dissolution in shallow rock salt layer and water table change. (6) Modern landform was developed. The dissolution collapse is often marked by a lake or a surface depression or a sinkhole and later filled up by sediments.

สาขาวิชาเทคโนโลยีธรณี
ปีการศึกษา 2544

ลายมือชื่อนักศึกษา.....
ลายมือชื่ออาจารย์ที่ปรึกษา.....

ACKNOWLEDGMENTS

The author would like to express his heartfelt and profound gratitude to this thesis adviser, Dr. Chongpan Chonglakmani, Chair of School of Geotechnology, Suranaree University of Technology for his advice, guidance and encouragement during the course of the research. Grateful acknowledgement is due to Associate Professor Dr. Kittitep Fuenkajorn and Dr. Friedrich Kuehn for their advice and suggestion and for serving as member of the Thesis Committee.

This contribution contains results of the co-operation program between the School of Geotechnology, Suranaree University of Technology (SUT), Department of Mineral Resource (DMR) and Federal Institute for Geoscience and Natural Resources (BGR), Germany.

Sincere thanks and appreciation are extended to Mr. Suebsak Solgosoom and Mr. Sakda Khundee, expert geologist from DMR. Eventually, this manuscript is dedicated to the author's parents for their everlasting support and encouragement.

Kitsana Malila

TABLE OF CONTENTS

	PAGE
Abstract (Thai)	I
Abstract (English)	II
Acknowledgments	III
Table of contents	IV
List of tables	VII
List of figures	IX
List of abbreviations	XIV

CHAPTER

I	INTRODUCTION	1
	1.1 General	1
	1.2 Research hypothesis	1
	1.3 Objective	2
	1.4 Scope and limitations of the study	2
	1.5 Location of research	3
	1.6 Research methodology	3
	1.6.1 Mapping process	3
	1.6.2 Field investigation and mapping	3
	1.6.3 Seismic, microgravity and electrical resistivity surveys	3
	1.6.4 Comprehensive interpretation and conclusion of all data	3
II	GEOLOGICAL SETTING	6
	2.1 General geology	6
	2.2.1 Permo-Carboniferous Sequence	6
	2.2.2 Permian and Triassic Pre-Khorat Sequence	6
	2.2.3 Jurassic-Cretaceous Sequence	9
	2.2 Tectonic events and deformation in the Khorat Plateau	11
	2.3 Geologic overview on Maha Sarakham Formation (Salt Formation)	12
	2.4 Salt structure	16
III	REMOTE SENSING	22
	3.1 Fundamental and terminology of remote sensing	22
	3.2 Remote sensing data	29
	3.3 Image processing	31
	3.3.1 Image registration (geocoding)	32
	3.3.2 Image enhancement	33

TABLE OF CONTENTS (Continued)

	PAGE
IV LINEAMENT ANALYSIS.....	36
4.1 Lineament terminology and application.....	36
4.2 Previous work in the Khorat Plateau.....	37
4.3 Methodology.....	41
4.3.1 Lineament information and data source collection....	41
4.3.2 Classification of lineament characteristic on image ...	41
4.4 Lineament density map.....	44
4.5 Lineament intersection density map.....	44
4.6 Lineament evaluation and deformation interpretation.....	51
V FIELD CHECKING.....	55
5.1 Geology of study area.....	55
5.2 Groundwater and surface water analysis.....	55
5.2.1 Electrical conductivity (EC).....	55
5.2.2 Total dissolved solids (TDS).....	56
5.2.3 Chloride content.....	56
5.2.4 Iron content.....	56
5.3 Results of groundwater and surface water sampling and assessments	59
VI GEOPHYSICAL EXPLORATION	62
6.1 General.....	62
6.1.1 Geophysical exploration area	62
6.1.2 Instruments	62
6.2 Electrical resistivity survey.....	63
6.2.1 Concept and theoretical background	63
6.2.2 Measuring resistivity.....	64
6.2.3 Interpretation of measurements	67
6.2.4 Results.....	68
6.2.5 Analysis	69
6.2.6 Discussions	72
6.2.7 Conclusions.....	72
6.3 Microgravity surveying.....	72
6.3.1 Basic theory of gravity.....	72
6.3.2 Measurement of gravity.....	73
6.3.3 Results and conclusions	74
6.4 Seismic survey.....	76
6.4.1 Concept and theoretical background	76
6.4.2 Ray path in multi-layered earth.....	76
6.4.3 Field investigation and acquisition parameter	77
6.4.4 Results and interpretations.....	78

TABLE OF CONTENTS (Continued)

	PAGE
VII SUMMARY AND CONCLUSIONS	80
7.1 Remote sensing and lineament analysis	80
7.2 Image classification types and salt accumulation model.....	80
7.2.1 Natural sinkhole and swamp salinity.....	80
7.2.2 Slope change with saline seep salinity.....	82
7.3 Remote sensing with geophysical survey.....	82
7.4 Proposed model for land subsidence and salt dissolution	82
7.5 Recommendation and future work	83
REFERENCES	93
APPENDIX	
APPENDIX A. Lineament raw data.	97
APPENDIX B. Electrical resistivity raw data.....	119
APPENDIX C. Rock salt boreholes.....	138
CURRICULUM VITAE	153

LIST OF TABLES

TABLE	PAGE
3.1 Spectral range of electromagnetic radiation utilized by remote-sensing sensor (After Erb, 1989)	27
3.2 The characteristics and principal applications of band and wavelength (After Lillesand and Kiefer, 1987)	28
3.3 Characteristics of MOMS-02 operating modes	30
3.4 Satellite data used for mapping in the Khorat project area.....	31
5.1 Soil salinity classes on the basis electrical conductivity (Baize, 1988).	57
5.2 Groundwater salinity classification based on total dissolved solids (Freeze and Cherry, 1979).....	57
5.3 Chloride classes for irrigation water (Mills, 2001)	57
5.4 Groundwater quality in geophysical survey area.....	58
5.5 Surface water quality in geophysical survey area.....	59
6.1 Electrical resistivity raw data including configuration array pattern at point1.....	68
A1 Lineament raw data (length and intersection) in sheet 1.....	99
A2 Lineament raw data (length and intersection) in sheet 2.....	99
A3 Lineament raw data (length and intersection) in sheet 3.....	100
A4 Lineament raw data (length and intersection) in sheet 4.....	100
A5 Lineament raw data (length and intersection) in sheet 5.....	101
A6 Lineament raw data (length and intersection) in sheet 6.....	101
A7 Lineament raw data (length and intersection) in sheet 7.....	102
A8 Lineament raw data (length and intersection) in sheet 8.....	102
A9 Lineament raw data (length and intersection) in sheet 9.....	103
A10 Lineament raw data (length and intersection) in sheet 10	103
A11 Lineament raw data (length and intersection) in sheet 11	104
A12 Lineament raw data (length and intersection) in sheet 12.	104
A13 Lineament raw data (length and intersection) in sheet 13	105
A14 Lineament raw data (length and intersection) in sheet 14.	105
A15 Lineament raw data (length and intersection) in sheet 15.	106
A16 Lineament raw data (length and intersection) in sheet 16.	106
A17 Lineament raw data (length and intersection) in sheet 17.	107
A18 Lineament raw data (length and intersection) in sheet 18.	107
A19 Lineament raw data (length and intersection) in sheet 19.	108
A20 Lineament raw data (length and intersection) in sheet 20.	108
A21 Lineament raw data (length and intersection) in sheet 21.	109
A22 Lineament raw data (length and intersection) in sheet 22.	109
A23 Lineament raw data (length and intersection) in sheet 23.	110
A24 Lineament raw data (length and intersection) in sheet 24.	110
A25 Lineament raw data (length and intersection) in sheet 25.	111
A26 Lineament raw data (length and intersection) in sheet 26.	111

LIST OF TABLES (Continued)

TABLE	PAGE
A27 Lineament raw data (length and intersection) in sheet 27	112
A28 Lineament raw data (length and intersection) in sheet 28	112
A29 Lineament raw data (length and intersection) in roll 1	113
A30 Lineament raw data (length and intersection) in roll 2	113
A31 Lineament raw data (length and intersection) in roll 3	114
A32 Lineament raw data (length and intersection) in roll 4	114
A33 Lineament raw data (length and intersection) in roll 5	115
A34 Lineament raw data (length and intersection) in roll 6	115
A35 Lineament raw data (length and intersection) in column 1	116
A36 Lineament raw data (length and intersection) in column 2	117
A37 Lineament raw data (length and intersection) in column 3	118
B1 Electrical resistivity raw data and configuration array pattern at point 1	120
B2 Electrical resistivity raw data and configuration array pattern at point 2	121
B3 Electrical resistivity raw data and configuration array pattern at point 3	122
B4 Electrical resistivity raw data and configuration array pattern at point 4	123
B5 Electrical resistivity raw data and configuration array pattern at point 5	124
B6 Electrical resistivity raw data and configuration array pattern at point 6	125
B7 Electrical resistivity raw data and configuration array pattern at point 7	126
B8 Electrical resistivity raw data and configuration array pattern at point 8	127
B9 Electrical resistivity raw data and configuration array pattern at point 9	128
B10 Electrical resistivity raw data and configuration array pattern at point 10 ..	129
B11 Electrical resistivity raw data and configuration array pattern at point 11 ..	130
B12 Electrical resistivity raw data and configuration array pattern at point 12 ..	131
B13 Electrical resistivity raw data and configuration array pattern at point 13 ..	132
B14 Electrical resistivity raw data and configuration array pattern at point 14 ..	133
B15 Electrical resistivity raw data and configuration array pattern at point 15 ..	134
B16 Electrical resistivity raw data and configuration array pattern at point 16 ..	135
B17 Electrical resistivity raw data and configuration array pattern at point 17 ..	136
B18 Electrical resistivity raw data and configuration array pattern at point 18 ..	137

LIST OF FIGURES

FIGURE		PAGE
1.1	Study area is located in the Khorat Basin covering Khong, Bua Yai, Non Daeng, Prathai districts in Nakhon Ratchasima province and Phon and Wang Noi districts in Khon Kaen province	4
1.2	The MOMS satellite image used was recorded on May 3, 1993 with 13.5x13.5 meter ² resolution; the False Color Composite (FCC) image was processed using RGB order in 4-2-1 respectively MOMS: German multispectra space sensor operated onboard the space shuttle (D2-Mission) Data provided by German Aerospace Establishment (DLR) and BGR.....	5
2.1	The Paleozoic rock in Northeast Thailand and adjacent area	7
2.2	The Geological map of Northeast Thailand (After Chuaviroj, 1997).....	8
2.3	Stratigraphy of Mesozoic Continental sediments with environments of deposition (After Piyasin, 1995).....	11
2.4	Lithostatigraphy and subdivisions of the Khorat Group and the Maha Sarakham Formation (Modified from Suwanich, 1986).....	15
2.5	The shapes of salt structures with structural evolution. Numbers indicate relative elevation x 100 m above base (After Hatcher, 1995).....	16
2.6	Salt distribution in Khorat Basin; (a) The contours show the depth of upper salt layer. (b) Upper salt in three dimensional view (The data from Potash exploration bore-holes, 1973-1982)	17
2.7	The differential loading mechanism (After Seni and Jackson, 1984).....	19
2.8	The salt folding structure initiated by gravity slides, gravity spreading and regional compression (After Warren, 1989)	19
2.9	The buoyancy mechanism (After Seni and Jackson, 1984).....	20
2.10	The salt pillow stage (After Seni and Jackson, 1983a).....	20
2.11	The diapir stage associated with the development of turtle structures and overhangs (After Seni and Jackson, 1983a).....	21
2.12	The post diapir stage associated (After Seni and Jackson, 1983a)	21
3.1	Remote sensing systems record the EM radiation after its interaction with the earth's surface (After Kronberg, 1985).....	24
3.2	Spectral characteristics of energy sources, atmospheric effects, and sensing system. Wavelength scale in logarithm (After Short, 2002).....	25
3.3	The types of electromagnetic spectrum in each wavelength (After Sabin, 1987)	26
3.4	The graph shows the typical reflectance spectra of three materials: water, dry bare soil and vegetation (After Gupta, 1991)	26
3.5	A digital image is a two-dimensional array of pixels. Each pixel has an intensity value (represented by a digital number) and a location address (referenced by its row and column numbers).....	27

LIST OF FIGURES (Continued)

FIGURE	PAGE
4.1	Contoured fracture density map of Amphoe Muang, Khon Kaen Province. Contoured at 5 mm interval cumulative fracture trace length per 10 mm diameter inventory circle (After Archwichai, 1991)..... 39
4.2	Deformation in Khorat Plateau interpreted from the Landsat 5 (After Chuaviroj, 1997) 40
4.3	Lineament map interpreted from MOMS imagery over part of Khong, Bua Yai, Kaeng Sanam Nang, Khon Sawan, Waeng Noi and Phon Districts..... 43
4.4	The joint geometry model. (A) Radial fractures due to tension in sharply folded stratum (After Archwichai, 1991). (B) Jointing in a folded stratum; T= tension joint, S = strike joints, D = dip joints, O = shear joint (After Blyth, 1990). (C) Joint structures developed in a large pluton (After Hatcher, 1995). (D) and (E) Joint in subsidence basin due to vertical maximum principle stress (after Hatcher, 1995)..... 45
4.5	Saline soil, sinkhole, swamp, major settlements, road net and rail ways (After Khundee, 2002) 46
4.6	(a) Map of lineament length density for the area shown in Figure 4.3. Contours are summation of length per 4 km ² grid cell. (b) Total dissolved solids distribution contour map of groundwater in Nakhon Ratchasima and adjacent area (Based on reports of the Groundwater Division, DMR, 1958-1996)..... 47
4.7	(a) Map of lineament intersection density for the area shown in Figure 4.3. Contours are summation of length per 4 km ² grid cell. (b) Total dissolved solids distribution contour map of groundwater in Nakhon Ratchasima and adjacent area (Based on reports of the Groundwater Division, DMR, 1958-1996)..... 48
4.8	(a) Map of lineament length density for the area shown in Figure 4.3. Contours are summation of length per 4 km ² grid cell. (b) Chloride distribution contour map of groundwater in Nakhon Ratchasima and adjacent area (Based on reports of the Groundwater Division, DMR, 1958-1996)..... 49
4.9	(a) Map of lineament intersection density for the area shown in Figure 4.3. Contours are summation of length per 4 km ² grid cell. (b) Chloride distribution contour map of groundwater in Nakhon Ratchasima and adjacent area (Based on reports of the Groundwater Division, DMR, 1958-1996)..... 50
4.10	Rose diagram of all lineament with 36 classes of 10 degree each. The numbers are prominent major joint set 52
4.11	Rose diagram shows strike direction of 28 square grid sheets with 10 km ² in each sheet..... 53
4.12	Predominant trends of lineament of the 3 domains (upper, middle and lower) of the study area..... 54

LIST OF FIGURES (Continued)

FIGURE	PAGE
5.1	Groundwater and surface water location in geophysical survey area. Yellow symbol is groundwater location and violet symbol is surface water location..... 60
5.2	The TDS contour of groundwater water (a) shows salinity higher than TDS contour of surface water (b) 61
6.1	The MOMS satellite image of study area recorded on May 3, 1993 with 13.5x13.5 m ² resolution. The numbers are vertical electric sounding points. The A-A' section is the seismic and microgravity survey line..... 63
6.2	Showing the Schlumberger configuration pattern..... 66
6.3	The example of curves fitting from RESIST87 software represents the depth, apparent resistivity and thickness at point 1 69
6.4	The apparent resistivity profile and interpretation along NW-SE direction with true scale and vertical exaggeration..... 70
6.5	The apparent resistivity profile and interpretation along east-west direction (lineament direction) 71
6.6	The topography elevation along the survey line (electrical resistivity, microgravity and seismic)..... 75
6.7	Bouguer gravity anomaly profile along the survey line 75
6.8	Off-end push spread configuration pattern..... 77
6.9	The part of seismic section showing the salt anticlinal folding in lineament direction at Ban Nong Phran Pan..... 78
6.10	The part of seismic section showing the salt flattening layer in red to slightly brown tone with rolling topography at Ban Khok Sa-At..... 79
6.11	The part of seismic section showing the salt flattening layer continued from Ban Khok Sa-At to Ban Khok Noi in red to slightly brown tone with rolling topography 79
7.1	Natural sinkholes on image are located on depression area at Ban Kao and Ban Wat, Khong district with water and salinity model in wet condition (Modified from Wentz, 1999)..... 84
7.2	Dry depression area without water in white to slightly blue on image at Ban Don Ta Nin and Ban Don Muang, Khong district and salinity model in dry condition (Modified from Wentz, 1999) 85
7.3	Circular feature on image at Ban Chot, Ban Nong Waeng Kaeo, Ban Nong Mek and Ban Nam Om representing outcrop and contact salinity model (Modified from Wentz, 1999)..... 86
7.4	The MOMS satellite image with vertical electric sounding and subsurface interpretation (same scale)..... 87
7.5	The MOMS satellite image with microgravity (Bouguer anomaly). The Bouguer values change at Ban Nong Pkan Pan and Ban Nong Nat (same scale) 88
7.6	The MOMS satellite image with part of seismic section showing the salt anticlinal folding in relation with lineament direction at Ban Nong Phran Pan..... 89

LIST OF FIGURES (Continued)

FIGURE	PAGE
7.7	MOMS satellite image with electrical resistivity, microgravity and seismicsection in the study area. Lineaments indicate the shallow salt structure..... 90
7.8	The conceptual model for land subsidence and salt dissolution in Khorat Basin in Late Cretaceous to Early Tertiary time (a) - (c)..... 91
7.9	The conceptual model for land subsidence and salt dissolution in Khorat Basin in Late Cretaceous to Early Tertiary time (d) - (f) 92
A1	(a) Diagram showing the location of sheets, rolls and columns for lineament analysis. (b) The node location in 1 sheet area. (c) The area for counting the lineament and intersection (4 km ²) with 2 km overlapping in each side. 98
B1	The curves fitting from RESIST87 software represents the depth, apparent resistivity and thickness at point 1 120
B2	The curves fitting from RESIST87 software represents the depth, apparent resistivity and thickness at point 2 121
B3	The curves fitting from RESIST87 software represents the depth, apparent resistivity and thickness at point 3 122
B4	The curves fitting from RESIST87 software represents the depth, apparent resistivity and thickness at point 4 123
B5	The curves fitting from RESIST87 software represents the depth, apparent resistivity and thickness at point 5 124
B6	The curves fitting from RESIST87 software represents the depth, apparent resistivity and thickness at point 6 125
B7	The curves fitting from RESIST87 software represents the depth, apparent resistivity and thickness at point 7 126
B8	The curves fitting from RESIST87 software represents the depth, apparent resistivity and thickness at point 8 127
B9	The curves fitting from RESIST87 software represents the depth, apparent resistivity and thickness at point 9 128
B10	The curves fitting from RESIST87 software represents the depth, apparent resistivity and thickness at point 10 129
B11	The curves fitting from RESIST87 software represents the depth, apparent resistivity and thickness at point 11 130
B12	The curves fitting from RESIST87 software represents the depth, apparent resistivity and thickness at point 12 131
B13	The curves fitting from RESIST87 software represents the depth, apparent resistivity and thickness at point 13 132
B14	The curves fitting from RESIST87 software represents the depth, apparent resistivity and thickness at point 14 133
B15	The curves fitting from RESIST87 software represents the depth, apparent resistivity and thickness at point 15 134
B16	The curves fitting from RESIST87 software represents the depth, apparent resistivity and thickness at point 16 135

LIST OF FIGURES (Continued)

FIGURE	PAGE
B17	The curves fitting from RESIST87 software represents the depth, apparent resistivity and thickness at point 17 136
B18	The curves fitting from RESIST87 software represents the depth, apparent resistivity and thickness at point 18 137
C1	Stratigraphy of potash exploration borehole number K-019 139
C2	Stratigraphy of potash exploration borehole number K-023 140
C3	Stratigraphy of potash exploration borehole number K-032 141
C4	Stratigraphy of potash exploration borehole number K-062 142
C5	Stratigraphy of potash exploration borehole number K-073 143
C6	Stratigraphy of potash exploration borehole number K-075 144
C7	Stratigraphy of potash exploration borehole number K-076 145
C8	Stratigraphy of potash exploration borehole number K-080 146
C9	Stratigraphy of potash exploration borehole number K-082 147
C10	Stratigraphy of potash exploration borehole number K-094 148
C11	Stratigraphy of potash exploration borehole number K-096 149
C12	Stratigraphy of potash exploration borehole number K-097 150
C13	Stratigraphy of potash exploration borehole number K-098 151
C14	Stratigraphy of potash exploration borehole number K-100 152

LIST OF ABBREVIATIONS

A	=	Cross-section area
A, B	=	Current electrode
$AB/2$	=	Half current electrode separation
b	=	The half separation between the measuring potential electrodes (M, N)
d	=	Electrode distance
F	=	Force attraction
g	=	Gravity acceleration
G	=	Universal gravitational constant; which is equal to the force in dynes between 2 small uniform spheres, each of mass 1gram with their centers 1cm apart.
I	=	The current between the current electrodes
K	=	Geometrical factor
L, l	=	The half-separation between the current electrodes (A, B)
m_1, m_2	=	2 masses
M, N	=	Potential electrode
$MN/2$	=	Half potential electrode separation
r	=	Distance between two mass
R	=	Electrical resistivity
\acute{I}_M, \acute{I}_N	=	Electric potential
V	=	The voltage at the measuring electrodes
\mathbf{r}, \mathbf{r}_a	=	Apparent resistivity

CHAPTER I

INTRODUCTION

1.1 General

The study is part of the technical components in the framework of the Thai-German Technical Cooperation Project “Environmental Geology for Regional Planning”. The work is carried out in cooperation with Federal Institute for Geosciences and Natural Resources (BGR), Department of Mineral Resources (DMR) and Suranaree University of Technology (SUT). The project activities in the Khorat Basin are related to the solution of the rock salt layers of Maha Sarakham Formation, which are at relative low depth below the surface.

Northeastern Thailand is a saucer-shaped tableland and is commonly known as the Khorat Plateau. It covers an area of about 155,000 square km. Surface elevations on the Khorat Plateau range from about 320 m in the northwest to about 100 m in the southeast and the average elevation is about 90-200 m above sea level. The terrain is rolling, and the hilltops generally slope to the southeast in conformity with the tilt of the land. This tilting created ranges of low hills, small lakes and mountains along the western and southern edges of the plateau, the Phetchabun and the Phanom Dong Rak mountains respectively. The plateau is drained by the Chi and Mun rivers and is bounded by the Mekong River (north and east on the Laos border). The plateau covered by impermeable soils are flooded during the rainy season (April–November) and parched during the dry season. The plateau includes the major towns of Khon Kaen, Nakhon Ratchasima, and Ubon Ratchathani, all of which are linked to Bangkok by rail and road. The Khorat plateau was formed by uplifting along two perpendicularly arranged crustal faults one trending north-south in the west and the other east-west in the south. As a result, the underlying sedimentary rocks were tilted rather than uniformly uplifted. The escarpments of these uplands overlook the plain of the Chao Phraya basin to the west and the Cambodian plain to the south.

1.2 Research hypothesis

Northeastern Thailand was previously regarded as an area of low potential in mineral resources. Rock salt and associated minerals had been discovered by the Department of Mineral Resources (DMR) from 1973-1982. The Khorat Basin contains a large evaporite basin of Cretaceous age which covers an area of about 33,000 square km. Salt and evaporite were included in the Maha Sarakham Formation which is part of the upper Khorat Group. The evaporite basin was structurally subdivided into Khorat and Sakon Nakhon Basins. The detailed study based on the bore-holes data was carried out to determine the origin, the structural setting, and the depositional environment of the salt formation (Yumuang, 1982).

Nowadays, the Khorat Plateau faces many problems caused by the underlying rock salt unit including industrial and traditional salt production in the Nakhon

Ratchasima province and adjacent areas. The problems are groundwater contamination, distribution of saline soil, land subsidence, and unstable ground. One factor comes from natural processes of salt solution by groundwater. In northeast of Thailand, salt accumulation in soil is considered to be derived principally from saline groundwater. Several theories have been proposed for salinization. All of them indicate that salinization is mainly related to the presence of rock salt strata of the Maha Sarakham Formation which are near or at the surface. To clarify the cause and associated relationship of the problems, remote sensing methodology, field checking and geophysical exploration are applied to solve the problem. Remote sensing should be integrated in the early stage of the exploration. Remote sensing can detect surface features related to unstable ground and saline soil. The interpretation of lineament features can locate areas best suited for geophysical exploration. In addition, remote-sensing can help to locate different types of hazardous zones.

Geophysical survey involving the electrical resistivity, microgravity and seismic methods can be used to determine the subsurface geologic formations and structures of the investigated area. The results of the geophysical investigation in conjunction with the remote sensing data, geological field checking and geochemistry can be used to clarify the geologic features related to soil salinity, land subsidence and unstable zones.

1.3 Objectives

The objectives of research are to investigate and to clarify the geologic features with related to land subsidence, unstable zones and saline soils caused by salt solution. The specific objectives of this research are:

- (1) to study the relationships between lineaments and subsidence/collapse sinkholes, swamps,
- (2) to study geologic background of linear features of different order and their relations to saline soils,
- (3) to clarify sources and processes of the salt dissolution, migration and accumulation at or near the surface, and
- (4) modeling the relationship between lineament density and salt features underneath the surface.

1.4 Scope and limitations of the study

The application of remote sensing in this study is based on ENVI 3.2 image processing software and the MOMs satellite data recorded in 1993 provided by BGR/DMR. Research areas are located in the Nakhon Ratchasima and Chaiyaphum province. The groundwater, surface water and soil samples are collected and are tested electrical conductivity in the field and total dissolved solids, chloride, and ferrous in the laboratory. The groundwater quality data are based on the reports of the Groundwater Division, Department of Mineral Resource (DMR). Specific

interesting features related to salt solution are selected for geophysical exploration to determine its subsurface strata and structure.

1.5 Location of research

The research area is located in Northeastern Thailand, covering Amphoe Bua Yai, Non Thai and Khong, Nakhon Ratchasima province and adjacent areas in Chaiyaphum province. The area is defined by latitude 15°-16°N and longitude 102°-103°E. The MOMS satellite image is shown in Figures 1.1 and 1.2.

1.6 Research methodology

1.6.1 Mapping processes

A. Update and clarification of the general structural setting in the greater investigated area (from geological map, lineament analysis, hydrogeological map and soil saline distribution map).

B. Image processing and interpretation of specific areas (Khong, Kham Sakae Saeng, Kaeng Sanam Nang and Prathai districts, Nakhon Ratchasima province and adjacent areas in Chaiyaphum and Khon Kaen provinces). Remote sensing data are mapped, processed and evaluated to detect specific terrain features related to unstable ground and saline soils. Specific features related to salt dissolution include e.g., lineament direction, distribution of swamps, drainage system and watersheds, indications of saline soils, sinkhole orientation, swamp pattern, moisture and vegetation differences and general land use and surface characters.

1.6.2 Field investigation and mapping

Field checking is an activity of the present research work to verify the results of remote sensing interpretation and mapping. Interviewing are also conducted with local people including the study of human activity, the changes of rock and soil features in 20-30 years ago, the change of land use and surface character, the profession which causes the distribution of saline soils and the process of traditional salt production are also conducted. The groundwater quality in geophysical survey will be tested for comparison with remote sensing interpretation. The seismic method is to investigate the different sub-surface rock layers. The seismic survey can also be applied to identify the movement of salt structures. Electrical resistivity method is used to investigate geological structure of rock/soil properties at different depth e.g., freshwater formation, brine-saturated formation, and rock salt formation.

1.6.3 Seismic, microgravity and electrical resistivity surveys

The survey areas are located near the town of Khong district in Nakhon Ratchasima province, northeastern Thailand on main Highway 2, approximately 70 kilometers from Nakhon Ratchasima. It covers an area of about 30 km² consisting of Ban Nong Bua, Ban Nong Phran Pan, Ban Khok Sa-at, Ban Khok Noi, Ban Nong Nat, Ban Noi and Ban Non Daeng.

1.6.4 Comprehensive interpretation and conclusion of all data.

This process is to clarify the relationships of different features, e.g. direction of lineaments and orientation of sinkholes, saline soils and lineaments, saline soils and

geomorphology, distribution of sinkholes and saline soils, geomorphology and sinkholes pattern, drainage system and orientation of sinkholes and direction of lineaments. Modeling of subsurface conditions that cause the characteristic features will be presented. Finally integrating features visible in remote sensing data and geophysical results can delineate the increasing salinization of the ground and potentially unstable ground.



Figure 1.1 Study area is located in the Khorat Basin covering Khong, Bua Yai, Non Daeng, Prathai districts in Nakhon Ratchasima province and Phon and Wang Noi districts in Khon Kaen province.

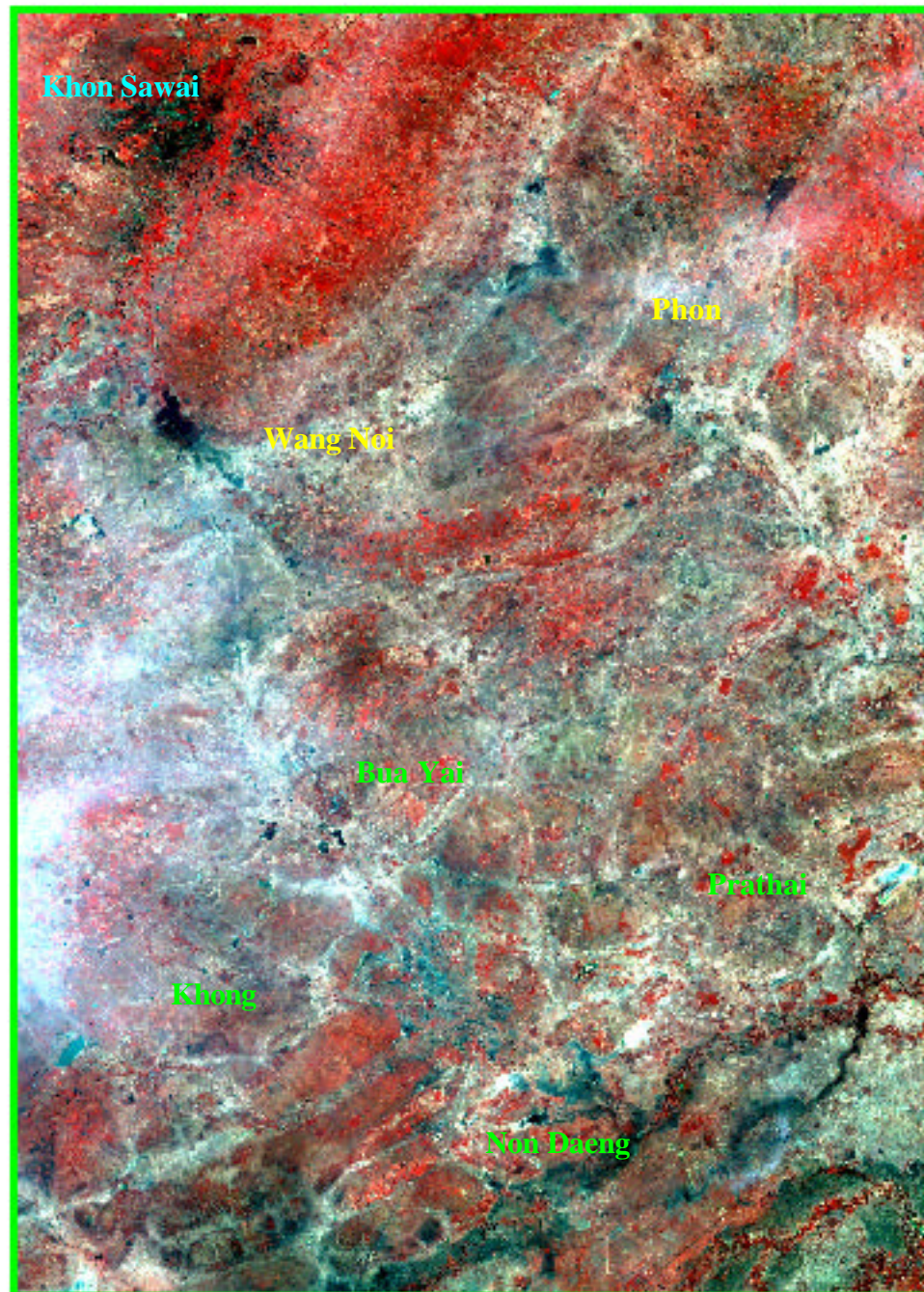


Figure 1.2 The MOMS satellite image used was recorded on May 3, 1993 with 13.5×13.5 meter² resolution; the False Color Composite (FCC) image was processed using RGB order in 4-2-1 respectively. MOMS: German multispectra space sensor operated onboard the space shuttle (D2-Mission). Data provided by German Aerospace Establishment (DLR) and BGR.

CHAPTER II

GEOLOGICAL SETTING

2.1 General geology

2.1.1 Permo-Carboniferous Sequence

The Silurian-Devonian rocks are the oldest rocks found in the Loei and Udon Thani provinces, northeastern Thailand. They consist mainly of metasediments and sedimentary rocks belonging to the Pak Chom Formation (Wongwanit, 2001). The Pak Chom Formation is composed of shale, limestone lens, chert, marble and schist. The depositional environments are continental and lagoonal swamps and graded to shallow marine environment (Piyasin, 1995). The orogenic event affected these rocks is poorly known, however it involved apparently large scale thrusting as well as volcanic activities and plutonism (Praditjan, 1995).

Chareonpravat and others (1984) classified the Devonian and Carboniferous rocks into two formations, namely the Nong Dok Bua Formation and the Wang Saphung Formation respectively in ascending order. The Nong Dok Bua Formation is Middle Devonian to Lower Carboniferous age. The Wang Saphung Formation is composed mainly of shale, limestone, sandstone and conglomerate of Carboniferous age and is exposed in Loei and some part of Udon Thani province. In Carboniferous period the depositional environments were continental reefal, lagoonal and graded to shallow marine (Chinoroje and Cole, 1995).

2.1.2 Permian and Triassic Pre-Khorat Sequence

Chonglakmani and Sattayarak (1978) classified the Permian sequence (Ratburi Group) in Loei-Phetchabun area into 3 units based on its age and depositional environment. The Nam Duk Formation is lower Permian age and it is deposited in a deep marine environment. The Pha Nok Khao Formation is middle Permian age and its depositional environment is a carbonate platform. The Hua Na Kham Formation is upper Permian age and it is deposited in a shallow marine environment. The distribution of these Permian units is shown in Figure 2.1. After the first stage of the second Indonesian orogeny probably in the Carnian, the Huai Hin Lat sediments were deposited in the separated half-grabens. The contacts with the older Permian rocks were more or less unconformable. The depositional environment was considered to be a fluvio-lacustrine type. Restricted basins were typical, and the limestone is believed to be a lacustrine deposit. According to the paleogeography it can be noted that, in some areas the Huai Hin Lat Formation comprises only redbeds, while in other areas it may contain a minor gray beds. Since the position of the Norian beds are located in the middle part of the sequence, the bases of the Huai Hin Lat Formation is considered to be Carnian.

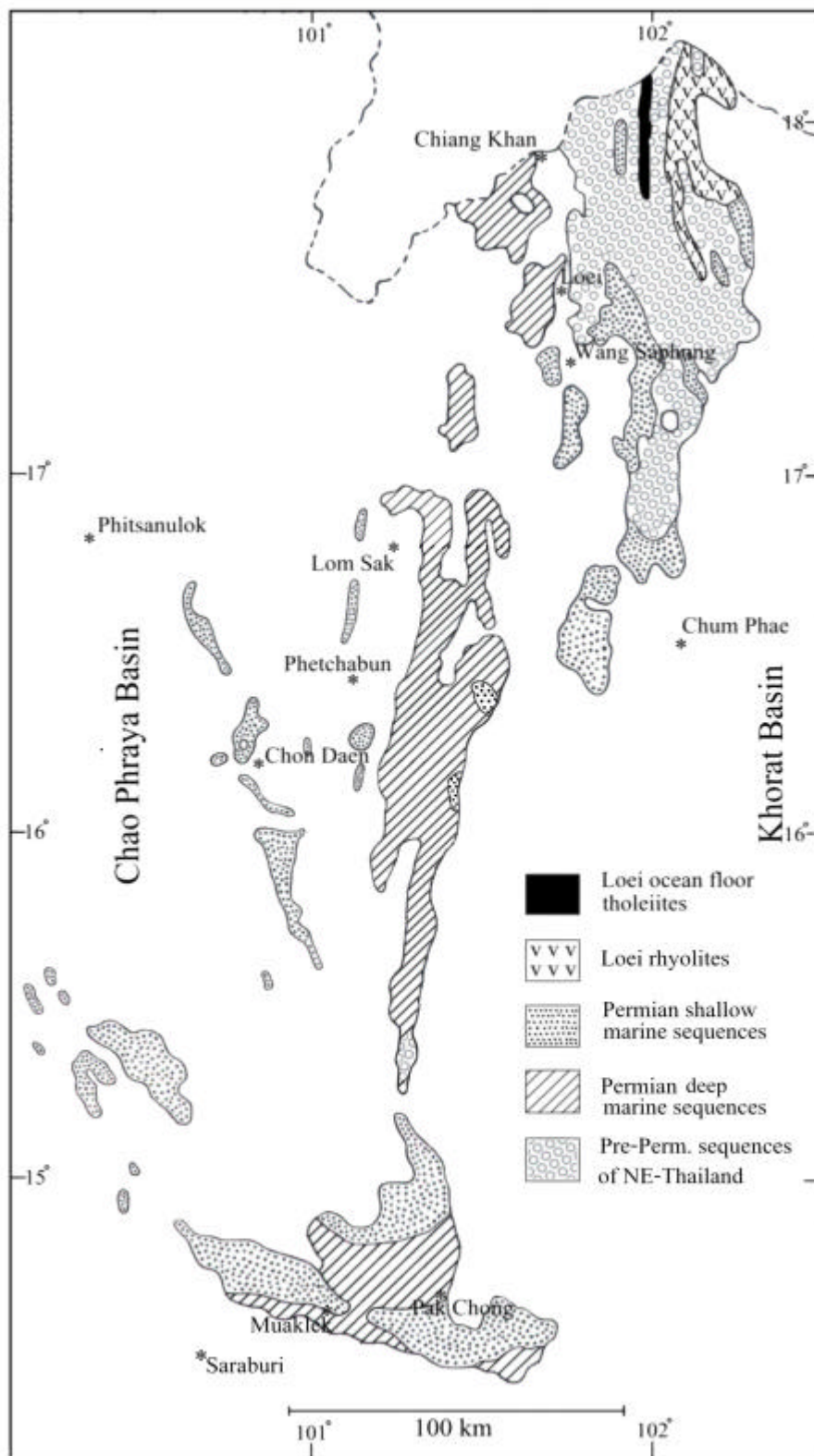


Figure 2.1 The Paleozoic rock in Northeast Thailand and adjacent area.

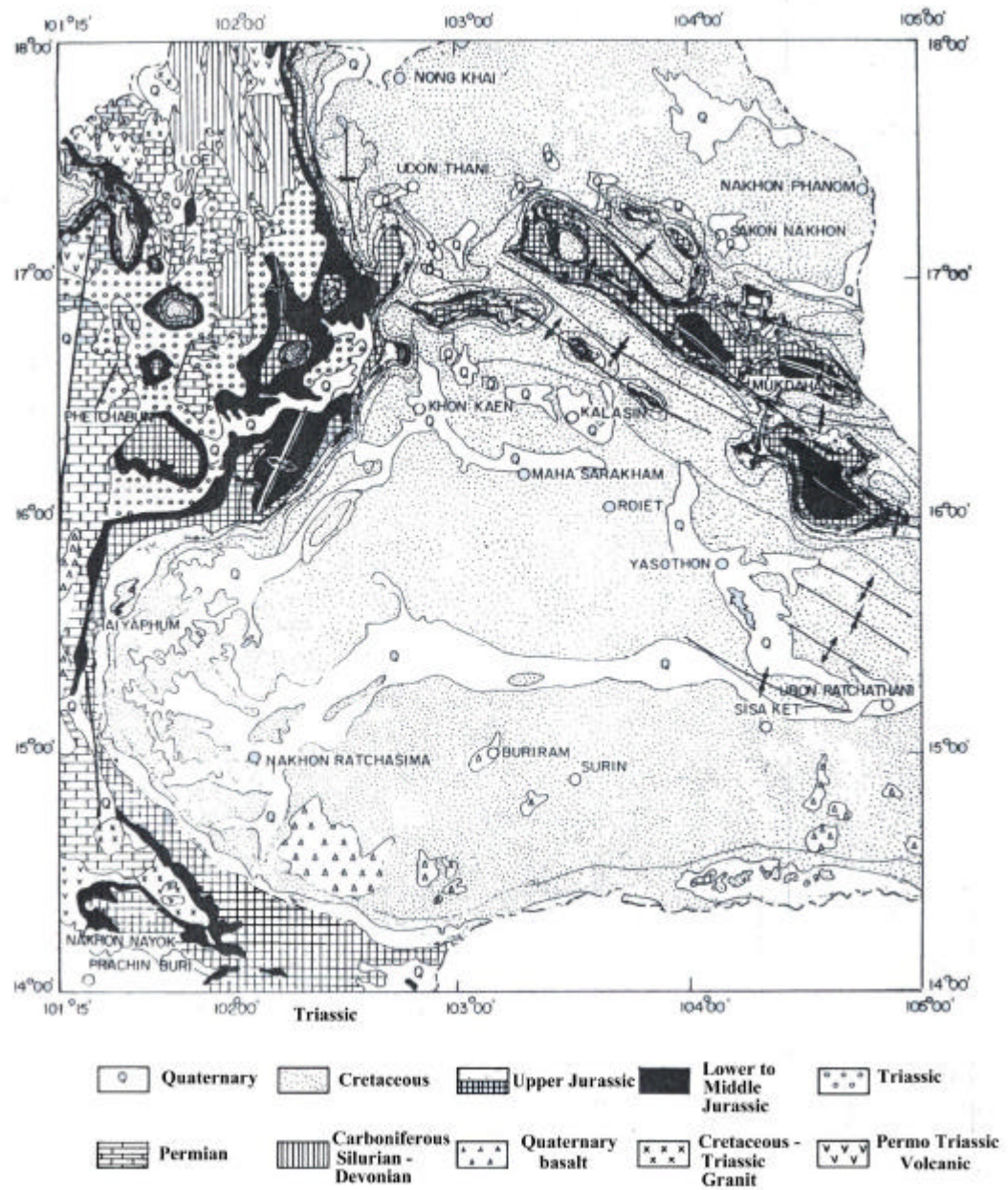


Figure 2.2 The Geological map of Northeast Thailand (After Chuaviroj, 1997).

2.1.3 Jurassic-Cretaceous Sequence

The Jurassic-Cretaceous continental red beds are widely distributed in Thailand and nearby countries, especially in northeastern region (Fig. 2.2). They belong to the Khorat Group and comprise predominantly red clastic sedimentary rock. Based on Metcalf (1996) the Khorat Basin is formed by flexural subsidence in front of orogenic belts. The evidence for supporting this process is based on the depocenter of the Khorat Basin which runs parallel with the Song Ma/Song Da suture lines and the Annamitic fold belt trend. Sattayarak (1983) reviewed and divided the Khorat Group and the overlying sediments into 8 Formations from bottom to top as follow (Fig. 2.3).

(1) The Nam Phong Formation

In the Late Triassic, just before or when all small separated basins were filled with the Huai Hin Lat sediments, the Nam Phong Formation started its accumulation. The deposits were transitionally changed into redbeds from the gray beds below. The Nam Phong Formation is the lowest formation of the continental Mesozoic Khorat Group. It is predominantly reddish brown resistant sandstone, siltstone and conglomerate. No fossil was found but its age is considered to be between those of the Huai Hin Lat and of the Phu Kradung Formations, i.e., Rhaetian. It was deposited in the fluvio-lacustrine environment.

(2) The Phu Kradung Formation

The Phu Kradung Formation is characterized predominantly by claystone in the lower part and with some massive sandstone intercalation in the middle part. While the upper part consists of massive sandstone interbedded with claystone. This unit rests unconformably on the Pre-Khorat rocks at a basin flanks. Ward and Bunnag (1964) noted the contact between the Nam Phong and Phu Kradung Formations at the alternating limestone zone. The interpreted marine ingression based on the presence of a plesiosaur tooth at Nong Bua Lam Phu was doubtful due to a recent discovery of the fresh water crocodile bones probably at the same locality. The fluvio-lacustrine depositional environment is again assigned to the Phu Kradung sediments. The claystones represented the flood plain deposits, while sandstones was interpreted as the channel sands of the meandering streams. The upper sequence characterized a gradual change to the overlying Phra Wihan Formation. The age of this formation is Early Jurassic.

(3) The Phra Wihan Formation

The Phra Wihan Formation comprises massive, resistant, light-coloured sandstone with some interbedded siltstone and conglomerate. Pebbly sandstone is usually encountered in the upper part of the section. The sequence reveals a deposition of braided streams. In some areas, it resembles the fluvio-lacustrine deposits. The age of the formation is considered to be the Middle to Late Jurassic.

(4) The Sao Khua Formation

The Sao Khua Formation is known as less resistant, reddish brown-coloured siltstone lying in between the more resistant sandstone units. It is predominantly deposited in fluvial environment. But the presence of marine pelecypods,

plesiosaur tooth, and ichthyosaur tooth, suggests some marine incursions. The age of the Sao Khua Formation is Late Jurassic to Early Cretaceous.

(5) The Phu Phan Formation

The Phu Phan Formation is characterized by massive beds of light-coloured, pebbly sandstone and conglomerate. The average thickness is about 80 meters, but at Nam Phung Dam site, it is about 400 meters thick. The middle part of the Nam Phung section comprises the redbeds containing Early Cretaceous pelecypods. In the northern part of the Khorat Plateau, the paleocurrent trending S-SW and/or W was recorded in the Phu Phan Formation which was similar to that of the Phra Wihan Formation (Sattayarak, 1983). Hahn (1982) considered the Phu Phan Formation as typical fluvial sediments.

(6) The Khok Kruat Formation

The Khok Kruat Formation consists predominantly of sandstone with some siltstone and claystone. It overlies conformably on the Phu Phan Formation. The fluvial environment is suggested and the deposition took place in an arid climate. Gypsum nodules and lenses were observed. The fossil found in its equivalent beds, the Ban Na Yo Formation points to the Late Cretaceous age.

(7) The Maha Sarakham Formation

The Maha Sarakham Formation is thought to rest unconformably on the underlying Khorat strata thus raising the problem about its status. This rock unit consists of the Lower, Middle and Upper Salt with 2 units of claystone in between. The unconformity does not show a strong discordance, thus a disconformity is suggested. The depositional basin is quite similar in shape to that of the older Khorat basin. The Khorat and Sakon Nakorn basins are structural basins formed after the deposition of the Maha Sarakham sediments. The age of this Formation is inferred as the Latest Cretaceous.

(8) The Phu Tok Formation

The Phu Tok Formation consists of two sandstone types, one with very large-scale crossbedding and the other with small wavy structures. Sattayarak and Sutheetorn (1979) mapped these strata as an informal formation. The sandstone was described as a red coloured, fine-grained, well-sorted and friable rock. The gross characteristics of this formation resemble an eolian deposit. The strata are found above the Khok Kruat Formation, but correlation with the Maha Sarakham Formation is not conclusive. It was probably deposited contemporaneously but in different environment with those of the rock salt. This formation, on the other hand, is possibly younger than the Maha Sarakham Formation as it overlies unconformably on the latter.

Suwanich (1995) proposed the "Nachuak Formation" as the top most formation in the Khorat Plateau. The type section of the Nachuak Formation was established from boreholes at Nachuak District, Maha Sarakham Province. This formation is composed mostly of fresh water limestone beds and sand-sized silica. They are mainly various kinds of white gray sedimentary rocks. The grain size of the rock

varies from clay to sand or larger to be nodules. He proposed that the Nachuak Formation was formed by the weathering of sandstone in the Phu Tok Formation and redeposited in shallow fresh water lake that subsided by the influence of salt tectonic. The lakes should be scattering on the basin of Khorat Plateau in the Quaternary age.

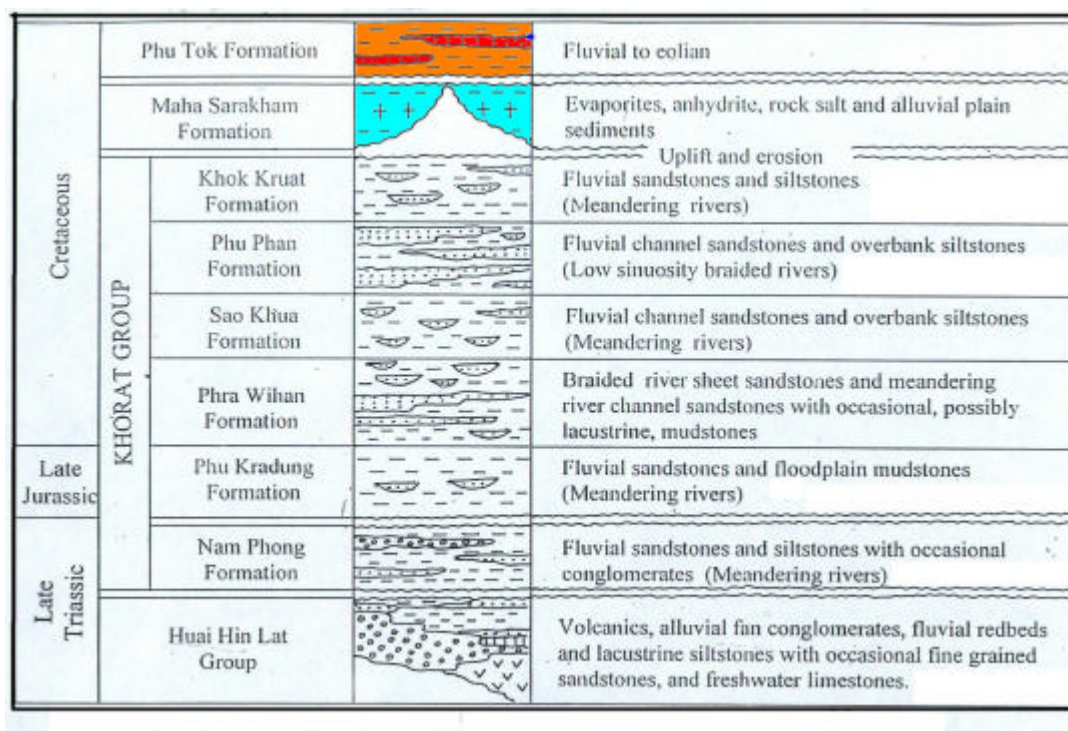


Figure 2.3 Stratigraphy of Mesozoic Continental sediments with environments of deposition (After Piyasin, 1995).

2.2 Tectonic events and deformation in the Khorat Plateau

The tectonic events of the Khorat Plateau can be divided into 3 episodes (Piyasin, 1995) as follow:

(1) Pre-Permo-Carboniferous

The igneous intrusion at the basement of the Yang Talat-1 well was dated as a middle Carboniferous age. This basement complex acts as buffer to protect the Plateau from the subsequent tectonic movements. The orogenic activity of the basement complex is very little known.

(2) Permo-Carboniferous

The lower clastic-carbonate and upper clastic of Permo-Carboniferous age deposited onlap on the basement complex at Yang Talat-1 on the western part of Phu Phan Range. The movement of Indosinian Phase II has generated reverse faults and propagation folds in this sedimentary facies accompanied by an extensive volcanic eruption and an uplift of the whole area above the sea level. The upper Triassic half-garbens were formed and the fluvial and lacustrine sediments were deposited in the garbens.

(3) Palaeocene (65 Ma)

The sediments of Khorat Group were deposited in the Khorat Basin without major tectonic movement. A minor unconformity is found at the base of Phra Wihan and Maha Sarakham Formations. The uplift at Early Palaeocene Epoch (65 Ma) was corresponded with the beginning of Himalayan deformation. The NW-SE trending movement in the later stage probably formed the Phu Phan anticlinorium.

Thanomsap (1992) studied the structural development on the Khorat Plateau and its western edge. He proposed four main stages of deformation in the studied areas. The structures formed in first stage show long and narrow shape of folding with N-S direction. The second stage is different phases of compressional movement in N-S and E-W directions. The third stage is the thrust of Nam Duk Formation over the Khorat red beds. Finally the active fault in the Phetchabun basin rim characterizes the fourth stage. He concluded that the axes of folding in the Khorat Plateau were prominent in N-S and E-W directions and were in perpendicular to each other.

2.3 Geologic overview on Maha Sarakham Formation (Salt Formation)

The Khorat Plateau of northeastern Thailand contains a large evaporite basin of Cretaceous age. It is divided into northern (Sakon Nakhon Basin) and southern (Khorat Basin) covering an area of about 50,000 km². The evaporite beds are included in the Maha Sarakham Formation (Sattayarak, 1985). These evaporites are thoroughly investigated by DMR aided by a UN Special Fund related to the Mekong Project (Japakasetr and Workman, 1978). It was planned to use the salts as a source for soda ash production by utilizing natural gas piped from the Gulf of Thailand. Additional feasibility study on Rock Salt and Soda Ash Project and Potash Engineering Project in Bamnet Narong area were conducted (Japakasetr, 1985).

Hite (1971) published his first report entitled "Potential for potash and related mineral resources, Khorat Plateau, Northeast Thailand and Central Laos". He first assumed that the salt bed is flat lying and recommended that the evaporite bed should be found in the other formation also. Japakasetr (1974) published the progressive report of potash investigation after the four holes drilling. All the first four holes were drilled in the northern basin in Udon Thani, Nongkhai, Sakon Nakhon and Nakhon Phanom Provinces. Sundharovat (1976) presented the idea of the origin of potash in northeast Thailand which was related with the warping of the rock in the Khorat Group, the transgression of sea water and the deposition of evaporites in later Tertiary or Pleistocene.

Sundharovat (1977) also discussed the hypothesis of low structure of potash in the small basin, which is disseminated in the Khorat Plateau. Thiramongkol (1978) proposed that rock salt was deposited in inland sea or lagoon environment in the Late Cretaceous and was affected later by epeirogenic movements as warping and block faulting. Hite and Japakasetr (1979) commented that differential loading affected the shape and attitude of rock salt strata. Hite (1982) published a report of potash investigation by emphasizing the three main structural areas of Bamnet Narong, Khon Kaen and Non Sung. But his idea about the genesis of salt anticline has been changed from the differential loading to paleochannel. Yumuang (1982) studied the boreholes

logging in Bamnet Narong area. He proposed that three times of marine transgression and regression had occurred and generated three units of rock salt and associate minerals.

Suwanich (1983) presented in the Conference on Geology and Mineral Resources of Thailand about the potash and rock salt in Thailand. He emphasized the genesis of salt dome which is formed by differential loading. The differential loading should occur after the lower salt had been deposited and the lower clastic started to deposit gradually. Sheldon (1984) published his report on phosphate exploration on the Khorat Plateau. He commented that the fourth cycle of transgression on the Khorat Plateau might be suitable for phosphate deposit and the basin structure was related to the salt tectonic and salt basin. He also supported the hypothesis of differential loading. Suwanich (1984) divided the Maha Sarakham Formation into 6 units from bottom to top as follow; lower salt, lower clastics, middle salt, middle clastics, upper salt and upper clastics.

Sattayarak (1985) separated the Maha Sarakham Formation from the Khorat Group on the ground that the depositional environment was changed from continental basin to marine basin. Warren (1989) proposed that where the Maha Sarakham rock salt is deeply buried, it becomes mobilized and may flow upwards to form salt domes and anticlinal structures. It might also be deformed into discordant bodies and lubricated filled in surrounding gaps and dragged adjacent strata. Mohamed et al (1995) studied detail stratigraphy of the Maha Sarakham Formation. They found that the sequence is not always consistent throughout the basin because of erosion, salt flowage, tectonic and natural dissolution. Donald (1996) compared the depositional characteristic of Khorat Basin with Sergipe, Brazil and Congo-Gabon. He summarized the common characteristics as follow:

- (1) The basin contains massive quantities of tachyhydrite.
- (2) The basin occurs directly on terrestrial sediments, with very little anhydrite and essentially no dolomite in or near the deposit.
- (3) There are subsequent basaltic intrusions in and adjacent to the deposit.

He concluded that the Maha Sarakham Formation is deposited in a terrestrial and not a marine environment. Warren (1999) commented that the Khorat and the Sakon Nakhon Basins are lack of $MgSO_4$ salts, indicating a likely time for continental or basinal brine source. Based on Suwanich (1984) and Mohamed et al., (1995) the stratigraphy of the Maha Sarakham Formation may be summarized as follow.

(1) Basal Anhydrite Member (Intersected thickness 0.75-6.20 m)

The Basal Anhydrite is found at the base of the Maha Sarakham Formation throughout both the Khorat and the Sakhon Nakhon basins. It conformably overlies the Khok Kruat sandstone of the Khorat Group. The generally reddish-coloured sandstone of the Khok Kruat Formation is typically greenish and may be Cu-stained

in proximity to this contact. Although in areas of slumping or dissolution the anhydrite layer locally varies in thickness from 0.75-6.20 m, but a thickness of 1.0 m characterizes the unit across the regional extent of the Maha Sarakham evaporites in the basin.

(2) Lower Salt Member (Intersected thickness 30.00-500.00 m)

The Lower Salt is the most widespread of the salt units in the Maha Sarakham Formation. Halite with accessory anhydrite is the dominant lithology. However, a zone rich in potash minerals characteristically occurs near the top of the unit. A layer of depositional-textured anhydrite up to 3.45 m in thickness separates the Lower Salt into upper and lower portions, and is correlatable throughout the basin. The contact with the Basal Anhydrite is sharp while that with the potash-rich zone is generally gradation.

(3) Lower Clastics Member (Intersected thickness 10.00-60.00 m)

The Lower Clastics Member comprises reddish brown claystone, invariably containing randomly oriented fractures filled with halite spar. Color of the claystone may be greenish-gray in the vicinity of the contacts with the underlying and overlying salt units.

(4) Middle Salt Member (Intersected thickness 20.00-180.00 m)

The Middle Salt comprises well-bedded halite with similar repetitive bed forms to those found in the upper part of the Lower salt. Rare sylvite and carnallite grains have sporadic occurrence and rarely a poorly developed potash zone may top the sequence.

(5) Middle Clastics Member (Intersected thickness 20.00-70.00 m)

The Middle Clastics Member consists of massive red to purple claystone and silty mudstone. Bedding in this unit is well defined with cryptalgal laminations and root traces.

(6) Upper Salt Member (Intersected thickness up to 20.00 m)

The Upper Salt is the least preserved halite member in the Khorat Basin because of later dissolution and possible non-deposition in some parts of the basin. However, salt beds when observed are the least deformed beds in the sequence.

(7) Upper Clastics Member (Thickness up to 687 m)

The Upper Clastics Member comprises pale reddish-brown silty claystone with minor sandy intervals. In this unit bedding is well defined and even laminations, root traces, and sets of cross beds are commonly observed. The unit is generally exhibits upward coarsening. The contact with the overlying Phu Thok is not defined.

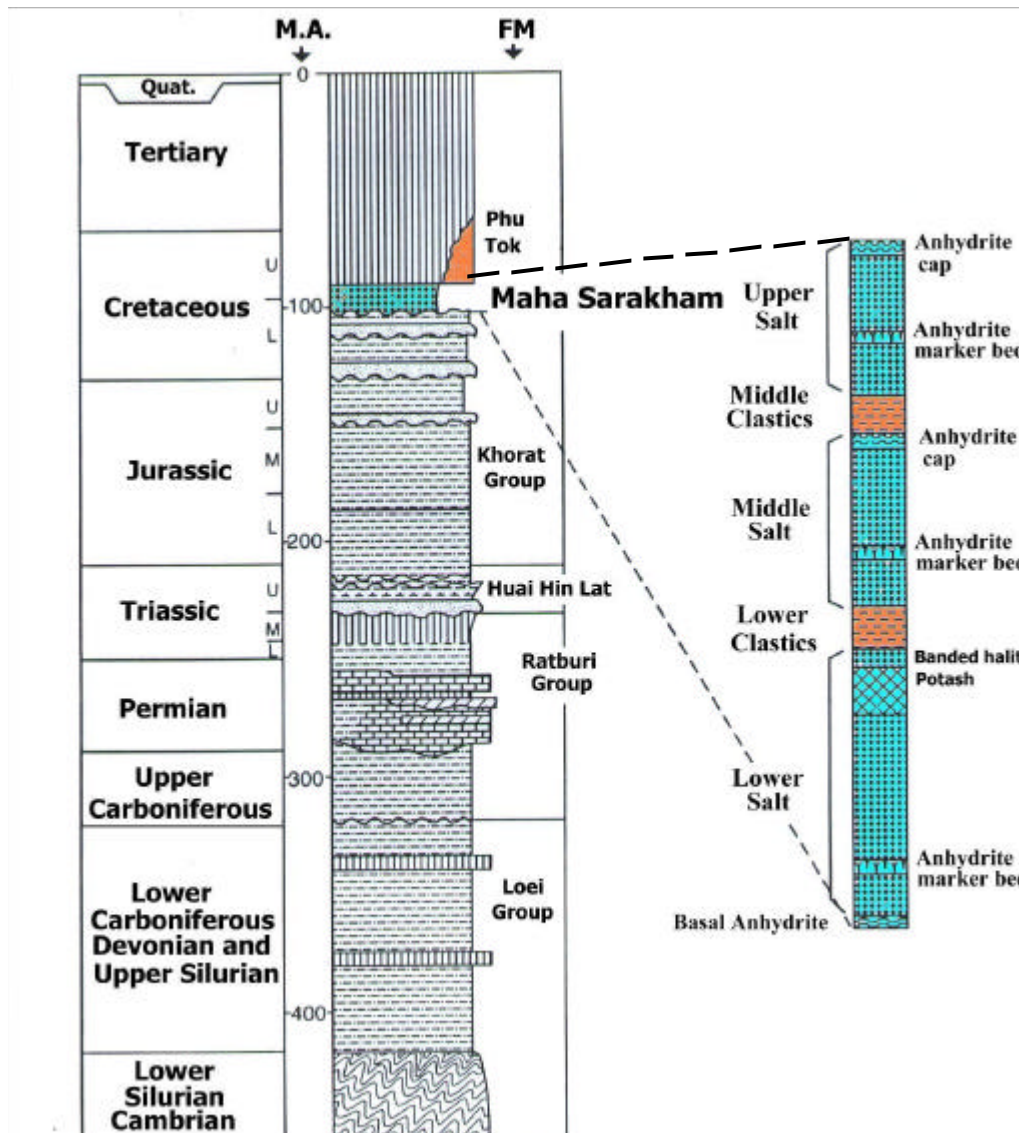


Figure 2.4 Lithostatigraphy and subdivisions of the Khorat Group and the Maha Sarakham Formation (Modified from Suwanich, 1986).

2.4 Salt Structure

Evaporite deposits occur in sedimentary sequence at shallow crustal levels in many parts of the world. Layers of rock salt undergo ductile deformation more readily than do the more common sedimentary rock types such as sandstone and limestone. Salt flows at surface conditions under the force of gravity and some tectonic environment. The density of salt contrasts with the greater density and strength of the enclosing sediments. A great variety of structures in subsurface can be ranging from shallow to deep. The internal structure of these salt features provides abundant evidence of plastic flow with fold, foliation and other structure as shown in Figure 2.5. In Northeastern Thailand, based on the detailed study of the bore-holes drilled in 1973-1982 the upper salt layer in the Khorat Basin can be plotted as shown in Figure 2.6.

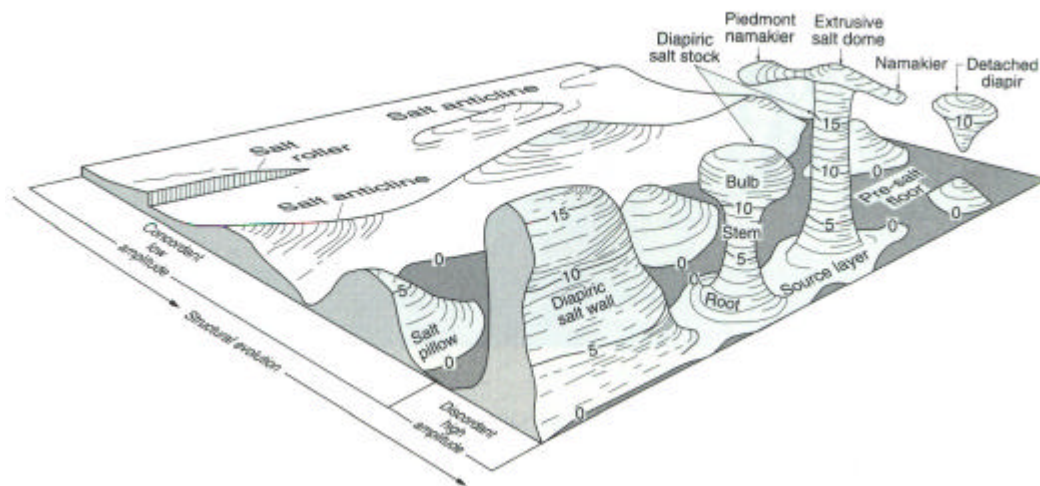
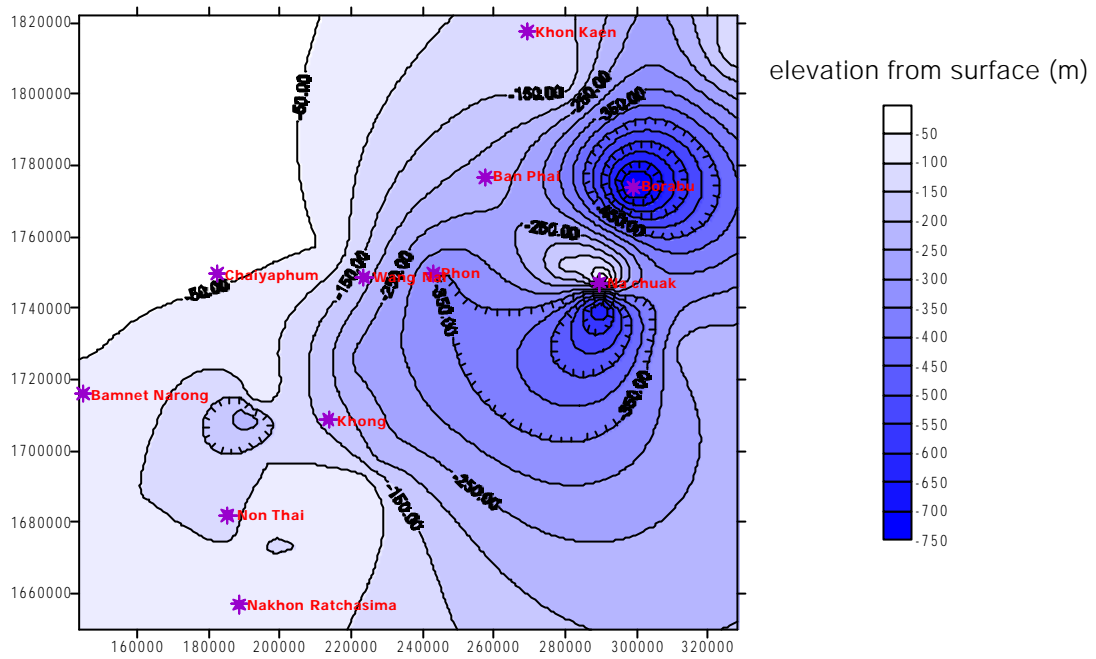
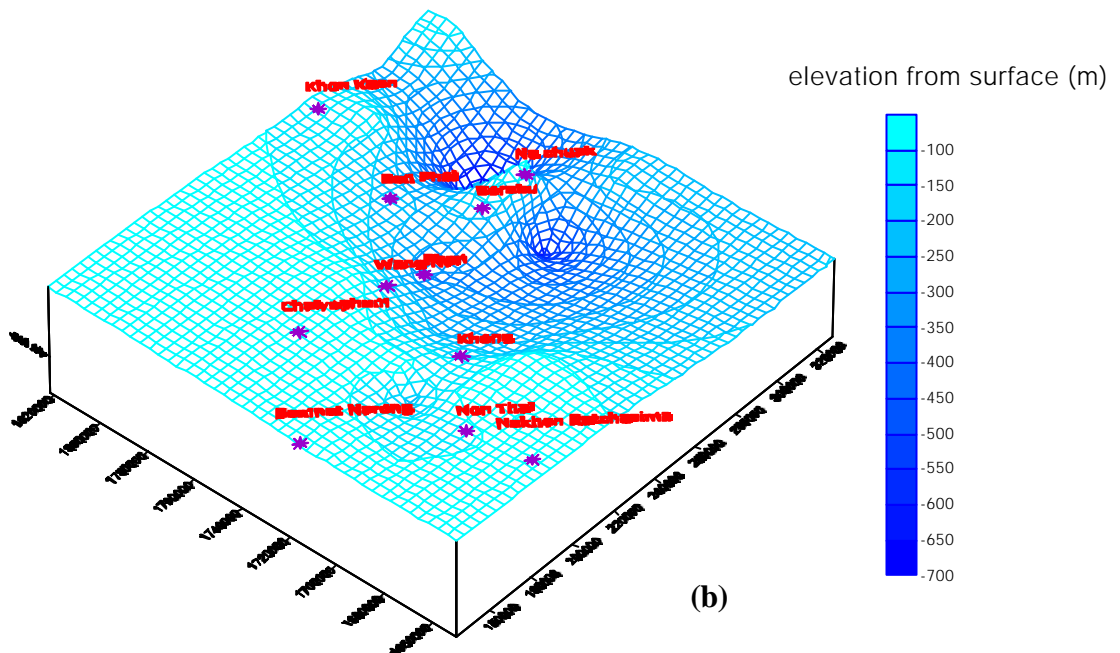


Figure 2.5 The shapes of salt structures with structural evolution. Numbers indicate relative elevation $\times 100$ m above base (After Hatcher, 1995).



(a)



(b)

Figure 2.6 Salt distribution in Khorat Basin; (a) The contours show the depth of upper salt layer. (b) Upper salt in three dimensional view (The data from Potash exploration bore-holes, 1973-1982).

Warren (1989) classified the mechanism controlling salt movement into two groups, a shallow group controlling salt flow at shallow depths of less than 600 m and a deeper group which is most important below such depths. In Northeastern Thailand, the Maha Sarakham Formation is considered to be shallow depths (<600m). Three major mechanisms are known as follow:

(1) Differential loading

The differential loading on top of the salt layer often occurs in areas of reefs and shoals or where deltas and/or submarine fans are prograding as depositional lobes over an underlying salt layer (Fig. 2.7).

(2) Gravity glide folding

The gravity glide folding causes the passive rise of salt into growing anticlines. The example of this process occurs in Gulf of Mexico. The mechanism commonly operates beneath the deep waters of the continental slope and margin (Fig. 2.8)

(3) Buoyancy

The buoyancy mechanism usually dominates at depths of > 600 m, but can operate at shallower depths under denser overburden. Such conditions can be found beneath well-cemented carbonate layers and reefs where densities often exceed 2.2 gm/cm³ only tens of meters below the surface (Fig. 2.9).

Warren (1989) also classified the development of salt structure into three stages as follow:

(1) Salt pillow stage

The pillow stage is a nonpiercement stage; sediments above the pillow are thin over a broad equidimensional area with maximum thinning over the crest of the structure (Fig. 2.10). The area above the pillow is often a topographic high, while the area between the pillows is often a topographic low or primary rim syncline created by salt withdrawal. Rim synclines are often areas of preferential sedimentation, that is sediment thick.

(2) Diapir stage

The diapir stage is a piercement stage, the rate of salt movement is so rapid that sediment is usually not preserved over the crest of the structure. During the diapir stage the salt is very near to, or at the surface and any overlying sediment is periodically eroded. Salt in the crest of the diapir is near or at the surface throughout the diapir stage. It is continually dissolved in the shallow subsurface.

The “**turtle structures**” also form in the diapir stage. They grow as the locus of maximum salt withdrawal moves closer and closer to the growing salt mass. This means that rim syncline also migrates toward the salt structure. As the area of salt withdrawal migrates closer and closer to the stem of the salt structure, the associated zone of subsidence moves closer and closer to the salt neck. Thus the area of primary

rim syncline of the pillow stage becomes a zone of relatively thicker sediment (Fig.2.11).

(3) Post diapir stage

The post diapir stage is the last stage of salt structure growth. By this time the salt supply is dwindling as the volume of salt flowing into the foot of the salt mass decreases (Fig. 2.12). The crest of the structure is once again buried, but still near the surface. It now feels the effects of meteoric waters as caprock carapace forms by dissolution and alteration to encase the upper few hundred meters of the structure. The buried crest means that sediment can once again be deposited over the crest of the structure and small, localized tertiary rim synclines can be adjacent to the diapir.

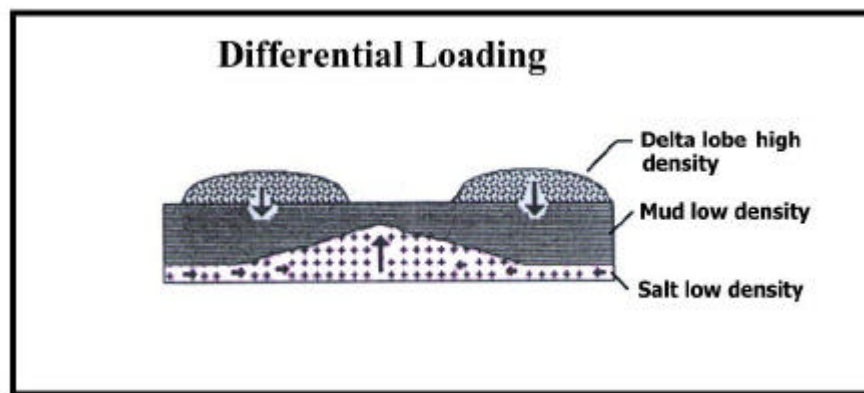


Figure 2.7 The differential loading mechanism (After Seni and Jackson, 1984).

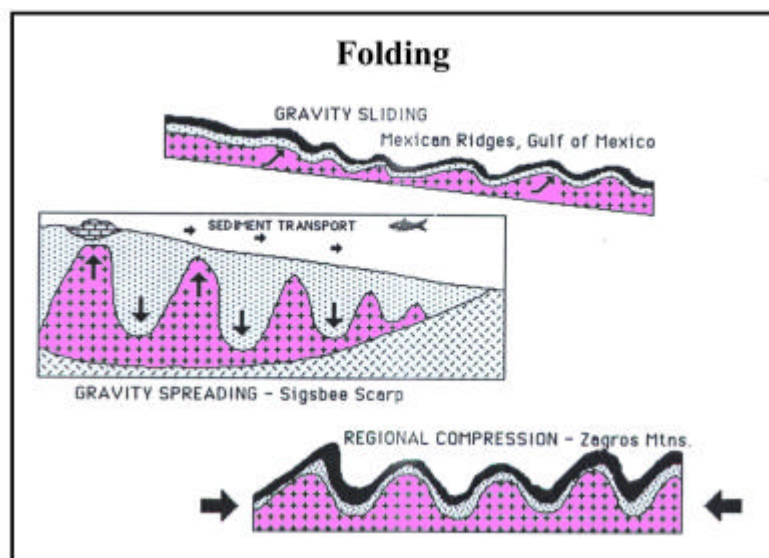


Figure 2.8 The salt folding structure initiated by gravity slides, gravity spreading and regional compression (After Warren, 1989).

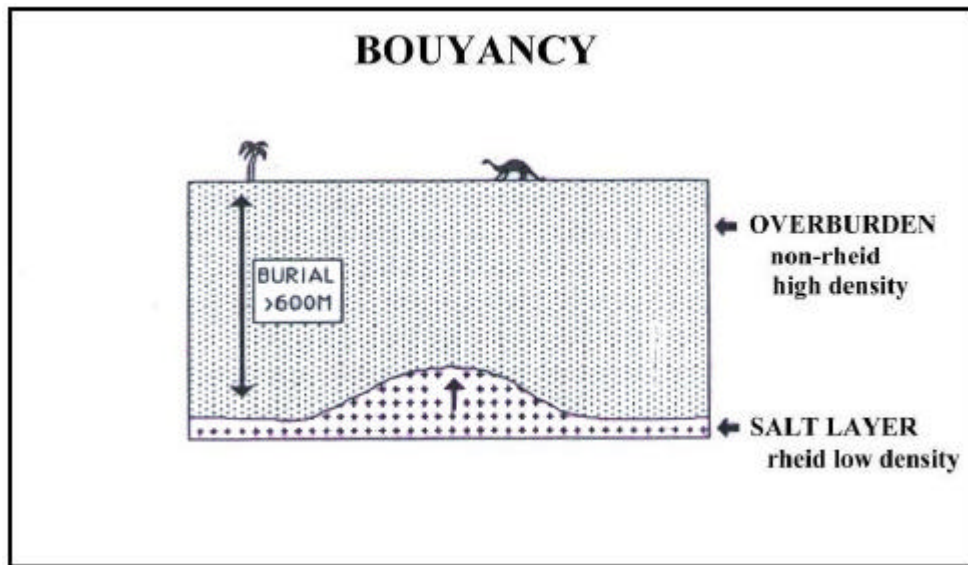


Figure 2.9 The Buoyancy mechanism (After Seni and Jackson, 1984).

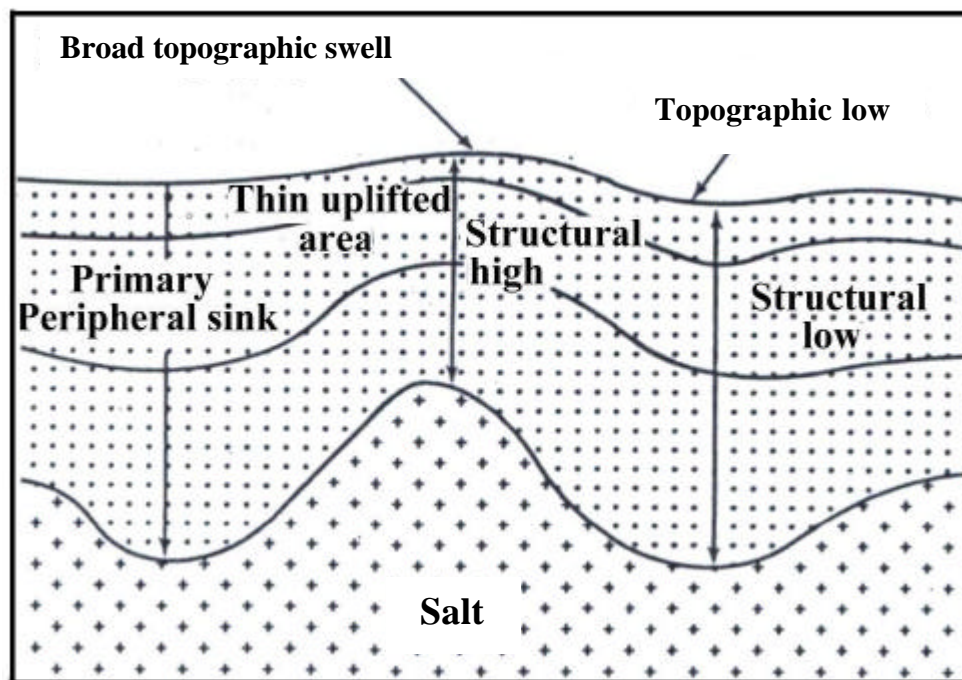


Figure 2.10 The salt pillow stage (After Seni and Jackson, 1983a).

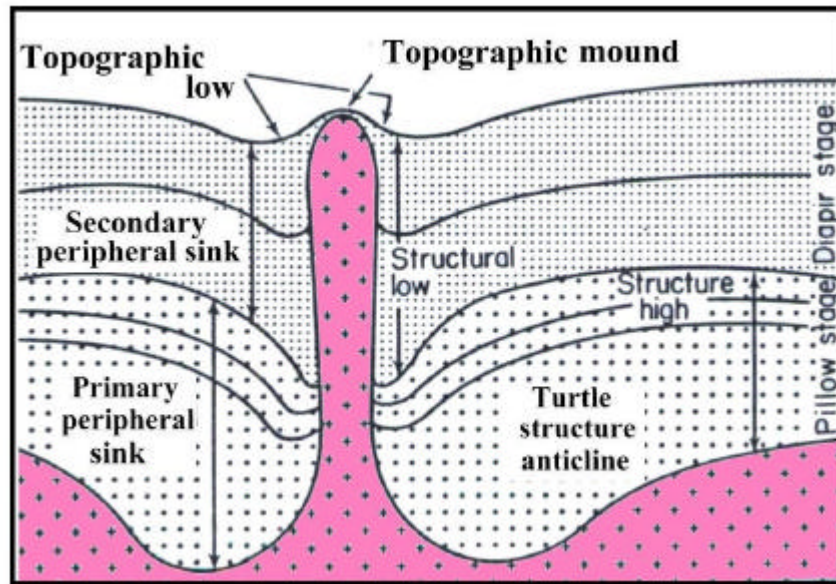


Figure 2.11 The diapir stage associated with the development of turtle structures and overhangs (After Seni and Jackson, 1983a).

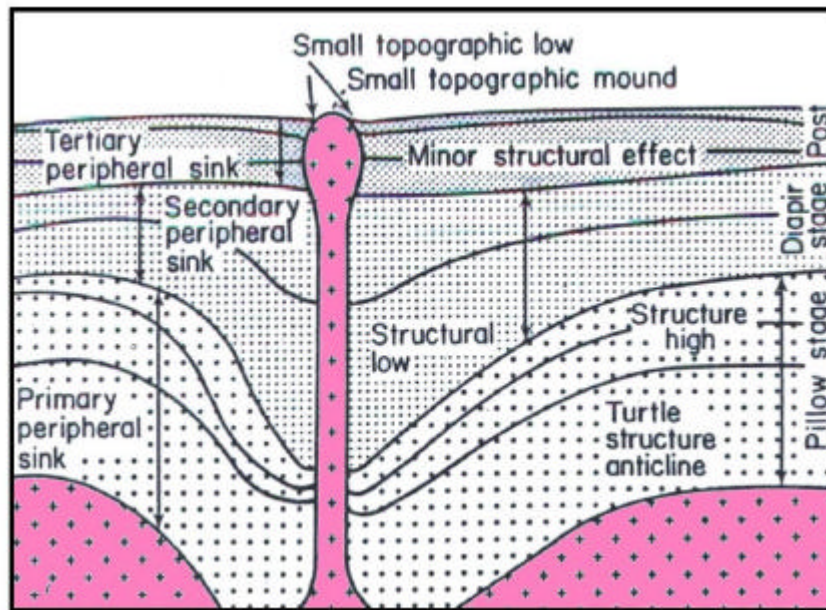


Figure 2.12 The post diapir stage (After Seni and Jackson, 1983a).

CHAPTER III

REMOTE SENSING

3.1 Fundamental and terminology of remote sensing

The term remote sensing refers to methods that employ electromagnetic energy, such as light, heat and radio waves as the means of detecting and measuring target characteristics (Sabins, 1997). Remote sensing uses sensors in satellites and airplanes to detect, to monitor, and to assess objects and processes at the earth's surface, without direct contact between the sensor and the targets. The remote sensing advantages can provide information for large areas, and in a relatively short time. In addition, the remote sensing is not limited by extremes in terrain or hazardous condition. Generally, remote sensing should be integrated into early stages of investigations and in conjunction with traditional mapping techniques. Remote sensing data is best suited for the following purposes:

- Preliminary assessment or characterization of an area prior to the application of the often more costly, time consuming, traditional assessment techniques such as field mapping, drilling, or geophysical measurements.
- Clarification of geoscientific problems that can be solved more effectively with the general perspective provided by an aircraft or satellite.
- Geoscientific assessment of regions of limited or no access, such as inaccessible terrain, hazardous sites, and disaster areas.

Remote sensing methods record electromagnetic (EM) radiation for obtaining information about the earth's surface (Fig. 3.1). Remote sensing utilizes EM radiation principally in the ultraviolet, visible light, infrared, and microwave portions of the EM spectrum as shown in Table 3.1 and Figures 3.2 and 3.3.

Most sensing devices record information about an object by measuring an object's transmission of electromagnetic from reflecting and radiating surfaces. The sun is the main source of the earth's incident EM radiation. Solar radiation can be absorbed or reflected by a surface, depending on the condition and properties of the materials. The proportions of reflection, absorption and penetration of the incident radiation at the earth's surface depend on the physical, structural and textural properties of the surface. The direct detection of minerals, rocks, soils, and vegetation using multispectral and hyperspectral remote sensing technologies requires knowledge of their spectral properties (reflectance spectra, spectral reflectance curves).

Reflectance spectra also called spectral signature define the percentage of incidence (solar) radiation that is reflected by a material, as a function of the wavelength of the radiation. When solar radiation hits a target surface, it may be transmitted, absorbed or reflected (Fig. 3.1 and 3.2). Different materials reflect and

absorb differently at different wavelengths. For any material, the amount of solar radiation that reflects, absorbs, or transmits varies with wavelength. This important property of matter makes it possible to identify different substances or classes and separate them by their spectral signatures (spectral curves), as shown in the Figure 3.4. In principle, a material can be identified from its spectral reflectance signature if the sensing system has sufficient **spectral resolution** to distinguish its spectrum from those of other materials. Depending on the wavelength and the nominal spectral location, principal applications can be matched with suitable satellite bands for classification. The applications in each band show in Table 3.2.

Remote sensing images are normally in the form of digital images. A digital image comprises of a two dimensional array of individual picture elements called **pixels** arranged in columns and rows (Fig. 3.5). Each pixel represents an area on the Earth's surface. A pixel has an intensity value and a location address in the two dimensional image. The intensity value represents the measured physical quantity such as the solar radiance in a given wavelength band reflected from the ground, emitted infrared radiation or backscattered radar intensity. This value is normally the average value for the whole ground area covered by the pixel. The intensity of a pixel is digitized and recorded as a digital number. Due to the finite storage capacity, a digital number is stored with a finite number of bits (binary digits). The number of bits determine the radiometric resolution of the image.

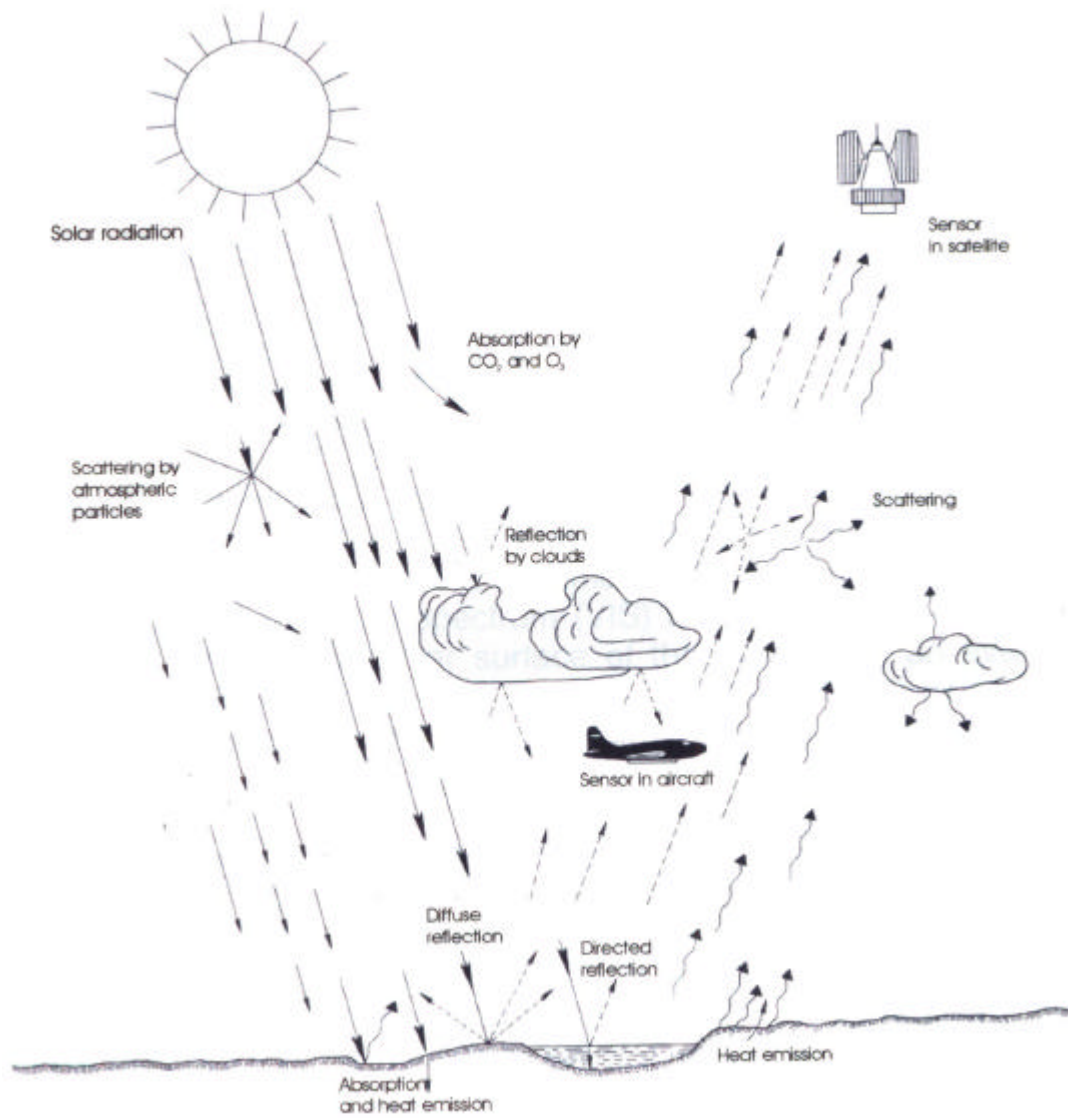


Figure 3.1 Remote sensing systems record the EM radiation after its interaction with the earth's surface (After Kronberg, 1985).

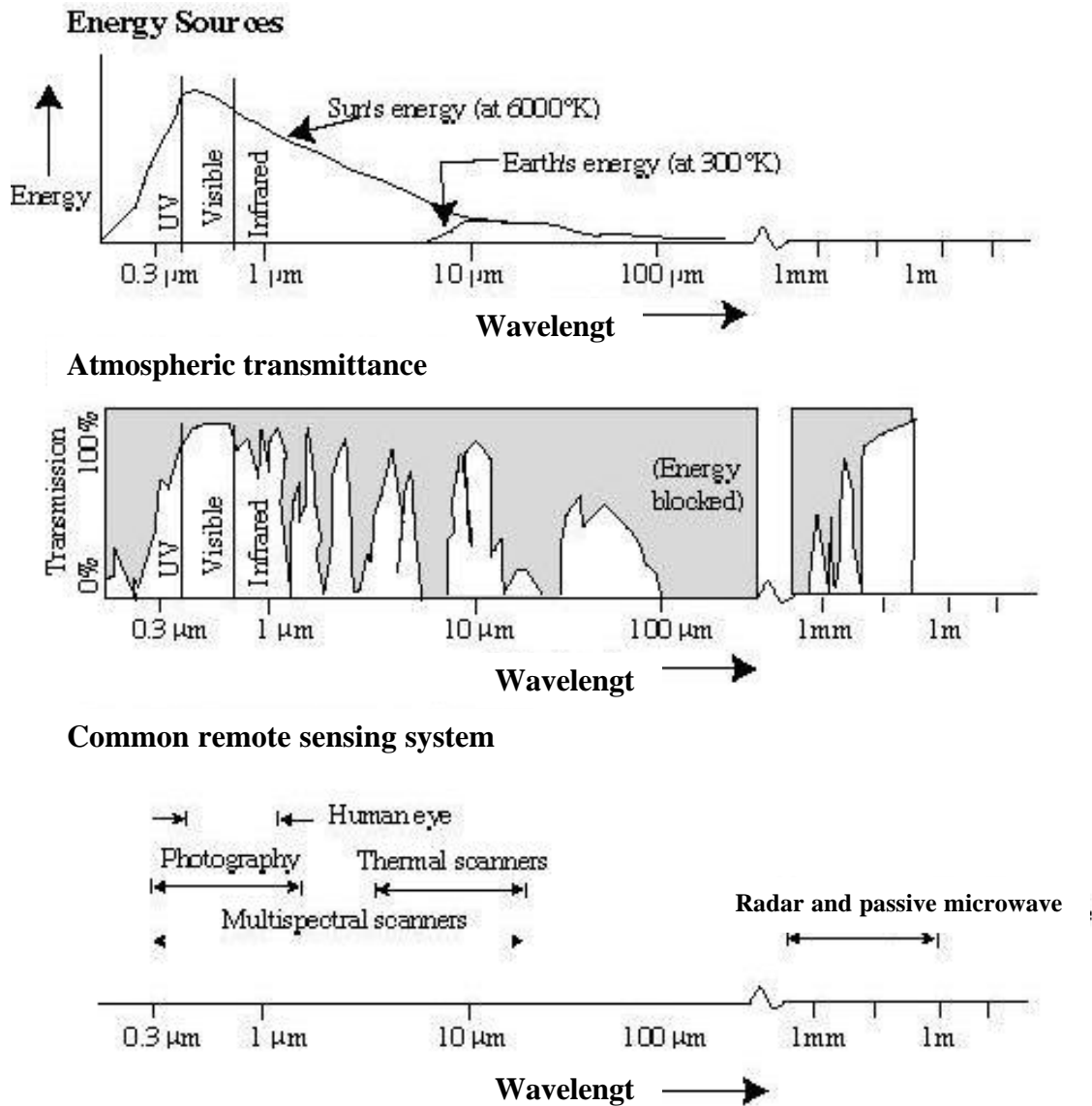


Figure 3.2 Spectral characteristics of energy sources, atmospheric effects, and sensing system. Wavelength scale in logarithm (After Short, 2002).

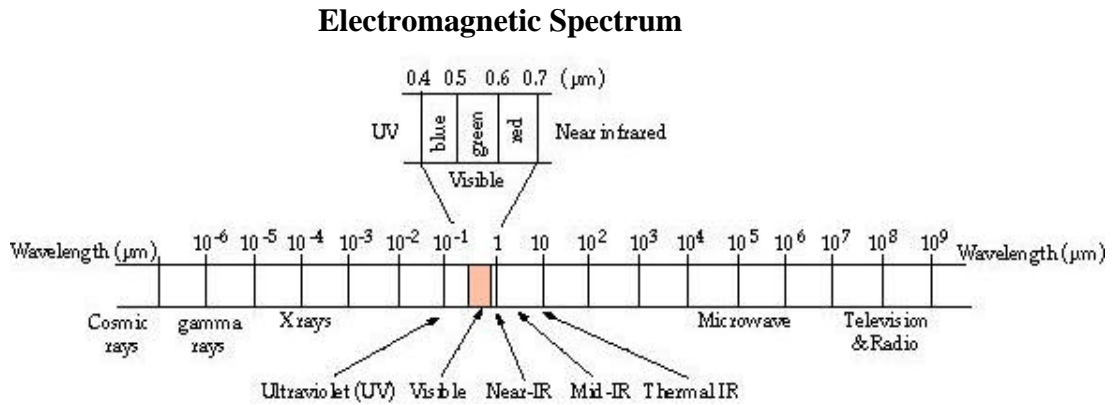


Figure 3.3 The types of electromagnetic spectrum in each wavelength (After Sabin, 1987) .

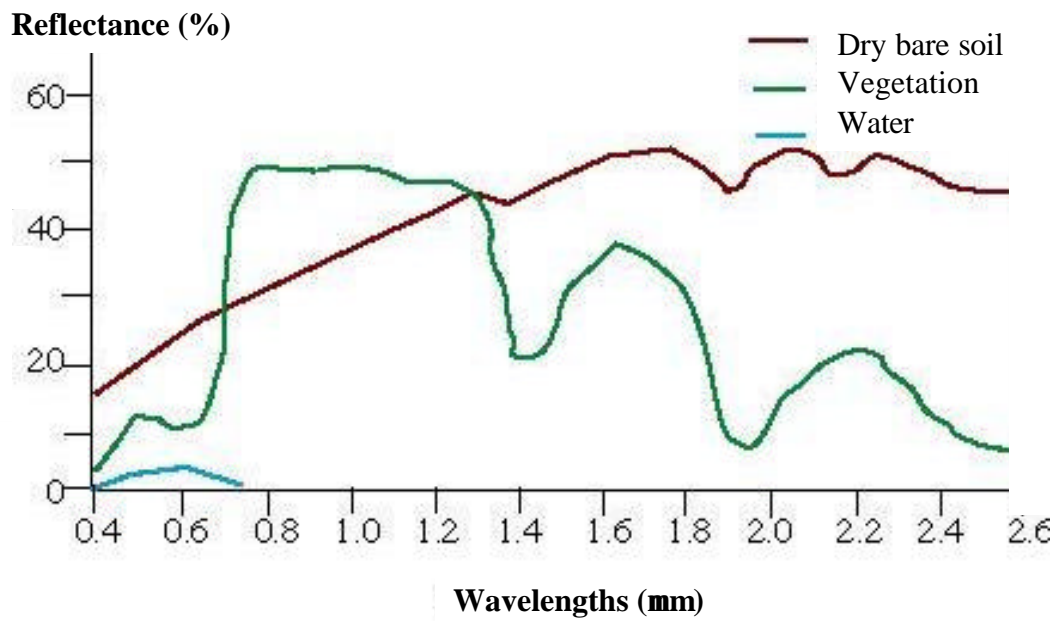


Figure 3.4 The graph shows the typical reflectance spectra of three materials: water, dry bare soil and vegetation (After Gupta, 1991).

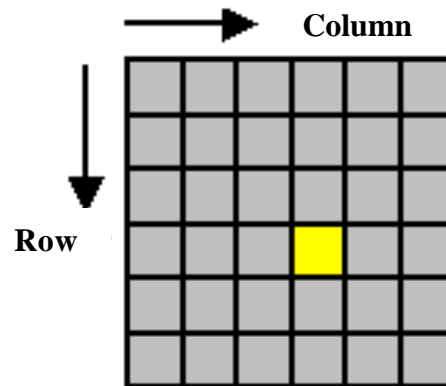


Figure 3.5 A digital image is a two-dimensional array of pixels. Each pixel has an intensity value (represented by a digital number) and a location address (referenced by its row and column numbers).

Table 3.1 Spectral range of electromagnetic radiation utilized by remote-sensing sensor (After Erb, 1989).

Radiation	Abbreviation	Wavelength λ (μm)
Near ultraviolet	NUV	0.315 - 0.38
Visible light	VIS	0.38 - 0.78
Near infrared	NIR-I	0.78 - 1.4
	NIR-II	1.4 - 3.0
Middle infrared (thermal infrared)	MIR	3.0 - 50.0
	MIR-I	3.0 - 5.5
	MIR-II	8.0 - 15.0
Far infrared	FIR	50.0 - 1000
Microwave (radar)	MW	1000 - 1×10^6

Table 3.2 The characteristics and principal applications of band and wavelength (After Lillesand and Kiefer, 1987)

Band	Wavelength (mm)	Nominal Spectral Location	Principal Applications
1	0.45-0.52	Blue	Designed for water body penetration, making it useful for coastal water mapping. Also useful for soil/vegetation discrimination, forest type mapping, and cultural feature identification.
2	0.52-0.60	Green	Designed to measure green reflectance peak of vegetation for vegetation discrimination and vigor assessment. Also useful for cultural feature identification.
3	0.63-0.69	Red	Designed to sense in a chlorophyll absorption region aiding in plant species differentiation. Also useful for cultural feature identification.
4	0.76-0.90	Near infrared	Useful for determining vegetation types, vigor, and biomass content, for delineating water bodies, and for soil moisture discrimination.
5	1.55-1.75	Short-wave infrared	Indicative of vegetation moisture content and soil moisture discriminations, and thermal mapping applications.
6	10.4-12.5	Thermal infrared	Useful in vegetation stress analysis, soil moisture discrimination, and thermal mapping applications.
7	2.08-2.35	Mid-infrared	Useful for discrimination of mineral and rock types. Also sensitive to vegetation moisture content.

3.2 Remote sensing data

Remote sensing data taken by different satellite observation systems was available for the remote sensing based mapping in the Khorat project area. The data was available in BGR archives and purchased by the Thai-German Environmental Geology Project. Data of the following Satellite Systems was acquired for the project and is now available on CDROM for further mapping and research in the DMR:

- MOMS D2 1993 Space Shuttle Mission, Germany/USA
- Landsat Thematic Mapper (TM), USA
- Landsat 7, USA

The MOMS satellite imaging systems is the main source in this study. The data taken and recorded by that system is characterized as follows:

MOMS (Modular Optical Multispectral Sensor):

The German Modular Optoelectronic Multispectral Stereo Scanner was launched on April 26, 1993 on board the Space Shuttle Mission STS-55. The data acquisition period lasted until May 6, 1993. During that time data were taken in different observation modes between +/- 28.5° geographic latitude.

Generally, the MOMS-02 sensor design is characterized by the following features:

- Stereo imagery
- High resolution imagery
- Multispectral imaging.

The nominal orbit altitude of the STS-55 Space Shuttle flight was 296 km. Depending on the recording mode the swath wide for the high resolution channel can be as much as 37 km (pixel size 4.5m x 4.5m), and 78 km (13.5m x 13.5m pixel). Due to the viewing angle of 24.4° of the two off-nadir channels 6 and 7 stereoscopic imagery is enabled. The MOMS-02 characteristics is shown in Table 3.3.

Table 3.3 Characteristics of MOMS-02 operating modes.

Channel	Mode	Orientation	Band Width	Pixel Size	Swath Width
1	multispectral	Nadir	449 - 511 n m	13.5 m x 13.5 m	78 / 43 km
2	multispectral	Nadir	532 - 576 n m	13.5 m x 13.5 m	78 / 43 km
3	multispectral	Nadir	645 - 677 n m	13.5 m x 13.5 m	78 / 43 km
4	multispectral	Nadir	772 - 815 n m	13.5 m x 13.5 m	78 / 43 km
5	high resolution	Nadir	512 - 765 n m	4.5 m x 4.5 m	37 / 27 km
6	stereo	+21.4°	524 - 763 n m	13.5 m x 13.5 m	78 / 43 km
7	stereo	-21.4°	524 - 763 n m	13.5 m x 13.5 m	78 / 43 km

Parts of the Khorat Plateau were covered by orbit 89 on May 3, 1993 (Data Take 31). This data take provided 8 multispectral images covering a 78 km width track between Amphoe Chayaphum in NE-Thailand and Nha Trang in Vietnam. The images 1, 2 and 3 of are cloud-free and in of high quality. The images 4 to 8 taken for parts of Eastern Thailand, Kampuchea and Vietnam are mainly covered by clouds and of limited use.

Multispectral data sets have been digitally processed and evaluated in the course of the project.

Landsat TM:

Spectral bands:	TM1:	0.45 - 0.52 nm (VIS)
	TM2:	0.52 - 0.60 nm (VIS)
	TM3:	0.63 - 0.69 nm (VIS)
	TM4:	0.76 - 0.90 nm (NIR)
	TM5:	1.55 - 1.75 nm (SWIR)
	TM7:	2.08 - 2.35 nm (SWIR)
	TM6:	10.40 - 12.50 μ m (TIR)

orbit altitude: 705 km

swath width: 170 km (170 km x 185 km standard image size)

pixel sizes (GIFOV): 30 m (VIS/NIR/SWIR)
120 m (TIR)

Landsat 7:

Spectral bands:	ETM1: 0.45 – 0.52 nm (VIS) ETM2: 0.52 - 0.60 nm (VIS) ETM3: 0.63 - 0.69 nm (VIS) ETM4: 0.76 - 0.90 nm (NIR) ETM5: 1.55 - 1.75 nm (SWIR) ETM6: 2.08 - 2.35 nm (SWIR) Band7: 10.40 - 12.50 μm (TIR) (2 TIR sensors, low/high gain)
orbit altitude:	705 km
swath width:	170 km (170 km x 185 km standard image size)
pixel sizes (GIFOV):	30 m (VIS/NIR/SWIR) 60 m (TIR) 15 m (Pan)

The data sets have been evaluated and interpreted for the Khorat project area as shown in Table 3.4:

Table 3.4: Satellite data used for mapping in the Khorat project area.

System	Data Acquisition Date	Path/Row	Comments
MOMS	03 May 1993	-	High quality, no cloud cover
Landsat TM	25 April 1994	128/049	Partly covered by dust
Landsat TM	06 March 1999	128/049	High quality, no cloud cover
Landsat TM	06 March 1999	128/050	High quality, no cloud cover
Landsat TM	06 March 1999	128/49/50 fl.	High quality, no cloud cover
Landsat 7	27 December 1999	128/049	good High quality, no cloud cover quality, no cloud cover
Landsat 7	27 December 1999	128/050	good quality, no cloud cover
Landsat 7	13 February 2000	128/049	High quality, no cloud cover
Landsat 7	13 February 2000	128/050	High quality, no cloud cover
Landsat 7	03 May 2000	128/049	Partly dusty, showing standing water
Landsat 7	03 May 2000	128/050	Partly dusty, showing standing water

All data was obtained from the officials providers was flight path oriented and corrected for radiometric and systematic errors.

3.3 Image processing

Image processing is applied to compensate data errors and geometric distortions, enhance and extract features related to thematic subjects being under investigation and to suppress redundant information. Standard tools of image processing have been used for digital processing of the satellite data. Digital image processing was applied to

- register the originally orbit oriented raster data over the UTM coordinates system
- enhance and to extract features that indicate targets of interest in the data.

In this study, the digital image processing is generally divided into two types as follow:

3.3.1 Image registration (geocoding)

Registration is the process of superimposing an over a map over another already registered data. The method of image registration or ‘geocoding’ can be divided into two types: ‘‘image-to-image-registration’’ and ‘‘image-to-map-registration’’.

Procedures and theoretical background are described by Gupta (1991), by Sabins (1997) and in the ‘‘ENVI 3.2. Users Guide’’ published in 1999. Selected image data of the Khorat area was rectified with reference to the 1:50,000 scale topographic maps (image-to-image-registration). Further imagery was geo-coded to this already registered satellite image using the image-to-image registration. The general concept and the procedures for the image registration as well as particular step are as follows:

(1) Image to map registration

The 1993 MOMS :mage was defined as the master image for the registration. It was registered using the image-to-map geocoding-techniques with reference to the Thai-Vietnam Datum, UTM, Zone 48, Thai/Vietnam datum (overlaps with zone 47 were extended to Zone 48 by definition). The topographical base was the official 1:50,000 scale topographic map series published by the Royal Thai survey Department of Thailand. The major steps of image registration are:

(2) The selection of the Ground Control Point (GCP)

The GCPs were collected from 1:50,000 topographic maps, 1969 editions for the Bua Yai / Khong area, and 1995 editions for the Phon / Khon Sawan area. GCPs are landmarks, which are uniquely located on the image and on the map. Best suitable landmarks for image registrations are cross-roads, bridges and railroad crossing. Because of the insufficient correspondence of the map road net, and the actually existing road net, it has been very difficult to cover the image with well-distributed and precise GCPs. However, the collection of the GCPs could be performed with the following RMS-Errors:

Landsat TM images: 0.723 pixel (30 m pixel size)

MOMS image: 0.917 pixel (13.5 m pixel size).

(3) The implementation of the registration and warping procedure

The warping procedure is the computing of affine projections that links the image and the map coordinate systems combined with an interpolation of the data (nearest, bilinear, cubic interpolation). For the warping procedure, the image processing software ENVI 3.4 was used to establish least squares polynomial equations to link the image coordinates (row/line-based) with the map coordinates.

Reference points are the GCPs. This process primarily performs a rotation of the scene with the respect to grid north (warping) in order to adjust the pixel-raster of the scene to the map grid.

Normally, registration is performed by changing the locations and the size of the origin pixels. Interpolation and resampling methods are applied to calculate the corresponding positions and the digital number values (DN) of the pixels in the output image. The commonly used methods of data interpolation and resampling are as follow:

- **Nearest neighbor method.** In this method, the point in the new grid simply acquires the digital number value of that point in the older grid that lies closest to it. The digital number value is not interpolated, but some of the old pixels are bodily shifted, leaving some pixels out.
- **Linear interpolation.** This method can be applied when interpolation in only one direction is required, either in scan direction or track direction. The values at new points in the grid are found by interpolating between the two neighboring values in one direction in the old grid.
- **Bilinear interpolation.** This is a two dimensional extension of the linear interpolation. It uses the surrounding four pixel values from the older grid. The procedure is first to interpolate along one direction, to obtain two intermediary digital number values, and then to interpolate in the second direction to obtain the final digital number value.

Polynomial warping of 1st degree has been applied to compute affined projections to link the image and the map coordinate systems. Bilinear interpolation has been applied to compute the digital number (DN) values in the warped image. Bilinair Interpolation uses the surrounding 4 pixels values from the older grid. As result of image registration, each pixel of the satellite image is assigned with pixel coordinate and a UTM coordinate as well.

3.3.2 Image Enhancements

Image enhancement is the modification of an image in order to alter its impact on the viewer. Generally, image enhancement change the original digital value, and it should be carried out after geo-coding. The purpose of image enhancement is to make the images more interpretable for specific applications. The general aim of image enhancement is to highlight features of thematic interest (lineament, rock and soil properties etc.,) and to suppress redundant information. Image enhancement can be divided into two groups:

Single Image Enhancement:

- Contrast Stretching
- Color-Coding
- Filtering:
 - Directional filtering
 - High pass/Edge Enhancement
 - Image Smoothing
 - RGB Color Coding

Multiple Image Enhancement:

- Addition and Subtraction
- Ratioing
- NDVI (NIR-R)/(NIR+R)
- Principal Component Transformation
- RGB-transformation
- Classification (Unsupervised, supervised)

Major tools applied for the enhancement of the Khorat Basin satellite data were contrast stretching, edge enhancement and RGB-Coding. The technical background and the general goals of selected image enhancement techniques are explained in the following section.

(1) Edge enhancement

The edge enhancement is an image processing technique that emphasizes the appearance of edges and lines in the image. Edge enhancement is achieved by spatial filtering or convolution using a box filter (Kernel). General goal of edge enhancement is to increase the brightness difference between each pixel and its immediate neighbors. In this way, “edges”, i.e. abrupt changes in brightness within the image, such as lines or boundaries, appears emphasized and the overall image appears sharper. Edge enhancement is a useful tool for structural geological mapping, e.g. lineament detection and interpretation.

(2) Contrast enhancement

The contrast enhancement is an image processing techniques that improves the contrast ratio of the image. The original narrow range of the digital values is also called contrast stretching (Sabins, 1997). The most frequently used contrast stretching type is the linear expansion of the digital value range. Depending on the distribution of the digital values in the input image, and depending on the interpretation targets, selected portions of the data can be expanded (e.g. piecewise linear). Apart from standard linear stretching, Gaussian, equalization, arbitrary, special user defined approaches or others can be applied. The distribution of the digital values of the image before and after linear stretching is defined by the histogram (Fig. 3.6).

(3) RGB-Color composite images

A color composite image is an image which was prepared by combining three undivided images with the colors Red, Green and Blue. It is one of the most simple ways to enhance features interest by digital image processing according the following steps:

- (3.1) Selection of the 3 single spectral bands, which show the highest differences in the locations of the clusters characterizing the investigation targets (Gupta, 1991),

- (3.2) Mixing of any the 3 primary additive colors **Red, Green** and **Blue** in various proportions defined by the grayscale values of the pixels of the 3 selected single bands of an n-dimensional multispectral data set.

The resulting colors of the color composite image are defined by **RGB Color Diagram** (Gupta, 1991). RGB-Transformation is one of the most frequently used techniques in image processing. It is mostly combined with contrast stretching applied to any of the three selected bands.

CHAPTER IV

LINEAMENT ANALYSIS

4.1 Lineament terminology and application

Lineament is any extensive linear surface on a planet, as a fault line or fracture line, that indicates the nature of the underlying crust. The term “lineament” is one of the most commonly used terms in geology. Hobbs (1904) first used the term lineament to define a “significant line of landscape which reveal the hidden architecture of rock basement”. Gupta (1991) summarized the application of lineament in different geological features, such as (1) shear zones/faults; (2) rift valleys; (3) truncation of outcrops; (4) fold axial traces; (5) joint and fracture traces; (6) topographic, vegetation, soil tonal changes alignment etc. It may then be reserved for cases where the origin is uncertain or compound. Lineaments are commonly interpreted as surface expressions of rock fractures which may provide pathways for upward from subsurface.

The term lineament has been used for a wide variety of geological features, over the wide range of scales. The study deals with the statistical analysis of linear features observed on the satellite images and investigates statistical changes of variable quantitative factors. These factors are length of individual lineament, their bearing, lineament density per unit area (lineament intersection incidence). The characterization of fracture surfaces is field of investigation that provides understanding about the relationship of geometry and macrostructure to the mechanical behavior of bedrock.

Photolineaments generally represent the surface traces of fractures in bedrock, projected more or less vertically upwards to the erosion surface by various mechanism (Bakliwal, 1978). Haman (1961) has separated lineament into two types, micro and macro lineaments. The microlineaments range in length from 0.1 km to 2.5 km and macrolineament are larger than 2.5 km. The techniques for obtaining lineaments from satellite image were investigated. It was based on the assumption that nearly all tectonic lineaments mapped on synoptic scale images are related to topographic features. The expressions of these lineaments are topographic relief, vegetation, land-use, soil salinity etc.

The genesis of the fractures is widely discussed by several authors. The origin of fractures is a synthesis of internal and external stress and occurrence of systematic fracturing is an apparently worldwide phenomenon (Bakliwal, 1978). Many studies have demonstrated the impact of faults, fractures and joints which are represented in photolineaments.

Fernandes and Rudolph (2000) studied the relationship between fracture lineament and groundwater-production capacity in Brazil. He proposed that the

lineament features in the study area indicate the orientation of the primary stress fields and fracture structures associated with the recent tectonic history that affected the region of the study. Teeuw (1995) used lineament interpretation incorporated with geographical information system to groundwater exploration in the United Kingdom. Janardhana and Reddy (1997) reported the research entitled “fracture pattern and electrical resistivity studies for groundwater exploration”. They studied the influence of structures such as fractures and faults in hard-rock area related to subsurface lithology. They established the relationship between electrical resistivity with fracture pattern, geological and hydrogeomorphological features.

In this study, the lineament data have been analyzed in satellite imagery in accompany with lineament density, lineament intersection density and rose diagram analysis.

4.2 Previous work in the Khorat Plateau

Jantaranipa and others (1981) reported on the “Application of Enhanced Landsat imagery to Mineral Resources of Loei Province, Northeastern Thailand”. They studied the mineral resources by lineament interpretation using enhanced technique. They interpreted the relationship of major and minor lineaments, lineament density contours, lineaments intersection density contours with indicated mineral zones.

Supajanya (1981) reported in his investigation of the collapsed-sinkhole as a promising source for shallow groundwater in the rural areas in Northeastern Thailand. His study indicated that the collapsed-sinkhole distributions were found in association with joint patterns within the region.

Archwichai (1991) published fracture density maps for groundwater development in Khon Kaen province, Northeastern Thailand. He attempted to apply fracture density maps as a guide for groundwater bore-hole location in fracture aquifers but no report on saline water in fracture density map. The mapping of fracture traces was achieved by aerial photographs and satellite image interpretation incorporating the analysis of corresponding topographic maps of the scale 1:50,000 and 1:250,000. The following conclusions were summarized (Fig. 4.1).

- (1) The regions with the higher fracture density are the more likely the regions to contain reliable quantity of groundwater.
- (2) The producing of the fracture density map of an interested area can be readily achieved providing that the accurate inferred fracture traces are available.
- (3) Considering regional groundwater exploration and development planning, the fracture density map shows high practical potential.

Chuaviroj (1997) studied the deformation in the Khorat Plateau by Landsat TM satellite images and aerial photograph interpretation. He recognized 3 episodes of deformation in Mesozoic rocks as follows (Fig. 4.2).

(1) Late Cretaceous

The first deformation (F1): The fold axes resulted from the first deformation are in the north-south direction. They indicate the compression resulted from the collision between the Shan-Thai and the Indochina plates. These phenomena can be observed at Phu Luang's trend in Loei province and Phu Wiang in Khon Kaen province.

(2) Lower Tertiary

The second deformation (F2): The Himalayan orogeny is the result of the collision between the Indian plate and the China plates. Consequently, the Phu Phan range was formed as a result of this deformation. It shows the northwest-southeast direction, which was affected, from the northeast-southwest compression.

(3) Miocene-Pleistocene

The third deformation (F3): The prolongation of the Himalayan orogeny probably induced the updoming in the third stage of deformation. The direction of interpreted compression movement is in the northwest-southeast. The fold axes are nearly parallel to the Kumpawapee syncline.

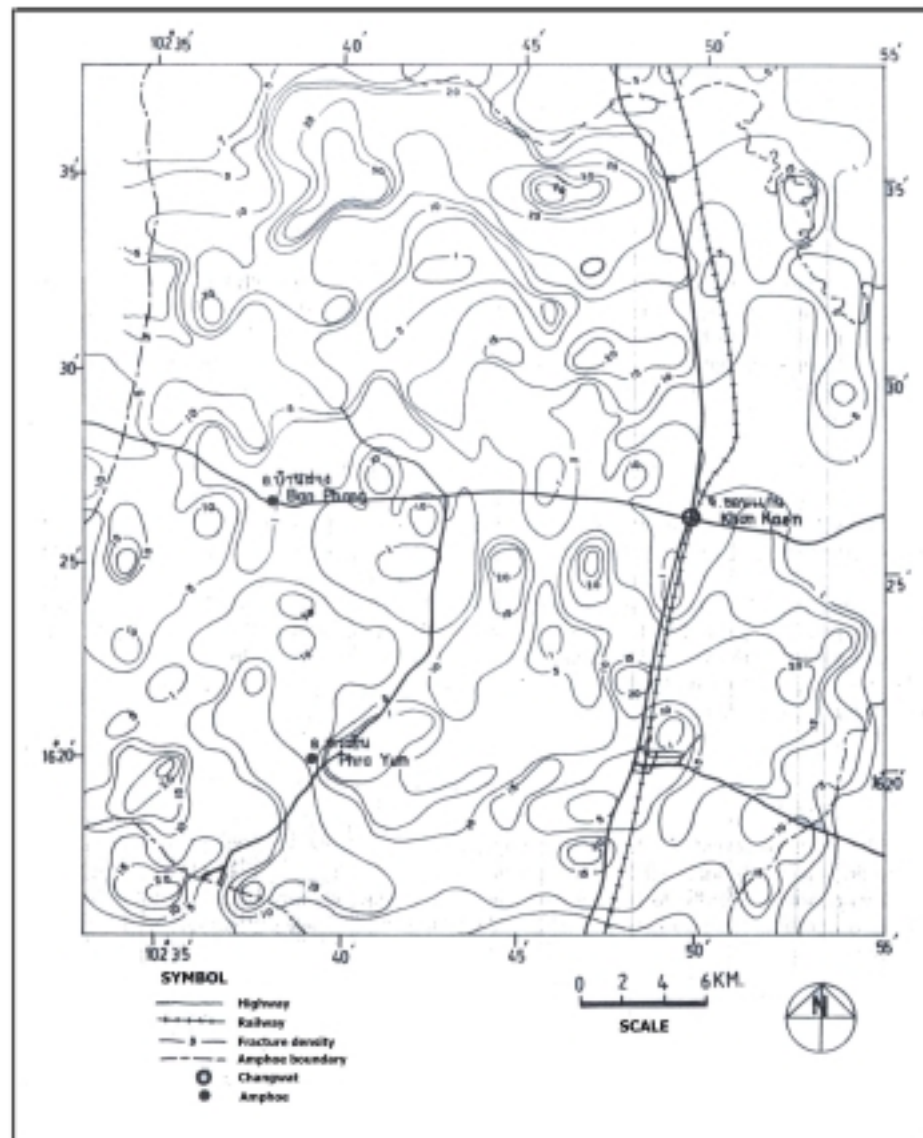


Figure 4.1 Contoured fracture density map of Amphoe Muang, Khon Kaen Province. Contoured at 5 mm interval cumulative fracture trace length per 10 mm diameter inventory circle (After Archwichai, 1991).

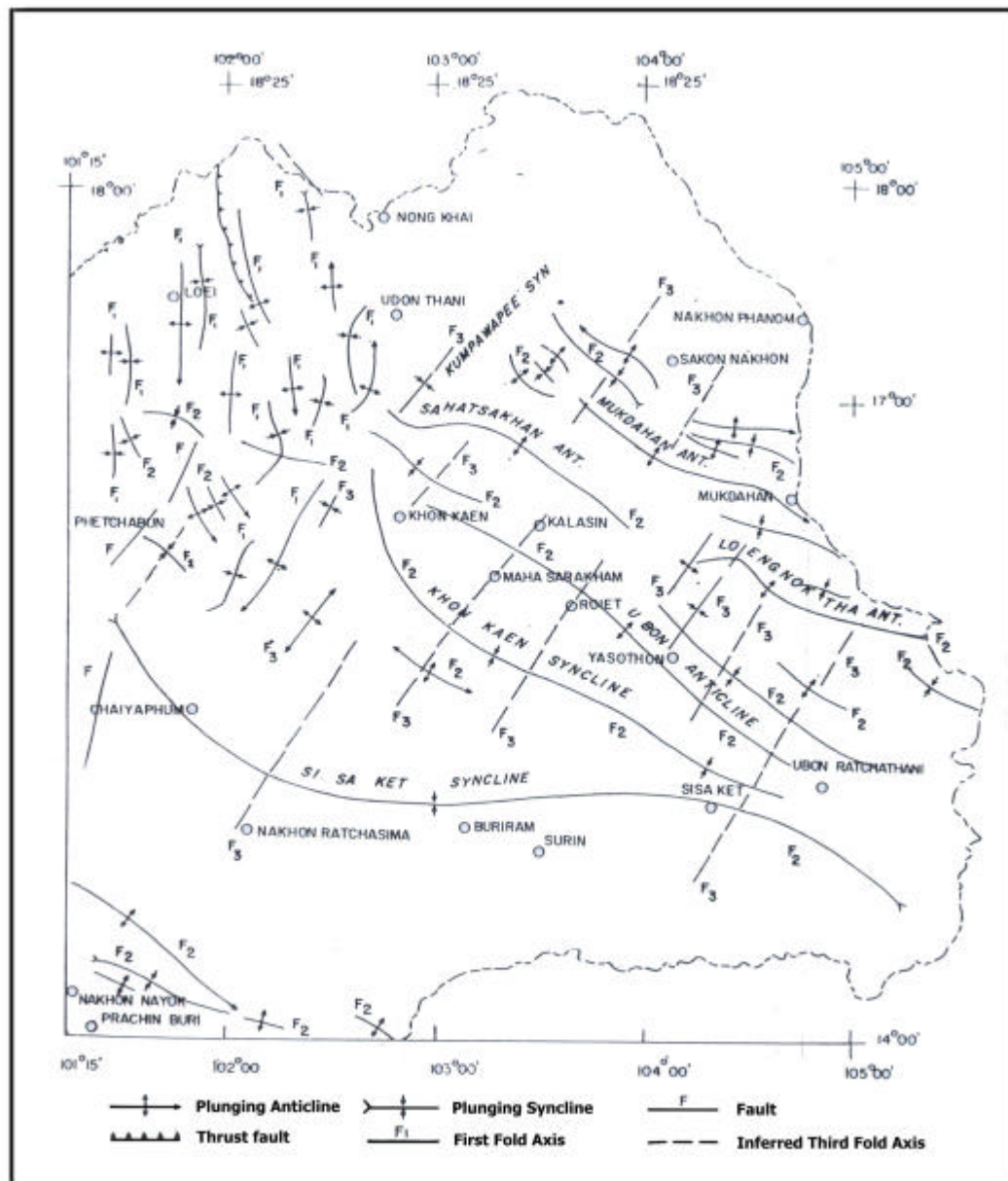


Figure 4.2 Deformation in Korat Plateau interpreted from the Landsat 5 (After Chuaviroj, 1997).

4.3 Methodology

4.3.1 Lineament information and data source collection

The principal data sets used for this analysis is MOMS satellite image with more resolution than Landsat TM image. The data was recorded in May 3, 1993 and recorded in digital format on CD-ROM. The data was loaded and processed on the workstation using ENVI 3.2 image processing software. The band selection in False Color Composites is 4-2-1 in red-green-blue (RGB) order. The lineaments have been analyzed by enhancing and stretching technique. The traces of lineaments were then visually recognized and drawn on transparencies overlaying the plotted images. After revisions and spot-checking in the field, the lineament map was digitized in Figure 4.3.

4.3.2 Classification of lineaments characteristic on image

There are many instances in geology of linear features, at a variety of scales and occurrence. Normally, they consist predominantly of joint, fracture, bedding, linear sand dunes, fault and fold. In Northeastern Thailand, on terrace and basin area lineaments are referred in long narrow area, which is high reflection by dry weathered soil along its trends. The weathering process of rocks is easy to start along lineament trends, especially in non-competent sediment (shale, clay, sandy clay or rock that clay is predominant) interbedded with competent rock (sandstone).

From satellite images, the combination process such as capillary phenomena, water run off, salt solution etc., produces salt contamination and dissolution feature near or at surface. When saline moisture contaminates near or at surface, the reflection from saline moisture was detected by satellite sensor. One kind of lineament feature in this study should be called “**salt lineament trace**”. Most of the detected sites were located on younger sediment of Tertiary age.

(1) Fracture and joint

Fracture and joint are occurring in a wide variety of rock types and tectonic environments. Hokjareon (1986), Archvichai (1991) and Chuaviroj (1997) believed that fractures and joints in this area were associated with regional folding and salt tectonic. The regional folding form anticline and syncline produced propagated fracture and joint within salt and overburden structure. Its forming was due to compression and tension. In fold stratum radial fracture was formed by tension and extension mechanism (Warren, 1999). Axial plane cleavage (fracture and joint) was developed from folding. On image, fracture and joint are short distance (minor lineament upto 3 km) and crossing prominent lineament in the western part.

(2) Rock Formation contact

One type of lineament is the contact between Khok Kruat Formation and Maha Sarakham Formation. Especially formation bearing rock salt and formation without rock salt will show prominent boundary due to its differential weathering level. Normally, the formation bearing rock salt is less resistant than the overlying Phu Tok Formation, which consists of siltstone, claystone and sandstone. Therefore the area occupied by formation bearing salt comprises low land. Some parts of this

will develop stream which is parallel with more elevated land of Phu Tok Formation. The lineament of rock boundary contact is found in Waeng Yai and Waeng Noi area.

Fracture maps are the best way to display the location of faults and fractures including major and minor joint set zones. The lineament length has been taken into account for grouping them into four classes based on the basis of their statistical distribution as follow:

- (1) **Lineament of first order:** for those longer than 6 km.
- (2) **Lineament of second order:** for lineaments having length between 3 km to 6 km long.
- (3) **Lineament of third order:** for lineaments less than 3 km long.
- (4) **Lineament of rock formations boundaries.**

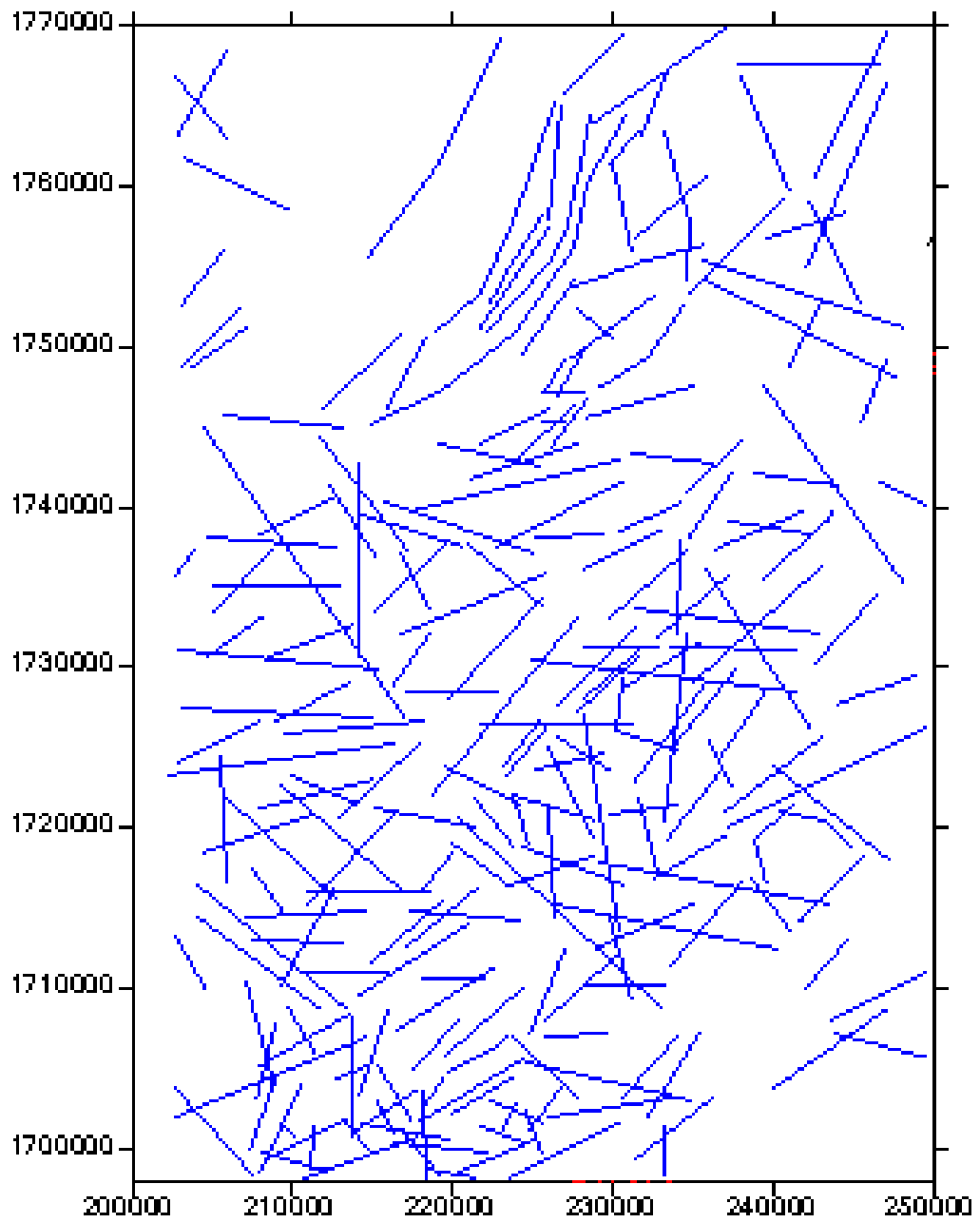


Figure 4.3 Lineament map interpreted from MOMS imagery over part of Khong, Bua Yai, Kaeng Sanam Nang, Khon Sawan, Waeng Noi and Phon Districts.

4.4 Lineament density map

Both density and orientation of lineament are important factors for delineation of the high permeability and unstable zone (Prost, 1994). In this part of the paper, fracture attributes are derived which are able to characterize the observed fracture system. The characteristics are including density, orientation, intersection, length and connectivity. The fundamental geometry of fracture and joint in geological structure are shown in Figure 4.4.

The lineament density map was derived from lineament base map as mentioned above. The “SURFER” software is used for the contour plotting. The density map could be prepared by two methods. The method employed in this study is called the “length frequency method”. This method is contouring the length of lineaments per unit area. The length of all lineaments within the grid square was then counted and the sum was plotted at the center of grid cell, until it covered all of the map. Then the sum of every four point adjacent cells was again plotted at the center of the larger cell (4 square kilometers or 2 by 2 km grid cell). Next, the values number in the UTM position was fixed and the density values including the true position were input to SURFER program. The program computed the density values and drew the contour. These values were used to define the contour intervals of the lineament density contour maps of all directions.

Figure 4.5 shows the saline map in the study area (Khundee, 2001). Figures 4.6 and 4.8 shows the lineament density map of the study area derived by the length frequency method and comparison between total dissolution solid and chloride content in the study area.

4.5 Lineament intersection density map

Based on the assumption that areas with high intersections of lineaments will be the areas of high intensity fractures and has the tendency to form unstable ground (Prost, 1994). It can be assumed that the area of high intersection density also is characterized by high permeability and high tendency for salinity.

The preparation of lineament intersection density map is also similar to those of the density map. The method is contouring the lineament intersection point per unit area (4 km²). This method is more convenient than the length frequency method. The procedure is counting the number of lineament intersection per unit area (4 square kilometers or 2 by 2 km grid cell) and the intersection values are contoured. The intersection contour values can be separated into 3 types as follow; high (more than 5 intersection per unit area), moderate (between 3-5 intersection per unit area), and low (less than 3 intersection per unit area). Figures 4.7 and 4.9 shows the fracture intersection density map of the study area and comparison between map, total dissolution solid and chloride content in the study area.

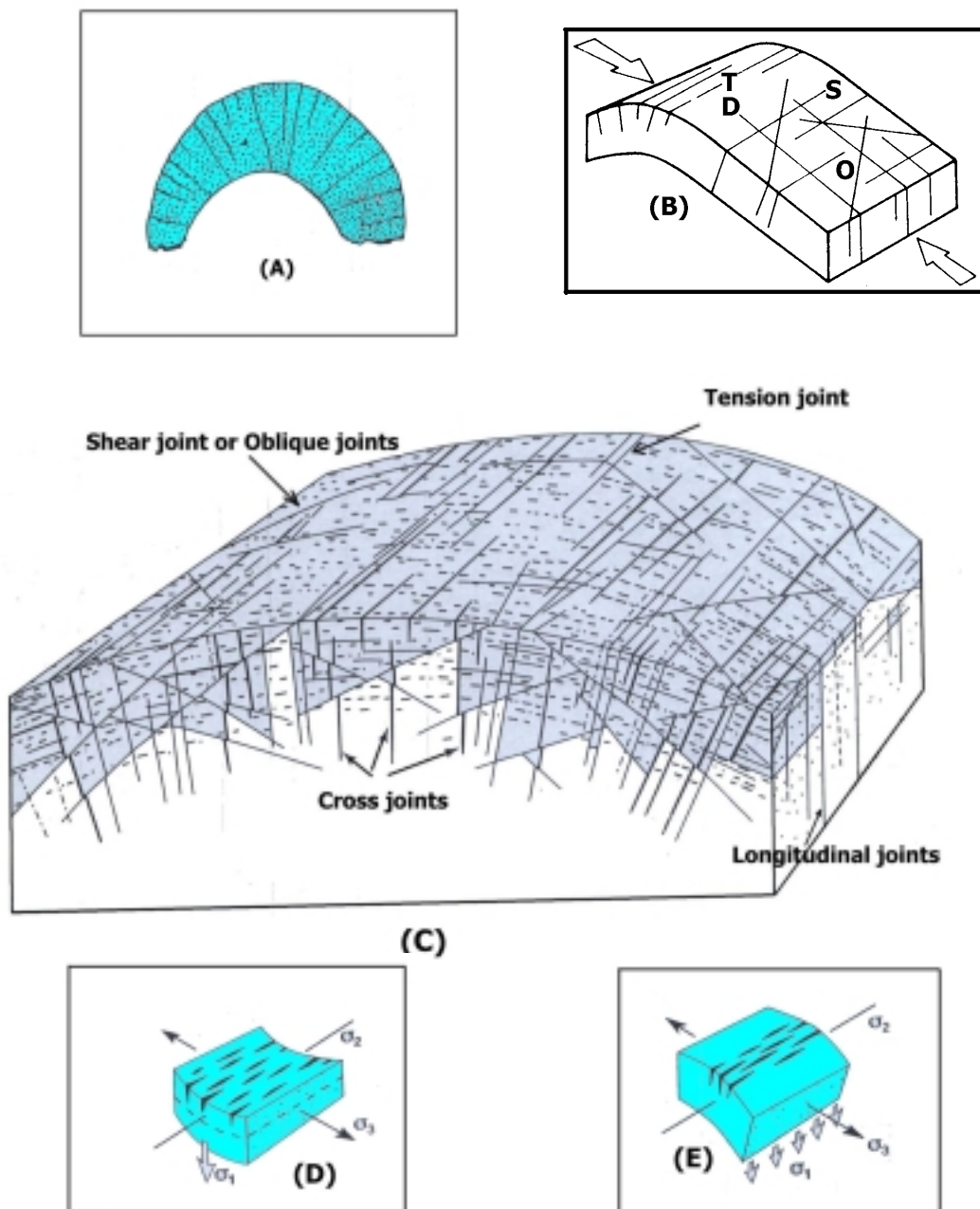


Figure 4.4 The joint geometry model. (A) Radial fractures due to tension in sharply folded stratum (After Archwichei, 1991). (B) Jointing in a folded stratum; T= tension joint, S = strike joints, D = dip joints, O = shear joint (After Blyth, 1990). (C) Joint structures developed in a large pluton (After Hatcher, 1995). (D) and (E) Joint in subsidence basin due to vertical maximum principle stress (After Hatcher, 1995).

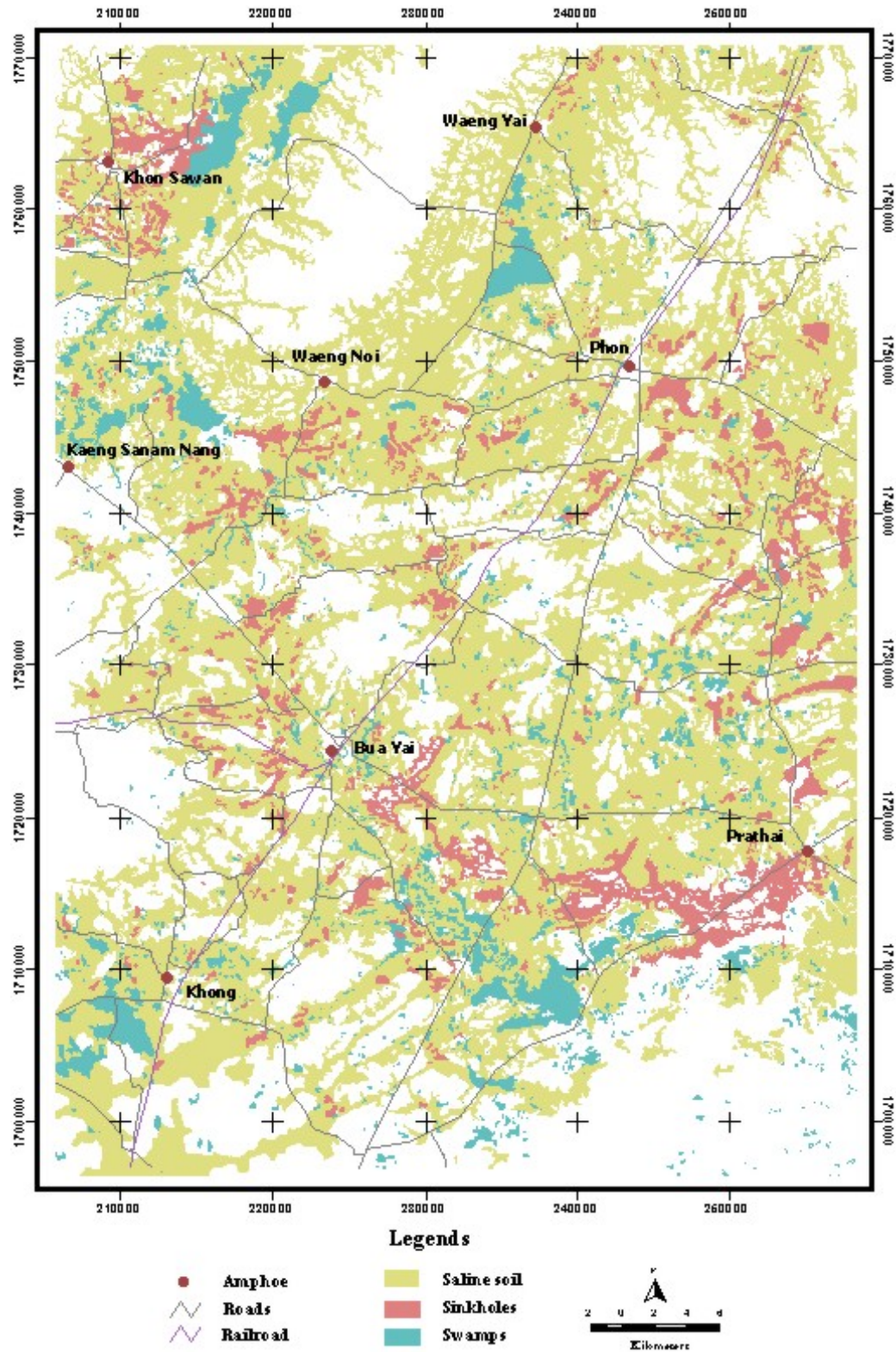
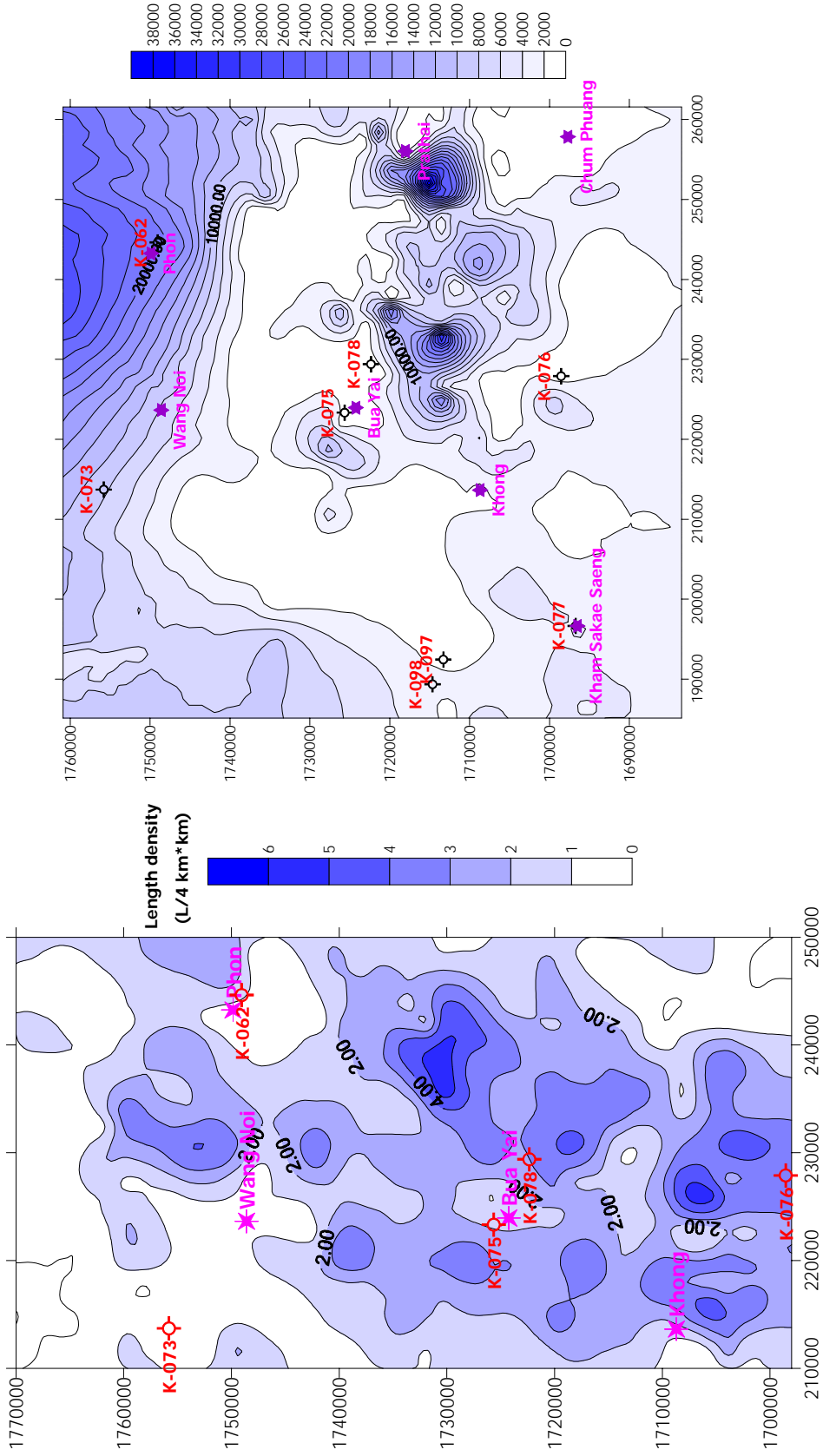
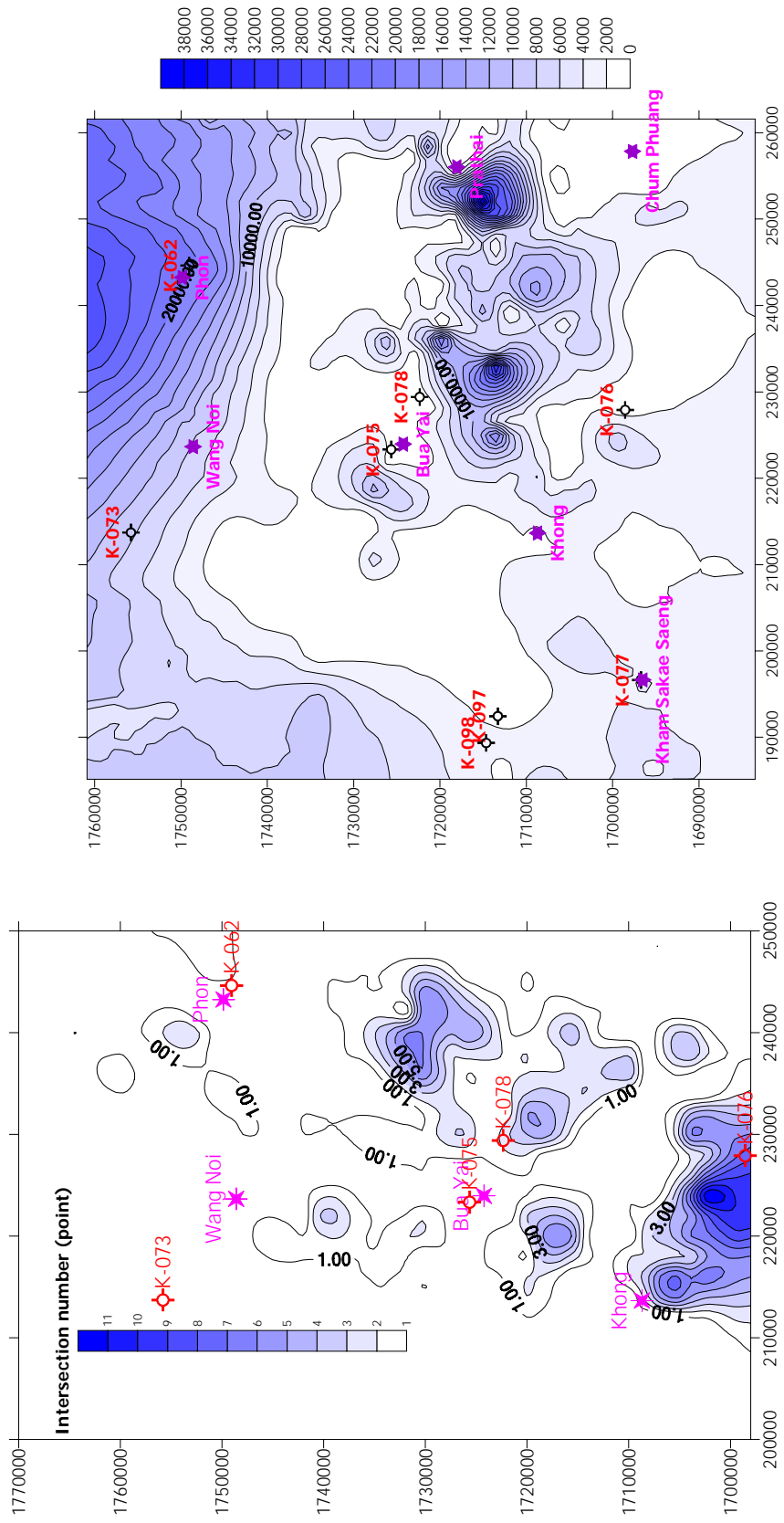
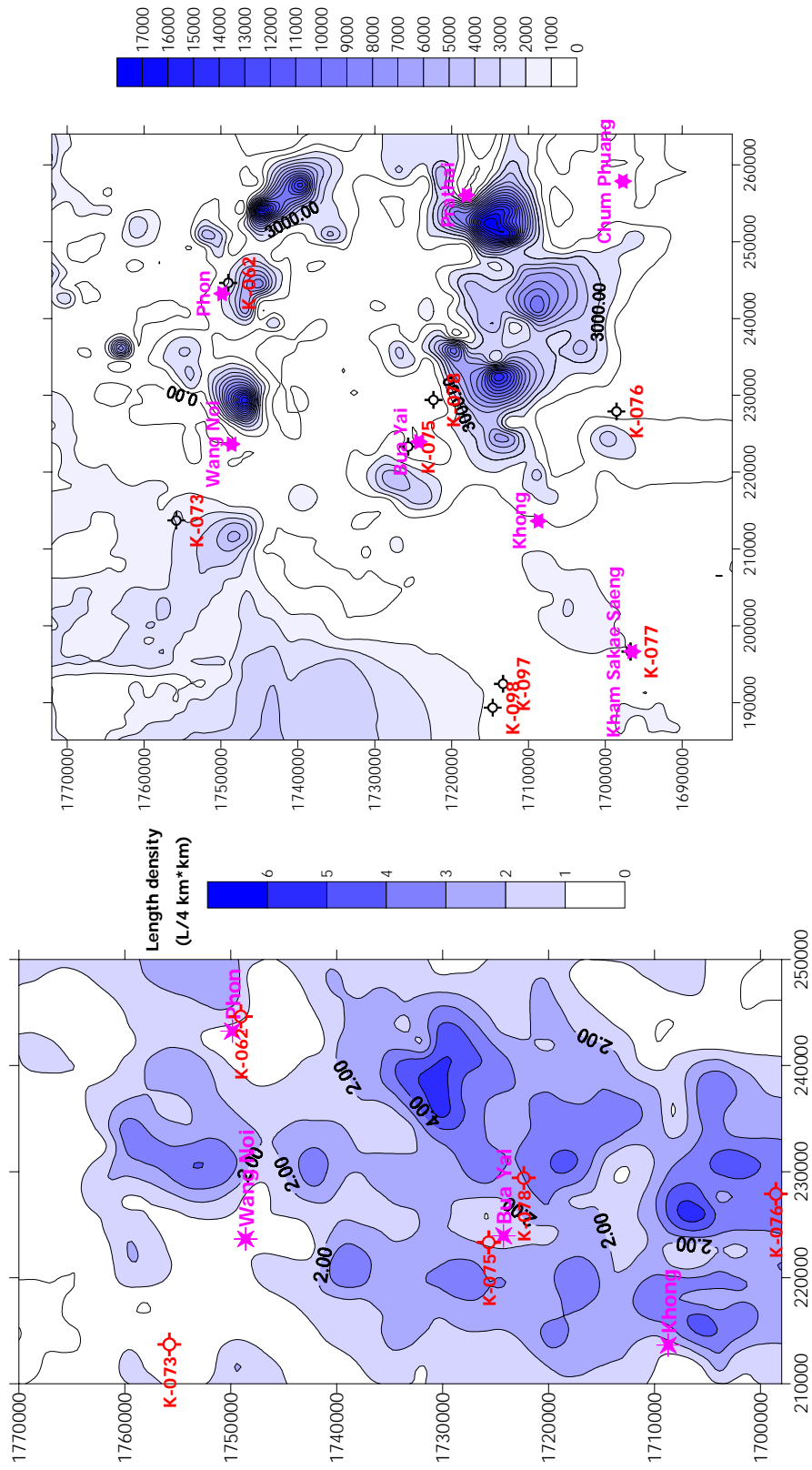
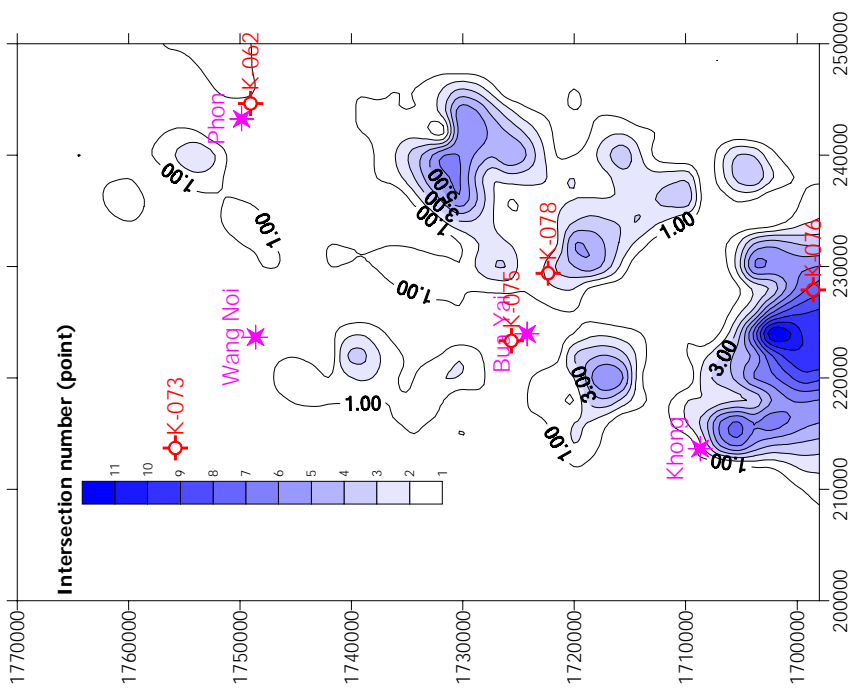
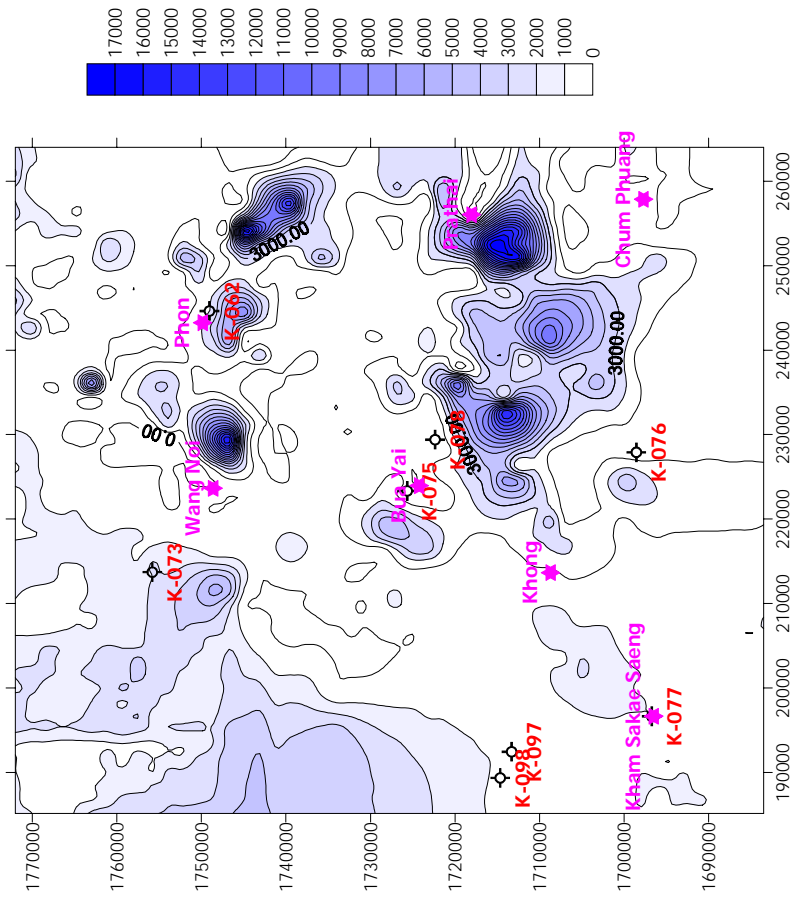


Figure 4.5 Saline Soil, Sinkholes, Swamps, Major Settlements, Road net and Rail Roads (After Khundee, 2001)









4.6 Lineament evaluation and deformation interpretation

The most reliable information obtained from linear fracture map is orientation data. Although, fracture orientation does not show dip direction but strike direction is important data for analyses. Rose diagram is a convenient way to display the orientation of major and minor fractures sets. The usual technique is to count the number of interpreted fractures in a given azimuth range. The total number of lineament observed is more than 240 lines on the MOMS image. The frequencies of the identified elements are graphically presented in rose diagrams in which the azimuth field has been divided into thirty six classes sectors with 10° each. The rose diagram was set up into 29 types. One is the total lineament in Figure 4.10 and the others are presented in 28 sheets with ten by ten kilometer grid cell shown in Figure 4.11. The prominent trend is divided into 3 part the upper, the middle and the lower as shown in Figure 4.12. Rose diagram interpretation can be summarized as follow:

Joint set number 1: This prominent set is trending in $N30^\circ-50^\circ E$ and is classified as first order lineament. It is located in the northern part of study areas between Waeng Noi and Chonabot anticlines and represents the boundary of the Khok Kruat Formation and the Maha Sarakham Formation. In the middle and the lower parts, this set exhibits second and third orders lineaments perpendicular to joint set number 2.

Joint set number 2: This prominent set is trending in $N35^\circ-60^\circ W$ and is belonged to first, second and third order lineaments. It represents the middle and the lower parts of the area. The Phu Phan up-lift axis is corresponding with this direction.

Joint set number 3: This prominent set is trending in $N10^\circ-25^\circ E$ and is belonged to second and third order lineaments. It represents predominantly the middle part. Fracture and joint are observed in this set forming dense network in the middle and the lower part.

Joint set number 4: This set is close to joint set number 1 trending $N65^\circ-75^\circ E$ and is belonged to first and second order lineaments. The Moon River is corresponding with this direction.

According to geological map by DMR (1999) and previous works by Thanosap (1992) and Chuaviroj (1997), the characteristic structure on the Khorat Plateau is closely related to folding with axes perpendicular to each other. The structural development in the study area can be divided into 2 stages.

(1) Lower Tertiary

The interpreted major lineaments from rose diagram (Figure 4.10) indicate a NW-SE trend. The major lineament in this trend was observed in the western part. These lineaments are long and prominent and are crossed by minor lineaments. The trend is corresponding to the Phu Phan up-lift axis. From tectonic history in the region, this trend was affected from the Himalayan orogeny in Early Tertiary time. The trend is also coincident with the Khon Kaen and the Si Sa Ket synclines

(Chuaviroj, 1997). The horizontal compressive stress of NE-SW direction was responsible for the fracture-tension deformation at that time.

(2) Miocene to Pleistocene

From MOMS image, these rocks are found in the middle and the lower parts of the area and are underlined by Maha Sarakham and Phu Tok Formations. Rose diagram analysis indicates is that the majority of lineament trends NE-SW. Based on Chuaviroj (1997) and Figure 4.10 the prominent lineament in this age corresponds to the third stage of deformation in the region. The major anomalies of lineament density and intersection density map indicate a regional compressive stress in NW-SE direction. The Waeng Noi anticline was affected by this stress regime. The interpreted salt asymmetrical folding structures are inferred to correspond with this direction. The minor lineaments close to the middle and the lower parts, trending N75°- 90°E or E-W are corresponding to the joint set number 4. They are short in length and belong to second and third order lineaments. This set is interpreted as shear or oblique joint occurred after forming of salt anticline structures.

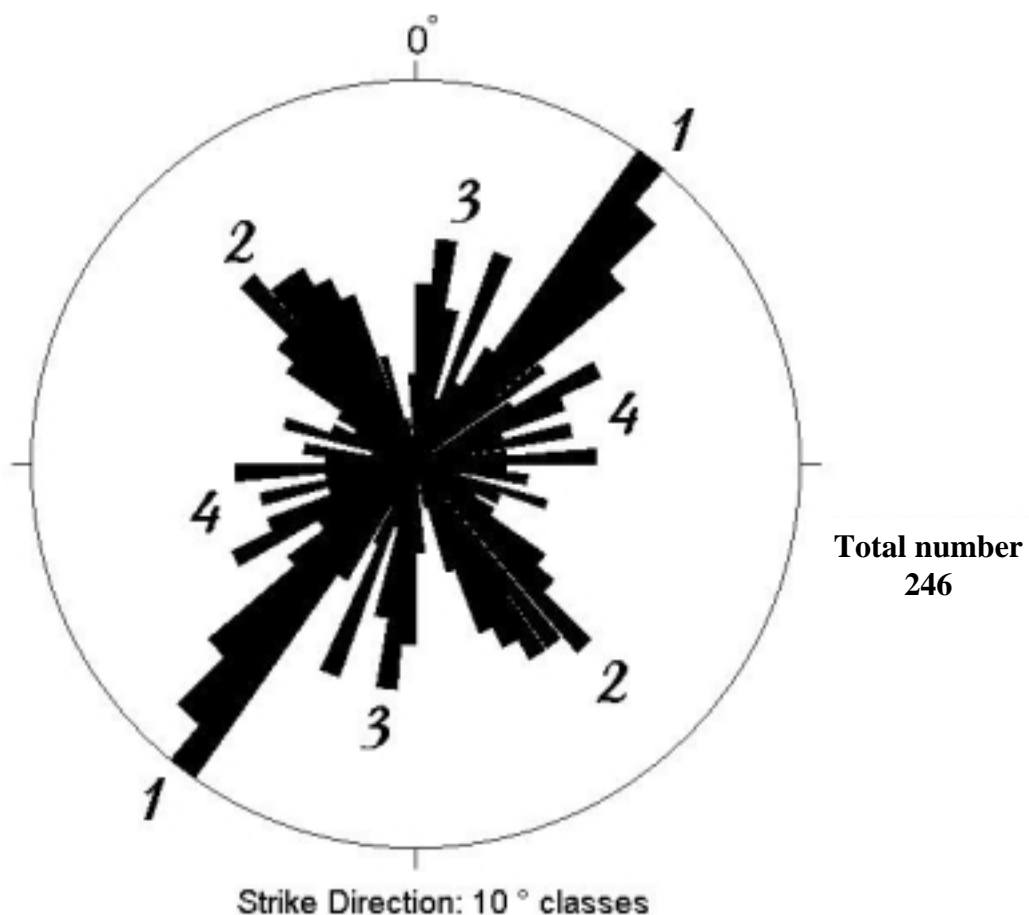


Figure 4.10 Rose diagram of all lineament with 36 classes of 10 degree each. The numbers are prominent major joint set.

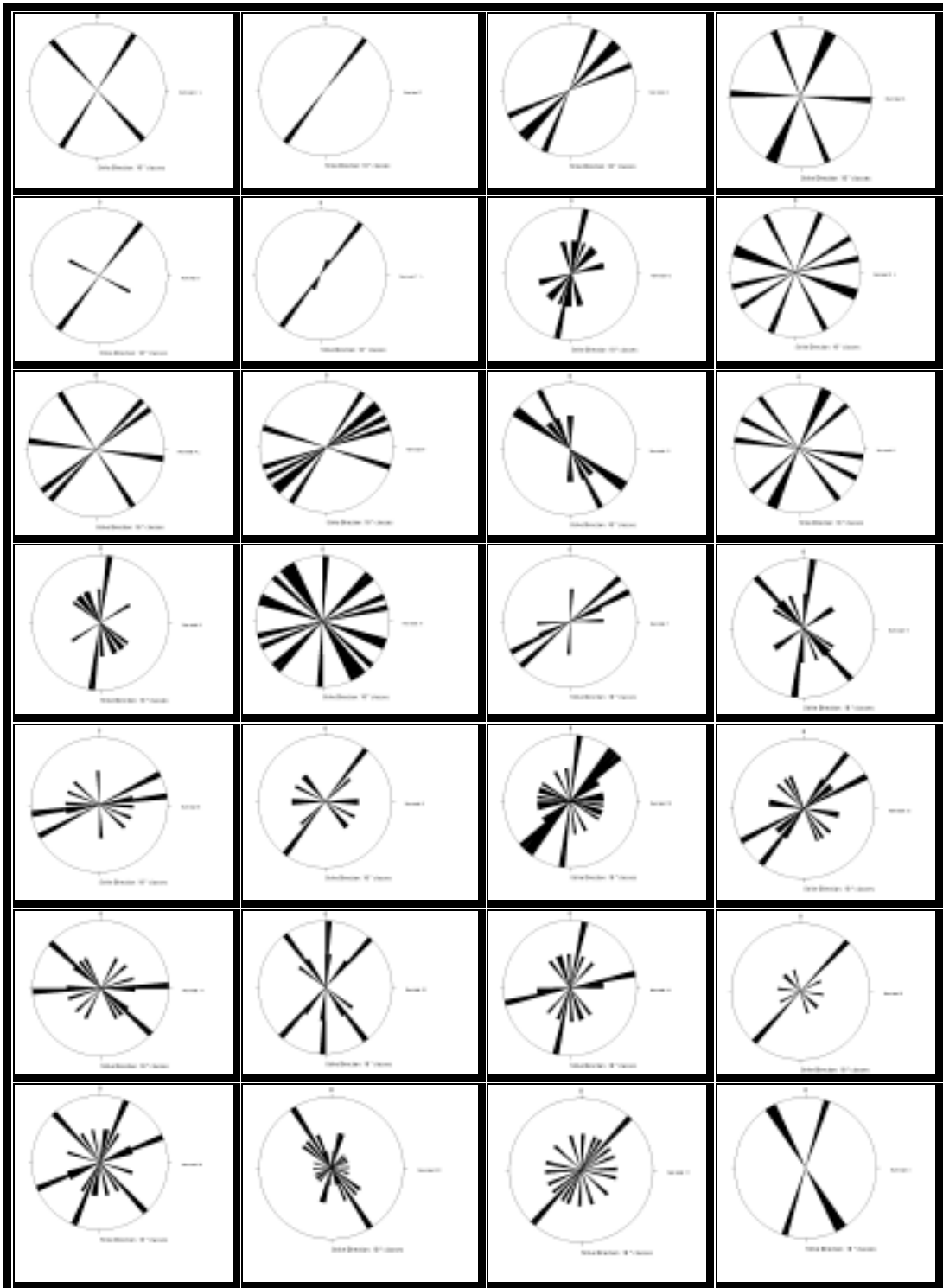


Figure 4.11 Rose diagram shows strike direction of 28 square grid sheets with 10 km² in each sheet.

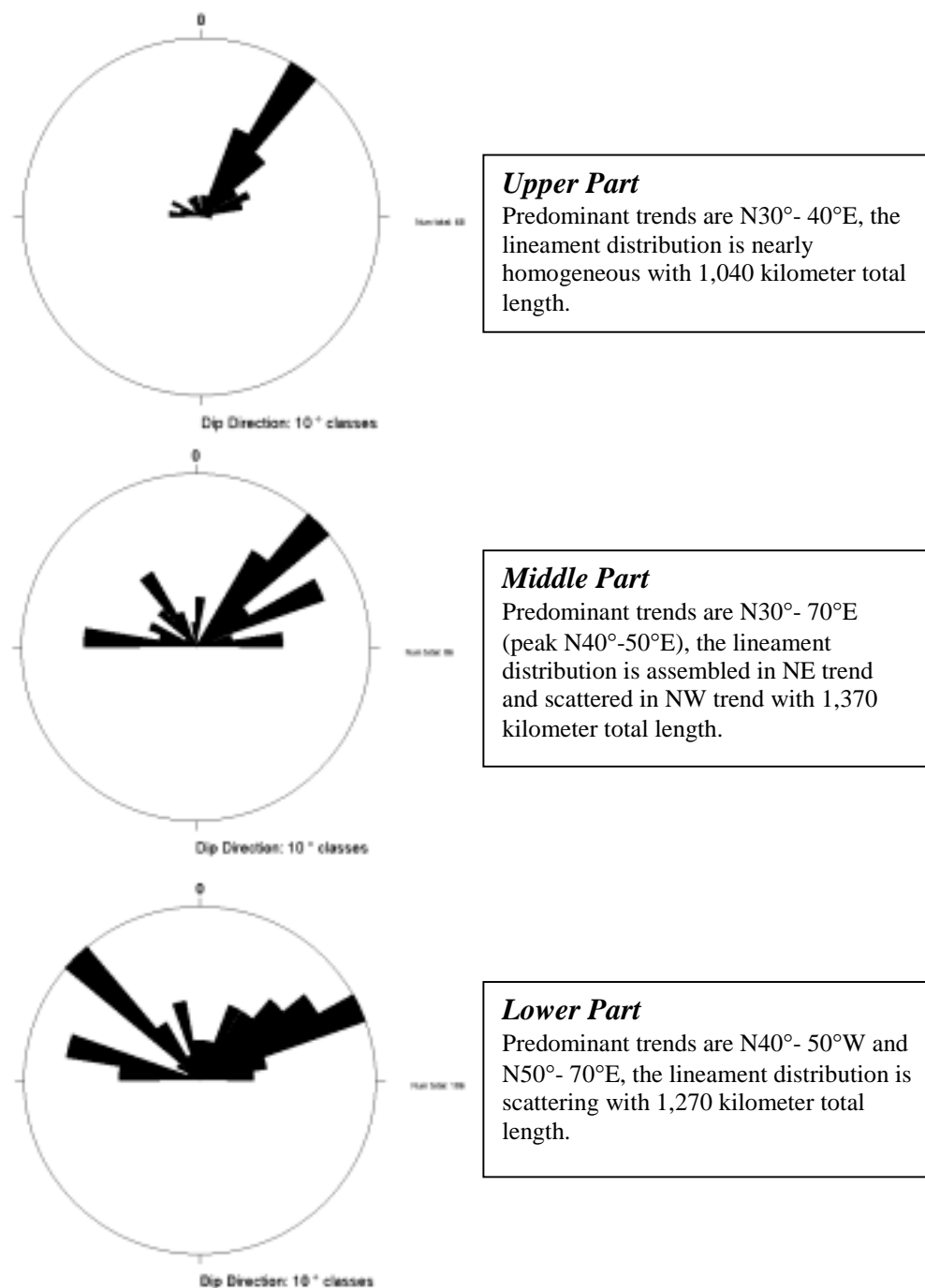


Figure 4.12 Predominant trends of lineament of the 3 domains (upper, middle and lower) of the study area.

CHAPTER V

FIELD CHECKING

The important aspect in the study strategies is field checking. The image interpretation should be checked in the field. This process is to clarify the relationships and correlate the geological, topographic features, surface water, groundwater quality with image interpretation. The groundwater and surface water were collected in geophysical survey area. The feature indicating subsidence and soil salinity area were recognized and classified.

5.1 Geology of study area

The study area is underlain by the sedimentary sequences known as the Khorat Group and the overlying sediments. The sediments overlying the Khorat Group is composed of Cretaceous and Tertiary sedimentary rock and is subdivided into the unconsolidated unit, Phu Tok and Maha Sarakham Formations respectively in descending order. The unconsolidated unit consists of Pleistocene to Quaternary alluvium sediment (Wongsomsak, 1986). From potash exploration bore-holes number K-023, K-032, K-019, K-082, K-100, K-098, K-094, K-096, K-097, K-080 and K-076 which are located close to the geophysical survey area, the unconsolidated unit comprises claystone interbedded with calcareous claystone/mudstone, sandstone and siltstone in general. Wongsomsak (1986) concluded that the unconsolidated unit is composed mainly of very fine-grained clastic sediments, i.e., semi-consolidated clay to claystone/mudstone. From field investigation, the outcrops along the survey line are represented by the very fine-grained sand, reddish brown calcareous siltstone and yellowish to reddish brown medium-grained sandstone respectively in descending order.

5.2 Groundwater and surface water analysis

This process is to clarify the relationships and correlate the groundwater and surface water quality with image interpretation. The samples were collected in geophysical survey area. The electrical conductivity (EC) was tested in the field. The total dissolved solids (TDS), iron content and chloride content were analyzed in the laboratory. The sample locations were plotted in Figure 5.1. The results of chemical analysis are as follow:

5.2.1 Electrical conductivity (EC)

Electrical conductivity (EC) is the standard measurement of the conductivity of materials. It therefore provides an indicator of the level of dissolved salts in a water and soil sample. It is commonly expressed in units of millisiemens per meter (mS/m) and corrected to a temperature of 25°C. The measurements may also be reported in units of decisiemens per meter (dS/m). The factor affecting soil electrical conductivity consists of pore-continuity, water content, cations exchange capacity,

depth, temperature and salinity. The classes of water and soil salinity based on electrical conductivity are tabulated in Table 5.1.

5.2.2 Total dissolved solids (TDS)

Total dissolved solids (TDS) is the sum of all solids dissolved in the water. They refer to any mineral, salts, metal, cations or anions dissolved in water. This includes anything present in water other than the pure water (H_2O) molecule and suspended solids. The natural sources of dissolved solids are rocks, bedrocks, and soils. As water comes in contact with them, minerals will dissolve to some degree. Geologic settings that include limestone (calcium carbonate) and halite (salt, sodium chloride), which readily dissolve in water, generally have waters with high TDS values. Based on Freeze and Cherry (1979), the salinity classification with total dissolved solids is tabulated in Table 5.2.

5.2.3 Chloride content

Chloride toxicity is taken into account with salinity evaluation as chloride sensitive plants are all in the low salt tolerance range. Irrigation water high in chloride may cause foliage burn, especially on salt sensitive plants, starting at the leaf tip and progressing back along the leaf margins or edges. A condition that may be aggravated by hot dry weather. The chloride ion can be toxic to plants with a low salt tolerance when taken up by their roots and absorbed through their leaves. The water quality as chloride contents is classified into three group, fresh water, brackish water and salty water as tabulated in Table 5.3.

5.2.4 Iron content

Iron is the fourth most abundant element, by weight, in the earth's crust. Natural waters contain variable amounts of iron depending on the geological area and other chemical components of the waterway. Dissolved iron in water is present in the ferrous state. Except at low pH values, ferrous iron is readily oxidized to ferric iron, an insoluble reddish brown precipitate on exposure to air and sunlight. The ferrous form Fe^{++} can persist in water void of dissolved oxygen and usually originates from groundwater or mines that are pumped or drained. Iron in domestic water supply systems stains laundry and porcelain. It appears to be more of a nuisance than a potential health hazard. Taste thresholds of iron in water are 0.1 mg/L for ferrous iron and 0.2 mg/L ferric iron, giving a bitter or an astringent taste. Water to be used in industrial processes should contain less than 0.2 mg/L iron.

The results of groundwater and surface water analysis in geophysical survey area are shown in Table 5.4 and 5.5.

Table 5.1 Soil salinity classes on the basis Electrical Conductivity (Baize, 1988).

Class	Description	EC at 25°C (mmho/cm)
0	Non-saline	<2.5
1	Slightly saline	2.5-5
2	Moderately saline	5-10
3	Saline	10-15
4	Strongly saline	15-20
5	Very strongly saline	20-27.5
6	Excessively saline	27.5-40
7	Hypersaline	>40

Table 5.2 Groundwater salinity classification based on Total Dissolved Solids (Freeze and Cherry, 1979).

Category	Total Dissolved Solids, TDS in mg/l
Fresh water	0-1,000
Brackish water	1,000-10,000
Saline water	10,000-100,000
Brine water	More than 100,000

Table 5.3 Chloride classes for irrigation water (Mills, 2001).

Chloride ion concentration	Suitability for irrigation
Less than 350 mg/L	1. Suitable all crops.
350 - 700 mg/L	2. Suitable for high, medium and low salt tolerant crops.
700 - 900 mg/L	3. Suitable for high and medium salt tolerance crops.
900 - 1300 mg/L	4. Suitable for high salt tolerant crops only.
Greater than 1300 mg/L	5. Too saline for irrigation of any crops.

Table 5.4 Groundwater quality in geophysical survey area.

No.	UTM. E	UTM. N	Electrical conductivity (mS/m)	Chloride (mg/l)	Total dissolved solids (mg/l)	Ferrous (mg/l)	Remark
1	228274	1704098	2790	670.0	1810	1.2	Paddy field
2	225401	1706256	4180	660.0	2720	46.0	Paddy field
3	225465	1706557	1340	220.0	871	0.5	Paddy field
4	226164	1706808	3660	550.0	2380	1.4	Lineament
5	226313	1706863	932	80.0	606	0.1	-
6	227486	1706510	819	46.0	532	0.1	Ban Sok Saeng
7	227589	1706524	763	16.0	496	9.1	Hill area
8	228213	1708500	6760	1790.0	4390	2.4	-
9	230702	1710273	12350	4220.0	8030	48.0	-
10	225254	1708958	3650	730.0	2370	0.5	Huai Ban Ngiu
11	225239	1708965	3710	770.0	2410	0.1	Huai Ban Ngiu
12	225153	1708906	1860	290.0	1210	0.1	Huai Ban Ngiu
13	228662	1708560	4920	1290.0	3200	14.0	Small hill/village
14	228671	1708468	4140	1020.0	2690	1.3	Small hill/village
15	229453	1708026	2770	610.0	1800	0.6	Paddy field
16	229306	1707935	1840	350.0	1200	0.1	Paddy field
17	225930	1703398	8600	2680.0	5590	6.7	Ban Nong Phan Pan
18	225666	1704128	3480	880.0	2260	0.2	-
19	225649	1704121	1400	220.0	910	0.1	-
20	225668	1704088	2320	500.0	1510	0.5	-
21	225208	1704275	578	6.4	376	0.2	Hill area
22	226809	1708737	7240	1740.0	4710	0.0	Ban Nong Nat

Table 5.5 Surface water quality in geophysical survey area.

No.	UTM. E	UTM. N	Electrical conductivity (mS/m)	Chloride (mg/l)	Total dissolved solids (mg/l)	Remark
1	228608	1702683	2000.00	560.0	1300	Paddy field
2	229768	1700712	3710.00	1090.0	2410	Paddy field
3	228130	1704307	1900.00	520.0	1240	Paddy field
4	228657	1705201	1280.00	340.0	832	Paddy field
5	228390	1704822	391.00	88.0	254	Paddy field
6	227241	1707008	286.00	13.0	186	Paddy field
7	227726	1706717	118.00	20.0	77	Temple
8	228123	1708327	150.00	6.4	98	Hill
9	226670	1708978	1050.00	220.0	683	Huai Ban Ngiu
10	226033	1708468	1100.00	290.0	715	Huai Ban Ngiu
11	225505	1709085	286.00	14.0	186	-
12	224810	1709966	82.00	2.4	53	Hill
13	225847	1708731	743.00	180.0	483	Huai Ban Ngiu
14	224618	1698435	7700.00	2400.0	5000	Paddy field
15	224221	1700589	517.00	120.0	336	-
16	231836	1708987	1950.00	490.0	1270	Small stream
17	230361	1708228	761.00	140.0	495	-
18	229357	1708359	345.00	42.0	224	Paddy field
19	230048	1705476	2410.00	680.0	1570	-
20	227364	1701922	250.00	16.0	162	-
21	226128	1703802	105.00	8.8	68	-
22	225948	1703740	131.00	12.0	85	-
23	235309	1709008	2170.00	610.0	1410	-
24	236214	1706949	3450.00	1030.0	2240	-
25	241106	1710739	1110.00	320.0	722	-

5.3 Results of groundwater and surface water sampling and assessments

Groundwater samplings were taken from existing wells of various aquifer emphasized on DMR wells and shallow wells dug by local people. Surface water samplings for analysis were collected from water body such as swamps, reservoir and pond including streams. Total dissolve Solids (TDS), Chloride content (Cl-), Iron content (Fe) and electrical conductivity (EC) are chemically analyzed for salinity assessment.

Distribution of surface and groundwater quality is directly related to topographic features. Either surface water or groundwater is fresh which often found on high land, especially elongated hills and rolling hills where are covered by tropical forest. Groundwater and surface water salinity often are high value on low land such as Ban Wat, Ban Kra Thin and Ban Rahan Khai areas where are located on the paddy field with depression area. Surface water quality sometime does not conform with groundwater salinity especially in low land where thick sediment layer such as sand overlies on thick clay layer. For example, the TDS and chloride content of groundwater at Ban Nong Phran Pan reservoir, are 5590 mg/l and 2680 mg/l for TDS and Cl respectively, but the surface water contains 85 mg/l in TDS and 12 mg/l in

Chloride content of surface water even though this area is located on flat land between hilly area (Fig. 5.2).

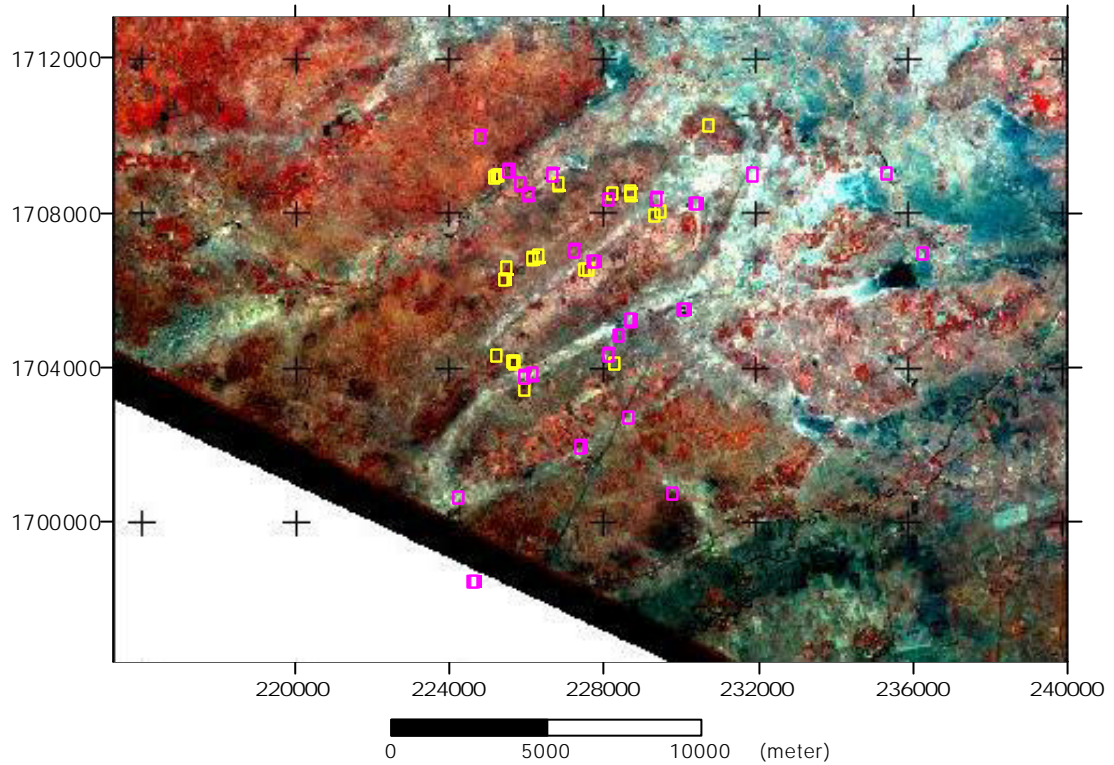
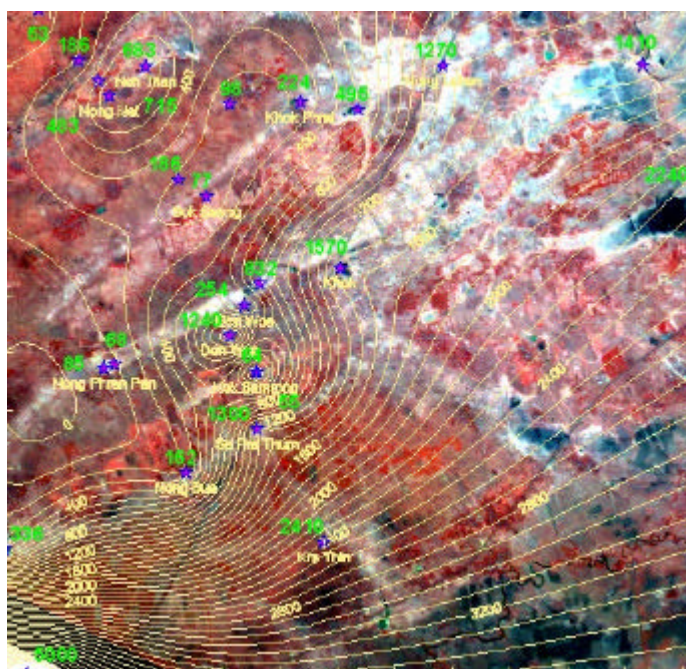
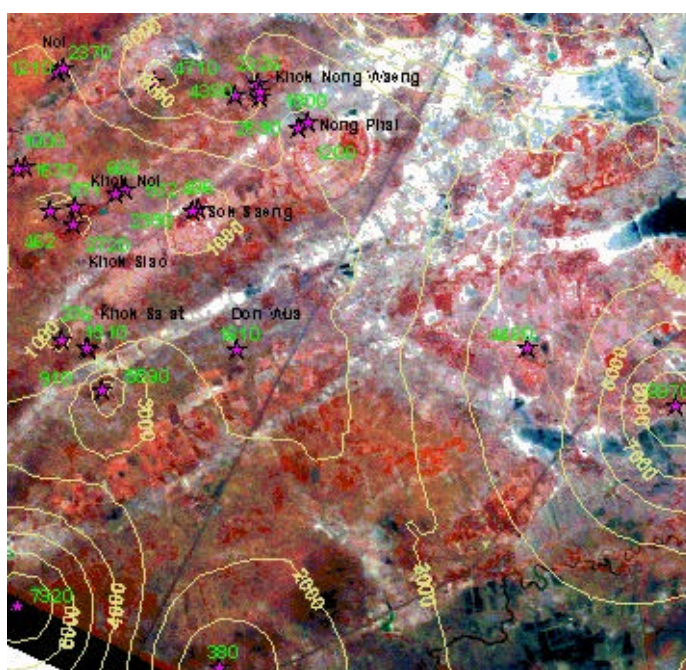


Figure 5.1 Groundwater and surface water location in geophysical survey area. Yellow symbol is groundwater location and violet symbol is surface water location.



(a)



(b)

★ TDS sampling point ~ TDS contour

Figure 5.2 The TDS contour of groundwater water (a) shows salinity higher than TDS contour of surface water (b).

CHAPTER VI

GEOPHYSICAL EXPLORATION

6.1 General

Northeastern Thailand is facing serious environmental problems of salt water contamination, soil salinization and sinkhole formation. The problems are related to the rock salt strata of the Maha Sarakham Formation which are widespread in the Khorat Plateau. Natural process of salt dissolution and structural setting of salt strata can be the cause of these problems. The geophysical exploration such as electrical resistivity, microgravity and seismicity can be used to determine the geological information at different depths e.g., fresh-water, brine-saturated, and rock salt formations including physical properties of rocks which are related to salt structure and overlying sedimentary strata.

6.1.1 Geophysical exploration area

The areas selected for geophysical exploration are located near the town of Khong district in Nakhon Ratchasima province, Northeastern Thailand on main Highway 2, approximately 70 kilometers from Nakhon Ratchasima. The areas are flat lying and rolling, with an elevation between 150-180 above mean sea level. It covers an area of about 30 km² consisting of Ban Nong Bua, Ban Nong Phran Pan, Ban Khok Sa-at, Ban Khok Noi, Ban Nong Nat, Ban Noi and Ban Non Daeng (Fig. 6.1).

6.1.2 Instruments

Electrical resistivity survey requires instruments to make electrical contact with the ground. The equipment used for electrical resistivity consists of Ammeter, Voltmeter, 4 electrodes (two for source/sink, two for volt meter/potential), connecting wire, power source (DC batteries in series or motor-driven generator) and IRIS resistivity instrument. Seismic survey uses seismograph recorder 24 channel, hydraulic weight drop of 50 kg, group geophone with 6 geophones/string, 4-wheel pick up car and accessories instruments. Microgravity use LaCoste & Romberg gravimeter model D.

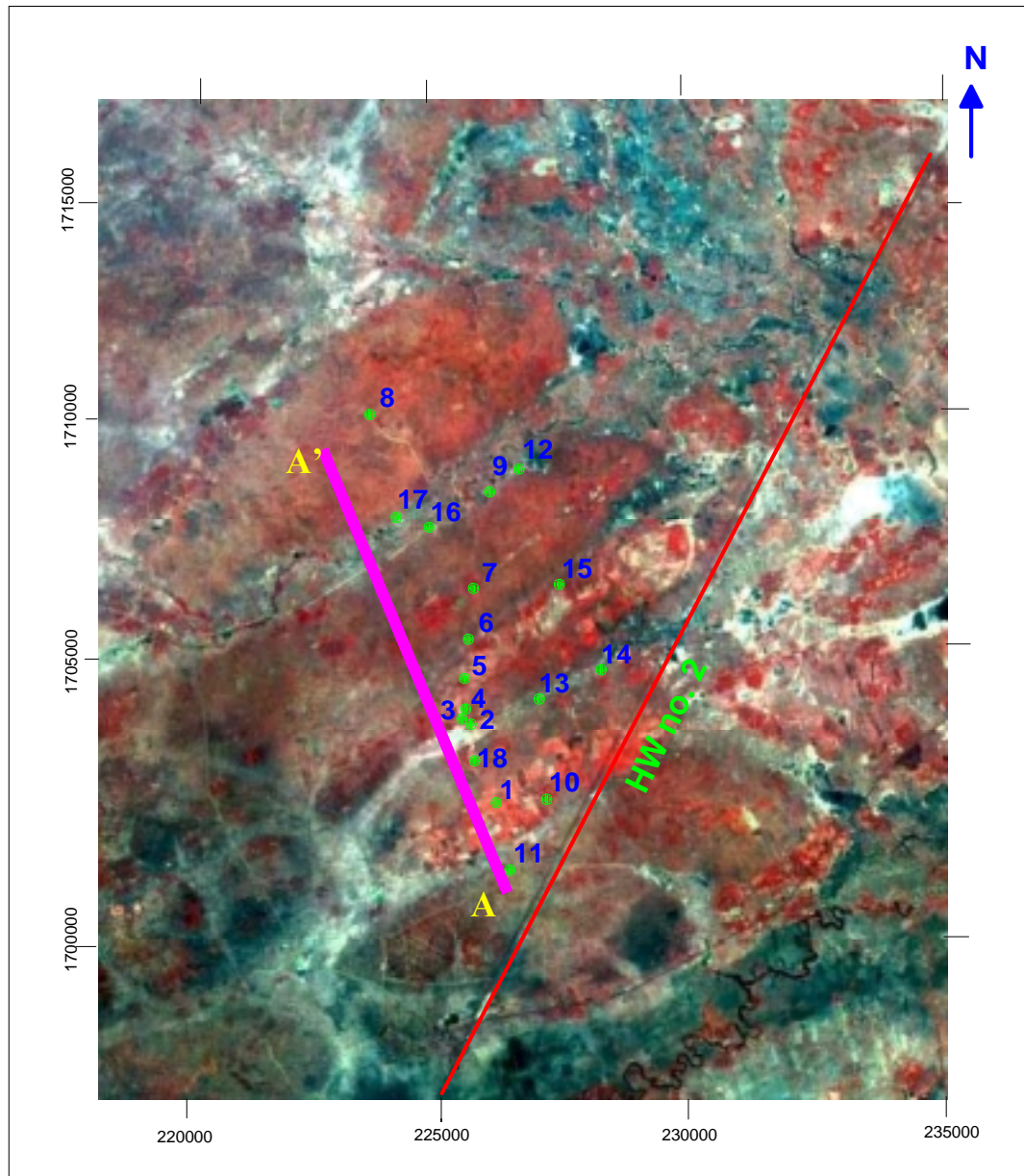


Figure 6.1 The MOMS satellite image of study area recorded on May 3, 1993 with $13.5 \times 13.5 \text{ m}^2$ resolution. The numbers are vertical electric sounding points. The A-A' section is the seismic and microgravity survey line.

6.2 Electrical Resistivity Survey

6.2.1 Concept and theoretical background

The electrical resistivity survey is based on the principal of the earth material acting as a resistor in a circuit. The basic behind electrical geophysical method is that different geologic materials have different electrical properties. The layers in the subsurface can be identified on the basis of these properties. An electrical current is

induced into the ground. The ability of that material to resist the current is measured. Because various earth materials exhibit characteristic resistivity values, they can be distinguished by using this method. Factors that affect the resistivity of earth material are degree of saturation, porosity, pore-fluid content, temperature, salinity, and thickness of clay or sand layers. Soils are more conductive than rocks, and saturated clays are more conductive than dry sands. Changes in pore water salinity also have great impact on ground conductivity. Applications of the electrical resistivity method include locating aquifers, salt water intrusions, and other ground water contamination problems. They can characterize bedrock by locating weathered zones, fractures, voids attributed to solution activity or determine depth to bedrock, and thickness of clay or sand layers.

Based on Sharma (1986); Robinson and Coruh (1988); Milsom (1996) and Yungul (1996), the property of the electrical resistivity of a material is usually expressed in terms of its resistivity. If the resistance between opposite faces of a conducting cylinder of length L and cross-section areas A is R , the resistivity is expressed as

$$\rho = \frac{RA}{L} \quad (6.1)$$

for an electrical circuit, Ohm's Law gives

$$R = \frac{V}{I} \quad (6.2)$$

where V and I are the potential difference across a resistor and the current passing through it, respectively. The resistance (R) of the layer is specified by its length (L) area of cross-section (A), and the resistivity (ρ). By definition (Eq. 6.1), equation 6.2 can be rewritten as

$$\frac{\Delta V}{L} = \frac{\rho I}{A} \quad (6.3)$$

or

$$\text{grade } V = \frac{\rho}{I} \quad (6.4)$$

6.2.2 Measuring resistivity

When the ground consists of a number of more or less horizontal layers. Knowledge of the vertical variation in resistivity is required. As the distance between the current electrodes is increased, so the depth to which the current penetrates is increased.

Measurements of ground conductivity or its inverse, resistivity can be used to delineate the boundaries between soil and rock, and between soil or rock strata of different water contents. The electrical current is directly introduced into the ground

through current electrodes. The resulting voltage potential difference is measured between a pair of potential electrodes. The current and the potential electrodes are generally arranged in a linear pattern. The apparent resistivity is the bulk average resistivity of all soils and rock influencing the flow of current. The popular pattern in vertical electric sounding (VES) is Wenner, Dipole-Dipole and Schlumberger configuration. Schlumberger pattern has been used to apply on this study. In the generalized Schlumberger configuration pattern, the spacing between potential electrodes is smaller than current electrodes. The current electrodes **A** and **B** are at equal distances **L** in opposite directions from the center of the array. The potential electrodes **M** and **N** are between **A** and **B** at equal distances **b** from the center of the array. The current electrodes located distance **2L** from each other, and potential electrodes located distance **MN** from each other, $2L > 5MN$ (Fig. 6.2). The survey uses an arrangement with a maximum separation in **AB** electrodes of 650 m sufficient to reach the desired investigation depth.

The measurement of apparent resistivity (ρ_a) is determined from Ohm's law using the potential difference (voltage) between two electrodes for a known current. At small spacing between electrodes, apparent resistivity is close to the resistivity of the upper layer. With increased space between electrodes, more current passes through the lower layer and apparent resistivity changes. Apparent resistivity never reaches the resistivity of the lower layer because some current always travels through the upper layer. Changes in apparent resistivity with electrode spacing depend on depth to the interface and the contrast in resistivity. Reynolds (1997) summarizes processes for the depth sounding. Measurements of the resistance (R) are made at the shortest electrodes separation and then at progressively larger spacing. At each electrodes separation, a values of apparent resistivity (ρ_a) is calculated using the measured resistance in conjugation with the appropriate **geometric factor** for the electrodes configuration and separation being used. The values of apparent resistivity are plotted on a graph (field curve) the X- and Y- axes of which represent the logarithm values of the current electrodes half-separation ($AB/2$) and the apparent resistivity (ρ_a), respectively.

In Figure 6.2, the source and sink electrodes are **A** and **B**, and the so-called potential electrodes are **M** and **N**. The electrodes are at distances d_1 and d_2 from the source and sink, and the **N** electrodes are at distances of d_3 and d_4 . According to Ohm's law, if the resistivity R is uniform, the electric potential v_M at the **M** electrodes will be

$$v_M = IR (1/d_1 - 1/d_2)/2\pi \quad (6.5)$$

and the potential v_N at the **N** electrodes will be

$$v_N = IR (1/d_3 - 1/d_4)/2\pi \quad (6.6)$$

Therefore, the difference in potential v_{MN} measured by the voltmeter will be

$$v_{MN} = v_M - v_N = IR (1/d_1 - 1/d_2 - 1/d_3 + 1/d_4)/2\pi \quad (6.7)$$

Equation (6.7) would then be a weighted average of resistivities in the difference materials within the zone between these equipotentials. Such a weighted average is called the apparent resistivity. Ordinarily, we do not know what different materials are presented at the time when the electrical survey is underway. Therefore, it is more appropriate to express a measurement as an apparent resistivity.

$$\text{When define } \rho_a = v_{MN}K/I \quad (6.8)$$

Where K is *geometrical factor* that depends on the electrodes arrangement. The geometrical factor is defined by the expression:

$$K = 2\pi/[1/d_1 - 1/d_2 - 1/d_3 + 1/d_4]^{-1} \quad (6.9)$$

From Schlumberger configuration pattern and Equation (6.9) the geometrical factor becomes

$$K = \frac{2\pi}{\frac{1}{L-b} - \frac{1}{L+b} - \frac{1}{L+b} + \frac{1}{L-b}} = \pi(L^2 - b^2)/2b \quad (6.10)$$

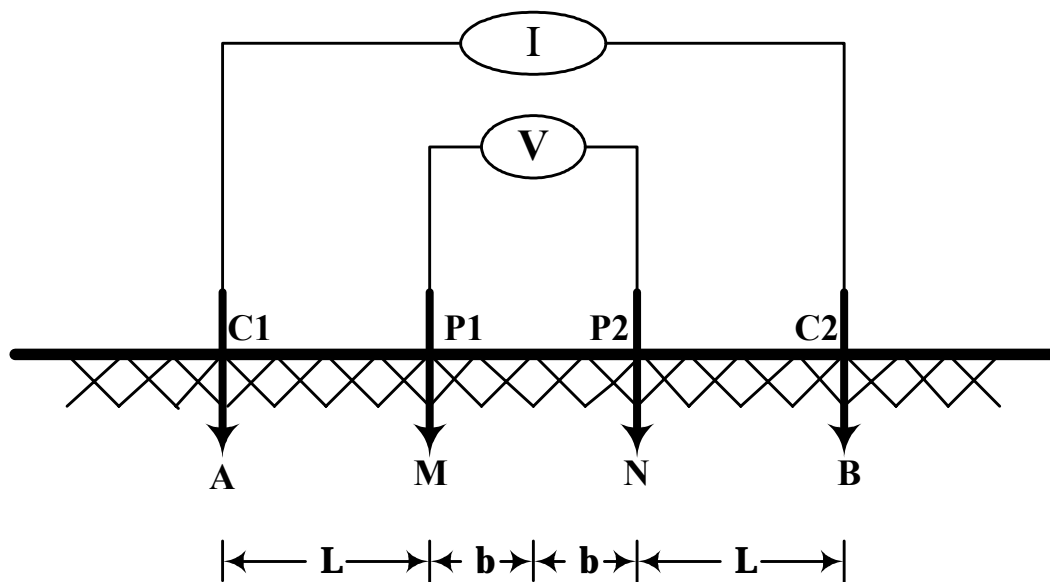


Figure 6.2 Showing the Schlumberger configuration pattern.

6.2.3 Interpretation of measurements

In the Schlumberger array, the depth to which the resistivity is averaged is roughly equal to half the separation between the current electrodes. From equation (6.8) and (6.10), The resistivity is computed using the formula:

$$\rho_a = \pi(L^2 - b^2) \quad (6.11)$$

where

- L = the half-separation between the current electrodes (A, B) measured in meters;
- b = the half separation between the measuring electrodes (M, N), in meters;
- V = the voltage at the measuring electrodes, in volts;
- I = the current between the current electrodes, in amperes.

This formula is based on the assumption that the ratio V/I is approximately equal to the voltage gradient, at the center of the electrode array. The resistivity as calculated from the above equation is not necessarily equal to the resistivity of the portion of the earth over which the measurement was made, due to the influence of the electrical properties of one layer on another layer. For this reason the value obtained from the above equation is termed the apparent resistivity. The interpretation process consists of deducing a likely set of true resistivity values which would be compatible with the observed apparent resistivity values. In many cases, there exists no single set of true resistivities that correspond to a particular set of apparent resistivities, and as such, the true resistivity cannot be uniquely determined. The apparent resistivity which would be measured over a series of uniform horizontal layers presents a fairly simple case, and since this is frequently a good first approximation to geologic conditions, the first step in the interpretation process normally involves determining what layer thickness and resistivities can explain the measured apparent resistivities.

Numerous investigations have produced resistivity curves for various geologic conditions using theoretical data. These curves have been plotted in terms of dimensionless variables and form the basis for the curve-matching technique of resistivity interpretation. A curve of the field data, in which the values of the observed apparent resistivity are plotted against electrode spacing on logarithmic graph paper, will have the same shape as the theoretical curves plotted in terms of dimensionless variables. By plotting the field data on graph paper of the same scale as the theoretical curves, the field data curve may be laid over the theoretical curves. The field curve is moved until the field points correspond or match with the points of the theoretical curves. The only requirement is that both sets of curve axes must be kept parallel. The depths and corresponding true resistivities are then read off of the field matched theoretical curve. It must be remembered, however, that there are available many differing sets of theoretical curves for many types of geologic settings and the curve matching process may become time consuming.

6.2.4 Results

Eighteen vertical electric sounding were applied along survey line from NW to SE and extended to E-W following lineament direction of satellite image. The total readings were 210 times. The apparent resistivity values can be grouped into 3 levels as follow; low (0-10 Ohm.m), medium (10-30 Ohm.m) and high resistivity (more than 30 Ohm.m). Apparent resistivity readings are separated into 158, 37, 15 times of low, medium and high resistivity respectively. The maximum depths approximately 450 meter below ground surface can be detected. At the shallow depth (0-30m), the apparent resistivity values are between 1.5-750 Ohm.m. Intervals between 10-85 m, the apparent resistivity values are varied from 0.6 to 15 Ohm.m. The data in this range are smooth and assembled but in the shallow depth are scattered. The apparent resistivity values at 85 meter and deeper (some points) are ranging between 5.3-25.3 Ohm.m. The results of raw data, curve fitting and computer program representing the depth, apparent resistivity and thickness are shown in Table 6.1 and Figure 6.3.

Table 6.1 Electrical resistivity raw data including configuration array pattern at point1.

Geophysical Exploration (Electrical Resistivity)											
Area:		<u>Khong district</u>		Station		<u>point1 225622E 1708126N</u>		Date		<u>05/26/01</u>	
Comment:		<u>direction N60°E</u>									
AB/2	MN/2	K	I	V _x	RES	AB/2	MN/2	K	I	V _x	RES
1.3	0.5	4.53	9.68	799.57	373.6	50	5	777.54	153.79	1.187	6.0
2.0	0.5	11.78	13.63	318.05	274.9	65	5	1319.47	67.66	0.370	7.2
3.2	0.5	31.38	18.22	90.516	155.9	80	5	2002.77	84.81	0.296	7.0
4.0	0.5	49.48	12.41	28.28	112.7	100	5	3133.74	136.97	0.350	8.0
5.0	0.5	77.75	15.69	17.06	84.6	100	20	753.98	130.14	1.304	7.6
6.5	0.5	131.95	12.36	3.75	40.1	130	20	1295.91	92.35	0.613	8.6
8.0	0.5	200.28	13.22	1.24	18.8	160	20	1979.20	142.93	0.894	12.4
10	0.5	313.37	50.53	2.62	16.3	200	20	3110.18	94.48	0.479	15.6
10	2	75.40	50.47	11.60	17.3	250	20	4877.32	352.23	0.777	10.8
13	2	129.59	28.05	1.78	8.2	320	20	8011.06	228.38	0.279	9.8
16	2	197.92	59.63	1.75	5.8	320	50	3138.50	230.14	0.668	9.1
20	2	311.02	63.76	1.047	5.1	400	50	4948.00	553.33	0.803	7.2
25	2	487.73	57.91	0.517	4.4	500	50	7775.65	194.29	0.122	4.9
32	2	801.11	191.80	1.402	5.9	650	50	13194.70	231.15	0.105	6.0
32	5	313.85	192.25	3.188	5.2						
40	5	494.80	152.33	1.762	5.7						

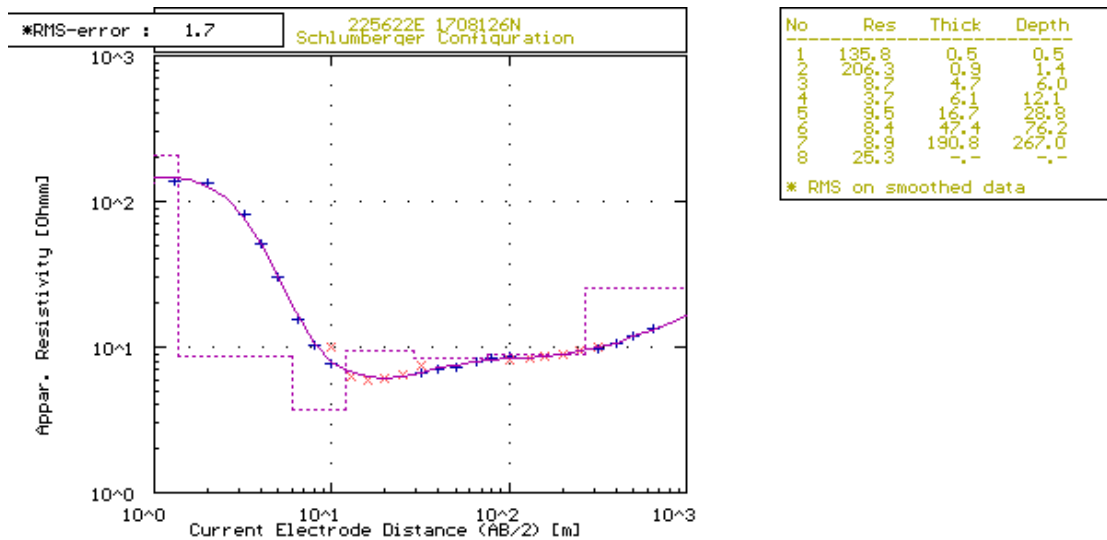
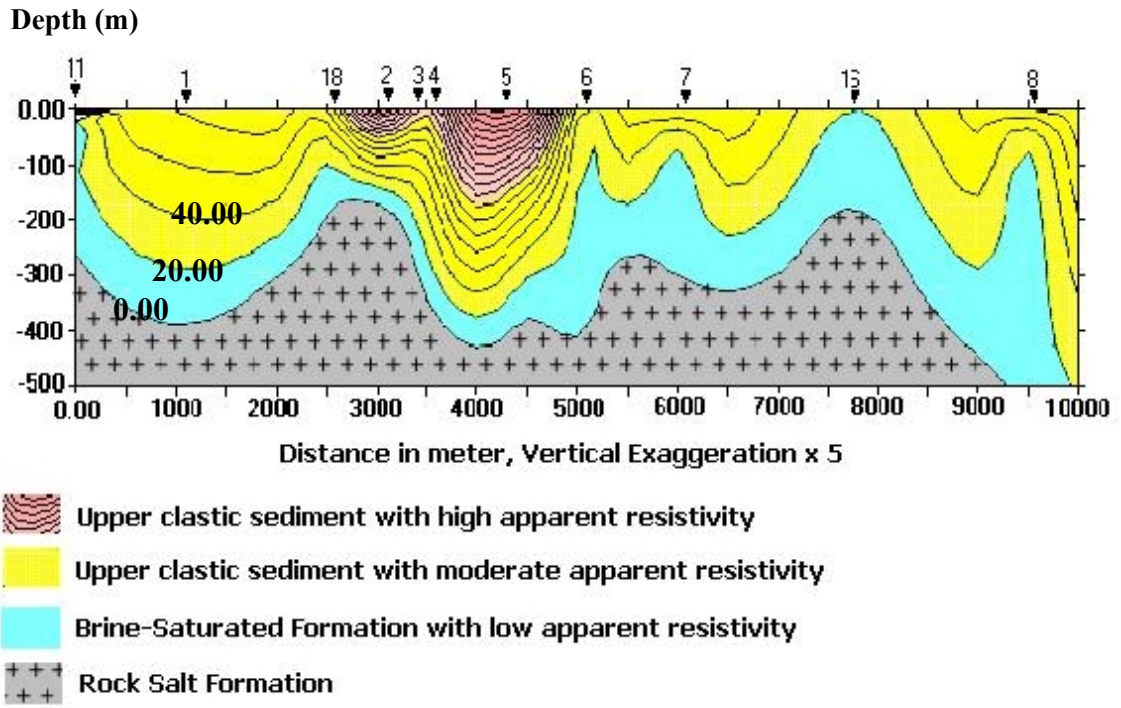


Figure 6.3 The example of curves fitting from RESIST87 software represents the depth, apparent resistivity and thickness at point 1.

6.2.5 Analysis

The data in the field consist of a graph of resistivity with electrode spacing. This curve is matched with a master curve on RESIST87 software. At depth between 1.5-30 m, the apparent resistivity values represent low to high resistivity zone. Based on Shama (1986) and Milsom (1997), the apparent resistivity values in this range can be interpreted to saline soil, clay, silt, sand and sandstone respectively in the increasing value order. From 30 - 120 m intervals, the apparent resistivity value is varied from 0.6 to 15 Ohm.m (low - medium resistivity zone). This zone is interpreted as mud, clay and claystone or brine-saturated formation. From Potash exploration boreholes, the rock salt units are found below clay layer. The apparent resistivity values below clay/claystone layer are ranging between 5.3-25.3 Ohm.m. Solgosoom (1999) recommended that the low resistivity zone (clay layer) is considered to be low conductor when comparing with salt layer (high conductor). He concluded that the layer below clay/claystone is rock salt formation (high resistivity). From curve fitting, iterative computer programs and interpretation, the salt layer and overburden along the survey line are shown in Figures 6.4 and 6.5.

Apparent resistivity profile along NW-SE direction



True scale along the survey line.

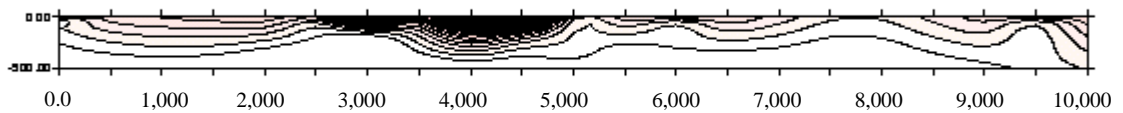


Figure 6.4 The apparent resistivity profile and interpretation along NW-SE direction with true scale and vertical exaggeration.

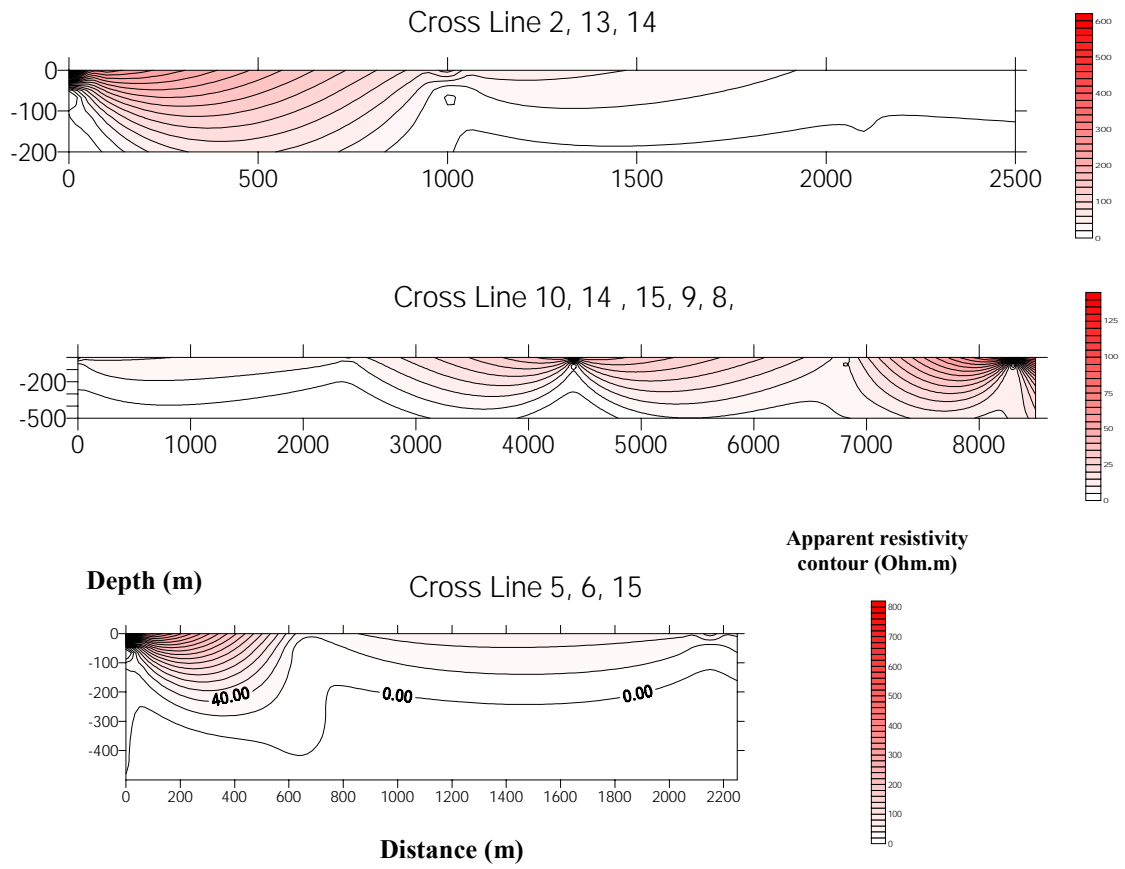


Figure 6.5 The apparent resistivity profile and interpretation along east-west direction (lineament direction).

6.2.6 Discussions

The image feature from satellite data shows parallel lineament in NE-SW direction. This feature is related to saline soil area, fracture, sinkhole and swamp. The result of the study indicates that the relationship between salt structure and lineament feature is significant. The salt structure in areas showing prominent lineament direction represents shallow depth (85-130 m.). The surface topography of underlying shallow salt shows swamp, natural reservoir and high salinity soil. In addition, based on earlier discussion in Chapter V the shallow groundwater is salty and brackish (at elevation 3-10 m from surface). It can be concluded that subsurface structure in study area is closely related with linear features such as fractures and faults. The limitation of resistivity surveys requires a fairly large area and far from power lines and grounded metallic structures. In high salinity areas, the over current is likely to occur when operating. Electrical resistivity analysis is not unique. More than one model may give an acceptable fit to the data (equivalence). It is also possible for some layers that are thin or have a small contrast in resistivity that is not resolved (suppression).

6.2.7 Conclusions

Electrical resistivity techniques are applied to determine the top of the Maha Sarakham rock salt unit, brine-saturated and fresh water formations. The interpretation of resistivity data requires background knowledge in stratigraphy and structural setting of the area. The fresh water, brine-saturated and rock salt formations interfaces are delineated by the apparent resistivity values. In fresh water formation, the apparent resistivity values are more than 30 Ohm.m. The apparent resistivity of brine-saturated formation is between 5-25 Ohm.m. The apparent resistivity of rock salt formation is between 1-10 Ohm.m. The rock salt formation is found at 85-300 meter depth. The brine-saturated formation is found above the rock salt unit between 30-300 meter depth. The fresh water formation appears at shallow depth (0-30 m). From the analysis and interpretation, salt structure is undulating following the anticlinal folding structure. Clay layer in the sequence may be considered as an important key bed which overlies conformably on the rock salt unit. The saline soil and groundwater contamination is likely to occur from the process after the formation of salt structure.

6.3 Microgravity surveying

6.3.1 Basic theory of gravity

Gravity survey involves the measurement of subsurface geology on the basis of variations in the Earth's gravitational field generated by differences of density between subsurface rock. The main control of rock density variation is its composition and porosity. Density increases with depth due to compaction and progressive cementation. Porosity is one of the main controls of density variation in sedimentary rocks.

When evaluating gravity data, a knowledge of the theory of gravity, and an appreciation of the acquisition and processing of gravity data should prove fruitful when interpretation subsequent geological anomalies.

The power with which 2 masses will attract one another is proportional to the given mass and conversely proportional to the square of the distance. This is known as 'Newton's Law of Gravitation' as Newton framed it in 1686. This can be expressed mathematically as:

$$\mathbf{F} = \mathbf{G} \mathbf{m}_1 \mathbf{m}_2 / \mathbf{r}^2 \quad (6.12)$$

when, \mathbf{F} = Force attraction,
 $\mathbf{m}_1, \mathbf{m}_2$ = 2 masses,
 \mathbf{r} = distance between two masses,
 \mathbf{G} = universal gravitational constant; which is equal to the force in dynes between 2 small uniform spheres, each of mass 1 gram with their centers 1 cm apart.

Force is related to mass by acceleration. This acceleration, termed the 'acceleration of gravity' (\mathbf{g}) was first measured by Galileo in his famous experiments at Pisa. The units which express the measurement of \mathbf{g} are known as the Gal (in honor of Galileo). The Gal is derived from using the basic law of mechanics. From Newton's second law and gravity acceleration, The force can be written as:

$$\mathbf{F} = \mathbf{m}_1 \mathbf{g} \quad (6.13)$$

when, \mathbf{F} = Force attraction,
 \mathbf{g} = Gravity acceleration.

The force in equation (1) and (2) is the same equation, so it can be rewritten as:

$$\mathbf{F} = \mathbf{G} \mathbf{m}_1 \mathbf{m}_2 / \mathbf{r}^2 = \mathbf{m}_1 \mathbf{g}$$

therefore, $\mathbf{g} = \mathbf{G} \mathbf{m}_2 / \mathbf{r}^2 \quad (6.14)$

However \mathbf{g} does vary. This is because the Earth is not a perfect homogenous sphere. If it was, then the gravity field at any point on the surface would be identical. Because variations in gravity are very small, units for gravity surveys are generally in milligals (mgal) where 1 mgal is one thousandth of 1 cm/s^2 . At sea level, the earth's gravitational acceleration is $\sim 9.8 \text{ m/s}^2$ or equivalently $\sim 980,000 \text{ mgal}$.

6.3.2 Measurement of gravity

Instruments that measure gravity are the pendulum, the torsion balance, and the gravimeter. A brief discussion of two of those instruments, namely the pendulum and the gravimeter are below.

The Lacoste-Romberg model D Gravimeter is chosen to use in this survey line. Because it has suitable for various respect such as, it is easily moved from place to place on account of this instrument is much smaller and light weight about 5 kg (total weight). Beside that, it is high sensitivity, gravity differences as 0.01 mgal can be

detected. Thus, it is accordingly high accurate gravity meter, which appropriated to use in this study.

For geological purposes, the main interest is localized shifts in the force of gravity. However, as already noted latitude and 'drift' corrections have to be accounted for. In addition, elevation, topography and tidal corrections must also be corrected. In gravity exploration, the determination of the gravity values can be summarized as below:

Absolute Gravity (g_{abs}) - The absolute determination of g at some point on the earth with a precision of better than one part in 1 million is an experiment that requires the greatest care. Almost all the earlier determinations used some form of swinging pendulum whose period is related to g .

Observed Gravity (g_{obs}) - Gravity readings observed at each gravity station after corrections have been applied for instrument drift and earth tides.

Latitude Correction (g_n) - Correction subtracted from g_{obs} that accounts for Earth's elliptical shape and rotation. The gravity value that would be observed if earth were a perfect (no geologic or topographic complexities), rotating ellipsoid is referred to as the normal gravity.

Free Air Corrected Gravity (g_{fa}) - The free-air correction accounts for gravity variations caused by elevation differences in the observation locations. The form of the Free-Air gravity anomaly, g_{fa} , is given by:

Bouguer Corrected Gravity (g_b) - The Bouguer correction is a first-order correction to account for the excess mass underlying observation points located at elevations higher than the elevation datum (sea level or the geoid). Conversely, it accounts for a mass deficiency at observation points located below the elevation datum.

6.3.3 Results and conclusions

In this study, the measurement points were located along the road at 20 m intervals in the 10000 meter distance. More than 500 data were read and collected. The measurements were conducted within one week. The survey including the collection of topographic elevation along the gravity survey line (Fig. 6.6). The two-dimensional gravity anomaly distributions corresponding to the underground structure along the survey lines are shown in Figure 6.7. It clearly shows that there are considerably low gravity anomalies (much more than -360 mGal) in two areas. These low gravity anomalies could be regarded as low density anomalies. Ban Nong Phran Pan and Ban Nong Nat (Fig. 6.7) can be interpreted as shallow salt unit when correlated with regional stratigraphy. The result of this study indicates that, (1) The Bouguer anomalies suddenly change at Ban Nong Pharn Pan (-365 mGal) and Ban Nong Nat (-363 mGal). (2) These locations are low elevation and natural reservoirs are present. (3) The lineament directions are also present trending NE-SW direction

at this point. (4) The salt structure underneath Ban Nong Phran Pan and Ban Nong Nat should be shallower than the other areas.

It is noticeable that the narrow long low lands between high-elevated land are corresponding with negative Bouguer gravity anomaly. On interpreting gravity data, shallow salt dome concept (Seni and Jackson, 1983; Jackson and Talbot, 1986) is employed as a working hypothesis. The negative Bouguer gravity anomaly should be a diapiric salt structure underneath the surface as an initial model of Warren model (1989).

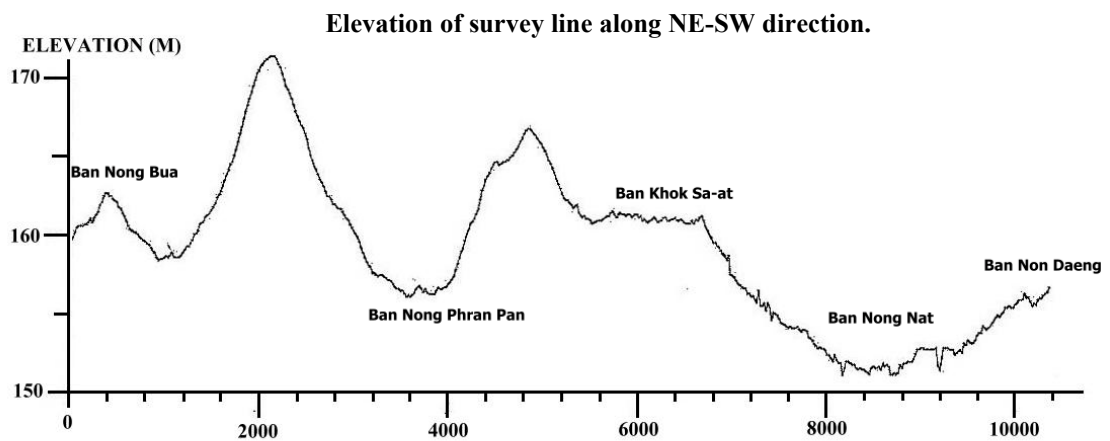


Figure 6.6 The topography elevation along the survey line (electrical resistivity, microgravity and seismic).

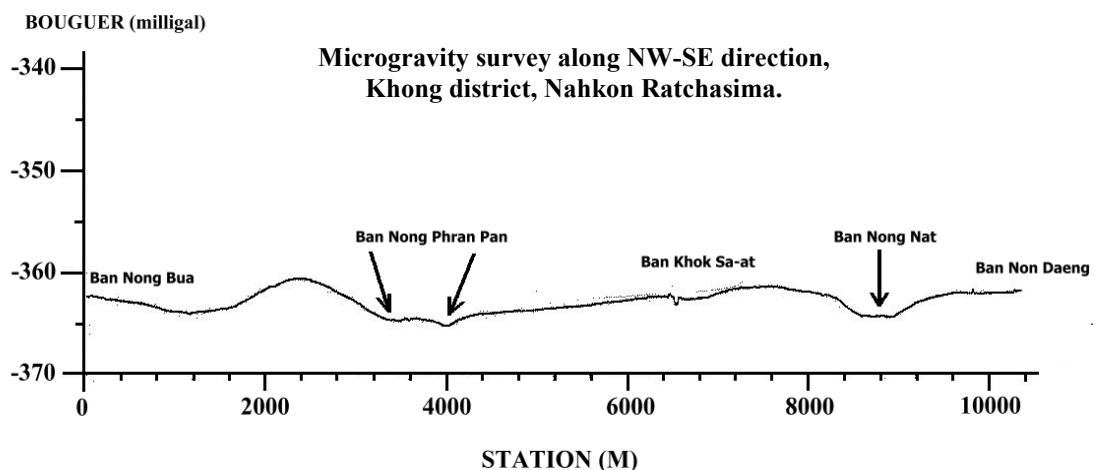


Figure 6.7 Bouguer gravity anomaly profile along the survey line.

6.4 Seismic survey

6.4.1 Concept and theoretical background

Seismic method is the most effective, and most expensive of all the geophysical exploration (Milsom, 1996). This method is based on differences in elastic properties of the soil and rock. When conducting seismic surveys, acoustic energy is put into the ground. Sources of acoustic energy include a hammer impacting a metallic plate, weight drops, vibrators, and different types of explosive sources. The acoustic waves propagate into the ground at a velocity dependent upon the density and elastic properties of the material through which they travel. When the waves reach an interface where the layer velocities change significantly, a portion of the energy is reflected back to the surface, and the rest is transmitted into the lower layer. Where the velocity of the lower layer is higher than that of the upper layer, a portion of the energy is critically refracted along the interface. Critically refracted waves travel along the interface at the velocity of the lower layer and continually refract energy back to surface. Receivers, laid out on the surface, record the incoming refracted and reflected waves.

6.4.2 Ray path in multi-layered earth

At an interface between 2 rock layers there is generally a change of propagation velocity resulting from differences in physical properties. At such an interface the energy within an incident seismic pulse is partitioned into transmitted and reflected pulses.

Total energy of the transmitted and reflected rays must equal the energy of the incident ray. The relative proportions of energy transmitted and reflected are determined by the contrast in acoustic impedance across the interface. The acoustic impedance of a rock is the product of its density and its compressional wave velocity. In general, the harder a rock the higher the acoustic impedance. The smaller the contrast in acoustic impedance across a rock interface the greater is the energy transmitted through the interface.

The “reflection coefficient” is the ratio of amplitude of the reflected ray to the amplitude of the incident ray. The transmission coefficient equals the ratio of amplitude of the transmitted ray to amplitude of the incident ray. Where all the incident energy is transmitted, there is no acoustic impedance across an interface. Normally, the bulk of seismic energy on a rock interface is transmitted and only a small proportion is reflected.

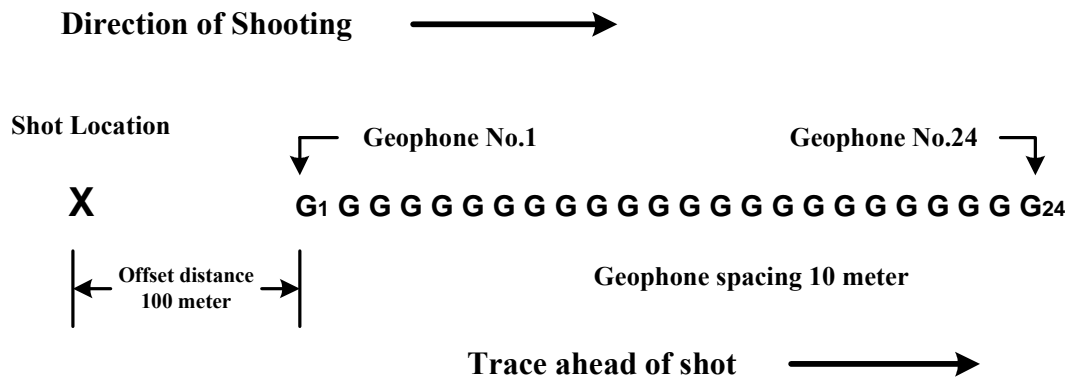


Figure 6.8 Off-end push spread configuration pattern.

6.4.3 Field investigation and acquisition parameter

This study used reflection survey method. The total of 1000 stations were measured and marked by wooden pegs with 10 meters interval. A portable seismic recording unit, OYO DAS 1, Japan, 24 channels and 6 geophones/string was employed to stored seismic data in a SEG-Y digital format. The survey uses Off-end push configuration as shown in Figure 6.8. The acquisition parameter and instruments used are as follow:

Source

Source type	Hydraulic weight drop, 50 kg
Shot point interval	20 meter
Offset distance	100 meter
Coverage	6 folds

Receiver

Geophone	Land type, group geophone, 6 geophones/string
Magnetic coil	Vertical to ground surface

Recording unit

Brand	OYO DAS 1, 24 channel
Digital data format	SEG-Y
Low cut filter	35 Hz
High cut filter	150 Hz
Sample rate	500 microsecond
Power supply	DC battery, 12 Volt, 24 Ah

Configuration

Type	Off-end push
Line	Straight

The reflection data processing were performed using SEISTRIX version 3.4 software. A processing procedure included trace editing, spherical divergence correction, deconvolution, filtering, normal move-out, staking and depth conversion.

6.4.4 Results and interpretations

More than 500 station with 20 meter geophones spacing were measured and recorded. From depth conversion and velocity analysis, the velocity of rock salt unit is 4000-4500 m/s and depth to the top of rock salt approximate 180-300 meter. The shape of rock salt unit is flattening and anticlinal folding. The areas of shallow salt structure are also located in the anticlinal folding structure at Ban Nong Phran Pan. The axes of salt anticline are NE-SW parallel with prominent lineament direction. The interpreted seismic sections along the survey lines are shown in Figures 6.9, 6.10 and 6.11.

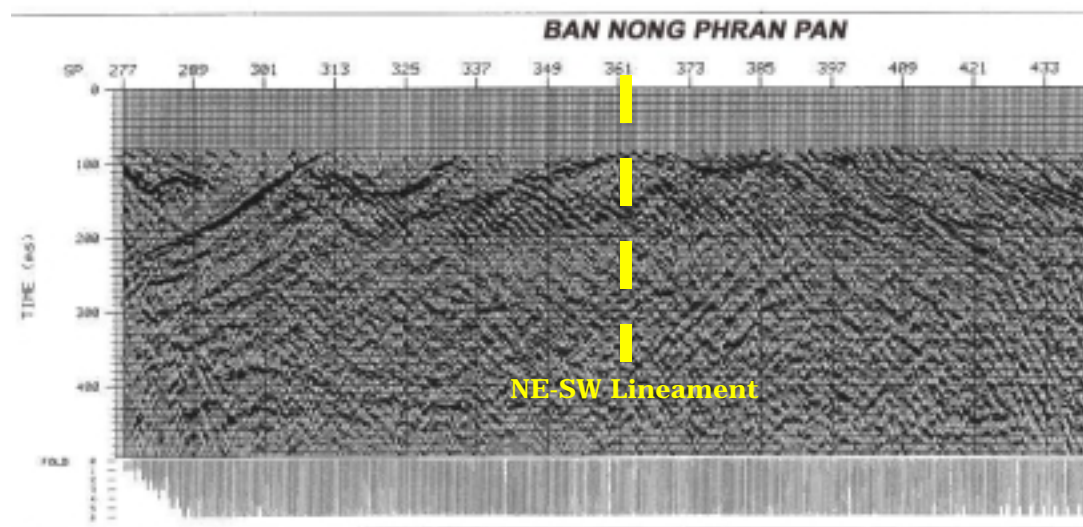


Figure 6.9 The part of seismic section showing the salt anticlinal folding in lineament direction at Ban Nong Phran Pan.

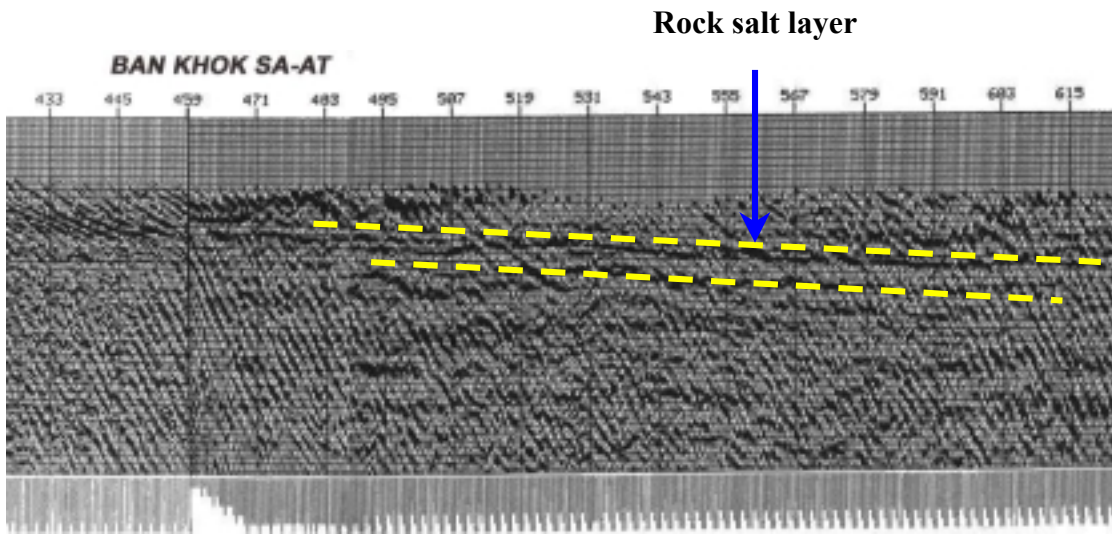


Figure 6.10 The part of seismic section showing the salt flattening layer in red to slightly brown tone with rolling topography at Ban Khok Sa-At.

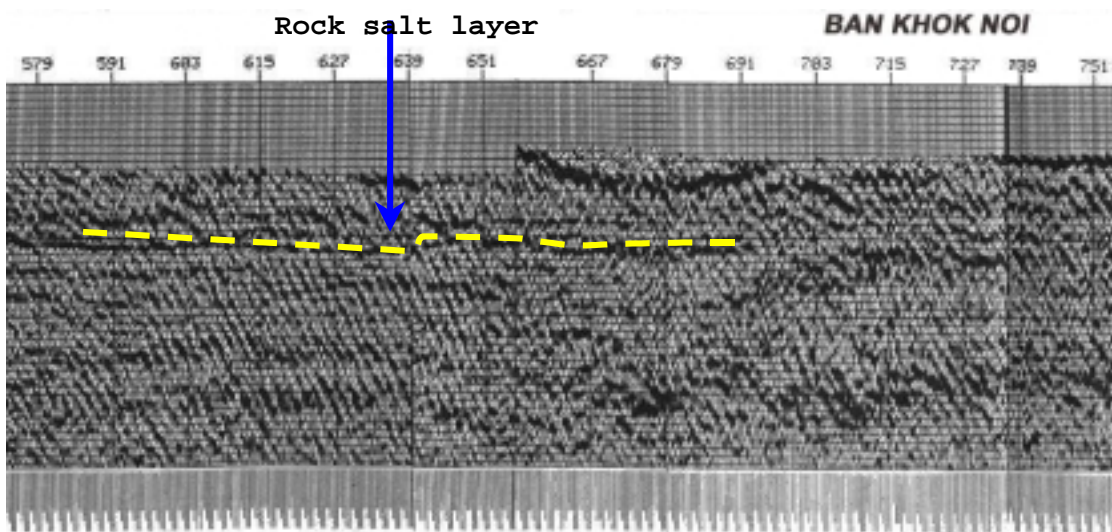


Figure 6.11 The part of seismic section showing the salt flattening layer continued from Ban Khok Sa-At to Ban Khok Noi in red to slightly brown tone with rolling topography.

CHAPTER VII

SUMMARY AND CONCLUSIONS

The results of the study show that the satellite images show typical features (texture, structure, color and tone) that correlate with the distribution of the soil salinity, structural setting and depth of the rock salt layers. From the integrated results of lineament analysis, geophysical exploration and field checking, the following conclusions are summarized.

7.1 Remote sensing and lineament analysis

Based on lineament density, intersection density map (Figs. 4.5 and 4.6) and comparison with soil salinity map (Khundee, 2001) and groundwater quality (DMR, 1958-1996), the soil salinity and the potential subsidence areas can be divided into 3 categories as follow.

- (1) High: more than 5 length density and 5 intersection per unit area.
- (2) Moderate: between 3-5 length density and 3-5 intersection per unit area.
- (3) Low: less than 3 length density and 3 intersection per unit area

The structural and deformation events can be interpreted in the study area based on lineament map (Fig. 4.3) and rose diagram analysis (Fig. 4.7). They can be divided into 2 stages as follow;

- (1) Lower Tertiary: The prominent lineament indicates a NW-SE trend. The trend is corresponding to the Phu Phan uplift axis and NE-SW horizontal compressive stress was responsible for the fracture-tension deformation.
- (2) Miocene to Pleistocene: The prominent lineament indicates a NE-SW trend. The trend is corresponding to the regional compressive stress in NW-SE direction. The interpreted salt asymmetrical folding structures are inferred to correspond with this direction.

7.2 Image classification types and salt accumulation model

The image classification types based on salinity model can be divided into 2 types as follow;

7.2.1 Natural sinkhole and swamp salinity

(A) Natural sinkholes

A natural sinkhole (depression area with circular feature) is one kind of features that indicate soil salinity and stage of salt dissolution underneath surface. Sinkholes are found in the areas underlain by rock salts within the Maha Sarakham Formation. The dissolution process was occurred after salt deposition accompanying with chemical weathering, tectonic and human activities. Sinkhole and depression

landform in Khorat basin are closely related with lineaments, particularly on its intersection (Khundee, 2001). Water moves along fractures lineament and dissolves the salt dome and the shallow salt layers beneath the surface.

The dissolution continues to take place over a long period of time. The dissolution cavities filled with water are formed below the water table. When the water table decreases over the years, the levels of groundwater in the caverns also decrease. While the water table increases, the water in the cavern helps to support the roof of caverns. This support is removed when the water table becomes drawn down, and thus the unsupported roof eventually becomes unstable and collapses to form a sinkhole. When sinkhole collapses, it will be filled with water as the water table is exposed at the surface. This small circular lake is called the sinkhole pond. Sinkholes on image appear circular on low land or depression area and show a dark (wet) to light tone (dry).

(B) Swamp salinity

Swamp is defined as the area of submerged standing water due to groundwater or surface water effect and the aquatic grass has generally covered the rim of swamp indicating that the groundwater table is quite shallow (Khundee, 2001). On the image, the swamp shape is similar to those of sinkholes. Swamp is the stage developed from natural sinkhole. After sinkhole occurred, sediment was deposited in depression area in rainy season alternating with the summer that the sinkhole is dry. These events have been repeated several times until depression area has been filled with thick layer of clastic particles. The depression area becomes shallow. The new sediment was composed of soil. The paddy field can grow in this nearly flat topography area. Swamp can be reversed to sinkhole stage by stimulating factors such as salt solution mining, groundwater pumping and groundwater level decrease in dry season. As mentioned above, the water quality in swamp is poor (slight to brackish salinity).

The two-type salinity as mentioned above can be divided into natural sinkhole and dry depression models (modified from Wentz, 1999). In natural sinkhole, the salinity occurs in depression area. Surface water flows slowly over and is trapped temporarily in the low lying areas until the water drains off and/or infiltrates the soil. The groundwater at the edge of the water body moves laterally upslope through the upper soil in an unsaturated state. Once the surface water has disappeared, groundwater from the water table rises by capillary action to the surface in the previously sinkhole area. Depression bottom seeps are well-defined on satellite image with dark to black tone and rounded edges (Fig. 7.1).

In depression area, the salinity occurs as a ring of salt immediately adjacent to a permanent water body. Water infiltrates from the pond into the permeable upper soil layer and moves laterally upslope as shallow groundwater in an unsaturated state through this layer. The water may also flow downward, raising the water table. Water from the lateral unsaturated flow and capillary rise from the water table emerges at the surface where it evaporates, leaving salts at the edge of the sloughs (Fig. 7.2).

7.2.2 Circular feature with outcrop and contact salinity

Outcrop salinity occurs where a permeable, water-bearing layer, such as a sandy layer, salt anticline or fracture bedrock layer, outcrops at or near the surface. Outcrop saline seeps occur in rows along a slope at similar elevations. In most cases, outcrop salinity is a form of primary salinity but may also be influenced by human alterations to the prairie ecosystem. Wongsomsak (1986) classified the salinity areas into three types as the hill area, the valley area and the basin area. The hill area is an example of outcrop salinity as it is located between boundary of the Maha Sarakham Formation and the Phu Tok Formation.

In its recharge areas the water percolates down through the soil profile beyond the root zone. The groundwater moves to a lower position in the landscape and here through capillary rise, reaches the surface, resulting in a saline seep. Contact salinity occurs where a permeable water-bearing surface layer thins out above a less permeable (e.g. fine textured) layer. This forces the groundwater flow closer to the surface (Fig. 7.3).

7.3 Remote sensing with geophysical survey

The image feature from satellite shows parallel lineament in NE-SW direction. From geophysical results, the relationship between salt structure, overlying sediment and fracture-lineament feature is significant. From geophysical results, the salt structure in areas showing prominent lineament direction represents shallow feature (100-130 m.). The surface topography of underlying shallow salt shows swamp, natural reservoir and high salinity with total dissolved solid, chlorine and electrical conductivity more than 4,500 mg/l, 1,500 mg/l, 7,000 mS/m respectively. On the other hand, salt structure is deeper at high topography with slightly brown to dark tone. The groundwater in this area is good quality. It can be concluded that subsurface structure in the study area is closely related with linear feature such as fractures and faults with white to light gray tone and long narrow trend. The comparison of image feature and geophysical results are shown in Figures 7.4, 7.5, 7.6, and 7.7.

7.4 Proposed model for land subsidence and salt dissolution

The conceptual model for land subsidence and salt dissolution can be summarized and shown in Figure 7.8 (a) - (c) and 7.9 (d)-(f) as follow:

Stage 1

In the Late Cretaceous, the Maha Sarakham Formation was deposited in a dry and arid environment in land-locked hypersaline lake. The unconformity was observed from Potash exploration bore-holes between Lower Anhydrite layer and siltstone of the Khok Kruat Formation.

Stage 2

In the Early Tertiary, the Phu Phan uplift was formed as a result of collision between the Indian plate and the Eurasian plate. The sediments of Phra Wihan, Phu Phan and Khok Kruat Formations were strongly eroded in the uplifted area. The

Maha Sarakham salt layers were generally folded with broad and shallow anticlinal and synclinal structure.

Stage 3

In the Early Tertiary, the Phu Thok Formation was deposited in an arid and semiarid environment by wind and fluvial processes. Salt flowage was developed probably driven by sediment loading and gravity glide folding. This process has destroyed the original flattening bedding features.

Stage 4

In the Early Tertiary to Miocene, fracture development was affected from the Himalayan orogeny. Dissolution process was continued to take place at shallow salt layer.

Stage 5

Miocene to Pleistocene, natural sinkhole was initiated by salt dissolution with capillary force, adhesion and water table change.

Stage 6

Pleistocene to Quaternary, modern landform was developed. The sediment particles transported to the dissolution collapse often marked by a lake or a surface depression or a sinkhole and soil salinity.

7.5 Recommendation and future work

This study uses remote sensing, geophysical exploration, geology, hydrogeology and field investigation data. Remote sensing is the tool for clarification of salt related questions and detected of the scope of environmental problems in the Khorat Basin. The geophysical exploration is used to determine the subsurface geologic formations to confirm the remote sensing interpretation. The study needs to use both methods for comparison, interpretation and conclusion. In this study, the remote sensing covers large area but geophysical exploration is limited in specific selected area.

The geophysical survey area is located near the basin center where salt layer is deeper than those of basin rim. The future geophysical work should be extended to the salt mining field and area near the basin rim. The electrical resistivity is a convenient and inexpensive tool to detect upper salt layer. The variation of overburden thickness in many locations is the main effect on resistivity values. The comparison of electrical resistivity result in the position of potash exploration borehole is important to calibrate the resistivity with geological structure. The regional gravity study is required to classify the salt structure. To prevent soil salinity and land subsidence problem, the traditional salt production and the disturbance activities of groundwater level and rock salt formation should be stopped in high lineament and high intersection density zone.

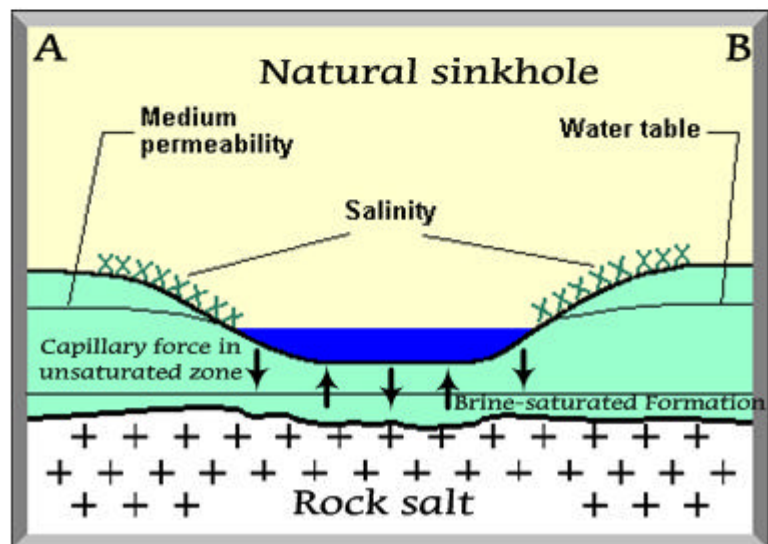
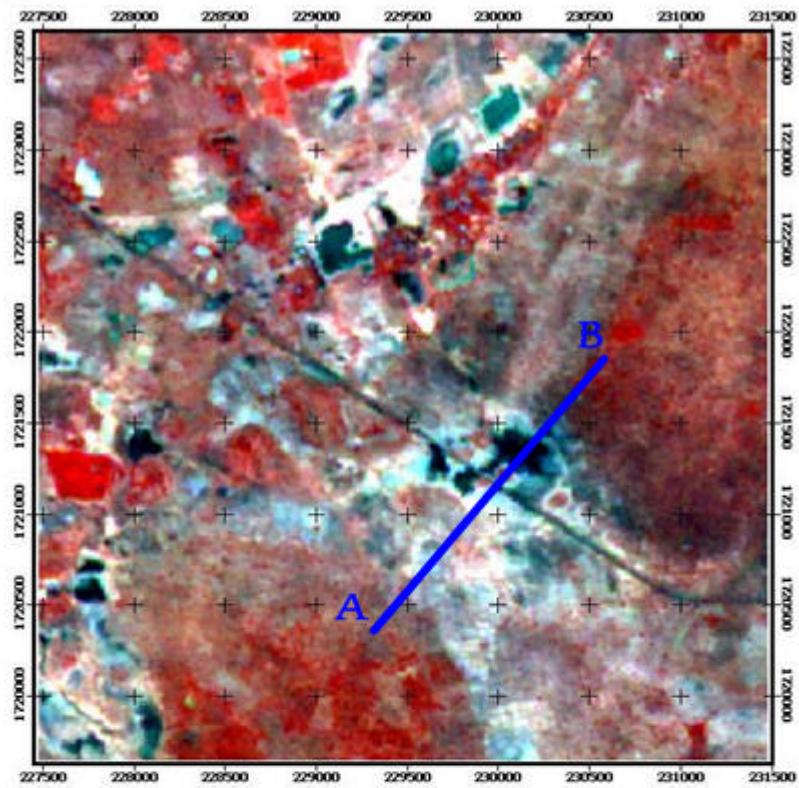


Figure 7.1. Natural sinkholes on image are located on depression area at Ban Kao and Ban Wat, Khong district with water and salinity model in wet condition (Modified from Wentz, 1999).

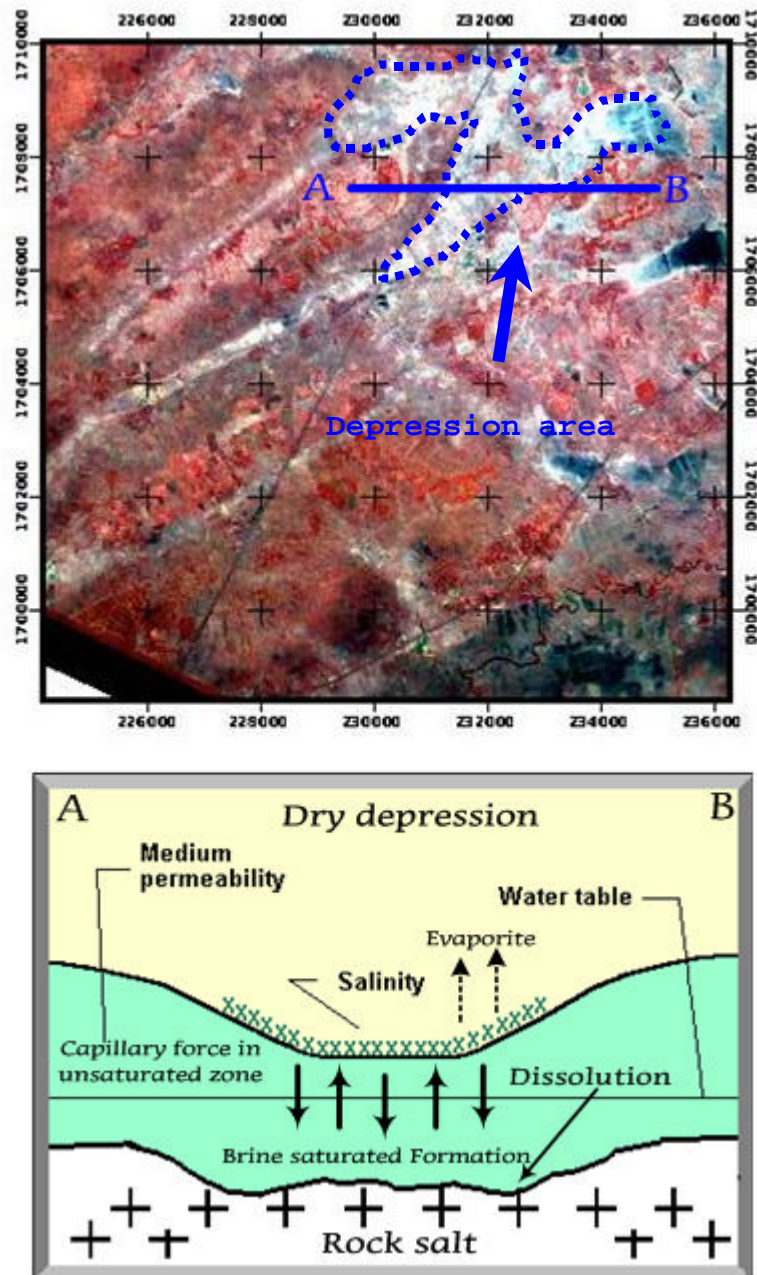


Figure 7.2 Dry depression area without water in white to slightly blue on image at Ban Don Ta Nin and Ban Don muang, Khong district and salinity model in dry condition (Modified from Wentz, 1999).

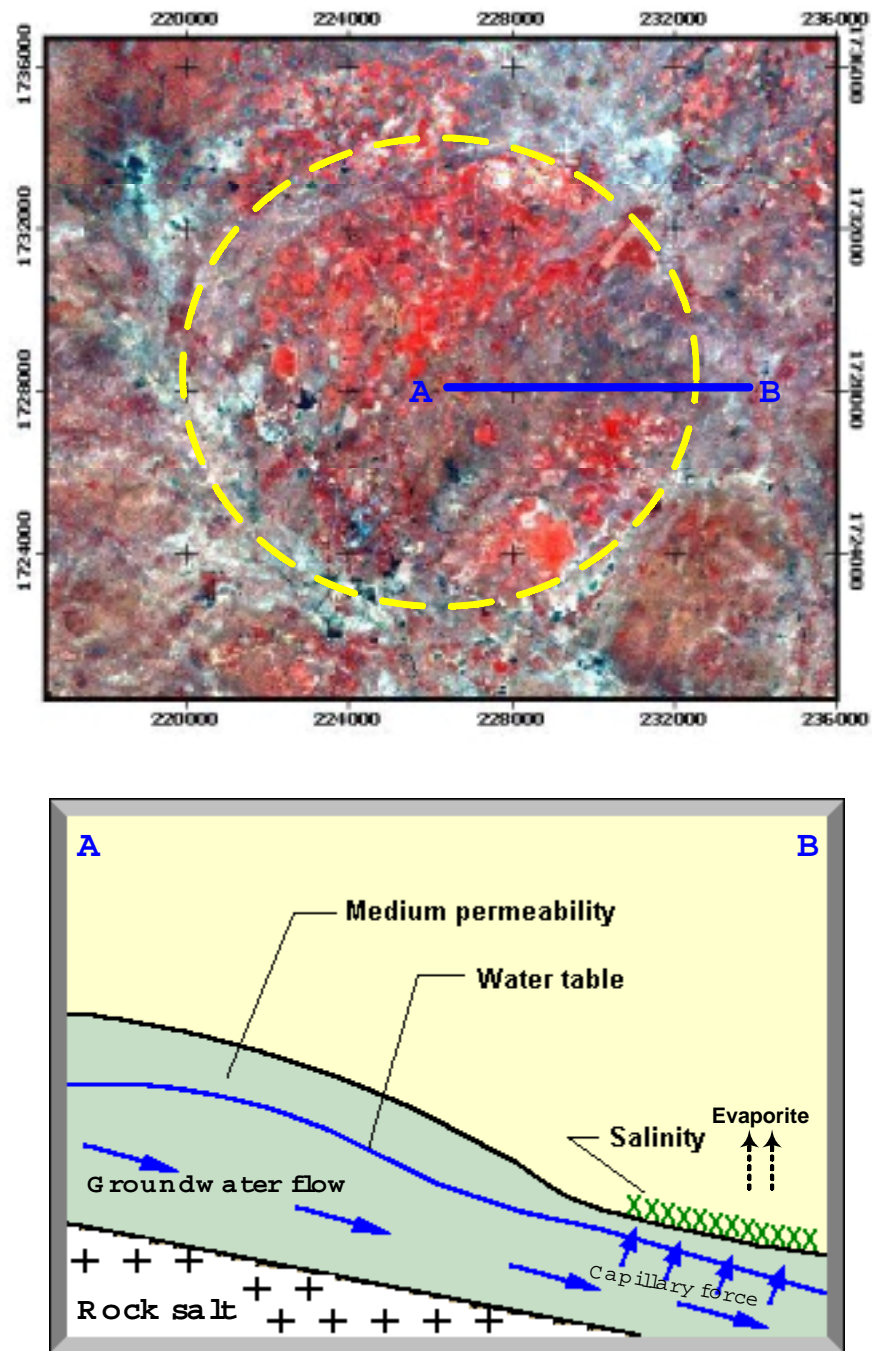
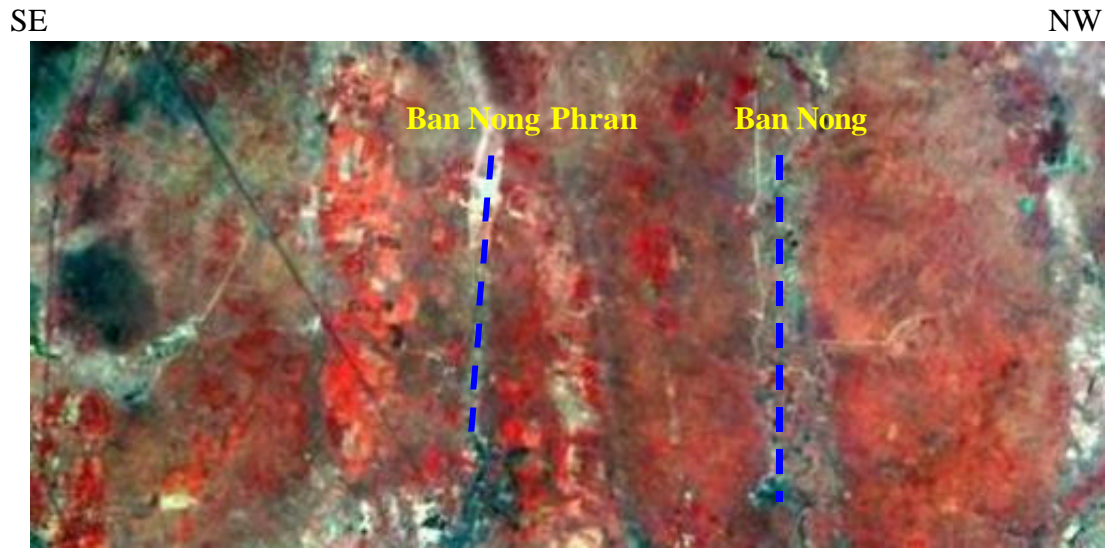


Figure 7.3 Circular feature on image at Ban Chot, Ban Nong Waeng Kaeo, Ban Nong Mek and Ban Nam Om representing outcrop and contact salinity model (Modified from Wentz, 1999).



--- Lineament

Apparent resistivity profile along NW-SE direction

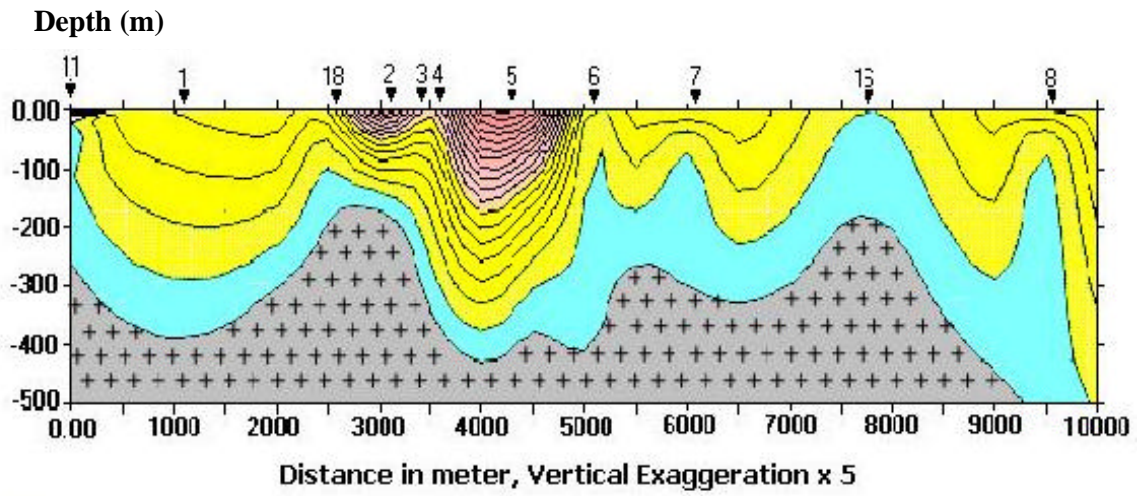
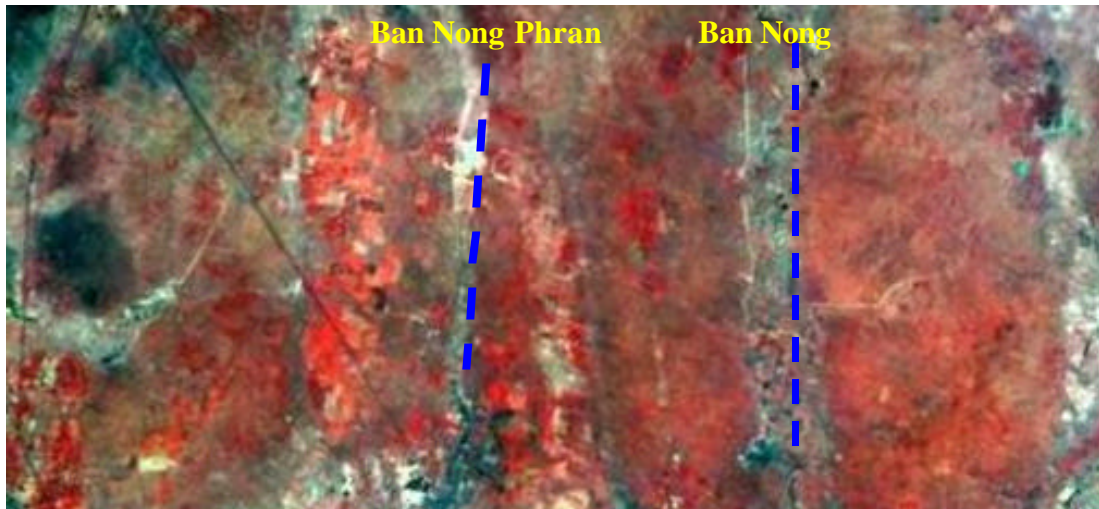


Figure 7.4 The MOMS satellite image with vertical electric sounding and subsurface interpretation (same scale).

SE

NW



--- Lineament

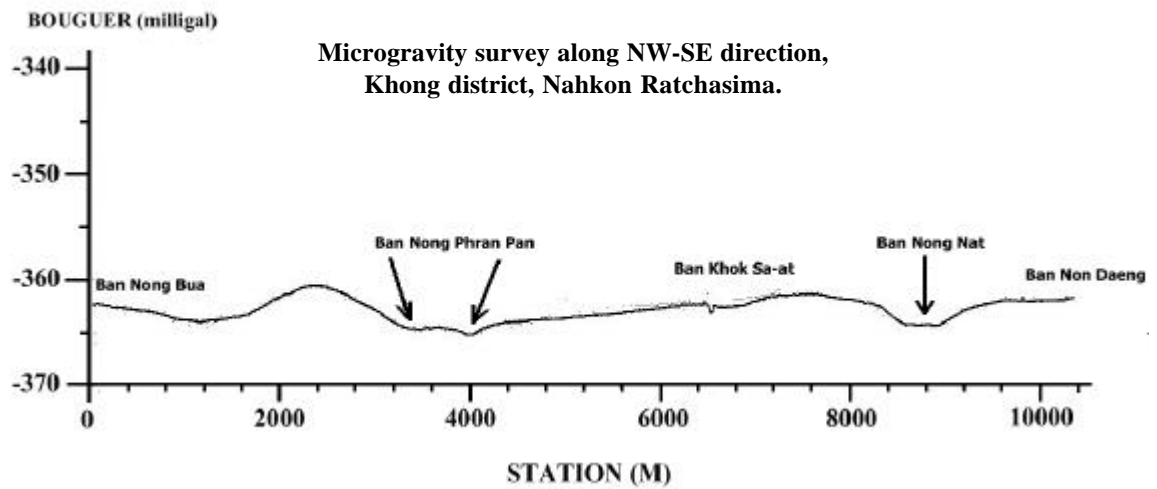


Figure 7.5 The MOMS satellite image with microgravity (Bouguer anomaly). The Bouguer values change at Ban Nong Pkan Pan and Ban Nong Nat (same scale).

SE

NW

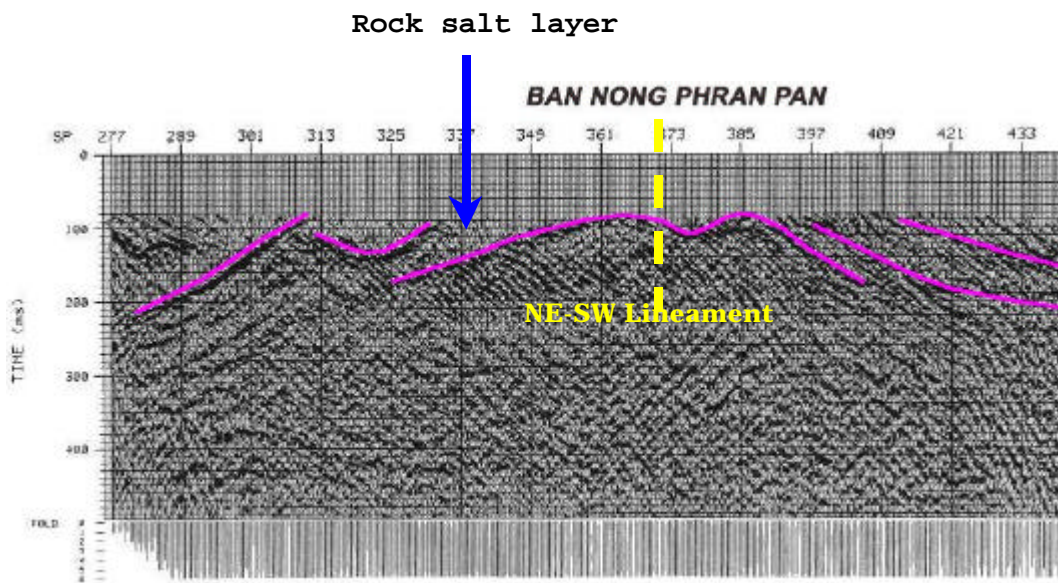
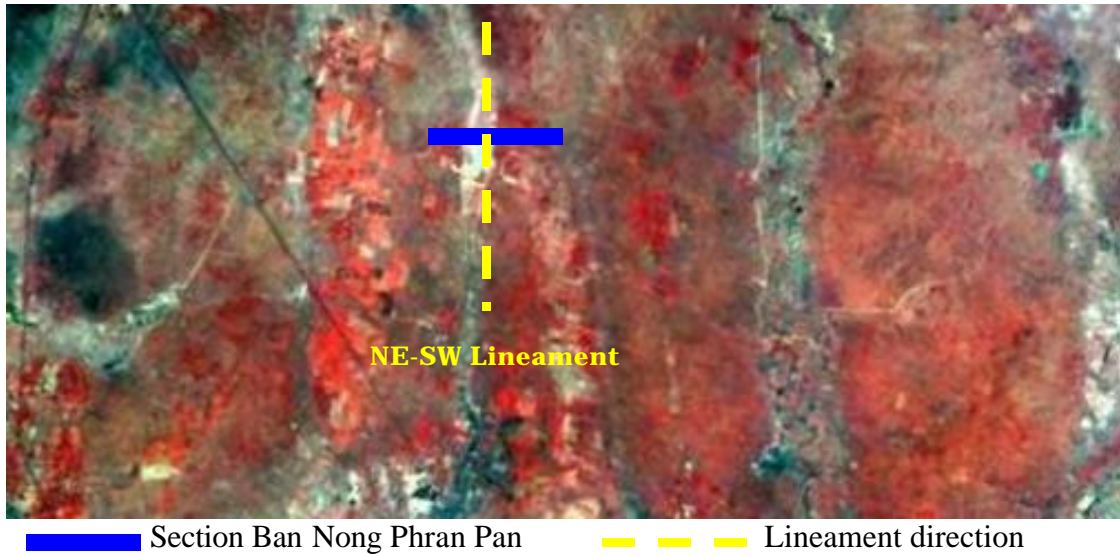
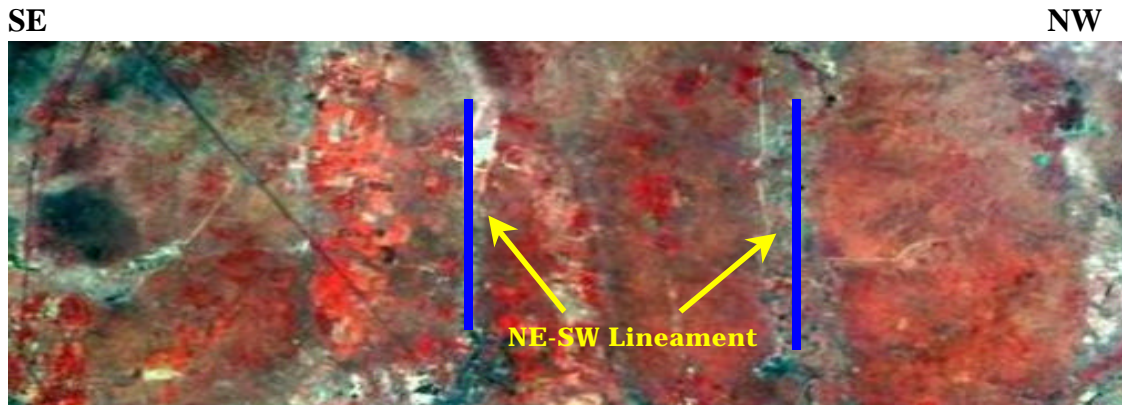


Figure 7.6 The MOMS satellite image with part of seismic section showing the salt anticlinal folding in relation with lineament direction at Ban Nong Phran Pan.



Apparent resistivity profile along NW-SE direction

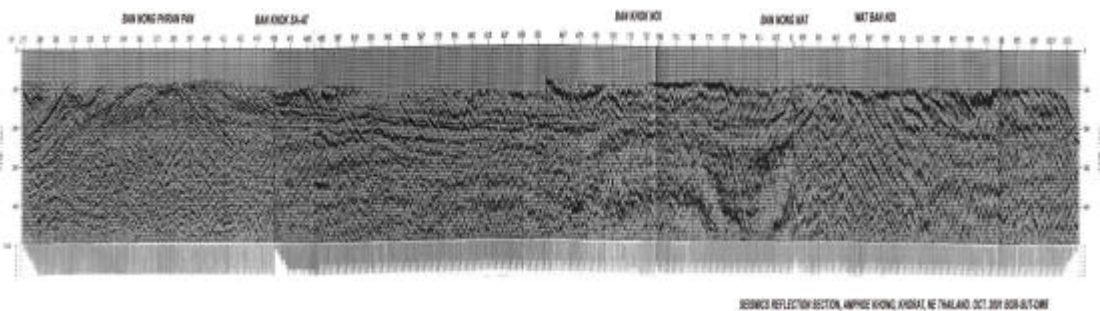
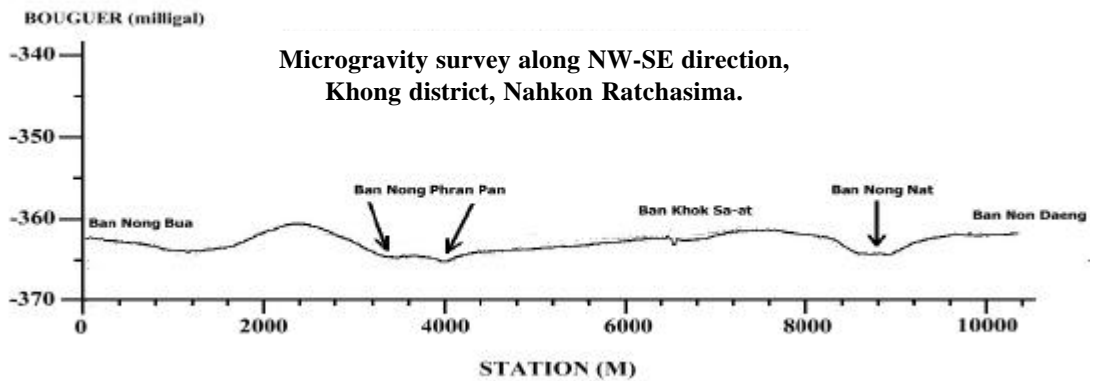
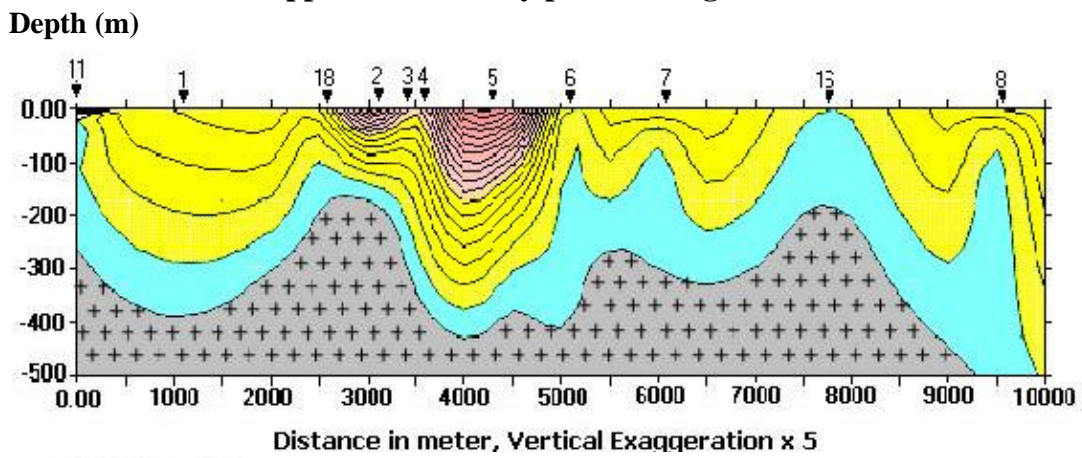


Figure 7.7 MOMS satellite image with electrical resistivity, microgravity and seismic section in the study area. Lineaments indicate the shallow salt structure.

Stage 1. Deposition of Maha Sarakham Formation (Late Cretaceous)

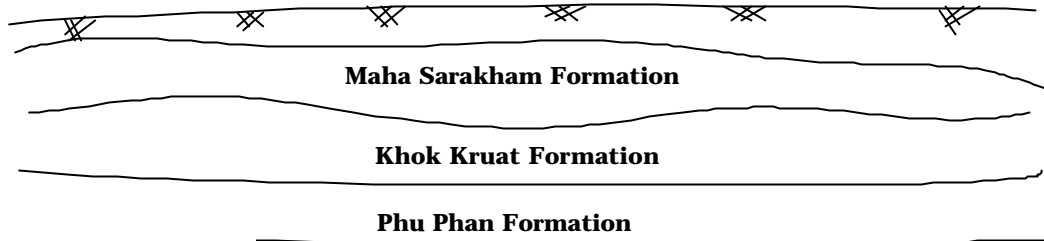


Figure 7.8 (a)

Stage 2. The Phu Phan uplift (Early Tertiary)

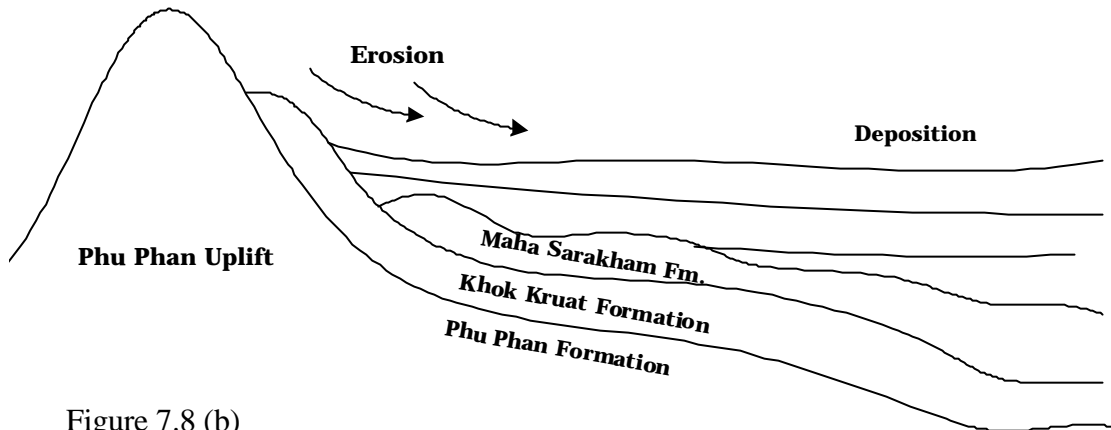


Figure 7.8 (b)

Stage 3. Deposition of Phu Thok Formation and initiation of salt flowage (Early Tertiary)

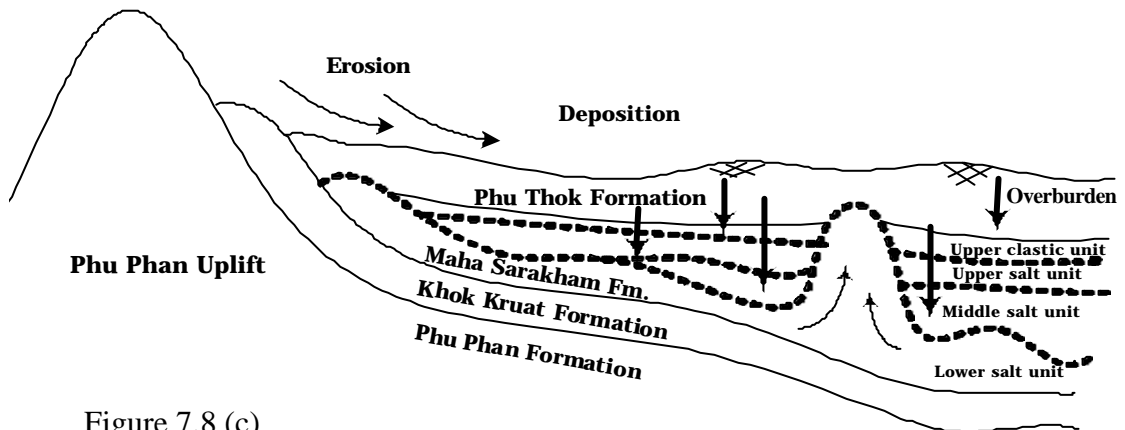
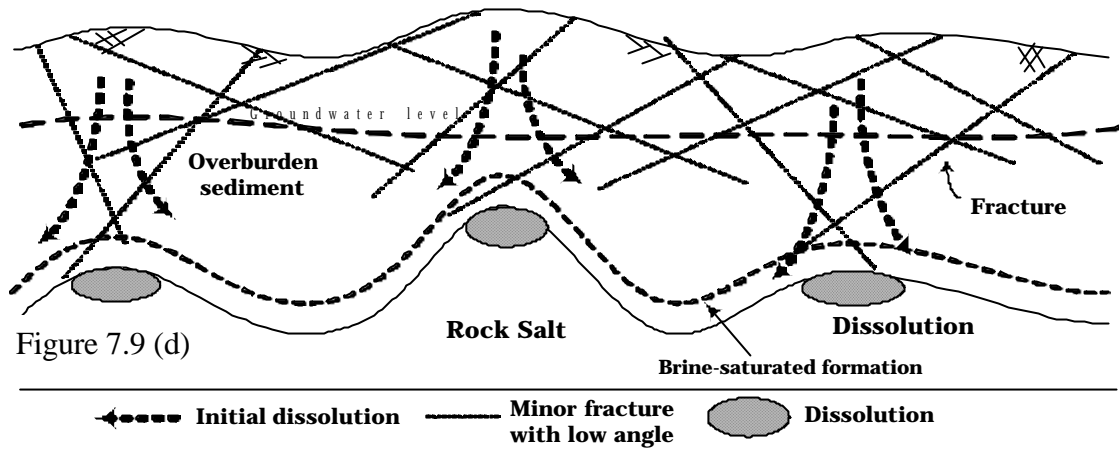


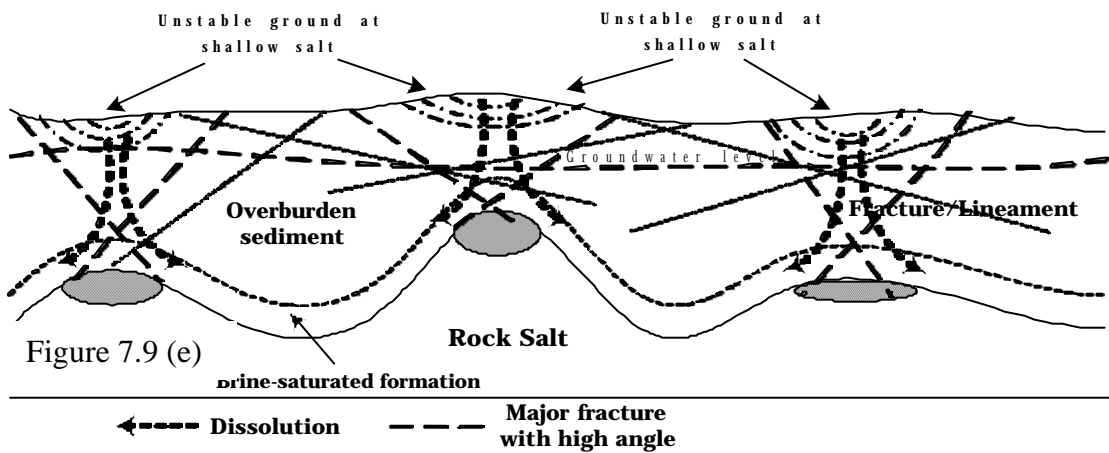
Figure 7.8 (c)

Figure 7.8 The conceptual model for land subsidence and salt dissolution in Khorat Basin in Late Cretaceous to Early Tertiary time (a) - (c).

Stage 4 Fracture development and continuation of rock salt dissolution (Early Tertiary to Miocene)



Stage 5 Unstable ground was initiated and development of natural sinkhole (Miocene to Pleistocene)



Stage 6 Development of modern landform after sinkhole collapsed (Pleistocene to Quaternary)

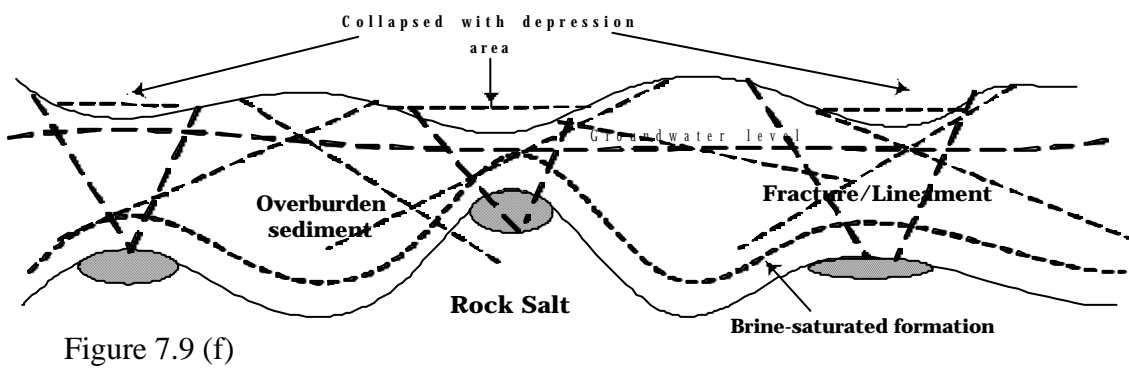


Figure 7.9 The conceptual model for land subsidence and salt dissolution in Khorat Basin in Early Tertiary to Quaternary time (d) - (f).

REFERENCES

- Archwichai, L. (1989). Fracture density map for groundwater development in Khon Kaen, Northeast Thailand. In **Proceedings of the annual technical meeting 1989 “Geology and mineral resources of Thailand, Indochina, and Myanmar” and IGCP-246 “Pacific Neogene events in Southeast Asia” (pp.59-68)**. Chiang Mai Univ. Thailand
- Bakliwal, P.C. (1978). Tectonic interpretation from lineament analysis using photogrammetrical techniques of Ranthambhor Fort area, Rajasthan, India. In **Proceeding of the Third Regional Conference on Geology and Mineral Resources of Southeast Asia (pp. 129-132)**, Bangkok, Thailand.
- Baize, D., (1988). **Soil science analyses: A guide to current use**. U.S.A.: John Wiley & Son.
- Blyth, F.G.H. and Freitas, M.H. (1984). **A geology for engineer**. Great Britain: Butler & Tounner Ltd.
- Chinoroje, O., and Cole, M.R. (1995). Permian carbonates in the Dao Ruang#1 exploration well-implications for petroleum potential, Northeast Thailand. In **Proceeding of the International Conference On: Geology, Geotechnology and Mineral Resources of Indochina (pp 563-578)**. Khon Kaen Univ: Khon Kaen, Thailand.
- Chonglakmani, C., and Sattayarak, N. (1978). Stratigraphy of the Huai Hin Lat Formation (Upper Triassic) in Northeastern Thailand. In **Proceeding of the Third Regional Conference on Geology and Mineral Resources of Southeast Asia (pp. 739-762)**, Bangkok, Thailand.
- Chuaviroj, S. (1997). Deformation in Khorat Plateau, Thailand. In **proceedings of the international conference on stratigraphy and tectonic evaluation of Southeast Asia and the South Pacific (pp.321-325)**, Bangkok, Thailand.
- Donald, E.G., (1996). **Potash Deposits, Processing, Properties and Uses**. Great Britain: Chapman and Hall.
- Erb, W., (1989). **Leitfaden der Spektrometrie**. Heidelberg Berlin New York: Springer.
- Freeze, R.A. and Cherry, J.A., (1979). **Groundwater**. Englewood Cliffs, NJ: Prentice Hall Inc.

- Geological Survey Division (1999). **Geological map of Thailand**, scale 1:2,500,000, Department of Mineral Resource, Bangkok.
- Gupta, R.P. (1991). **Remote sensing geology**. New York: Springer Heidelberg Berlin.
- Haman, P.J., (1961). Lineament analysis on aerial photographs exemplified in the North Sturgeon Lake area, Alberta. **West Canadian Research Publication of Geology and related sciences**. 1:1-20.
- Hatcher, R.D. Jr, (1995). **Structural geology, principals, concepts and problems**. New Jersey:Prentice-Hall, Inc.
- Hite, R.J., (1971). Potential for potash and related mineral resources, Khorat Plateau, Northeast Thailand and central Laos. Unpublished. **U.S. Geol. Survey project report, (IR)EA-1**.
- Hite, R.J. and Japakasetr, T., (1979). Potash deposits of the Khorat Plateau. **Thailand and Laos, Econ. Geol. Vol. 74. No.2**. DMR: Bangkok, Thailand.
- Hite, R.J., (1982). Progress report on the potash deposits of the Khorat Plateau, Thailand. In **project report Thailand investigation (IR) TH-25**, U.S. Geological surveys open-file report 82-1096.
- Janardhana Raju, N., Reddy, T.V.K., (1998). Cases and solution: Fracture pattern and electrical resistivity studies for groundwater exploration [On-line]. India: Springer. Abstract from: FirstSearch File:Agricola Item: ISSN: 0943-0105.
- Japakasetr, T. and Suwanich, P., (1978). Potash and rock salt in Thailand. **Economic Geology Division (pp. A1-A252)**. DMR: Bangkok, Thailand.
- Japakasetr, T., (1985). Review on Rock Salt and Potash Exploration in Northeast Thailand. **Conference on Geology and Mineral Resources Development of the Northeast, Thailand (pp.135-147)**. Khon Kaen University: Khon Kaen.
- Japakasetr, T., and Workman, R. D., (1981). Evaporite deposition of Northeast Thailand. In **Michel T. Halbouty (ed.). Energy resources of Pacific region (pp 179-178)**. AAPG studies in Geology#12.
- Jantaranipa, W., Vongprommek, R., Sukko, T. and Preammanee, J., (1981). Application of enhance Landsat imagery to mineral resources of Loei province, Northeastern Thailand. In **Econ. Geol. Bulletin No. 30**, DMR. Bangkok.
- Khundee, S. (2001). The study of satellite image with structural geology with related to soil salinity and sinkhole in Northeast Thailand. **Annual meeting of geological surveys division (pp 138-146)**, Sept. DMR. Bangkok (in thai).

- Kuehn, F., King, T., Hoerig, B., and Peters, D., (2000). **Remote sensing for site characterization**. Germany: Springer.
- Lillesand, T.M. and Kiefer, R.W., (1987). **Remote Sensing and Image Interpretation**, 2nd Ed. New York: John Wiley & Sons.
- Metcalf, I. (1997). The palaeo-tethys and Palaeozoic-Mesozoic tectonic evolution of Southeast Asia. In **proceedings of the international conference on stratigraphy and tectonic evaluation of Southeast Asia and the South Pacific (pp.260-272)**, Bangkok, Thailand.
- Milsom, J. (1996). **Field Geophysics**. England: John Wiley & Sons.
- Mohamed, E.I.T., Cherdsak, U., Lee, C., and Warren, K., (1995). Cretaceous Saline Deposits of The Maha Sarakam Formation in The Khorat Basin, Northeastern Thailand. In **the workshop on Proceeding of the International Conference On: Geology, Geotechnology and Mineral Resources of Indochina**. Khon Kaen Univ: Khon Kaen, Thailand.
- Piyasin, S., (1995). The Hydrocarbon Potential of Khorat Plateau Intern. In **Proceeding of the International Conference On: Geology, Geotechnology and Mineral Resources of Indochina (pp 551-562)**. Khon Kaen Univ: Khon Kaen, Thailand.
- Pradidtan, S., (1995). Petroleum exploration in Northeast Thailand: The Revealed Results and Its Potential. In **Proceeding of the International Conference On: Geology, Geotechnology and Mineral Resources of Indochina (pp 589-600)**. Khon Kaen Univ: Khon Kaen, Thailand.
- Prost, G.L. (1994). **Remote sensing for geologists: A guide to image interpretation**. Amsterdam, The Netherlands: Gordon and Breach Science Publishers.
- Racey, A., Stokes, R.B., Lovatt-Smith, P., Love, M.A. (1997). Late Jurassic collision in Northeast Thailand and the significance of the Khorat Group. In **Proceedings of the international conference on stratigraphy and tectonic evaluation of Southeast Asia and the South Pacific (pp.412-413)**. Bangkok, Thailand.
- Sabins, F.F. (1987). **Remote sensing: principles and interpretation**, 2nd edition. New York: Freeman and Company.
- Sattayarak, N., (1983). Continental Mesozoic stratigraphy of Thailand. In **Conference on geology and mineral resource of Thailand**. Bangkok.
- Sattayarak, N., (1985). Review on Geology of Khorat Plateau. In **Conference on Geology and Mineral Resources Development of the Northeast, Thailand (pp.23-30)**. Khon Kaen Univ: Khon Kaen, Thailand.

- Sattayarak, N., and Polachan, S., (1990). Rock salt beneath the Khorat Plateau, In **Proc. Annual Tech. Meeting of DMR (pp.1-14)**. DMR: Bangkok, Thailand.
- Seni, S.J. and Jackson, M. P. A. (1983a). Evolution of salt structures, east Texas diapir province, Part I: Sedimentary record of halokinesis. **A.A.P.G. Bulletin**. V. 67: 1219-1244.
- Sharma, P.V. (1986). **Geophysical Methods in Geology**. New Jersey: Prentice-Hall.
- Sheldon, R.P. (1984). Phosphate resource assessment and exploration in Thailand, **Thai Department of Mineral Resource**. 1: 1-52.
- Solgosoom, S. (1999). Report on **“Geophysical Exploration to detect sinkhole in Ban Non Sabang, Sakhon Nakhon”**. Geophysical survey section. Department of Mineral Resources. Thailand (in thai).
- Suwanich, P., (1995). Nachuak Formation in Khorat Plateau. **In Proceeding of the International Conference On: Geology, Geotechnology and Mineral Resources of Indochina (pp 63-71)**. Khon Kaen Univ: Khon Kaen, Thailand.
- Teeuw, R.M., (1995). Groundwater exploration using remote sensing and a low-cost geographical information system [On-line]. UK: Springer. Abstract from: FirstSearch File:Agricola Item: ISSN: 0941-2816.
- Thanomsap, S. (1992). Structural developmenr on the Khorat Plateau and its western adjacent area. **In proceedings of the technology conference on development geology for Thailand into the year 2000 (pp 29-38)**. Department of Geology, Chulalongkorn Univ, Bangkok, Thailand.
- Wongsomsak, S. (1986). Salinity in Northeast Thailand. **Southeast Asian Studies, Vol.24** (pp 133-153), No. 2, September. Japan.
- Warren, J.K. (1989). **Evaporite sedimentology: Importance in Hydrocarbon accumulation**. New Jersey: Prentice Hall.
- Warren, J.K. (1999). **Evaporites: their evolution and economics**. Oxford. U.K: Blackwewll Science.
- Wentz, D., (1999). **Salinity Classification, Mapping and Management in Alberta** [On-line]. Available: <http://www.agric.gov.ab.ca/sustain/soil/salinity/>
- Yumuang, S., (1982). **Evaporite Deposits in the Maha Sarakam Formation, in Bamnet Narong area, Changwat Chaiyapum**. Dept. Geol., Graduate School, Chulalongkorn Univ.

APPENDIX A
LINEAMENT RAW DATA

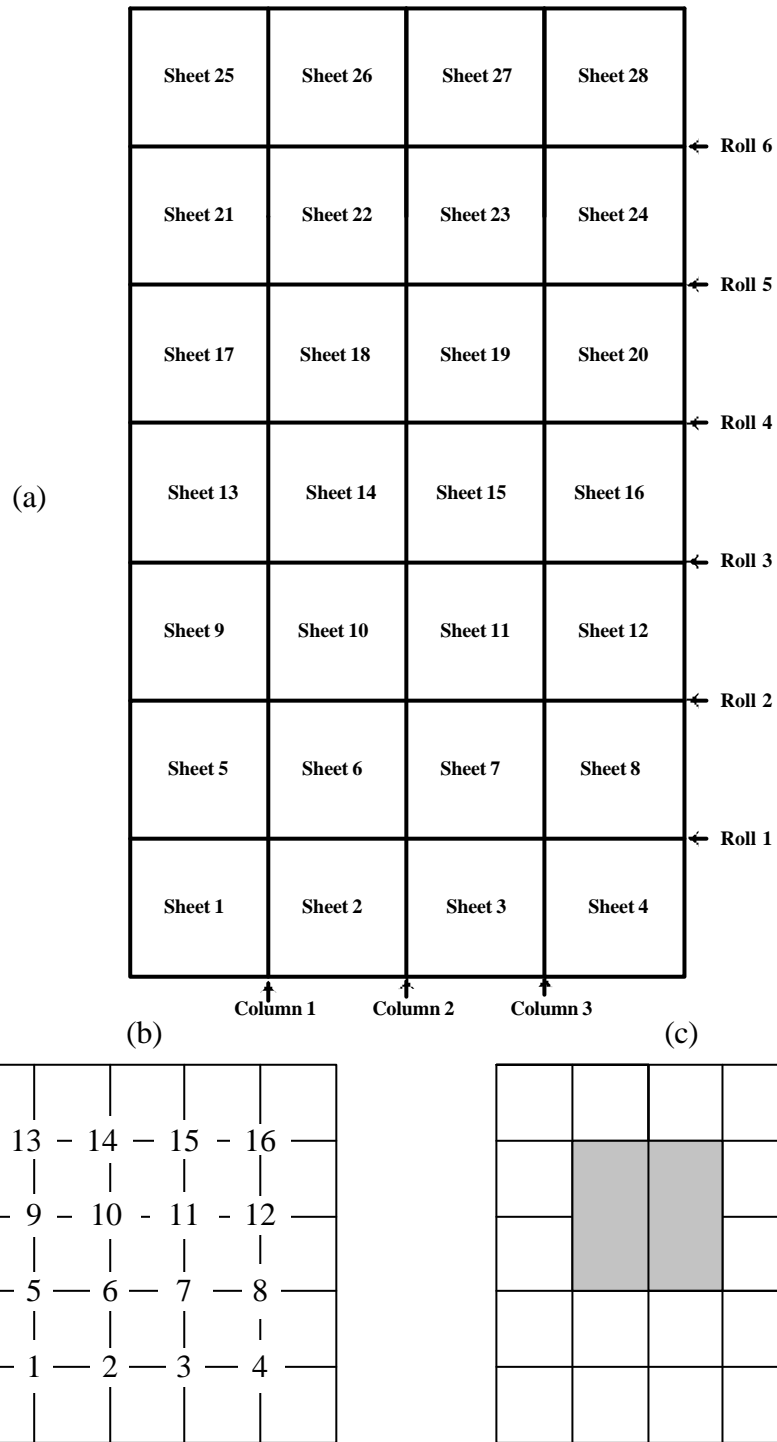


Figure A1. (a) Diagram showing the location of sheets, rolls and columns for lineament analysis. (b) The node location in 1 sheet area. (c) The area for counting the lineament and intersection (4 km^2) with 2 km overlapping in each side.

Table A1. Lineament raw data (length and intersection) in sheet 1.

Node No.	UTM E.	UTM N.	Intersection (point)	Major Lineament (Km.)	Minor Lineament (Km.)	Total distances (Km.)	Length density (Km/4 km ²)
1	212000	1702000	1	3.7	0.4	4.1	1.0
2	214000	1702000	4	2.4	3.4, 4.2	10	2.5
3	216000	1702000	7	0.9, 1.9	2.6, 3.0, 3.8, 4.4	16.6	4.2
4	218000	1702000	5	0.7, 0.8, 2.3	0.6, 1.2, 2.4, 2.8	11	2.8
5	212000	1704000	1	1.9, 2.4	0.6, 1.2, 2.6, 2.8	11.5	2.9
6	214000	1704000	5	0.2, 2.3	1.2, 1.2, 2.0, 4.2	14.9	3.7
7	216000	1704000	6	0.3, 1.4, 1.8	0.8, 1.2, 2.0, 3.8, 4.2	15.5	3.9
8	218000	1704000	3	0.3, 1.1, 1.5	0.6, 0.6, 1.0, 2.6	7.7	1.9
9	212000	1706000	0	0.5, 1.5	0	2	0.5
10	214000	1706000	7	2.3	2.0, 2.0, 3.4, 4.2,	13.9	3.5
11	216000	1706000	8	2.3	1.2, 1.8, 2.6, 3.4, 4.2, 4.4	19.9	5.0
12	218000	1706000	2	2.3	1.0, 1.4, 1.8, 2.4	8.9	2.2
13	212000	1708000	0	0.5	0	0.5	0.1
14	214000	1708000	3	0	2.0, 2.8, 4.2	9	2.3
15	216000	1708000	4	0.9	2.0, 2.8, 3.8, 4.4	13.9	3.5
16	218000	1708000	2	1.9	1.0, 1.2, 3.8, 4.0	11.9	3.0

Table A2. Lineament raw data (length and intersection) in sheet 2.

Node No.	UTM E.	UTM N.	Intersection (point)	Major Lineament (Km.)	Minor Lineament (Km.)	Total distances (Km.)	Length density (Km/4 km ²)
1	222000	1702000	8	4.2	1.4	5.6	1.4
2	224000	1702000	13	2.6	3.4, 4.2	10.2	2.6
3	226000	1702000	7	0.6, 1.2, 1.4	2.6, 3.0, 3.8, 4.4	17	4.3
4	228000	1702000	3	1.2, 3.4	0.6, 1.2, 2.4, 2.8	11.6	2.9
5	222000	1704000	5	0.2	0.6, 1.2, 2.6, 2.8	7.4	1.9
6	224000	1704000	7	0.6, 2.4	1.2, 1.2, 2.0, 4.2	11.6	2.9
7	226000	1704000	3	0.4, 0.6, 2.4, 2.4	0.8, 1.2, 2.0, 3.8, 4.2	15.2	3.8
8	228000	1704000	2	5	0.6, 0.6, 1.0, 2.6	9.8	2.5
9	222000	1706000	4	1.4	0	1.4	0.4
10	224000	1706000	2	2.6	2.0, 2.0, 3.4, 4.2	14.2	3.6
11	226000	1706000	1	2.0, 2.2, 2.4	1.2, 1.8, 2.6, 3.4, 4.2, 4.4	24.2	6.1
12	228000	1706000	0	1.2, 1.6, 3.4, 3.8	1.0, 1.4, 1.8, 2.4	16.6	4.2
13	222000	1708000	2	1.2, 1.4	0	2.6	0.7
14	224000	1708000	0	3.4	2.0, 2.8, 4.4	12.6	3.2
15	226000	1708000	0	1.6, 2.2, 2.8	2.0, 2.8, 3.8, 4.4	19.6	4.9
16	228000	1708000	0	1.2, 3.0, 4.2	1.0, 1.2, 3.8, 4.0	18.4	4.6

Table A3. Lineament raw data (length and intersection) in sheet 3.

Node No.	UTM E.	UTM N.	Intersection (point)	Major Lineament (Km.)	Minor Lineament (Km.)	Total distances (Km.)	Length density (Km/4 km ²)
1	232000	1702000	5	1.0, 2.4, 3.2, 4.4	0.2, 0.6, 1.8, 2.6	16.2	4.1
2	234000	1702000	0	4.2, 4.6	0.2	9	2.3
3	236000	1702000	0	2.6, 4.4	1.0, 1.6	9.6	2.4
4	238000	1702000	2	3	1.4, 3.4, 4.2	12	3.0
5	232000	1704000	4	1.6, 2.6, 2.6	2.0, 3.2, 3.8	15.8	4.0
6	234000	1704000	0	1.2, 4.4, 4.4	1.0, 2.4	13.2	3.3
7	236000	1704000	1	1.2, 4.4, 4.4	0.8, 2.4	13.2	3.3
8	238000	1704000	4	3.4, 4.6	0.6, 1.2, 2.4, 4.0	16.2	4.1
9	232000	1706000	1	0.2, 4.0	0.4, 0.8, 2.4, 5.0	12.8	3.2
10	234000	1706000	0	4.4	0.8, 2.2, 3.6	11	2.8
11	236000	1706000	1	0.2, 4.4	1.6, 2.8	13.2	3.3
12	238000	1706000	3	0.4, 4.0	3.4, 5.2	13	3.3
13	232000	1708000	1	0.8	0.4, 2.2, 2.4, 2.6, 2.6	11	2.8
14	234000	1708000	0	0	1.4, 3.6	5	1.3
15	236000	1708000	0	0	0.2, 0.2, 1.6	2	0.5
16	238000	1708000	0	1	0.2, 0.8, 2.8	3.8	1.0

Table A4. Lineament raw data (length and intersection) in sheet 4.

Node No.	UTM E.	UTM N.	Intersection (point)	Major Lineament (Km.)	Minor Lineament (Km.)	Total distances (Km.)	Length density (Km/4 km ²)
1	242000	1702000	0	0	2	2	0.5
2	244000	1702000	0	0	0	0	0.0
3	246000	1702000	0	0	0	0	0.0
4	248000	1702000	0	0	0	0	0.0
5	242000	1704000	0	0	2.4	2.4	0.6
6	244000	1704000	0	0	1	1	0.3
7	246000	1704000	0	0	2.2	2.2	0.6
8	248000	1704000	0	0	1.2	1.2	0.3
9	242000	1706000	0	0.2	0.2, 1.6	2	0.5
10	244000	1706000	0	0	1	1	0.3
11	246000	1706000	0	0	3.6	3.6	0.9
12	248000	1706000	1	0	0.6, 4.8	5.4	1.4
13	242000	1708000	0	0	1.8	1.8	0.5
14	244000	1708000	0	0	0	0	0.0
15	246000	1708000	0	0	1.4	1.4	0.4
16	248000	1708000	1	0	1.4, 2.0, 4.0	7.4	1.9

Table A5. Lineament raw data (length and intersection) in sheet 5

Node No.	UTM E.	UTM N.	Intersection (point)	Major Lineament (Km.)	Minor Lineament (Km.)	Total distances (Km.)	Length density (Km/4 km ²)
1	212000	1712000	1	1.8	0.6, 2.4, 3.6	8.4	2.1
2	214000	1714000	0	0.2	1.2, 1.8, 2.2, 4.8	9.2	2.3
3	216000	1716000	5	1.0, 3.6	4.0, 4.4, 5.0	18	4.5
4	218000	1718000	4	3.0, 3.6	2.2, 4.2, 4.4	17.4	4.4
5	212000	1712000	0	0	2.0, 3.0, 4.2	9.2	2.3
6	214000	1714000	1	1.0, 2.4	1.8, 4.0, 5.2	14.4	3.6
7	216000	1716000	4	1.2, 3.6, 4.4	0.6, 1.0, 4.0, 4.0	18.8	4.7
8	218000	1718000	4	0.2, 4.2, 4.8	0.2, 0.6, 1.0, 4.2	15.2	3.8
9	212000	1712000	0	0.2	1.2, 1.6, 4.4	7.4	1.9
10	214000	1714000	0	2.2, 3.6	0.2, 1.2, 3.2	10.4	2.6
11	216000	1716000	0	1.0, 3.8, 4.4	0.4, 0.6, 1.2, 1.4	12.8	3.2
12	218000	1718000	6	0.2, 3.6, 4.4	2.8, 3.4, 3.6	18	4.5
13	212000	1712000	1	0	1.2, 3.2, 3.2	7.6	1.9
14	214000	1714000	1	3.4	1.4, 3.2, 3.2	11.2	2.8
15	216000	1716000	0	3.4	0.4, 0.6, 0.8, 4.6	9.8	2.5
16	218000	1718000	5	1.2	1.2, 2.6, 3.6, 4.8	13.4	3.4

Table A6. Lineament raw data (length and intersection) in sheet 6.

Node No.	UTM E.	UTM N.	Intersection (point)	Major Lineament (Km.)	Minor Lineament (Km.)	Total distances (Km.)	Length density (Km/4 km ²)
1	222000	1712000	1	2.8, 4.6	0.4, 2.6	10.4	2.6
2	224000	1714000	1	0.2, 0.4, 5.0	1.0, 1.4, 1.6	9.6	2.4
3	226000	1716000	1	2.8, 3.0	0.6, 3.8	10.2	2.6
4	228000	1718000	1	0.6, 3.8	2.4	6.8	1.7
5	222000	1712000	0	0.4, 0.8, 1.2	0.6, 3.6	6.6	1.7
6	224000	1714000	2	2.6, 3.4	3.4, 5.0	14.4	3.6
7	226000	1716000	2	4.2, 4.4	2.4, 4.0	15	3.8
8	228000	1718000	0	0.2, 1.4, 4.4	1	7	1.8
9	222000	1712000	1	0.4, 1.2	0.8, 2.4, 4.2	9	2.3
10	224000	1714000	3	1.8, 2.6	1.6, 2.2, 3.2, 3.4	14.8	3.7
11	226000	1716000	2	1.2, 2.0, 4.4	1.2, 2.4, 4.8	10.8	2.7
12	228000	1718000	1	1.4, 2.6, 4.4	0.4, 2.8	11.6	2.9
13	222000	1712000	2	0	2.4, 4.2, 4.6	11.2	2.8
14	224000	1714000	1	2.8	0.2, 1.4, 3.2	7.6	1.9
15	226000	1716000	0	2.6, 3.2	0.2, 1.2, 1.6	8.8	2.2
16	228000	1718000	1	0.4, 1.2, 3.4, 5.0	0.4, 1.6	12	3.0

Table A7 Lineament raw data (length and intersection) in sheet 7.

Node No.	UTM E.	UTM N.	Intersection (point)	Major Lineament (Km.)	Minor Lineament (Km.)	Total distances (Km.)	Length density (Km/4 km ²)
1	232000	1712000	0	0.2, 1.0	1.2, 3.4	5.8	1.5
2	234000	1714000	5	3.2	1.6, 1.8, 2.2, 2.2, 4.2	15.2	3.8
3	236000	1716000	8	5.4	1.6, 2.8, 4.2, 4.4	12.2	3.1
4	238000	1718000	3	3	0.4, 1.6, 2.2, 3.0	10.2	2.6
5	232000	1712000	2	0.4, 2.0, 3.2	1.2, 1.4	8.2	2.1
6	234000	1714000	6	2.2, 4.2, 5.2	1.0, 1.2, 1.4, 1.6, 2.6	19.4	4.9
7	236000	1716000	6	2.0, 3.0, 4.4	1.0, 3.2, 4.0	17.2	4.3
8	238000	1718000	1	4	1.4, 4.6	10	2.5
9	232000	1712000	4	2.0, 5.2	3.4, 3.6	14.2	3.6
10	234000	1714000	5	2.4, 3.0, 4.2, 4.2	0.6, 1.0	15.4	3.9
11	236000	1716000	4	2.2, 2.8, 4.4, 4.4	1.0, 1.6	16.4	4.1
12	238000	1718000	3	0.4, 2.0, 4.2, 4.2	0.4, 4.0	15.2	3.8
13	232000	1712000	5	0.2, 2.4, 4.2	0.8, 4.2, 4.6	16.4	4.1
14	234000	1714000	3	1.4, 4.2, 4.6	0.6, 2.6, 2.8	16.2	4.1
15	236000	1716000	2	3.0, 3.6, 4.2	0.6, 0.6, 2.0	14	3.5
16	238000	1718000	2	0.6, 2.4, 4.2	0.8, 2.6	10.6	2.7

Table A8. Lineament raw data (length and intersection) in sheet 8.

Node No.	UTM E.	UTM N.	Intersection (point)	Major Lineament (Km.)	Minor Lineament (Km.)	Total distances (Km.)	Length density (Km/4 km ²)
1	242000	1712000	1	3.4	1.2	4.6	1.2
2	244000	1714000	0	3.8	0	3.8	1.0
3	246000	1716000	0	1.6	2	3.6	0.9
4	248000	1718000	0	0	4.4	4.4	1.1
5	242000	1712000	1	4.4	4	4.8	1.2
6	244000	1714000	0	3.8	0.4, 2.4	6.6	1.7
7	246000	1716000	1	1.2, 1.6	1.6, 2.6	7	1.8
8	248000	1718000	1	1.2	0.2, 1.6, 2.4	5.4	1.4
9	242000	1712000	2	0.6, 4.4	0.4, 0.6, 4.4	10.4	2.6
10	244000	1714000	2	1.4, 4.4	2.0, 4.2	11	2.8
11	246000	1716000	2	1.4, 4.4	1.6, 3.6	11	2.8
12	248000	1718000	1	2.8	0.2, 4.6	7.6	1.9
13	242000	1712000	1	3.2, 4.4	0.4, 1.4	9.4	2.4
14	244000	1714000	3	0.8, 3.0, 4.2	1.6, 1.6	11.2	2.8
15	246000	1716000	2	0.8, 2.0, 3.0	1	6.8	1.7
16	248000	1718000	0	0.2, 1.6	1.5	3.3	0.8

Table A9. Lineament raw data (length and intersection) in sheet 9.

Node No.	UTM E.	UTM N.	Intersection (point)	Major Lineament (Km.)	Minor Lineament (Km.)	Total distances (Km.)	Length density (Km/4 km ²)
1	212000	1722000	1	2.8	4.2, 2.0	9	2.3
2	214000	1724000	2	1.4	1.4, 1.6, 3.2, 4.2	11.8	3.0
3	216000	1726000	3	0	1.4, 1.6, 3.2, 3.6, 3.8	13.6	3.4
4	218000	1728000	3	0	1.0, 2.2, 4.2, 4.2, 4.4	16	4.0
5	212000	1722000	1	4.4	2.8, 3.8	10.2	2.6
6	214000	1724000	1	4.2	0.2, 0.4, 1.4, 2.8	9	2.3
7	216000	1726000	1	4.4	1.4, 1.8, 2.2	9.2	2.3
8	218000	1728000	2	4.4	1.2, 4.0, 4.4	14	3.5
9	212000	1722000	1	0.6	0.6, 4.2, 4.4	9.8	2.5
10	214000	1724000	1	2.2	0.6, 0.8, 3.2, 4.2	11	2.8
11	216000	1726000	1	4.4	0.8, 1.1, 3.4, 4.3	14	3.5
12	218000	1728000	1	4.4	3.0, 4.2, 4.3	15.9	4.0
13	212000	1722000	0	0	0.9, 4.2	5.1	1.3
14	214000	1724000	0	0	0.7, 1.7, 4.2	6.6	1.7
15	216000	1726000	1	0	0.7, 2.0, 3.4, 4.2	10.3	2.6
16	218000	1728000	1	0	3.0, 4.3, 5.0	12.3	3.1

Table A10. Lineament raw data (length and intersection) in sheet 10.

Node No.	UTM E.	UTM N.	Intersection (point)	Major Lineament (Km.)	Minor Lineament (Km.)	Total distances (Km.)	Length density (Km/4 km ²)
1	222000	1722000	2	0	0.5, 1.7, 2.0, 2.7, 4.0	10.9	2.7
2	224000	1724000	1	2.1	0.9, 1.2, 4.2	8.4	2.1
3	226000	1726000	2	1.0, 1.5, 2.6	2.3, 4.1	11.5	2.9
4	228000	1728000	4	0.7, 0.8, 1.5, 3.0	0.4, 1.9, 4.6	12.9	3.2
5	222000	1722000	0	2.8	0.2, 1.7, 4.8	9.5	2.4
6	224000	1724000	0	0.8, 1.8	3.2	5.8	1.5
7	226000	1726000	1	0.2, 0.5	0.4, 2.7	3.8	1.0
8	228000	1728000	3	0.2, 0.6, 1.2, 3.6	0.4, 4.6	10.6	2.7
9	222000	1722000	1	1.8, 2.8	1.5, 1.6, 4.2	11.9	3.0
10	224000	1724000	1	0.7, 1.8	0.2, 2.9, 2.2	7.8	2.0
11	226000	1726000	0	0.2, 0.3, 2.4	0.1, 0.4, 0.8	4.2	1.1
12	228000	1728000	1	0.1, 1.2, 2.4, 5.0	0	8.7	2.2
13	222000	1722000	2	2.0, 4.2	0.7, 1.5, 2.0, 4.2	14.6	3.7
14	224000	1724000	1	0.2, 2.6	2.2, 2.7, 2.9	10.6	2.7
15	226000	1726000	1	3.4	0.4, 4.2	8	2.0
16	228000	1728000	2	2.4, 3.0, 3.4	3.4	12.2	3.1

Table A11. Lineament raw data (length and intersection) in sheet 11.

Node No.	UTM E.	UTM N.	Intersection (point)	Major Lineament (Km.)	Minor Lineament (Km.)	Total distances (Km.)	Length density (Km/4 km ²)
1	232000	1722000	2	5	0.4, 2.0, 2.0, 4.2	13.6	3.4
2	234000	1724000	1	3.2	0.6, 4.2, 4.6	9.4	2.4
3	236000	1726000	1	0.8, 2.8, 4.2	0.6, 0.6, 1.2, 2.4	12.6	3.2
4	238000	1728000	2	4	1.3, 1.4, 2.2, 3.6	12.5	3.1
5	232000	1722000	1	1.4, 1.8, 3.8	2.0, 3.2, 3.8	16	4.0
6	234000	1724000	4	4.4	3.2, 3.8, 4.2	15.6	3.9
7	236000	1726000	3	4.4	0.1, 0.2, 1.4, 1.6, 2.0, 2.2	11.9	3.0
8	238000	1728000	3	1.6	3.4, 4.0, 4.3	13.3	3.3
9	232000	1722000	3	0.2, 2.6, 3.6, 4.4	0.2, 0.6, 1.2, 2.0, 2.2, 2.8	19.8	5.0
10	234000	1724000	7	0.1, 3.4, 4.2	0.1, 0.2, 0.2, 0.6, 1.6, 3.4, 3.8	17.6	4.4
11	236000	1726000	6	2.6, 3.4	0.8, 1.4, 1.5, 2.0, 2.4	14.1	3.5
12	238000	1728000	5	1.2, 1.4	0.6, 4.0, 4.4, 4.4	16	4.0
13	232000	1722000	2	0.1, 0.6, 0.8, 1.2, 2.6, 4.2	0.4, 0.8, 2.4	13.1	3.3
14	234000	1724000	4	0.1, 1.2, 2.2, 4.4	0.6, 3.1, 3.8	15.4	3.9
15	236000	1726000	7	0.2, 3.4, 4.2	0.2, 1.4, 1.7, 2.3, 3.2, 4.0	20.6	5.2
16	238000	1728000	5	1.2, 4.2	0.4, 1.0, 1.4, 2.8, 3.2, 4.2	18.4	4.6

Table A12. Lineament raw data (length and intersection) in sheet 12.

Node No.	UTM E.	UTM N.	Intersection (point)	Major Lineament (Km.)	Minor Lineament (Km.)	Total distances (Km.)	Length density (Km/4 km ²)
1	242000	1722000	1	2.1	1.4, 2.6, 3.8	9.9	2.5
2	244000	1724000	2	0.6, 1.2, 2.0, 4.6	1.4, 4.4	14.2	3.6
3	246000	1726000	3	2.8, 2.9, 3.6, 4.6	2.1	16	4.0
4	248000	1728000	1	0.4, 0.8, 2.2, 4.2, 5.0	0	12.6	3.2
5	242000	1722000	2	0.1	2.1, 2.4, 3.4	8.1	2.0
6	244000	1724000	2	1.5	0.4, 1.8, 2.0, 4.0	9.7	2.4
7	246000	1726000	2	1.7, 3.3	5.3	10.3	2.6
8	248000	1728000	1	1.8, 4.6	2.6	9	2.3
9	242000	1722000	1	2.6	1.0, 2.0, 4.0	9.6	2.4
10	244000	1724000	1	0.1	0.4, 4.8	5.3	1.3
11	246000	1726000	0	0.1	0.9, 2.4, 3.2	6.6	1.7
12	248000	1728000	0	0.2, 1.2	2.4, 2.4	6.2	1.6
13	242000	1722000	3	2.2, 4.4, 5.2	2.4, 1.4	15.6	3.9
14	244000	1724000	3	2.0, 4.5	2.6, 3.1	12.2	3.1
15	246000	1726000	2	3	1.4, 5.0	9.4	2.4
16	248000	1728000	0	0.7, 1.4	0.1, 2.4	4.6	1.2

Table A13. Lineament raw data (length and intersection) in sheet 13.

Node No.	UTM E.	UTM N.	Intersection (point)	Major Lineament (Km.)	Minor Lineament (Km.)	Total distances (Km.)	Length density (Km/4 km ²)
1	212000	1732000	1	4.4	1.5, 3.2	9.1	2.3
2	214000	1734000	1	4.3	0.8, 1.2, 4.0	10.3	2.6
3	216000	1736000	1	3	1.4, 3.2	7.6	1.9
4	218000	1738000	1	0.8, 3.2	4.6	8.6	2.2
5	212000	1732000	1	0	0.4, 0.8, 2.1, 3.4	6.7	1.7
6	214000	1734000	1	0	1.8, 4.3, 4.3	10.4	2.6
7	216000	1736000	1	2.2	1.1, 1.4, 4.4	9	2.3
8	218000	1738000	2	5.2	1.5, 1.6, 2.2, 2.6	9.1	2.3
9	212000	1732000	1	0	4.0, 4.2, 4.3	12.5	3.1
10	214000	1734000	1	1.0, 1.3	2.2, 4.1, 4.3	12.9	3.2
11	216000	1736000	2	1.3, 4.8	3.8, 4.0	13.9	3.5
12	218000	1738000	2	4	1.0, 2.6	7.6	1.9
13	212000	1732000	0	0	1.0, 2.6	3.6	0.9
14	214000	1734000	1	2.0, 3.6	1.0, 4.2	10.8	2.7
15	216000	1736000	2	4.4, 5.0	1.0, 4.4	14.8	3.7
16	218000	1738000	2	1.6, 3.8	1.4, 3.8	10.6	2.7

Table A14. Lineament raw data (length and intersection) in sheet 14.

Node No.	UTM E.	UTM N.	Intersection (point)	Major Lineament (Km.)	Minor Lineament (Km.)	Total distances (Km.)	Length density (Km/4 km ²)
1	222000	1732000	1	0.1, 1.4, 1.8, 3.9	3.6	10.8	2.7
2	224000	1734000	0	3.6	0.4, 1.0, 2.2	7.2	1.8
3	226000	1736000	0	0.4, 4.8	1.0, 1.4	7.6	1.9
4	228000	1738000	0	2.4, 3.1	0	5.5	1.4
5	222000	1732000	1	0.5, 4.2	0.3, 2.0, 3.5	10.5	2.6
6	224000	1734000	1	3	3.4, 3.6	10	2.5
7	226000	1736000	0	4.6	0.6, 1.6	6.8	1.7
8	228000	1738000	1	4.4	2.2	6.6	1.7
9	222000	1732000	2	2.0, 4.2	0.4, 2.2, 2.6, 2.6	14	3.5
10	224000	1734000	2	2	2.8, 2.8, 5.1	12.7	3.2
11	226000	1736000	1	2	0.5, 1.7, 3.0, 3.1	10.3	2.6
12	228000	1738000	2	1.4, 1.8, 4.0	0.8, 4.4	12.4	3.1
13	222000	1732000	3	0.8, 2.4, 4.2, 5.0	0.4, 3.4, 3.6	19.8	5.0
14	224000	1734000	3	2.6, 3.1, 4.6	0.5, 2.0, 4.6	17.4	4.4
15	226000	1736000	1	3.2, 4.6	1.6, 2.2, 3.2	14.8	3.7
16	228000	1738000	1	1.2, 1.4, 4.2	0.4, 1.6	8.8	2.2

Table A15. Lineament raw data (length and intersection) in sheet 15.

Node No.	UTM E.	UTM N.	Intersection (point)	Major Lineament (Km.)	Minor Lineament (Km.)	Total distances (Km.)	Length density (Km/4 km ²)
1	232000	1732000	2	1.0, 2.4, 3.6	1.2	8.2	2.1
2	234000	1734000	1	0.4, 2.8	1.0, 1.6, 2.2	8	2.0
3	236000	1736000	1	1.2	0.6, 1.0, 2.6, 3.4, 4.2	13	3.3
4	238000	1738000	5	3.2	0.6, 0.9, 1.0, 1.1, 1.4, 1.8, 2.5, 2.6, 2.6	16.6	4.2
5	232000	1732000	2	1.0, 2.4, 2.6	0.2, 2.4	8.6	2.2
6	234000	1734000	0	1	1.0, 1.1	3.1	0.8
7	236000	1736000	0	1.2	0.4, 0.8, 3.8	6.2	1.6
8	238000	1738000	3	3.4	0.4, 1.4, 4.2, 4.4	13.8	3.5
9	232000	1732000	1	1.2, 1.4, 2.2, 3.4	0.2, 0.6	9	2.3
10	234000	1734000	0	0.1, 3.6	2.6	6.3	1.6
11	236000	1736000	0	0.1, 1.4	1.2, 4.8	7.5	1.9
12	238000	1738000	1	0	2.8, 3.4, 4.1	10.3	2.6
13	232000	1732000	0	1.2, 3.3, 4.8	0	9.3	2.3
14	234000	1734000	0	0.1, 3.4, 3.6	1.4	8.5	2.1
15	236000	1736000	0	1.0, 1.4, 2.6, 4.6	4	13.6	3.4
16	238000	1738000	1	4.6	0.8, 1.4, 2.9	9.7	2.4

Table A16. Lineament raw data (length and intersection) in sheet 16.

Node No.	UTM E.	UTM N.	Intersection (point)	Major Lineament (Km.)	Minor Lineament (Km.)	Total distances (Km.)	Length density (Km/4 km ²)
1	242000	1732000	4	3.6, 4.2	1.0, 1.6, 1.6, 3.9, 4.3	20.2	5.1
2	244000	1734000	5	4.4, 5.4	1.4, 4.8	16	4.0
3	246000	1736000	2	3.0, 4.4	0.7, 1.2, 2.8	12.1	3.0
4	248000	1738000	0	2.3	0.6, 4.0	6.9	1.7
5	242000	1732000	3	0.1, 4.2	4.0, 4.6	12.9	3.2
6	244000	1734000	2	3.1, 4.4	1.0, 1.6, 2.7	12.8	3.2
7	246000	1736000	1	4.0, 5.7	1.4	11.1	2.8
8	248000	1738000	0	1.0, 3.1	0.9	5	1.3
9	242000	1732000	1	0	1.0, 1.3, 1.7, 2.9	6.9	1.7
10	244000	1734000	1	0.1	0.1, 0.4, 1.1, 2.0, 3.4	7.1	1.8
11	246000	1736000	2	2.8	0.6, 2.0, 4.9	10.3	2.6
12	248000	1738000	1	2.9	1.4, 2.6	6.9	1.7
13	242000	1732000	0	0	1.9, 3.0, 3.4	8.3	2.1
14	244000	1734000	1	0	0.2, 4.0, 4.8	9	2.3
15	246000	1736000	2	0	3.4, 3.5, 3.6	10.5	2.6
16	248000	1738000	1	1.2	1.0, 1.4, 2.4	6	1.5

Table A17. Lineament raw data (length and intersection) in sheet 17.

Node No.	UTM E.	UTM N.	Intersection (point)	Major Lineament (Km.)	Minor Lineament (Km.)	Total distances (Km.)	Length density (Km/4 km ²)
1	212000	1742000	0	5	0	5	1.3
2	214000	1744000	0	3.6	0	3.6	0.9
3	216000	1746000	0	0.2	0	0.2	0.1
4	218000	1748000	0	3	0.8	3.8	1.0
5	212000	1742000	0	2.4	0	2.4	0.6
6	214000	1744000	0	1	3.8	4.8	1.2
7	216000	1746000	0	0	4.3	4.3	1.1
8	218000	1748000	0	2	4.2	6.2	1.6
9	212000	1742000	0	0.1	1.0, 1.2, 1.6	3.9	1.0
10	214000	1744000	0	0	3.6	3.6	0.9
11	216000	1746000	0	0	4.2	4.2	1.1
12	218000	1748000	0	0	2.5	2.5	0.6
13	212000	1742000	0	0	4.0, 4.8	8.8	2.2
14	214000	1744000	0	0	2.4	2.4	0.6
15	216000	1746000	0	0	0	0	0.0
16	218000	1748000	0	0	0.8	0.8	0.2

Table A18. Lineament raw data (length and intersection) in sheet 18.

Node No.	UTM E.	UTM N.	Intersection (point)	Major Lineament (Km.)	Minor Lineament (Km.)	Total distances (Km.)	Length density (Km/4 km ²)
1	222000	1742000	1	1.2, 2.0	0	3.2	0.8
2	224000	1744000	0	0	1	1	0.3
3	226000	1746000	0	0.3	0.5, 1.2, 3.2	5.2	1.3
4	228000	1748000	1	0	2.2, 2.4, 4.0	8.6	2.2
5	222000	1742000	0	3.7	1.2	4.9	1.2
6	224000	1744000	0	3.6	1.0, 1.1	5.7	1.4
7	226000	1746000	0	1.2	0.5, 3.2	4.9	1.2
8	228000	1748000	0	0	2.2, 4.0	6.2	1.6
9	222000	1742000	0	3.7	2.0, 3.7	9.4	2.4
10	224000	1744000	0	4.6	3.7	8.3	2.1
11	226000	1746000	0	1.4, 3.0	0	4.4	1.1
12	228000	1748000	0	2.2	0.2	2.4	0.6
13	222000	1742000	0	0.1	2.8, 4.4	7.3	1.8
14	224000	1744000	0	0.1, 0.5, 1.4	1.3, 4.0	7.3	1.8
15	226000	1746000	0	0.1, 0.8, 3.8	0.3, 1.0	6	1.5
16	228000	1748000	0	0.1, 5.0	0.3	5.4	1.4

Table A19. Lineament raw data (length and intersection) in sheet 19.

Node No.	UTM E.	UTM N.	Intersection (point)	Major Lineament (Km.)	Minor Lineament (Km.)	Total distances (Km.)	Length density (Km/4 km ²)
1	232000	1742000	1	4.4	1.5, 1.6, 2.4, 4.0	13.9	3.5
2	234000	1744000	0	1.4, 4.5	1.2, 1.7	8.8	2.2
3	236000	1746000	0	2.0, 2.4	1.4	5.8	1.5
4	238000	1748000	0	0.1, 0.4	3.4	3.9	1.0
5	232000	1742000	2	0.1	0.3, 1.8, 2.4, 3.8, 5.0	13.4	3.4
6	234000	1744000	2	2.4	0.3, 1.0, 1.7, 2.3, 3.8	11.5	2.9
7	236000	1746000	0	0.5, 4.4	1.4	6.3	1.6
8	238000	1748000	0	0.1, 3.2	3.4	6.7	1.7
9	232000	1742000	4	0.1, 2.9	1.8, 2.2, 2.4, 2.4, 2.6, 2.8	17.2	4.3
10	234000	1744000	3	1.6, 2.4, 2.8	1.0, 1.5, 2.3, 2.4, 2.7	16.7	4.2
11	236000	1746000	0	3.6, 4.5	0	7.1	1.8
12	238000	1748000	0	2.0, 4.2	0	6.2	1.6
13	232000	1742000	3	0.5, 1.5, 2.2, 2.8	2.4, 3.1	12.5	3.1
14	234000	1744000	3	1.6, 2.5, 3.8	1.3, 1.6, 3.0	13.8	3.5
15	236000	1746000	1	0.2, 2.4, 4.0	1.6	8.2	2.1
16	238000	1748000	0	1.0, 2.0, 2.2	0	5.2	1.3

Table A20. Lineament raw data (length and intersection) in sheet 20.

Node No.	UTM E.	UTM N.	Intersection (point)	Major Lineament (Km.)	Minor Lineament (Km.)	Total distances (Km.)	Length density (Km/4 km ²)
1	242000	1742000	1	5	0.1, 1.6, 1.8	8.5	2.1
2	244000	1744000	0	2	1.2, 2.2	5.4	1.4
3	246000	1746000	0	3	4.3	7.3	1.8
4	248000	1748000	1	5	3.4	8.4	2.1
5	242000	1742000	0	2.2	0.8	3	0.8
6	244000	1744000	0	2.0, 2.2	0	4.2	1.1
7	246000	1746000	0	5	0	5	1.3
8	248000	1748000	0	3	0	3	0.8
9	242000	1742000	0	0.5	0	0.5	0.1
10	244000	1744000	0	2.6	0	2.6	0.7
11	246000	1746000	0	0.5	0	0.5	0.1
12	248000	1748000	0	0.5	0.1	0.6	0.2
13	242000	1742000	0	0.5	0	0.5	0.1
14	244000	1744000	0	0.8	0.2	1	0.3
15	246000	1746000	1	0.8, 1.4	2.9	5.2	1.3
16	248000	1748000	1	4	2.8	6.8	1.7

Table A21. Lineament raw data (length and intersection) in sheet 21.

Node No.	UTM E.	UTM N.	Intersection (point)	Major Lineament (Km.)	Minor Lineament (Km.)	Total distances (Km.)	Length density (Km/4 km ²)
1	212000	1752000	0	0	4.2	4.2	1.1
2	214000	1754000	0	0	0.3, 1.6	1.9	0.5
3	216000	1756000	0	0	0	0	0.0
4	218000	1758000	0	0	0	0	0.0
5	212000	1752000	0	0	3.2	3.2	0.8
6	214000	1754000	0	0	0.8	0.8	0.2
7	216000	1756000	0	0.2	0	0.2	0.1
8	218000	1758000	0	0.2	0	0.2	0.1
9	212000	1752000	0	0	0.1, 0.8	0.9	0.2
10	214000	1754000	0	0	0.8, 2.4	3.2	0.8
11	216000	1756000	0	0.8	3	3.8	1.0
12	218000	1758000	0	2.8	0.5	3.2	0.8
13	212000	1752000	0	0	4.6	4.6	1.2
14	214000	1754000	0	0	4.7	4.7	1.2
15	216000	1756000	0	0.7	3	3.7	0.9
16	218000	1758000	0	4	0.5	4.5	1.1

Table A22. Lineament raw data (length and intersection) in sheet 22.

Node No.	UTM E.	UTM N.	Intersection (point)	Major Lineament (Km.)	Minor Lineament (Km.)	Total distances (Km.)	Length density (Km/4 km ²)
1	222000	1752000	0	0.1, 0.5	0	0.6	0.2
2	224000	1754000	0	3.6	0	3.6	0.9
3	226000	1756000	0	1.6, 4.0	0	5.6	1.4
4	228000	1758000	0	2.2	3.4, 4.0	9.6	2.4
5	222000	1752000	0	2.6	0	2.6	0.7
6	224000	1754000	0	0.7, 0.8	0	1.5	0.4
7	226000	1756000	0	1.4, 2.8	0	4.2	1.1
8	228000	1758000	0	0.5, 2.8	1.2, 2.0	6.5	1.6
9	222000	1752000	0	5	0.6	5.6	1.4
10	224000	1754000	0	3.2	0	3.2	0.8
11	226000	1756000	0	3.4	0	3.4	0.9
12	228000	1758000	0	4.5	0	4.5	1.1
13	222000	1752000	0	1.2, 2.6	3.3	7.1	1.8
14	224000	1754000	0	0.4, 4.5	1.2	6.1	1.5
15	226000	1756000	0	0.4, 0.8, 1.4	0	2.6	0.7
16	228000	1758000	0	4.6	0	4.6	1.2

Table A23. Lineament raw data (length and intersection) in sheet 23.

Node No.	UTM E.	UTM N.	Intersection (point)	Major Lineament (Km.)	Minor Lineament (Km.)	Total distances (Km.)	Length density (Km/4 km ²)
1	232000	1752000	1	0.6, 3.0, 3.4, 5.0	0.8, 0.8, 1.0	14.6	3.7
2	234000	1754000	1	0.4, 2.8	1.8, 3.2	8.2	2.1
3	236000	1756000	0	3.2	1.1, 2.3, 3.6	10.2	2.6
4	238000	1758000	0	1.6, 1.6, 2.6	1.0, 1.0	7.8	2.0
5	232000	1752000	1	0.8, 1.2, 2.2, 2.4, 3.2	0.8, 2.4, 3.7	16.7	4.2
6	234000	1754000	1	0.8, 1.2, 2.3, 2.6	3.2	10.1	2.5
7	236000	1756000	1	1.6	1.0, 1.8, 3.5	7.9	2.0
8	238000	1758000	2	1.6, 1.9	1.2, 1.8, 3.2	9.7	2.4
9	232000	1752000	0	0.7, 1.6, 2.2, 2.2, 3.4	1.9, 2.2, 3.0	17.2	4.3
10	234000	1754000	0	0.7, 2.2, 2.2, 3.4	0.8	9.3	2.3
11	236000	1756000	1	2	4	6	1.5
12	238000	1758000	3	1.0, 4.6	2.0, 2.6	10.2	2.6
13	232000	1752000	0	2.4, 4.0, 4.4	0.7, 4.2	15.7	3.9
14	234000	1754000	1	1.7, 2.6, 4.6	0.7, 1.2, 2.6	13.4	3.4
15	236000	1756000	1	0.5, 1.9	0.8, 4.0	7.2	1.8
16	238000	1758000	1	3.2, 4.0	0.9	8.1	2.0

Table A24. Lineament raw data (length and intersection) in sheet 24.

Node No.	UTM E.	UTM N.	Intersection (point)	Major Lineament (Km.)	Minor Lineament (Km.)	Total distances (Km.)	Length density (Km/4 km ²)
1	242000	1752000	2	3.4, 3.6	3.4	10.4	2.6
2	244000	1754000	0	4.3, 5.0	0.4	9.7	2.4
3	246000	1756000	1	0.8, 2.6, 4.6	1.9	9.9	2.5
4	248000	1758000	1	0.4, 0.8, 4.4	1.9, 2.6	10.1	2.5
5	242000	1752000	3	1.8, 3.6, 3.7	1.2, 5.4	15.7	3.9
6	244000	1754000	0	0.7, 4.4	1.4, 3.0	9.5	2.4
7	246000	1756000	0	2.2, 2.8	2.2	7.2	1.8
8	248000	1758000	1	2.7	0.6, 4.6	7.9	2.0
9	242000	1752000	1	0.3, 2.2	1.0, 2.6	6.1	1.5
10	244000	1754000	0	0	1.4, 5.0	6.4	1.6
11	246000	1756000	2	2	1.9, 2.4, 3.6	9.9	2.5
12	248000	1758000	3	4.2	4.0, 4.2	12.4	3.1
13	242000	1752000	0	1.0, 1.6	0	2.6	0.7
14	244000	1754000	0	2	2.4	4.4	1.1
15	246000	1756000	1	1.6, 2.5	1.0, 1.9, 2.4	9.4	2.4
16	248000	1758000	3	0.2, 1.5, 4.8	1.9, 3.5	11.9	3.0

Table A25. Lineament raw data (length and intersection) in sheet 25.

Node No.	UTM E.	UTM N.	Intersection (point)	Major Lineament (Km.)	Minor Lineament (Km.)	Total distances (Km.)	Length density (Km/4 km ²)
1	212000	1762000	1	0	2.4, 4.0	6.4	1.6
2	214000	1764000	0	0	1.2	1.2	0.3
3	216000	1766000	0	0	0	0	0.0
4	218000	1768000	0	0	0	0	0.0
5	212000	1762000	1	0	3.6, 4.2	7.8	2.0
6	214000	1764000	0	0	0	0	0.0
7	216000	1766000	0	0	0	0	0.0
8	218000	1768000	0	0	0	0	0.0
9	212000	1762000	0	0	1.2, 3.0	4.2	1.1
10	214000	1764000	0	0	0.8	0.8	0.2
11	216000	1766000	0	0	0	0	0.0
12	218000	1768000	0	0	0	0	0.0
13	212000	1762000	0	0	0.7	0.7	0.2
14	214000	1764000	0	0	0.7	0.7	0.2
15	216000	1766000	0	0	0	0	0.0
16	218000	1768000	0	0	0	0	0.0

Table A26. Lineament raw data (length and intersection) in sheet 26.

Node No.	UTM E.	UTM N.	Intersection (point)	Major Lineament (Km.)	Minor Lineament (Km.)	Total distances (Km.)	Length density (Km/4 km ²)
1	222000	1762000	0	4.6	2.2	6.8	1.7
2	224000	1764000	0	2.2	4.6	6.8	1.7
3	226000	1766000	0	4	2.2	6.2	1.6
4	228000	1768000	0	0.8, 2.4	0	3.2	0.8
5	222000	1762000	0	3.6	0	3.6	0.9
6	224000	1764000	0	4.8	3.2	8	2.0
7	226000	1766000	0	4	4.9	8.9	2.2
8	228000	1768000	0	4.3	1.4	5.7	1.4
9	222000	1762000	0	1.2	0	1.2	0.3
10	224000	1764000	0	4.2	0.8	5	1.3
11	226000	1766000	0	1.7, 1.8	3.6	7.1	1.8
12	228000	1768000	0	4	1.7	5.7	1.4
13	222000	1762000	0	0	0	0	0.0
14	224000	1764000	0	1.6	0	1.6	0.4
15	226000	1766000	0	1.6	1.2	2.8	0.7
16	228000	1768000	0	1.8	1.2	3	0.8

Table A27. Lineament raw data (length and intersection) in sheet 27.

Node No.	UTM E.	UTM N.	Intersection (point)	Major Lineament (Km.)	Minor Lineament (Km.)	Total distances (Km.)	Length density (Km/4 km ²)
1	232000	1762000	0	1.6, 2.4, 3.6	3.3	10.9	2.7
2	234000	1764000	1	0.2, 2.5, 2.6, 2.6	0.4, 3.5	11.8	3.0
3	236000	1766000	2	0.8, 2.5, 3.0, 3.0	2	11.3	2.8
4	238000	1768000	1	0.8, 0.8, 1.6, 2.5	1.4	7.1	1.8
5	232000	1762000	0	1.6, 1.8	1.4, 1.4	6.2	1.6
6	234000	1764000	0	0.4, 0.7, 2.6	1.4, 2.7	7.8	2.0
7	236000	1766000	0	0.6, 1.0, 2.0, 5.0	0	8.6	2.2
8	238000	1768000	0	0.5, 3.9, 4.2	0	8.6	2.2
9	232000	1762000	0	0	2.4	2.4	0.6
10	234000	1764000	0	0	5.2	5.2	1.3
11	236000	1766000	0	1.8	3	4.8	1.2
12	238000	1768000	1	1.6, 4.0	0	5.6	1.4
13	232000	1762000	0	0	0	0	0.0
14	234000	1764000	0	0	2.6	2.6	0.7
15	236000	1766000	0	0	2.6	2.6	0.7
16	238000	1768000	0	0.4	0	0.4	0.1

Table A28. Lineament raw data (length and intersection) in sheet 28.

Node No.	UTM E.	UTM N.	Intersection (point)	Major Lineament (Km.)	Minor Lineament (Km.)	Total distances (Km.)	Length density (Km/4 km ²)
1	242000	1762000	0	0.8	0	0.8	0.2
2	244000	1764000	0	4	0	4	1.0
3	246000	1766000	0	2.8	0	2.8	0.7
4	248000	1768000	0	0.1, 4.0	0	4.1	1.0
5	242000	1762000	0	2	0	2	0.5
6	244000	1764000	0	3.4	0	3.4	0.9
7	246000	1766000	0	1	0	1	0.3
8	248000	1768000	0	2	4.2	6.2	1.6
9	242000	1762000	0	1.2, 2.8	1.1	4.1	1.0
10	244000	1764000	0	0.3, 1.3	3	4.6	1.2
11	246000	1766000	0	0	4.2	4.2	1.1
12	248000	1768000	0	0.1	4.2	4.2	1.1
13	242000	1762000	0	3	1	4	1.0
14	244000	1764000	0	0.4	1	1.4	0.4
15	246000	1766000	0	0	4	4	1.0
16	248000	1768000	0	0	4.2	4.2	1.1

Table A29. Lineament raw data (length and intersection) in roll 1.

Node No.	UTM E.	UTM N.	Intersection (point)	Major Lineament (Km.)	Minor Lineament (Km.)	Total distances (Km.)	Length density (Km/4 km ²)
1	212000	1710000	1	3	1.7	4.7	1.2
2	214000	1710000	0	0.1	0.7, 1.4, 3.4	5.6	1.4
3	216000	1710000	2	1.2	0.6, 1.8, 2.0, 2.8, 4.1	12.5	3.1
4	218000	1710000	2	0.8, 3.2	2.0, 2.4, 3.2, 4.3	15.9	4.0
5	222000	1710000	1	1.4, 2.8, 3.6	1.2, 1.6	10.6	2.7
6	224000	1710000	1	0.5, 1.4, 4.0	0.5, 1.6	8	2.0
7	226000	1710000	1	0.9, 5.0	1.4, 3.8	11.1	2.8
8	228000	1710000	1	3.4, 3.8	1.1, 2.5	10.8	2.7
9	232000	1710000	0	1	3.6, 4.2	8.8	2.2
10	234000	1710000	1	0	0.7, 2.2, 4.3	11	2.8
11	236000	1710000	4	2.8	1.7, 2.2, 4.3	11	2.8
12	238000	1710000	3	4	2.2, 3.0	9.2	2.3
13	242000	1710000	0	0	0	0	0.0
14	244000	1710000	0	0	0	0	0.0
15	246000	1710000	0	0	1.8	1.8	0.5
16	248000	1710000	0	0	0.2, 1.8, 2.0	4	1.0

Table A30. Lineament raw data (length and intersection) in roll 2.

Node No.	UTM E.	UTM N.	Intersection (point)	Major Lineament (Km.)	Minor Lineament (Km.)	Total distances (Km.)	Length density (Km/4 km ²)
1	212000	1720000	1	0	1.4, 3.2, 4.0	8.6	2.2
2	214000	1720000	2	0	1.4, 4.0, 4.2, 4.4	14	3.5
3	216000	1720000	2	0	1.4, 1.6, 4.4, 4.4	11.8	3.0
4	218000	1720000	1	0	0.4, 1.0, 1.6, 2.1, 4.3	9.4	2.4
5	222000	1720000	3	0	0.4, 0.5, 2.0, 2.6, 4.4	9.9	2.5
6	224000	1720000	1	0.8	1.2, 4.2	6.2	1.6
7	226000	1720000	1	0.8, 1.4, 2.4, 2.4	4.1	11.1	2.8
8	228000	1720000	2	0.5, 2.3, 3.8, 4.4	0.1, 0.3, 2.0	13.4	3.4
9	232000	1720000	5	3.0, 3.3	0.4, 0.9, 1.2, 2.7, 3.6	15.1	3.8
10	234000	1720000	3	0.4, 1.0, 3.2, 4.0	1.3, 2.7	12.6	3.2
11	236000	1720000	2	0.2, 0.7, 2.9, 4.0	0.6, 1.3, 4.0	13.7	3.4
12	238000	1720000	2	4	1.4, 2.1, 4.0	11.5	2.9
13	242000	1720000	0	2.2, 3.2	1.0, 1.2	7.6	1.9
14	244000	1720000	1	0.8, 1.3, 3.0, 4.0	1.2	10.3	2.6
15	246000	1720000	1	1.3, 1.4, 2.8, 3.6	0	9.1	2.3
16	248000	1720000	0	0.5, 2.2, 2.6, 3.0	0	8.3	2.1

Table A31. Lineament raw data (length and intersection) in roll 3.

Node No.	UTM E.	UTM N.	Intersection (point)	Major Lineament (Km.)	Minor Lineament (Km.)	Total distances (Km.)	Length density (Km/4 km ²)
1	212000	1730000	1	4.2	2.8	6.8	1.7
2	214000	1730000	1	4.2	0.9, 2.2	7.3	1.8
3	216000	1730000	1	4.2	3.2	7.4	1.9
4	218000	1730000	0	0.6, 4.2	1.9, 3.6	10.3	2.6
5	222000	1730000	2	0.1, 1.8, 2.0, 4.0	2.8	10.7	2.7
6	224000	1730000	0	0.1, 0.8	3.0, 4.2	8.1	2.0
7	226000	1730000	1	3.4	1.2, 4.2	8.8	2.2
8	228000	1730000	1	5	3	8	2.0
9	232000	1730000	1	3.7, 4.8	2	10.5	2.6
10	234000	1730000	3	4.3	2.2, 2.2, 2.8, 4.6	16.1	4.0
11	236000	1730000	6	4.3	1.2, 2.2, 3.8, 4.0, 4.0, 4.0	23.5	5.9
12	238000	1730000	6	4.2	0.3, 0.4, 0.8, 1.0, 1.2, 1.6, 1.7, 2.5, 4.0, 4.4	22.1	5.5
13	242000	1730000	6	2.6, 4.4, 5.0	1.0, 1.0, 1.2, 4.1	19.3	4.8
14	244000	1730000	6	1.8, 2.4, 4.4	0.5, 4.0, 4.2	17.3	4.3
15	246000	1730000	3	3	0.5, 1.0, 2.8, 4.0	11.3	2.8
16	248000	1730000	0	0.1, 0.2, 0.8	0.6, 2.8	4.5	1.1

Table A32. Lineament raw data (length and intersection) in roll 4.

Node No.	UTM E.	UTM N.	Intersection (point)	Major Lineament (Km.)	Minor Lineament (Km.)	Total distances (Km.)	Length density (Km/4 km ²)
1	212000	1740000	0	2.2	0	2.2	0.6
2	214000	1740000	0	5	0	5	1.3
3	216000	1740000	1	2.6, 3.2	0	5.8	1.5
4	218000	1740000	1	1.2, 4.0	2	7.2	1.8
5	222000	1740000	4	0.7, 2.2, 4.0, 4.2	0.8, 3.0	14.9	3.7
6	224000	1740000	2	0.6, 3.0, 4.2	1.3	9.1	2.3
7	226000	1740000	0	2.2, 4.2	1.3	7.7	1.9
8	228000	1740000	0	4.0, 0.2	0.1, 3.3	7.6	1.9
9	232000	1740000	1	3.6, 4.4	0.2, 1.6	9.8	2.5
10	234000	1740000	0	4.2, 4.6	0	8.6	2.2
11	236000	1740000	0	1.6, 2.0, 3.0	0	6.6	1.7
12	238000	1740000	0	0.6, 4.0	0	4.6	1.2
13	242000	1740000	1	2.8	0.1, 1.7, 4.1	8.7	2.2
14	244000	1740000	1	0	1.2, 1.4, 2.2, 2.2	7	1.8
15	246000	1740000	1	0.4	0.8, 2.4, 4.3	7.9	2.0
16	248000	1740000	1	4	1.0, 1.2, 3.4	9.6	2.4

Table A33. Lineament raw data (length and intersection) in roll 5.

Node No.	UTM E.	UTM N.	Intersection (point)	Major Lineament (Km.)	Minor Lineament (Km.)	Total distances (Km.)	Length density (Km/4 km ²)
1	212000	1750000	0	0	1.5, 3.2, 4.4	9.1	2.3
2	214000	1750000	0	0	2.2, 2.4	4.6	1.2
3	216000	1750000	0	0	0	0	0.0
4	218000	1750000	0	0	2.2	2.2	0.6
5	222000	1750000	0	0.6	1.4, 1.8	3.8	1.0
6	224000	1750000	0	0	1.0, 1.2	2.2	0.6
7	226000	1750000	0	0	1.1, 3.0	4.1	1.0
8	228000	1750000	0	2.8, 3.0	0.6, 0.8	7.2	1.8
9	232000	1750000	1	0.4, 2.4, 3.0, 4.7	0.6, 0.8	11.9	3.0
10	234000	1750000	2	1.8, 4.0	0.6, 3.3	9.7	2.4
11	236000	1750000	1	0.6, 5.0	2.5	8.1	2.0
12	238000	1750000	0	2.4, 4.2	0	6.6	1.7
13	242000	1750000	0	1.6	0.2	1.8	0.5
14	244000	1750000	0	4	0	4	1.0
15	246000	1750000	2	1.7, 4.4	4.4	10.5	2.6
16	248000	1750000	2	3.6, 4.5	4.5	12.6	3.2

Table A34. Lineament raw data (length and intersection) in roll 6.

Node No.	UTM E.	UTM N.	Intersection (point)	Major Lineament (Km.)	Minor Lineament (Km.)	Total distances (Km.)	Length density (Km/4 km ²)
1	212000	1760000	0	0	0.1, 1.2, 4.4	5.7	1.4
2	214000	1760000	0	0	1.2, 2.0	3.2	0.8
3	216000	1760000	0	0	0	0	0.0
4	218000	1760000	0	1.4	0	1.4	0.4
5	222000	1760000	0	3.6	4.8	8.4	2.1
6	224000	1760000	0	1.8, 2.6	3.8	8.2	2.1
7	226000	1760000	0	2.0, 2.4	0	4.4	1.1
8	228000	1760000	0	0.4, 3.4	0	3.8	1.0
9	232000	1760000	0	0.4, 4.0, 4.2	4	12.6	3.2
10	234000	1760000	1	0.4, 4.0, 4.2	1.3, 1.8, 3.0	14.7	3.7
11	236000	1760000	2	0.5, 4.0	1.8, 2.9	9.2	2.3
12	238000	1760000	1	0.1, 0.5, 4.0	1.6	6.2	1.6
13	242000	1760000	0	1.7	0	1.7	0.4
14	244000	1760000	0	4.1	0	4.1	1.0
15	246000	1760000	0	4.2	0	4.2	1.1
16	248000	1760000	0	2.8, 3.8	0	6.6	1.7

Table A35. Lineament raw data (length and intersection) in column 1.

Node No.	UTM E.	UTM N.	Intersection (point)	Major Lineament (Km.)	Minor Lineament (Km.)	Total distances (Km.)	Length density (Km/4 km ²)
1	220000	1702000	7	2.4, 3.6	0.4, 0.8, 1.2, 2.2, 2.6	13.2	3.3
2	220000	1704000	6	2.4	0.8, 1.3, 1.3, 1.4, 1.9, 2.4, 4.2	15.7	3.9
3	220000	1706000	4	3.7	0.1, 0.7, 2.2, 4.0, 4.2	14.9	3.7
4	220000	1708000	3	3.7	0.4, 0.4, 1.0, 2.4, 2.8, 3.2	13.9	3.5
5	220000	1710000	0	2.2, 4.0	0.4, 0.6, 1.2, 1.3, 2.4	12.4	3.1
6	220000	1712000	0	2.1, 4.0	0.9, 1.4, 2.0	10.4	2.6
7	220000	1714000	1	1.0, 3.3	0.9, 2.0	7.2	1.8
8	220000	1716000	6	3.3, 2.6	0.8, 1.9, 2.4, 4.0	15	3.8
9	220000	1718000	6	1.2	1.6, 4.0, 4.0, 5.2	16	4.0
10	220000	1720000	2	0	0.3, 0.6, 1.6, 3.6, 4.6	10.7	2.7
11	220000	1722000	2	0	0.3, 0.6, 2.0, 3.9, 4.0	10.8	2.7
12	220000	1724000	1	4.1	2.0, 2.4, 3.9	12.4	3.1
13	220000	1726000	0	4.1	3.6, 4.2	11.9	3.0
14	220000	1728000	1	1.9, 4.0	2.4, 3.6, 4.2	16.1	4.0
15	220000	1730000	2	1.8, 4.0, 4.2	1.2, 1.9	13.1	3.3
16	220000	1732000	2	0.1, 4.0, 4.6	0.8, 2.6	12.1	3.0
17	220000	1734000	1	1.5, 4.0	0.8, 1.1, 1.7	9.1	2.3
18	220000	1736000	1	0.4, 4.0	1.5, 1.6, 2.4	9.9	2.5
19	220000	1738000	2	1.4, 2.0, 4.0	1.4, 1.5, 4.5	14.8	3.7
20	220000	1740000	2	1.4, 4.0, 4.8	1.4, 3.2	14.8	3.7
21	220000	1742000	1	1.9, 4.4	0.8	7.1	1.8
22	220000	1744000	2	1.2, 2.0	1.7, 2.0	6.9	1.7
23	220000	1746000	2	0.3, 1.2	4.8	6.3	1.6
24	220000	1748000	0	0	3.8	3.8	1.0
25	220000	1750000	0	0	0.8	0.8	0.2
26	220000	1752000	0	0.2	0	0.2	0.1
27	220000	1754000	0	1.8	0	1.8	0.5
28	220000	1756000	0	1.4, 2.1	0.7	4.2	1.1
29	220000	1758000	0	4.8	1.8	6.6	1.7
30	220000	1760000	0	4.8	1	5.8	1.5
31	220000	1762000	0	2.2	0	2.2	0.6
32	220000	1764000	0	0.1	0	0.1	0.0
33	220000	1768000	0	0	0	0	0.0
34	220000	1770000	0	0	0	0	0.0

Table A36. Lineament raw data (length and intersection) in column 2.

Node No.	UTM E.	UTM N.	Intersection (point)	Major Lineament (Km.)	Minor Lineament (Km.)	Total distances (Km.)	Length density (Km/4 km ²)
1	230000	1702000	6	1.7, 3.2, 3.6	0.6, 2.0, 2.2, 2.8, 3.0	19.1	4.8
2	230000	1704000	6	0.3, 2.0, 2.6	1.8, 2.2, 2.4, 2.8, 3.8	17.9	4.5
3	230000	1706000	1	1.8, 2.4, 2.8	0.8, 3.1, 3.4	14.3	3.6
4	230000	1708000	0	0.8, 2.4, 2.4	0.4, 0.8, 1.2, 2.4, 2.6	13	3.3
5	230000	1710000	0	0.2, 1.0, 4.0	0.4, 0.7, 1.7	8	2.0
6	230000	1712000	0	1.2, 1.4	0.3, 1.0	3.9	1.0
7	230000	1714000	0	0.3, 2.6	0	2.9	0.7
8	230000	1716000	2	2.6, 2.6, 3.9	2.6	11.7	2.9
9	230000	1718000	5	1.4, 2.2, 2.5, 4.8	0.7, 2.6, 4.2	18.4	4.6
10	230000	1720000	4	0.7, 2.1, 2.2, 3.2	0.7, 3.0, 3.8	15.7	3.9
11	230000	1722000	3	0.6, 1.9, 2.6	0.4, 1.6, 2.4, 2.9	12.4	3.1
12	230000	1724000	1	0.2, 1.2, 2.7, 3.4	0.5, 1.0, 2.1	11.1	2.8
13	230000	1726000	3	2.8, 3.5, 4.2, 4.2	0.2, 0.4	15.3	3.8
14	230000	1728000	3	0.6, 1.2, 4.2, 5.2	1.2	12.4	3.1
15	230000	1730000	1	1.2, 2.4, 3.8	1.2	8.6	2.2
16	230000	1732000	2	0.1, 0.7, 1.2, 4.8	1.2	8	2.0
17	230000	1734000	2	2.8, 4.2	4.6	11.6	2.9
18	230000	1736000	2	1.1, 2.6, 3.2	3.4	10.3	2.6
19	230000	1738000	1	1.1, 3.2, 3.7	0.2	8.2	2.1
20	230000	1740000	1	1.0, 4.2	1.8, 2.4	9.4	2.4
21	230000	1742000	1	4.2	0.2, 1.6, 2.5, 3.5, 4.3	16.3	4.1
22	230000	1744000	0	0	0.2, 0.6, 1.4, 1.6, 2.6, 4.6	11	2.8
23	230000	1746000	1	0.6	0.1, 0.6, 1.0, 2.6	4.9	1.2
24	230000	1748000	1	0.6, 2.2, 2.4	0.8	6	1.5
25	230000	1750000	0	2.4, 3.0, 3.2, 3.4	1.1, 1.8	14.9	3.7
26	230000	1752000	0	1.0, 1.3, 5.4	3.8, 4.4	15.9	4.0
27	230000	1754000	0	0.7, 2.8, 3.8	4.6, 4.6	16.5	4.1
28	230000	1756000	0	0.1, 1.2, 4.4	1.9, 2.1, 3.0	12.7	3.2
29	230000	1758000	0	3.6, 4.2	0.6, 2.4	10.8	2.7
30	230000	1760000	0	4.2, 4.4	0.3	8.9	2.2
31	230000	1762000	0	3.1, 3.9	0.2, 1.2, 1.9	10.3	2.6
32	230000	1764000	0	1.2, 1.9	0	3.1	0.8
33	230000	1768000	0	2	0	2	0.5
34	230000	1770000	0	1.8	0	1.8	0.5

Table A37. Lineament raw data (length and intersection) in column 3.

Node No.	UTM E.	UTM N.	Intersection (point)	Major Lineament (Km.)	Minor Lineament (Km.)	Total distances (Km.)	Length density (Km/4 km ²)
1	240000	1702000	1	0	2.7, 4.4	7.1	1.8
2	240000	1704000	3	1.3, 2.6	2.9, 3.7	10.5	2.6
3	240000	1706000	3	0.6, 1.3	2.4, 4.8	9.1	2.3
4	240000	1708000	0	1	2.5, 2.5	6	1.5
5	240000	1710000	0	1	0.9	1.9	0.5
6	240000	1712000	0	0.2, 1.4	0.9, 2.6	5.1	1.3
7	240000	1714000	2	4.3	1.7, 4.8	10.8	2.7
8	240000	1716000	4	2.4, 4.2	0.4, 2.1, 2.7	11.8	3.0
9	240000	1718000	2	4.2, 4.6	0.2, 0.8	9.8	2.5
10	240000	1720000	1	1.8, 3.0	1.4, 3.4	9.6	2.4
11	240000	1722000	1	1.8	3.5, 4.8	10.1	2.5
12	240000	1724000	4	1.6	1.4, 1.7, 1.9, 2.2, 4.3	13.1	3.3
13	240000	1726000	5	4	1.4, 1.7, 4.3, 4.4	15.8	4.0
14	240000	1728000	4	2.4, 3.2, 4.2	0.8, 3.6, 4.2	18.6	4.7
15	240000	1730000	6	0.7, 2.6, 4.2	0.3, 0.4, 0.6, 1.1, 3.2, 3.8, 4.2	21.1	5.3
16	240000	1732000	6	0.1, 4.2	0.4, 1.9, 2.5, 2.8, 3.2, 4.0	19.1	4.8
17	240000	1734000	4	4.2	1.6, 4.2, 4.3, 4.5	18.8	4.7
18	240000	1736000	2	0	0.4, 0.6, 0.9, 1.1, 1.8, 2.8, 3.4	11	2.8
19	240000	1738000	1	2.1	0.4, 0.6, 1.2, 1.4, 3.4	9.1	2.3
20	240000	1740000	0	2.1, 2.9	0.2, 2.9	8.1	2.0
21	240000	1742000	1	2.9	0.4, 4.0	7.3	1.8
22	240000	1744000	0	1	2.8	3.8	1.0
23	240000	1746000	0	2.7	0	2.7	0.7
24	240000	1748000	0	1.4, 1.7	0	3.1	0.8
25	240000	1750000	0	3.4	0.2	3.6	0.9
26	240000	1752000	2	1.0, 1.2, 1.6, 1.7	2.8	8.3	2.1
27	240000	1754000	3	1.0, 1.2, 3.7	2.4, 3.4	11.7	2.9
28	240000	1756000	2	1.9, 2.1, 2.7	3.3	10	2.5
29	240000	1758000	1	4.2, 4.3	0	8.5	2.1
30	240000	1760000	0	1.7, 4.0	0	5.7	1.4
31	240000	1762000	0	1.7	0	1.7	0.4
32	240000	1764000	1	2.0, 2.0	0	4	1.0
33	240000	1768000	1	1.6, 5.0	0	6.6	1.7
34	240000	1770000	0	3.4	0	3.4	0.9

APPENDIX B
ELECTRICAL RESISTIVITY RAW DATA



Geophysical Exploration (Electrical Resistivity)

Table B1 Electrical resistivity raw data and configuration array pattern at point1.
Area: Khong district Station: point1 225622E 1708126N Date: 05/26/01
Comment: direction N60°E

AB/2	MN/2	K	I	V _x	RES	AB/2	MN/2	K	I	V _x	RES
1.3	0.5	4.53	9.68	799.57	373.6	50	5	777.54	153.79	1.187	6.0
2.0	0.5	11.78	13.63	318.05	274.9	65	5	1319.47	67.66	0.370	7.2
3.2	0.5	31.38	18.22	90.516	155.9	80	5	2002.77	84.81	0.296	7.0
4.0	0.5	49.48	12.41	28.28	112.7	100	5	3133.74	136.97	0.350	8.0
5.0	0.5	77.75	15.69	17.06	84.6	100	20	753.98	130.14	1.304	7.6
6.5	0.5	131.95	12.36	3.75	40.1	130	20	1295.91	92.35	0.613	8.6
8.0	0.5	200.28	13.22	1.24	18.8	160	20	1979.20	142.93	0.894	12.4
10	0.5	313.37	50.53	2.62	16.3	200	20	3110.18	94.48	0.479	15.6
10	2	75.40	50.47	11.60	17.3	250	20	4877.32	352.23	0.777	10.8
13	2	129.59	28.05	1.78	8.2	320	20	8011.06	228.38	0.279	9.8
16	2	197.92	59.63	1.75	5.8	320	50	3138.50	230.14	0.668	9.1
20	2	311.02	63.76	1.047	5.1	400	50	4948.00	553.33	0.803	7.2
25	2	487.73	57.91	0.517	4.4	500	50	7775.65	194.29	0.122	4.9
32	2	801.11	191.80	1.402	5.9	650	50	13194.70	231.15	0.105	6.0
32	5	313.85	192.25	3.188	5.2						
40	5	494.80	152.33	1.762	5.7						

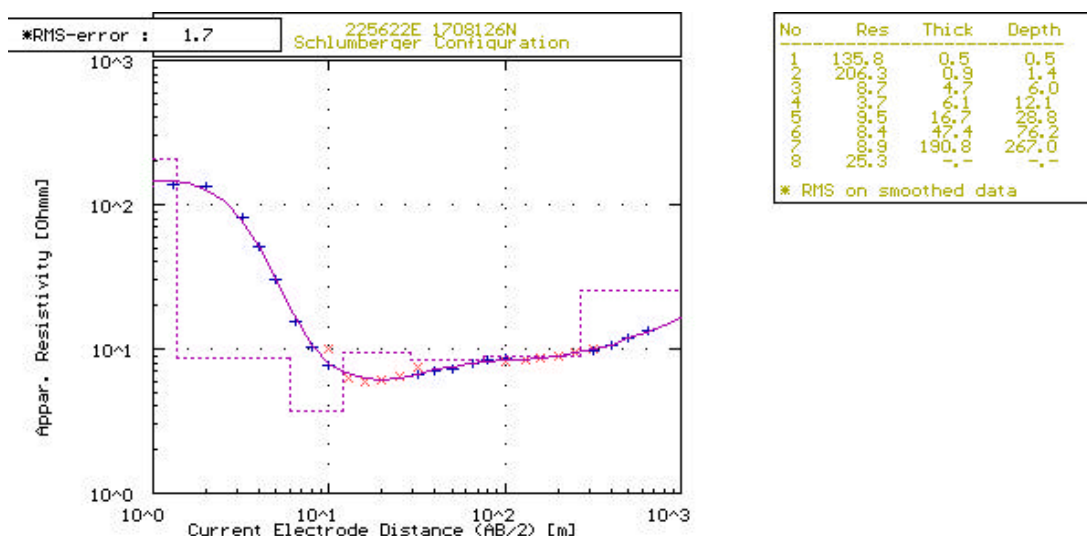


Figure B1 The curves fitting from RESIST87 software represents the depth, apparent resistivity and thickness at point 1.



Geophysical Exploration (Electrical Resistivity)

Table B2 Electrical resistivity raw data and configuration array pattern at point 2.
Area: Khong district **Station:** point2 226200E 1703790N **Date:** 06/26/01
Comment: Wat Nong Phran Pan

AB/2	MN/2	K	I	V _x	RES	AB/2	MN/2	K	I	V _x	RES
1.3	0.5	4.53	50.70	4474.725	399.41	32	2	801.11	336.66	1.152	2.74
2.0	0.5	11.78	68.88	1892.159	323.60	32	5	313.85	342.29	2.573	2.36
3.2	0.5	31.38	74.06	438.945	185.98	40	5	494.80	372.49	1.814	2.41
4.0	0.5	49.48	70.28	169.759	119.52	50	5	777.54	732.49	2.325	2.47
5.0	0.5	77.75	106.44	111.413	81.38	65	5	1319.47	629.41	1.116	2.34
6.5	0.5	131.95	86.20	33.962	51.99	80	5	2002.77	418.69	0.452	2.16
8.0	0.5	200.28	76.18	10.134	26.64	105	5	3133.74	443.35	0.277	2.16
10	0.5	313.37	83.07	3.897	14.70	105	20	834.82	439.18	1.194	2.27
10	2	75.40	87.72	17.521	15.06	130	20	1295.91	1177.48	2.102	2.31
13	2	129.59	72.31	2.999	5.37	176	20	1979.20	33.426	0.362	2.5
16	2	197.92	127.68	2.213	3.43	200	20	3110.18	769.29	0.685	2.77
20	2	311.02	116.25	1.127	3.01	250	20	4877.32	1629.37	1.059	3.2
25	2	487.73	147.37	0.906	2.99	320	20	8011.06	256.12	0.104	3.25
						320	50	3138.50	316.46	0.132	3.34

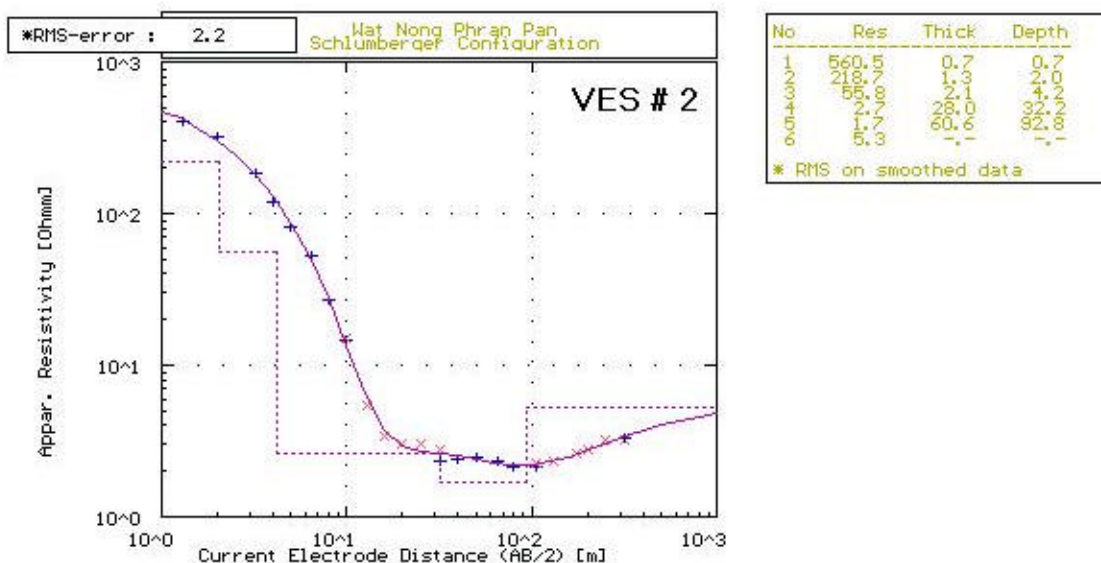


Figure B2 The curves fitting from RESIST87 software represents the depth, apparent resistivity and thickness at point 2.



Geophysical Exploration (Electrical Resistivity)

Table B3 Electrical resistivity raw data and configuration array pattern at point 3.

Area: Khong district **Station:** point3 226290 1704000N **Date:** 06/27/01

Comment: 250 m North of Wat Nong Phran Pan

AB/2	MN/2	K	I	V _x	RES	AB/2	MN/2	K	I	V _x	RES
1.3	0.5	4.53	185.71	2067.008	50.42	32	2	801.11	1047.00	6.321	4.77
2.0	0.5	11.78	118.96	276.835	27.41	32	5	313.85	1060.96	16.069	4.75
3.2	0.5	31.38	110.06	30.029	8.56	40	5	494.80	960.48	8.827	4.55
4.0	0.5	49.48	149.27	19.176	6.53	50	5	777.54	258.65	1.337	4.02
5.0	0.5	77.75	138.84	11.877	6.65	65	5	1319.47	58.09	0.148	3.44
6.5	0.5	131.95	126.45	6.535	6.82	80	5	2002.77	217.42	0.355	3.27
8.0	0.5	200.28	176.72	5.770	6.54	100	5	3133.74	284.53	0.248	2.73
10	0.5	313.37	486.17	10.023	6.46	100	20	753.98	284.31	1.009	2.67
10	2	75.40	480.93	36.884	5.78	130	20	1295.91	222.38	0.466	2.71
13	2	129.59	119.67	5.291	5.73	160	20	1979.20	246.57	0.343	2.75
16	2	197.92	308.03	9.035	5.80	200	20	3110.18	889.19	0.824	2.88
20	2	311.02	1323.42	23.920	5.62	250	20	4877.32	334.23	0.208	3.03
25	2	487.73	1799.20	18.368	4.98	320	20	8011.06	623.40	0.290	3.72
						320	50	3138.50	403.09	0.458	3.60
						400	50	4948.00	528.84	0.515	4.10

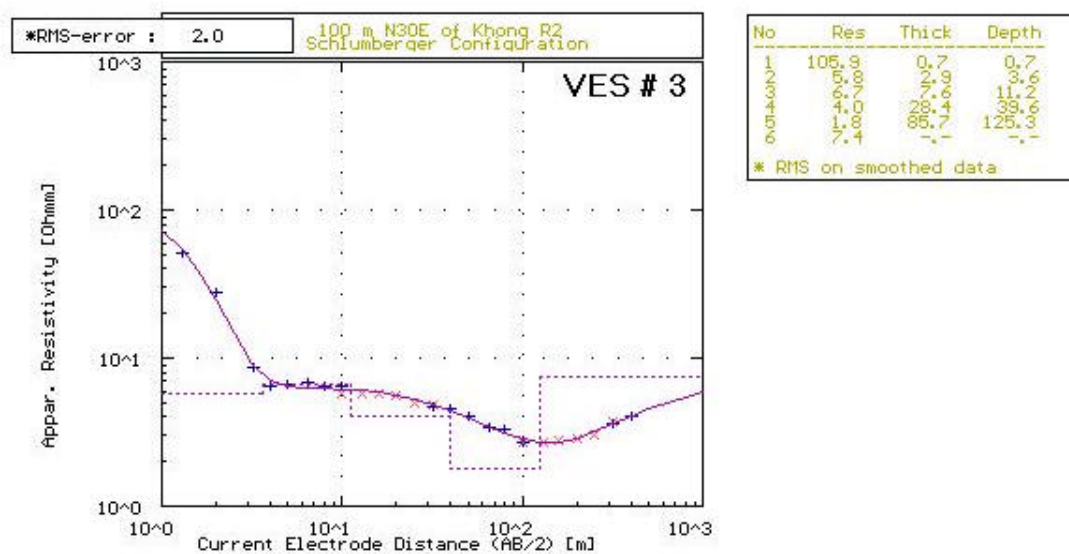


Figure B3 The curves fitting from RESIST87 software represents the depth, apparent resistivity and thickness at point 3.



Geophysical Exploration (Electrical Resistivity)

Table B4 Electrical resistivity raw data and configuration array pattern at point 4.
Area: Khong district **Station:** point4 226079E 1704479N **Date:** 07/01/01
Comment: Ban Khok Sa-At **Direction** N60°E

AB/2	MN/2	K	I	V _x	RES	AB/2	MN/2	K	I	V _x	RES
1.3	0.5	4.53	123.75	3173.12	116.0	50	5	777.54	469.23	3.916	6.5
2.0	0.5	11.78	103.71	626.184	71.1	65	5	1319.47	154.24	0.782	6.7
3.2	0.5	31.38	115.68	64.538	17.5	80	5	2002.77	52.33	0.188	7.2
4.0	0.5	49.48	113.56	24.195	10.5	100	5	3133.74	214.70	0.451	6.6
5.0	0.5	77.75	108.84	10.333	7.4	100	20	753.98	215.21	1.869	6.5
6.5	0.5	131.95	143.11	6.957	6.4	130	20	1295.91	312.88	1.564	6.5
8.0	0.5	200.28	124.50	3.989	6.4	160	20	1979.20	177.83	0.567	6.3
10	0.5	313.37	93.96	1.574	5.2	200	20	3110.18	137.50	0.267	6.0
10	2	75.40	58.28	3.996	5.2	250	20	4877.32	128.40	0.148	5.6
13	2	129.59	94.91	3.748	5.1	320	20	8011.06	379.65	0.226	4.8
16	2	197.92	97.77	2.515	5.1	320	50	3138.50	380.46	0.582	4.8
20	2	311.02	129.46	2.176	5.2	400	50	4948.00	498.35	0.474	4.7
25	2	487.73	122.46	1.453	5.8	467	50	6775.75	296.79	0.219	5.0
32	2	801.11	90.54	0.703	6.2	500	50	7775.40	309.30	0.198	5.0
32	5	313.85	92.08	1.767	6.0	650	50	13194.70	203.78	0.145	6.5
40	5	494.80	305.62	3.831	6.2						

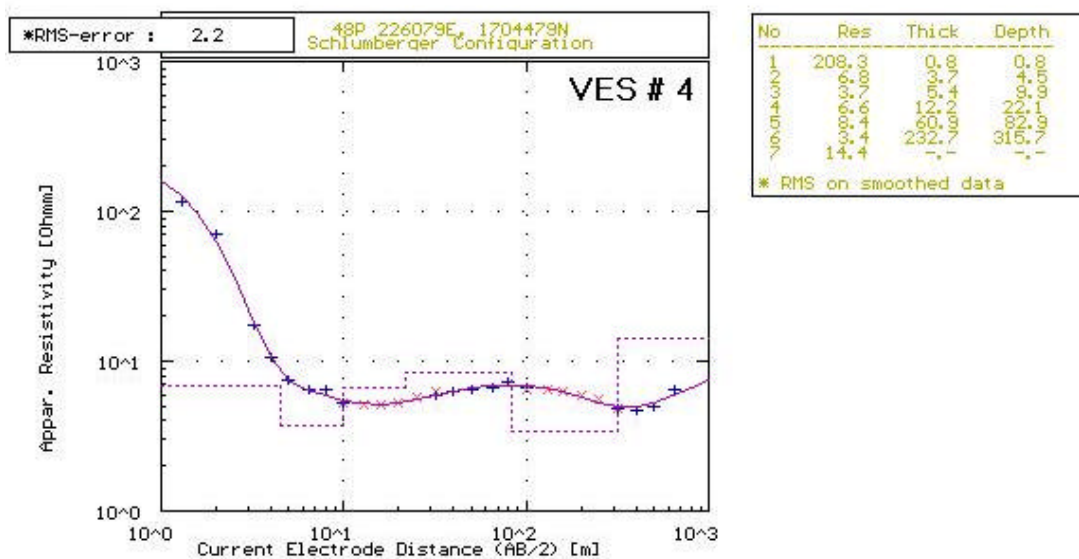


Figure B4 The curves fitting from RESIST87 software represents the depth, apparent resistivity and thickness at point 4.



Geophysical Exploration (Electrical Resistivity)

Table B5 Electrical resistivity raw data and configuration array pattern at point 5.
Area: Khong district Station: point5 226163E 1705106N Date: 06/31/01
Comment:

AB/2	MN/2	K	I	V _x	RES	AB/2	MN/2	K	I	V _x	RES
1.3	0.5	4.53	9.68	799.574	373.6	50	5	777.54	153.79	1.187	6.0
2.0	0.5	11.78	13.63	318.046	274.9	65	5	1319.47	67.66	0.370	7.2
3.2	0.5	31.38	18.22	90.516	155.9	80	5	2002.77	84.81	0.296	7.0
4.0	0.5	49.48	12.41	28.281	112.7	100	5	3133.74	136.97	0.350	8.0
5.0	0.5	77.75	15.69	17.061	84.6	100	20	753.98	130.14	1.304	7.6
6.5	0.5	131.95	12.36	3.753	40.1	130	20	1295.91	92.35	0.613	8.6
8.0	0.5	200.28	13.22	1.240	18.8	160	20	1979.20	142.93	0.894	12.4
10	0.5	313.37	50.53	2.620	16.3	200	20	3110.18	94.48	0.479	15.6
10	2	75.40	50.47	11.599	17.3	250	20	4877.32	352.23	0.777	10.8
13	2	129.59	28.05	1.779	8.2	320	20	8011.06	228.38	0.279	9.8
16	2	197.92	59.63	1.750	5.8	320	50	3138.50	230.14	0.668	9.1
20	2	311.02	63.76	1.047	5.1	400	50	4948.00	553.33	0.803	7.2
25	2	487.73	57.91	0.517	4.4	500	50	7775.65	194.29	0.122	4.9
32	2	801.11	191.80	1.402	5.0	650	50	13194.70	231.15	0.105	6.0
32	5	313.85	192.25	3.188	5.2						
40	5	494.80	152.33	1.762	5.7						

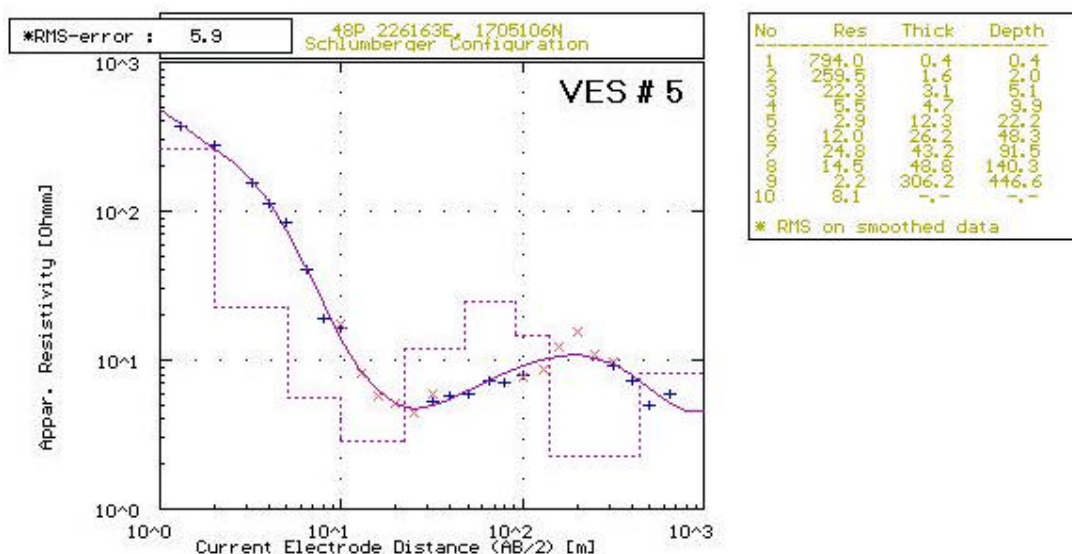


Figure B5 The curves fitting from RESIST87 software represents the depth, apparent resistivity and thickness at point 5.



Geophysical Exploration (Electrical Resistivity)

Table B6 Electrical resistivity raw data and configuration array pattern at point 6.
Area: Khong district **Station:** point6 226090E 1707073N **Date:** 07/13/01
Comment: Direction N30°E

AB/2	MN/2	K	I	V _x	RES	AB/2	MN/2	K	I	V _x	RES
1.3	0.5	4.53	479.19	2247.050	21.2	50	5	777.54	360.89	2.420	5.2
2.0	0.5	11.78	593.86	838.160	16.6	65	5	1319.47	143.45	0.656	6.0
3.2	0.5	31.38	533.91	198.122	11.6	80	5	2002.77	151.38	0.483	6.4
4.0	0.5	49.48	598.54	118.416	9.8	100	5	3133.74	421.16	0.973	7.2
5.0	0.5	77.75	760.68	85.856	8.8	100	20	753.98	420.22	4.128	7.4
6.5	0.5	131.95	1005.80	58.224	7.6	130	20	1295.91	161.07	0.992	8.0
8.0	0.5	200.28	516.06	20.416	7.2	160	20	1979.20	149.55	0.633	8.4
10	0.5	313.37	399.37	5.684	4.5	200	20	3110.18	148.84	0.418	8.7
10	2	75.40	325.95	29.091	6.7	250	20	4877.32	205.12	0.366	8.7
13	2	129.59	570.02	26.373	6.0	320	20	8011.06	177.34	0.210	9.5
16	2	197.92	291.14	8.659	5.9	320	50	3138.50	177.46	0.555	9.8
20	2	311.02	384.49	6.218	5.0	400	50	4948.00	342.30	0.721	10.4
25	2	487.73	160.10	1.572	4.8	500	50	7775.40	100.58	0.153	11.8
32	2	801.11	145.98	0.849	4.7	650	50	13194.70	385.75	0.376	12.9
32	5	313.85	169.64	2.441	4.5						
40	5	494.80	175.32	1.743	4.9						

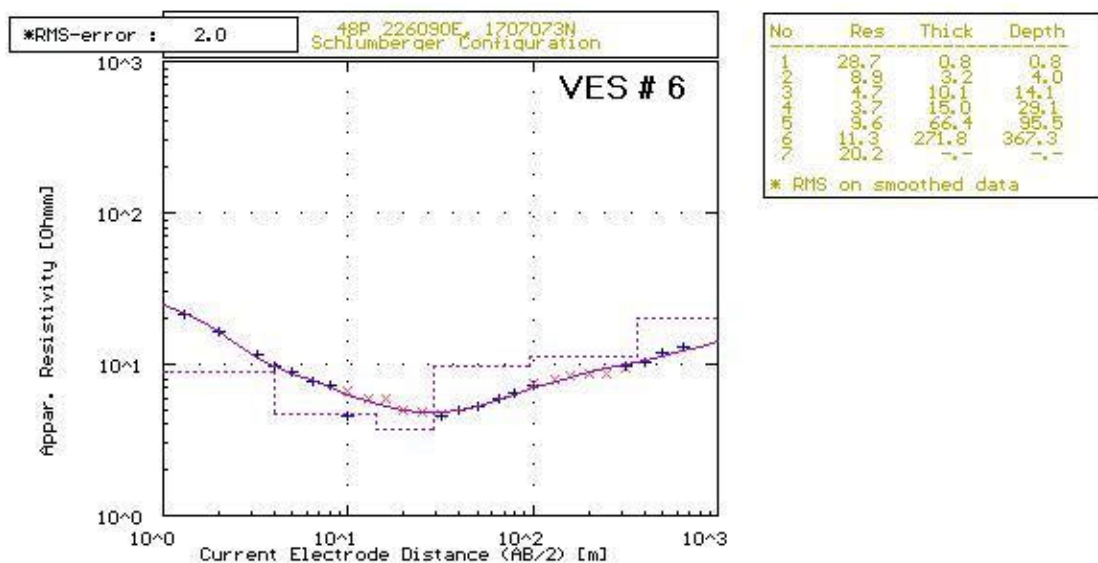


Figure B6 The curves fitting from RESIST87 software represents the depth, apparent resistivity and thickness at point 6.



Geophysical Exploration (Electrical Resistivity)

Table B7 Electrical resistivity raw data and configuration array pattern at point 7.
Area: Khong district **Station:** point7 226233E 1706724N **Date:** 07/07/01
Comment: Direction N55°E

AB/2	MN/2	K	I	V _x	RES	AB/2	MN/2	K	I	V _x	RES
1.3	0.5	4.53	123.87	3727.497	136.1	50	5	777.54	311.21	2.933	7.3
2.0	0.5	11.78	261.91	2987.651	134.4	65	5	1319.47	799.59	4.807	7.9
3.2	0.5	31.38	202.91	522.643	81.1	80	5	2002.77	417.42	1.726	8.3
4.0	0.5	49.48	204.82	214.417	51.8	100	5	3133.74	432.31	1.183	8.6
5.0	0.5	77.75	188.81	72.527	29.9	100	20	753.98	434.24	4.656	8.1
6.5	0.5	131.95	194.70	23.029	15.6	130	20	1295.91	915.48	5.953	8.4
8.0	0.5	200.28	261.25	13.466	10.3	160	20	1979.20	320.77	1.411	8.7
10	0.5	313.37	189.12	4.642	7.7	200	20	3110.18	355.00	1.025	9.0
10	2	75.40	191.25	25.420	10.0	250	20	4877.32	301.48	0.587	9.5
13	2	129.59	174.42	8.435	6.3	320	20	8011.06	661.62	0.815	9.9
16	2	197.92	177.18	5.329	6.0	320	50	3138.50	657.46	2.007	9.6
20	2	311.02	231.34	4.566	6.1	400	50	4948.00	260.74	0.563	10.7
25	2	487.73	340.25	4.551	6.5	500	50	7775.40	333.20	0.513	12.0
32	2	801.11	234.02	2.191	7.5	650	50	13194.70	365.50	0.369	13.3
32	5	313.85	228.04	4.857	6.7						
40	5	494.80	475.34	6.726	7.0						

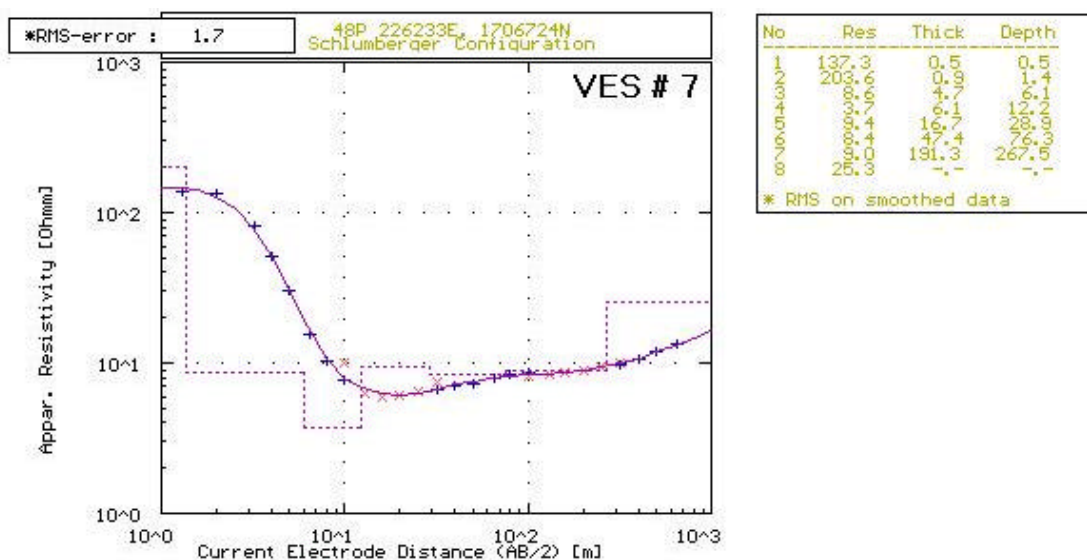


Figure B7 The curves fitting from RESIST87 software represents the depth, apparent resistivity and thickness at point 7.



Geophysical Exploration (Electrical Resistivity)

Table B8 Electrical resistivity raw data and configuration array pattern at point 8.
Area: Khong district Station: point8 225514N 1710134E Date: 07/14/01
Comment: Ban Don Tan, Direction N50°E

AB/2	MN/2	K	I	V _x	RES	AB/2	MN/2	K	I	V _x	RES
1.3	0.5	4.53	146.10	2370.129	73.4	50	5	777.54	286.96	3.636	9.9
2.0	0.5	11.78	139.82	441.678	37.2	65	5	1319.47	120.07	0.925	10.2
3.2	0.5	31.38	122.35	63.861	16.4	80	5	2002.77	130.18	0.677	10.4
4.0	0.5	49.48	93.01	24.655	13.1	100	5	3133.74	129.92	0.446	10.8
5.0	0.5	77.75	171.06	22.590	10.3	100	20	753.98	124.68	1.702	10.3
6.5	0.5	131.95	155.64	11.289	9.6	130	20	1295.91	125.04	1.040	10.8
8.0	0.5	200.28	236.70	10.819	9.2	160	20	1979.20	111.50	0.618	11.0
10	0.5	313.37	172.05	4.637	8.4	200	20	3110.18	279.55	1.030	11.5
10	2	75.40	171.98	18.983	8.3	250	20	4877.32	166.90	0.408	11.9
13	2	129.59	176.14	11.020	8.1	320	20	8011.06	296.26	0.446	12.1
16	2	197.92	168.48	6.888	8.1	320	50	3138.50	411.17	1.502	11.5
20	2	311.02	99.97	2.532	7.9	400	50	4948.00	438.68	1.075	12.1
25	2	487.73	167.72	2.863	8.3	500	50	7775.40	295.98	0.494	13.0
32	2	801.11	290.14	3.202	8.8	650	50	13194.70	671.39	0.807	15.9
32	5	313.85	392.00	11.163	8.9						
40	5	494.80	199.85	3.853	9.5						

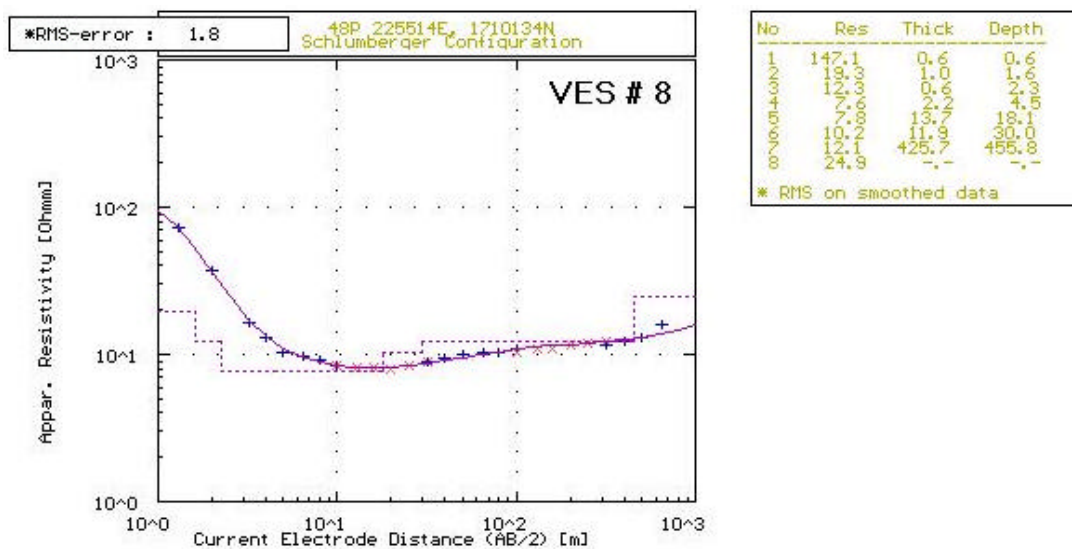


Figure B8 The curves fitting from RESIST87 software represents the depth, apparent resistivity and thickness at point 8.



Geophysical Exploration (Electrical Resistivity)

Table B9 Electrical resistivity raw data and configuration array pattern at point 9.
Area: Khong district **Station:** point9 226712N 1708862E **Date:** 07/14/01
Comment: Direction N70°E

AB/2	MN/2	K	I	V _x	RES	AB/2	MN/2	K	I	V _x	RES
1.3	0.5	4.53	1050.48	1173.508	5.1	50	5	777.54	2102.30	21.343	7.9
2.0	0.5	11.78	871.94	334.509	4.5	65	5	1319.47	1291.56	8.254	8.4
3.2	0.5	31.38	919.45	99.848	3.4	80	5	2002.77	1641.22	7.153	8.7
4.0	0.5	49.48	643.04	45.271	3.5	100	5	3133.74	1862.40	5.349	9.0
5.0	0.5	77.75	648.95	27.425	3.3	100	20	753.98	1859.32	21.184	8.6
6.5	0.5	131.95	915.02	23.136	3.3	130	20	1295.91	2339.86	15.855	8.8
8.0	0.5	200.28	683.22	12.283	3.6	160	20	1979.20	2125.35	9.162	8.5
10	0.5	313.37	867.97	11.108	4.0	200	20	3110.18	499.60	1.366	8.5
10	2	75.40	851.73	43.185	3.8	250	20	4877.32	739.43	1.278	8.4
13	2	129.59	804.74	27.494	4.8	320	20	8011.06	699.52	0.696	8.0
16	2	197.92	1160.45	28.601	4.9	320	50	3138.50	694.48	1.793	8.1
20	2	311.02	1565.02	27.817	5.5	400	50	4948.00	741.99	1.190	7.9
25	2	487.73	1417.02	17.116	5.9	500	50	7775.40	1518.15	1.633	8.4
32	2	801.11	2098.80	17.352	6.6	650	50	13194.70	1248.11	0.925	9.8
32	5	313.85	2097.77	46.234	6.9						
40	5	494.80	1790.34	26.889	7.4						

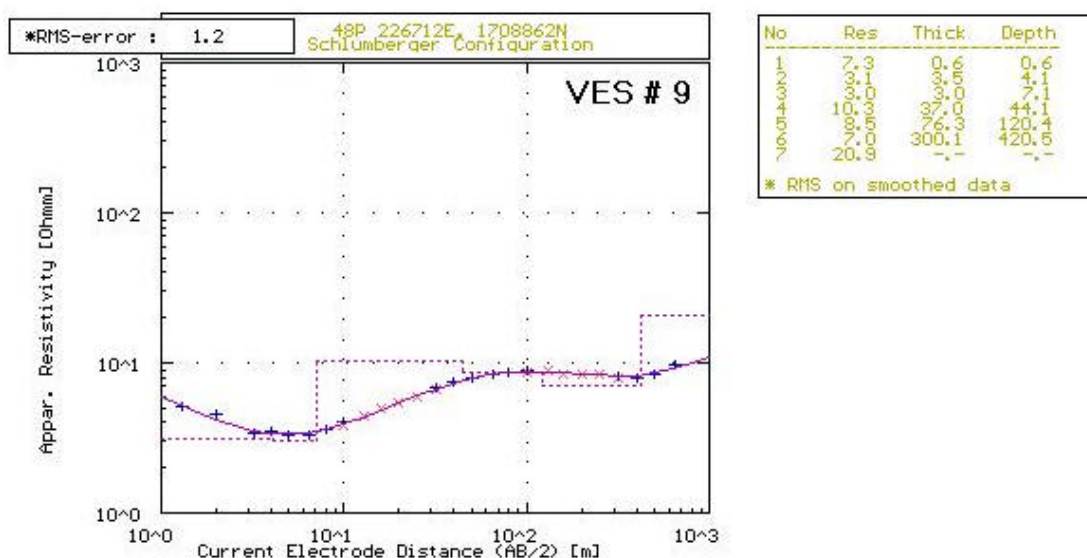


Figure B9 The curves fitting from RESIST87 software represents the depth, apparent resistivity and thickness at point 9.



Geophysical Exploration (Electrical Resistivity)

Table B10 Electrical resistivity raw data and configuration array pattern at point 10.
Area: Khong district **Station:** point10 227470N 1701950E **Date:** 07/15/01
Comment:

AB/2	MN/2	K	I	V _x	RES	AB/2	MN/2	K	I	V _x	RES
1.3	0.5	4.53	1091.79	3597.264	14.9	50	5	777.54	159.61	0.433	2.1
2.0	0.5	11.78	696.43	1032.589	17.5	65	5	1319.47	884.14	1.291	1.9
3.2	0.5	31.38	407.59	232.310	17.9	80	5	2002.77	888.91	0.685	1.5
4.0	0.5	49.48	199.49	66.380	16.5	100	5	3133.74	847.65	0.458	1.7
5.0	0.5	77.75	332.59	60.791	14.2	100	20	753.98	854.36	1.963	1.7
6.5	0.5	131.95	230.55	18.118	10.4	130	20	1295.91	1412.87	1.667	1.5
8.0	0.5	200.28	271.31	10.479	7.7	160	20	1979.20	978.92	0.728	1.5
10	0.5	313.37	421.02	7.814	5.8	200	20	3110.18	796.59	0.355	1.5
10	2	75.40	395.50	30.329	5.8	250	20	4877.32	901.08	0.315	1.7
13	2	129.59	495.37	17.126	4.5	320	20	8011.06	1377.41	0.367	2.1
16	2	197.92	619.80	12.816	4.1	320	50	3138.50	1379.37	0.931	2.1
20	2	311.02	684.07	8.454	3.8	400	50	4948.00	1033.46	0.553	2.6
25	2	487.73	582.00	5.013	2.8	500	50	7775.40	331.97	0.141	3.0
32	2	801.11	684.06	2.310	2.7	650	50	13194.70	785.07	0.284	4.8
32	5	313.85	676.74	5.905	2.7						
40	5	494.80	1012.33	5.219	2.6						

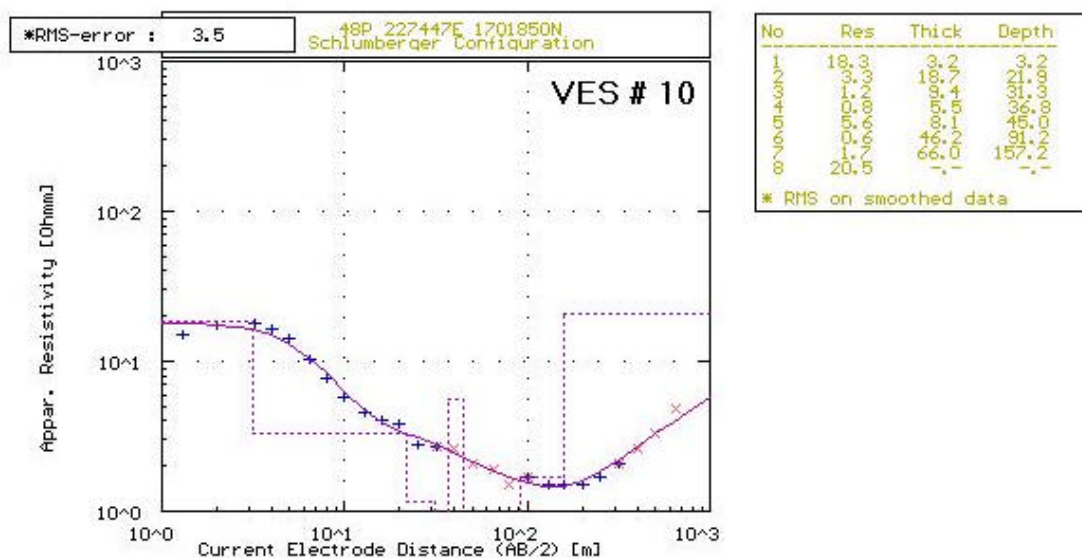


Figure B10 The curves fitting from RESIST87 software represents the depth, apparent resistivity and thickness at point 10.



Geophysical Exploration (Electrical Resistivity)

Table B11 Electrical resistivity raw data and configuration array pattern at point 11.
Area: Khong district **Station:** point11 226965N 1700900E **Date:** 07/15/01
Comment: Ban Nong Bou

AB/2	MN/2	K	I	V _x	RES	AB/2	MN/2	K	I	V _x	RES
1.3	0.5	4.53	913.58	2377.138	11.8	50	5	777.54	394.36	1.376	9.7
2.0	0.5	11.78	875.15	527.428	7.1	65	5	1319.47	339.11	0.784	10.1
3.2	0.5	31.38	612.65	132.206	6.8	80	5	2002.77	881.82	1.433	10.3
4.0	0.5	49.48	586.38	94.502	8.0	100	5	3133.74	498.93	0.530	10.2
5.0	0.5	77.75	851.65	63.896	5.8	100	20	753.98	1291.54	18.299	10.7
6.5	0.5	131.95	847.74	37.971	5.9	130	20	1295.91	378.37	3.281	11.2
8.0	0.5	200.28	929.53	27.988	6.0	160	20	1979.20	807.28	4.681	11.5
10	0.5	313.37	784.85	15.466	6.2	200	20	3110.18	808.07	2.868	11.0
10	2	75.40	671.16	52.837	5.9	250	20	4877.32	623.85	1.256	9.8
13	2	129.59	853.64	40.699	6.2	320	20	8011.06	334.84	0.343	8.2
16	2	197.92	590.21	18.892	6.3	320	50	3138.50	329.27	0.865	8.2
20	2	311.02	608.50	11.328	5.8	400	50	4948.00	976.99	1.329	6.7
25	2	487.73	546.14	1.981	8.8	500	50	7775.40	932.92	0.665	5.5
32	2	801.11	795.31	1.857	1.9	650	50	13194.70	1317.08	0.525	5.3
32	5	313.85	787.58	7.195	9.9						
40	5	494.80	947.04	4.898	9.6						

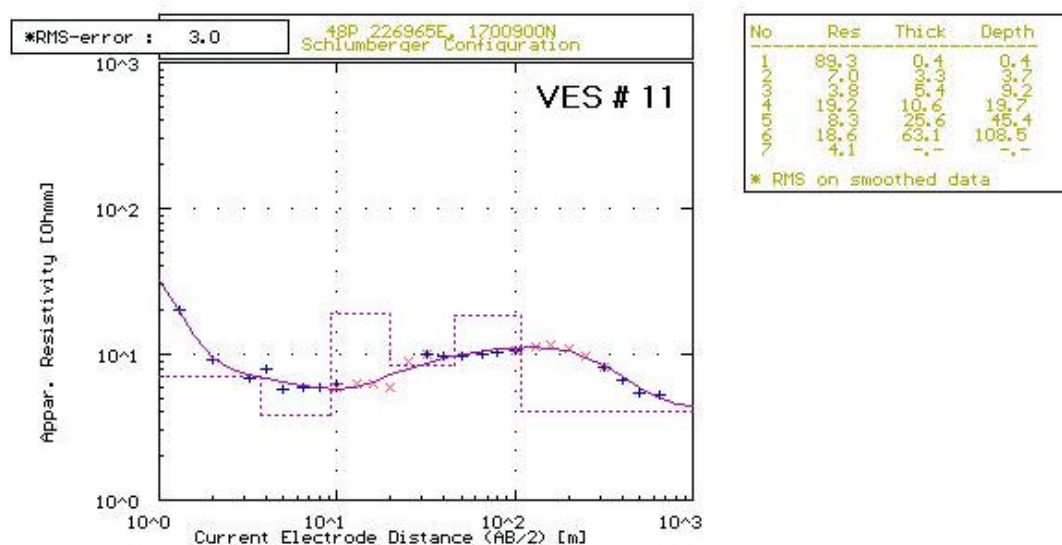


Figure B11 The curves fitting from RESIST87 software represents the depth, apparent resistivity and thickness at point 11.



Geophysical Exploration (Electrical Resistivity)

Table B12 Electrical resistivity raw data and configuration array pattern at point 12.
Area: Khong district **Station:** point12 226965N 1700900E **Date:** 07/19/01
Comment: Direction N45°E

AB/2	MN/2	K	I	V _x	RES	AB/2	MN/2	K	I	V _x	RES
1.3	0.5	4.53	2156.30	927.251	1.9	50	5	777.54	2180.52	22.266	7.9
2.0	0.5	11.78	1525.60	331.181	2.6	65	5	1319.47	1947.88	12.157	8.2
3.2	0.5	31.38	786.41	71.087	2.8	80	5	2002.77	2031.42	8.199	8.1
4.0	0.5	49.48	1992.98	101.516	2.5	100	5	3133.74	2111.32	5.467	8.1
5.0	0.5	77.75	1962.91	66.624	2.6	100	20	753.98	2062.47	22.128	8.1
6.5	0.5	131.95	1620.32	37.208	3.0	130	20	1295.91	2129.12	13.282	8.1
8.0	0.5	200.28	1639.52	26.889	3.3	160	20	1979.20	1940.75	7.722	7.9
10	0.5	313.37	2256.82	25.744	3.6	200	20	3110.18	1747.34	4.239	7.5
10	2	75.40	2258.12	103.467	3.5	250	20	4877.32	2188.67	3.202	7.1
13	2	129.59	2112.11	77.129	4.7	320	20	8011.06	1710.58	1.359	6.4
16	2	197.92	1962.54	52.221	5.3	320	50	3138.50	1810.13	3.738	6.5
20	2	311.02	2125.17	39.828	5.8	400	50	4948.00	1975.99	2.558	6.4
25	2	487.73	2158.87	28.393	6.4	500	50	7775.40	1973.98	1.674	6.6
32	2	801.11	1852.58	16.041	6.9	650	50	13194.70	1808.06	1.101	8.0
32	5	313.85	1611.39	36.795	7.2						
40	5	494.80	1267.19	19.286	7.5						

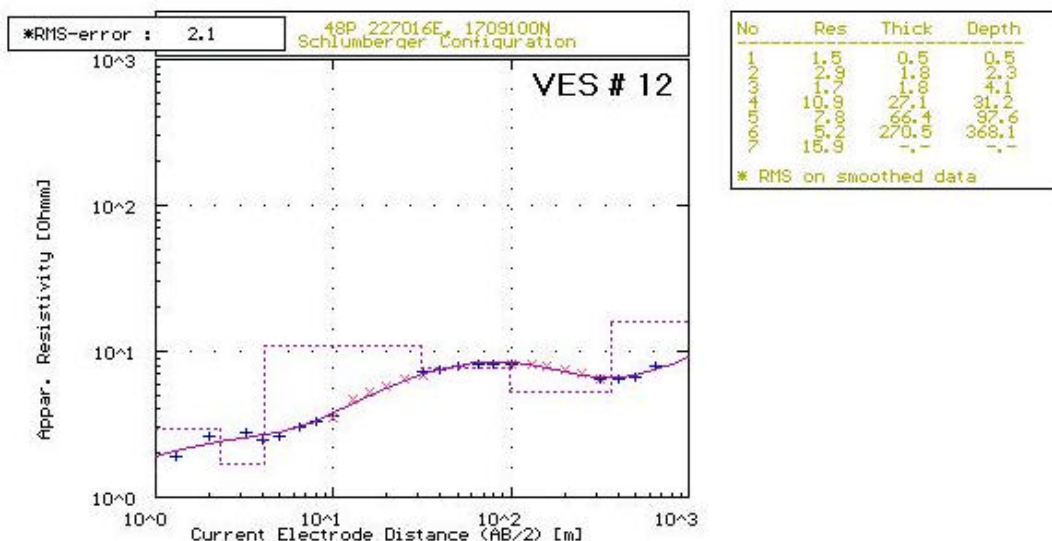


Figure B12 The curves fitting from RESIST87 software represents the depth, apparent resistivity and thickness at point 12.



Geophysical Exploration (Electrical Resistivity)

Table B13 Electrical resistivity raw data and configuration array pattern at point 13.
Area: Khong district Station: point13 227019N 1704236E Date: 07/19/01
Comment: Direction N40°E

AB/2	MN/2	K	I	V _x	RES	AB/2	MN/2	K	I	V _x	RES
1.3	0.5	4.53	238.10	3129.877	59.5	50	5	777.54	612.60	2.956	3.8
2.0	0.5	11.78	196.41	669.714	46.6	65	5	1319.47	1920.44	5.507	3.8
3.2	0.5	31.38	278.13	158.537	17.9	80	5	2002.77	1211.44	2.043	3.4
4.0	0.5	49.48	258.60	63.024	12.1	100	5	3133.74	903.98	0.925	3.2
5.0	0.5	77.75	316.15	40.593	10.0	100	20	753.98	912.67	3.738	3.1
6.5	0.5	131.95	350.83	13.297	5.0	130	20	1295.91	1331.43	3.333	3.2
8.0	0.5	200.28	195.72	3.700	3.8	160	20	1979.20	1848.67	2.981	3.2
10	0.5	313.37	297.77	3.066	3.2	200	20	3110.18	1079.51	0.994	2.9
10	2	75.40	278.96	11.683	3.2	250	20	4877.32	644.43	0.470	3.6
13	2	129.59	194.49	5.093	3.4	320	20	8011.06	340.42	0.174	4.1
16	2	197.92	681.54	11.528	3.3	320	50	3138.50	342.46	0.415	3.8
20	2	311.02	621.25	6.764	3.4	400	50	4948.00	317.09	0.262	4.1
25	2	487.73	1162.48	10.061	4.2	500	50	7775.40	1217.18	0.801	5.1
32	2	801.11	706.11	3.943	4.5						
32	5	313.85	826.41	11.280	4.3						
40	5	494.80	689.02	5.697	4.1						

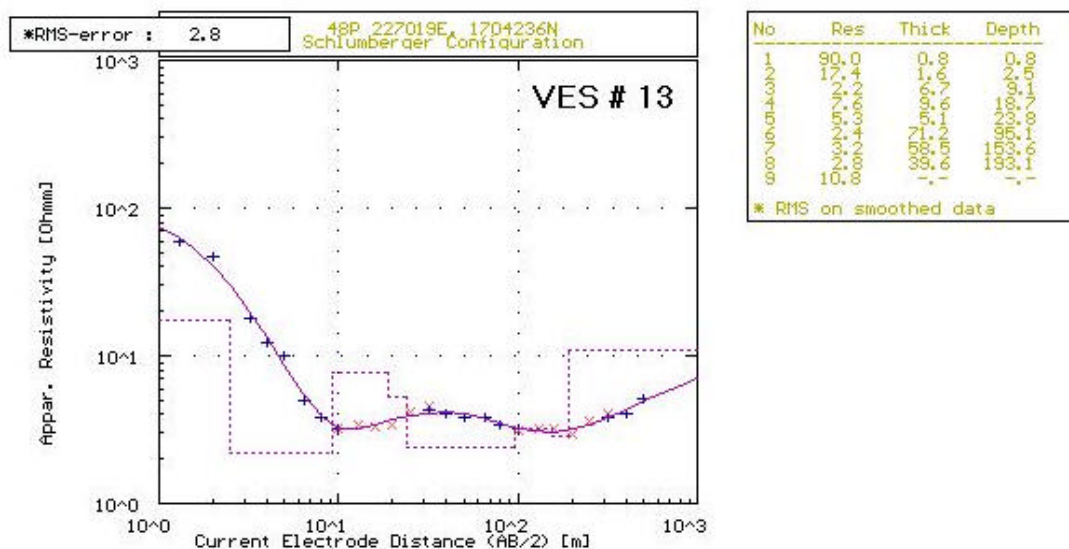


Figure C13 The curves fitting from RESIST87 software represents the depth, apparent resistivity and thickness at point 13.



Geophysical Exploration (Electrical Resistivity)

Table B14 Electrical resistivity raw data and configuration array pattern at point 14.
Area: Khong district **Station:** point14 228151N 1704815E **Date:** 07/19/01
Comment: Direction N65°E

AB/2	MN/2	K	I	V _x	RES	AB/2	MN/2	K	I	V _x	RES
1.3	0.5	4.53	317.43	426.230	6.6	50	5	777.54	222.76	0.646	2.3
2.0	0.5	11.78	270.23	110.305	4.8	65	5	1319.47	929.09	1.457	2.1
3.2	0.5	31.38	426.18	50.671	3.7	80	5	2002.77	800.84	0.194	1.7
4.0	0.5	49.48	472.95	34.990	3.7	100	5	3133.74	570.06	0.296	1.6
5.0	0.5	77.75	669.34	31.142	3.6	100	20	753.98	598.88	1.256	1.6
6.5	0.5	131.95	511.98	14.150	3.6	130	20	1295.91	192.84	0.255	1.7
8.0	0.5	200.28	582.33	10.529	3.6	160	20	1979.20	1732.00	1.385	1.6
10	0.5	313.37	654.13	7.613	3.6	200	20	3110.18	1039.23	0.596	1.8
10	2	75.40	650.21	31.767	3.7	250	20	4877.32	373.67	0.157	2.1
13	2	129.59	1363.22	36.793	3.5	320	20	8011.06	235.77	0.091	3.1
16	2	197.92	1505.02	25.394	3.4	320	50	3138.50	117.63	0.093	2.5
20	2	311.02	1204.33	12.794	3.3	400	50	4948.00	923.16	0.622	3.3
25	2	487.73	421.40	2.988	3.4	500	50	7775.40	1029.48	0.544	4.1
32	2	801.11	355.63	1.316	3.0						
32	5	313.85	360.22	3.293	2.9						
40	5	494.80	1034.84	5.636	2.7						

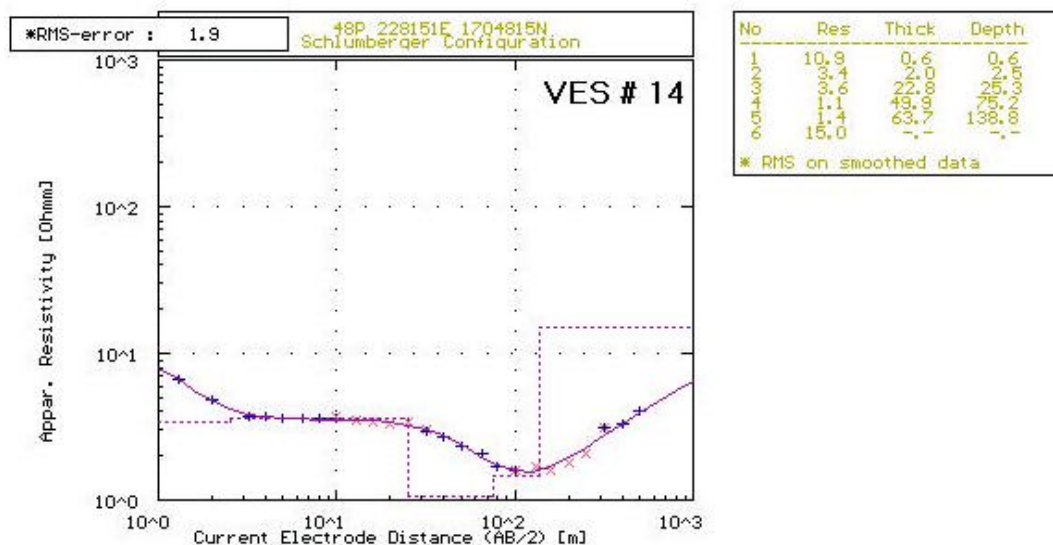


Figure B14 The curves fitting from RESIST87 software represents the depth, apparent resistivity and thickness at point 14.



Geophysical Exploration (Electrical Resistivity)

Table B15 Electrical resistivity raw data and configuration array pattern at point 15.
Area: Khong district **Station:** point15 227340N 1706660E **Date:** 07/20/01
Comment: Direction N48°E

AB/2	MN/2	K	I	V _x	RES	AB/2	MN/2	K	I	V _x	RES
1.3	0.5	4.53	294.74	3358.140	51.5	50	5	777.54	847.51	6.452	5.9
2.0	0.5	11.78	236.90	880.409	43.8	65	5	1319.47	645.91	3.090	6.3
3.2	0.5	31.38	234.76	191.212	25.6	80	5	2002.77	1003.73	3.443	6.9
4.0	0.5	49.48	212.07	79.865	18.6	100	5	3133.74	830.86	1.976	7.5
5.0	0.5	77.75	176.90	30.282	13.3	100	20	753.98	825.24	7.932	7.2
6.5	0.5	131.95	211.46	13.758	8.6	130	20	1295.91	456.54	2.839	8.1
8.0	0.5	200.28	116.98	3.685	6.3	160	20	1979.20	512.06	2.184	8.4
10	0.5	313.37	175.62	2.966	5.3	200	20	3110.18	650.53	1.848	8.8
10	2	75.40	172.96	11.702	5.1	250	20	4877.32	187.36	0.353	9.2
13	2	129.59	175.20	6.385	4.7	320	20	8011.06	478.55	0.564	9.4
16	2	197.92	196.45	4.826	4.9	320	50	3138.50	472.86	1.522	10.1
20	2	311.02	271.84	4.392	5.0	400	50	4948.00	615.80	1.351	10.9
25	2	487.73	339.52	3.041	5.7	500	50	7775.40	190.25	0.291	11.9
32	2	801.11	515.79	3.710	5.8	650	50	13194.70	197.00	0.206	13.8
32	5	313.85	593.56	8.686	5.4						
40	5	494.80	821.54	9.511	5.7						

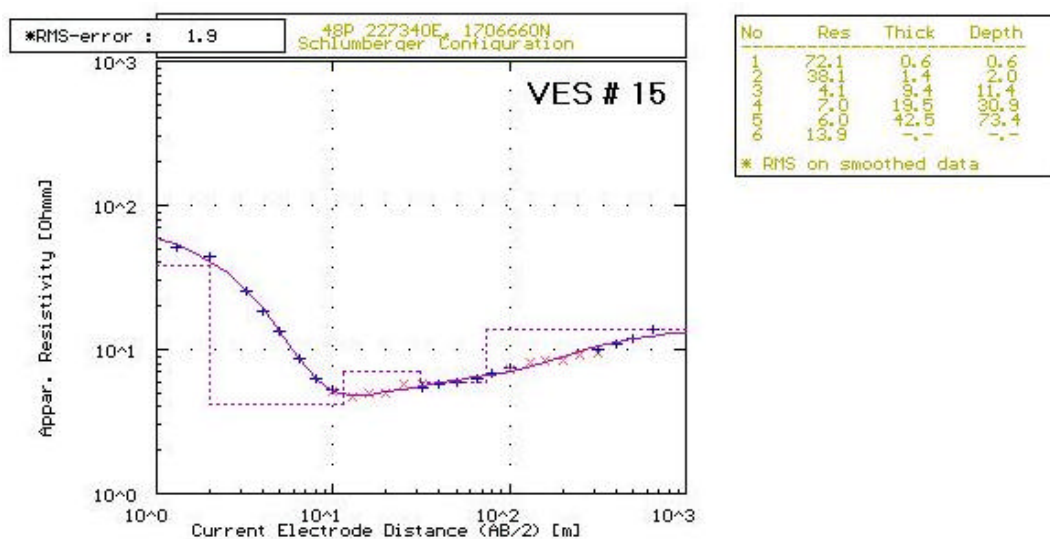


Figure B15 The curves fitting from RESIST87 software represents the depth, apparent resistivity and thickness at point 15.



Geophysical Exploration (Electrical Resistivity)

Table B16 Electrical resistivity raw data and configuration array pattern at point 16.
Area: Khong district **Station:** point16 225622N 1708162E **Date:** 07/20/01
Comment:

AB/2	MN/2	K	I	V _x	RES	AB/2	MN/2	K	I	V _x	RES
1.3	0.5	4.53	1036.45	859.351	3.8	50	5	777.54	1002.96	10.271	6.6
2.0	0.5	11.78	756.92	280.793	4.4	65	5	1319.47	1079.46	5.083	6.2
3.2	0.5	31.38	806.90	118.718	4.6	80	5	2002.77	1011.16	2.832	5.6
4.0	0.5	49.48	400.51	33.809	4.2	100	5	3133.74	1681.28	2.693	5.0
5.0	0.5	77.75	524.92	26.565	3.9	100	20	753.98	1678.09	12.937	5.8
6.5	0.5	131.95	610.81	16.773	3.6	130	20	1295.91	795.31	2.930	4.8
8.0	0.5	200.28	872.07	14.167	3.3	160	20	1979.20	1537.08	3.132	4.0
10	0.5	313.37	1353.01	14.315	3.3	200	20	3110.18	2256.09	2.518	3.5
10	2	75.40	1350.79	56.760	3.2	250	20	4877.32	2085.05	1.371	3.2
13	2	129.59	1015.15	27.754	3.5	320	20	8011.06	971.81	0.435	3.6
16	2	197.92	945.10	17.760	3.7	320	50	3138.50	970.44	1.097	3.5
20	2	311.02	926.52	11.611	3.9	400	50	4948.00	2307.43	1.953	4.2
25	2	487.73	853.61	7.696	4.4	500	50	7775.40	807.92	0.547	5.3
32	2	801.11	1581.63	9.422	4.8	650	50	13194.70	1181.63	0.622	6.9
32	5	313.85	1627.61	32.519	6.3						
40	5	494.80	1478.46	19.262	6.4						

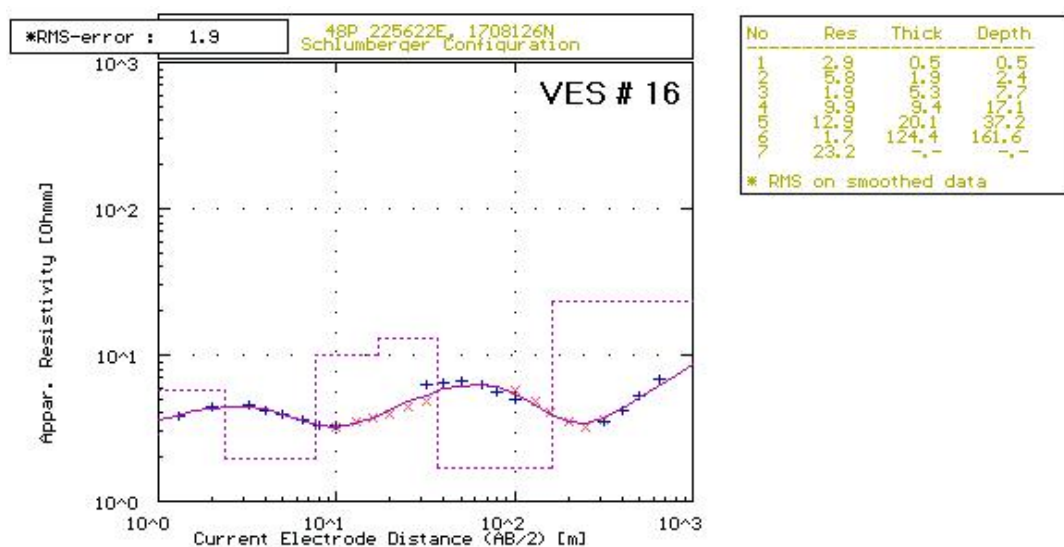


Figure B16 The curves fitting from RESIST87 software represents the depth, apparent resistivity and thickness at point 16.



Geophysical Exploration (Electrical Resistivity)

Table B17 Electrical resistivity raw data and configuration array pattern at point 17.
Area: Khong district **Station:** point17 225180N 1708619E **Date:** 07/20/01
Comment:

AB/2	MN/2	K	I	V _x	RES	AB/2	MN/2	K	I	V _x	RES
1.3	0.5	4.53	1171.39	704.678	2.7	50	5	777.54	1456.46	14.725	7.9
2.0	0.5	11.78	1341.16	311.819	2.7	65	5	1319.47	1527.61	9.546	8.2
3.2	0.5	31.38	1046.57	95.412	2.9	80	5	2002.77	1151.84	4.973	8.6
4.0	0.5	49.48	930.93	56.906	3.0	100	5	3133.74	1166.70	3.259	8.8
5.0	0.5	77.75	776.72	31.837	3.2	100	20	753.98	1161.34	13.880	9.0
6.5	0.5	131.95	1126.45	29.901	3.5	130	20	1295.91	1698.75	11.396	8.7
8.0	0.5	200.28	1103.13	20.909	3.8	160	20	1979.20	1633.94	6.771	8.2
10	0.5	313.37	1036.64	13.456	4.1	200	20	3110.18	2019.33	4.747	7.3
10	2	75.40	881.78	48.013	4.1	250	20	4877.32	1439.85	1.905	6.5
13	2	129.59	973.31	33.875	4.5	320	20	8011.06	1755.07	1.309	6.0
16	2	197.92	647.45	16.046	4.9	320	50	3138.50	1746.19	3.314	6.0
20	2	311.02	1189.77	19.894	5.2	400	50	4948.00	1460.15	1.793	6.1
25	2	487.73	1244.02	14.739	5.8	500	50	7775.40	965.49	0.801	6.5
32	2	801.11	1302.68	10.296	6.3	650	50	13194.70	401.14	0.248	8.2
32	5	313.85	1293.52	26.877	6.5						
40	5	494.80	1366.78	19.753	7.2						

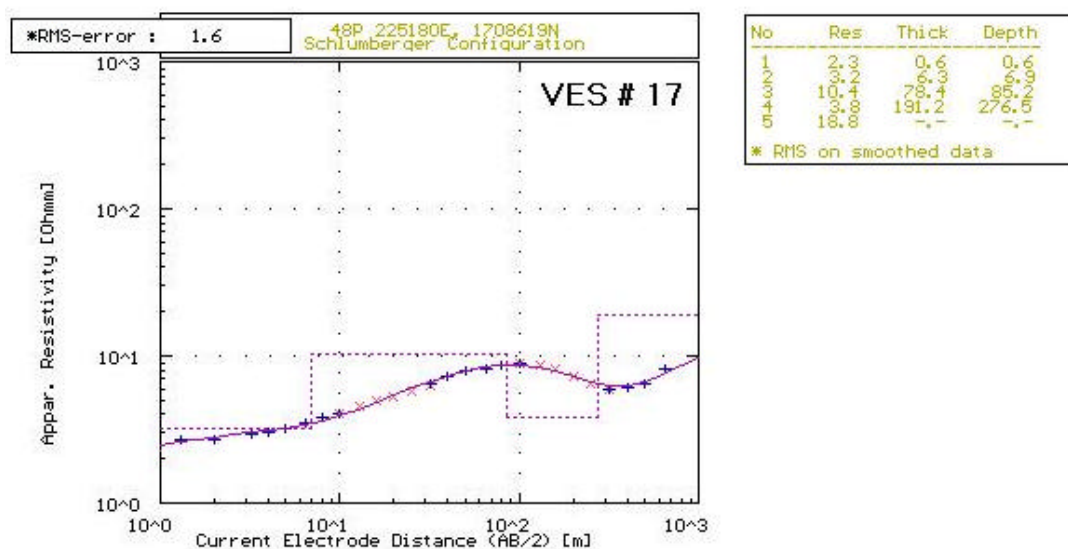


Figure B17 The curves fitting from RESIST87 software represents the depth, apparent resistivity and thickness at point 17.



Geophysical Exploration (Electrical Resistivity)

Table B18 Electrical resistivity raw data and configuration array pattern at point 18.
Area: Khong district **Station:** point18 226193N 1703256E **Date:** 07/20/01
Comment:

AB/2	MN/2	K	I	V _x	RES	AB/2	MN/2	K	I	V _x	RES
1.3	0.5	4.53	34.52	580.940	76.1	50	5	777.54	131.77	1.205	7.2
2.0	0.5	11.78	26.37	84.105	37.6	65	5	1319.47	116.88	0.665	7.5
3.2	0.5	31.38	46.61	24.035	16.2	80	5	2002.77	255.08	0.942	7.4
4.0	0.5	49.48	117.15	25.177	10.6	100	5	3133.74	120.08	0.286	7.5
5.0	0.5	77.75	33.04	3.181	7.5	100	20	753.98	127.28	1.186	7.4
6.5	0.5	131.95	26.60	1.161	5.8	130	20	1295.91	182.75	0.961	6.8
8.0	0.5	200.28	30.20	0.826	5.5	160	20	1979.20	315.12	0.952	6.0
10	0.5	313.37	43.77	0.738	5.3	200	20	3110.18	310.48	0.517	5.2
10	2	75.40	43.88	2.389	4.1	250	20	4877.32	325.66	0.288	4.3
13	2	129.59	146.38	4.888	4.3	320	20	8011.06	729.52	0.359	3.9
16	2	197.92	100.50	2.375	4.7	320	50	3138.50	730.30	0.887	3.8
20	2	311.02	171.11	3.088	5.6	400	50	4948.00	424.02	0.345	4.0
25	2	487.73	249.20	2.944	5.8	500	50	7775.40	373.08	0.210	4.4
32	2	801.11	221.60	1.454	7.0						
32	5	313.85	214.41	3.386	6.7						
40	5	494.80	157.35	2.548	6.7						

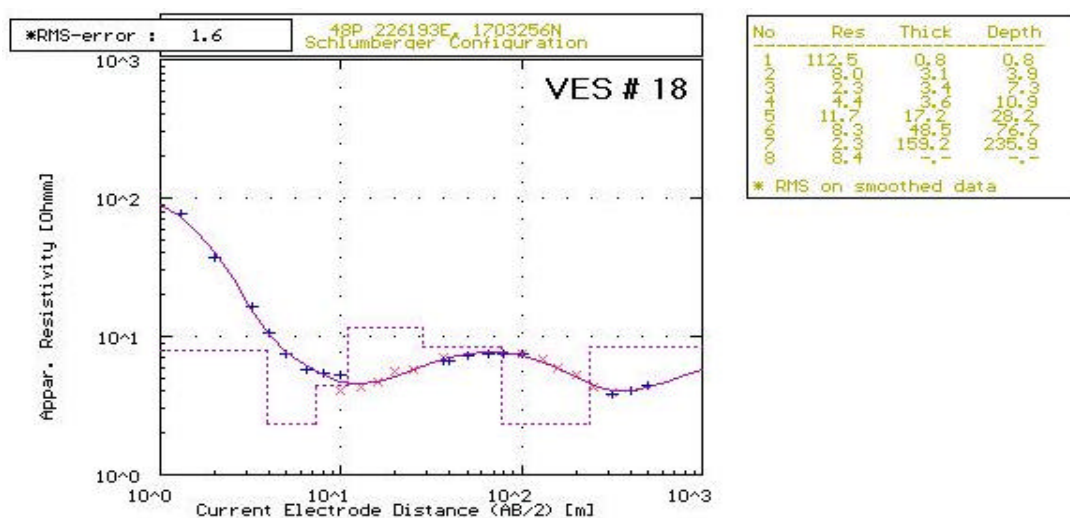


Figure B18 The curves fitting from RESIST87 software represents the depth, apparent resistivity and thickness at point 18.

APPENDIX C
ROCK SALT BOREHOLES

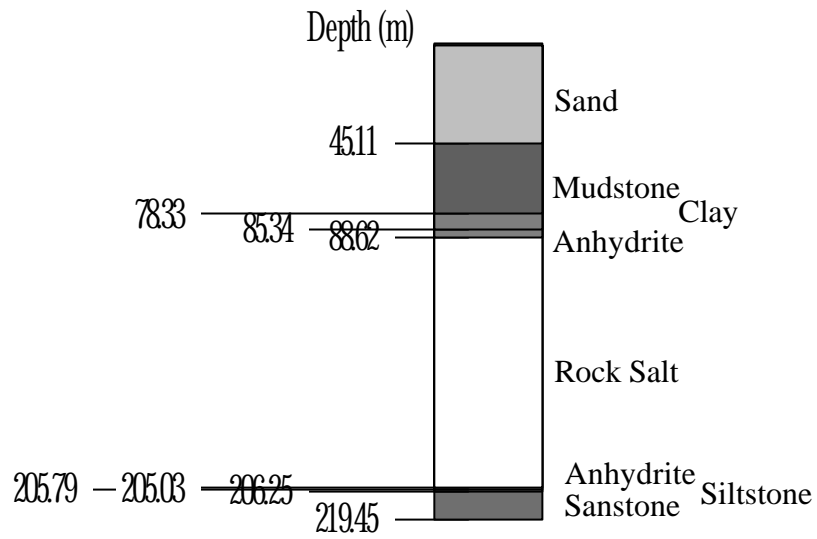
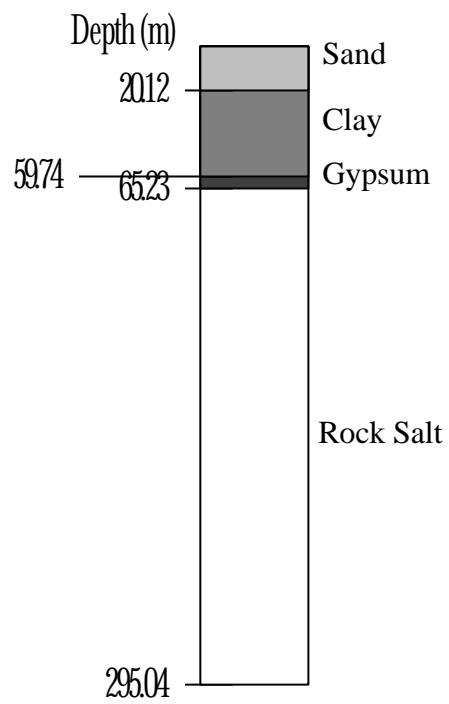


Figure C1 Stratigraphy of potash exploration borehole number K-019.



N. B. Hole was abandoned in rock salt

Figure C2 Stratigraphy of potash exploration borehole number K-023.

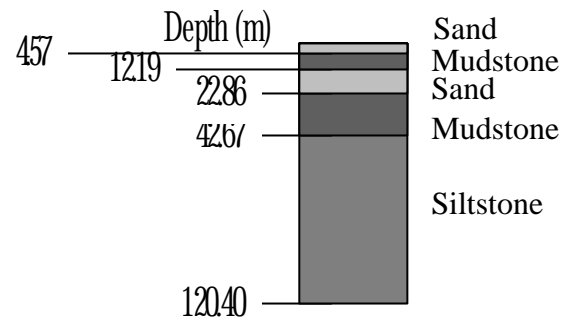


Figure C3 Stratigraphy of potash exploration borehole number K-032.

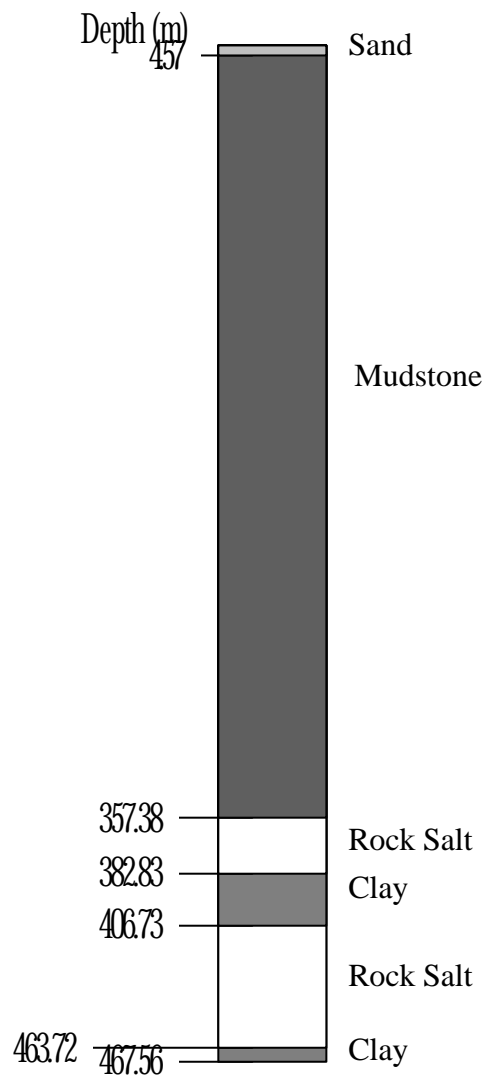


Figure C4 Stratigraphy of potash exploration borehole number K-062.

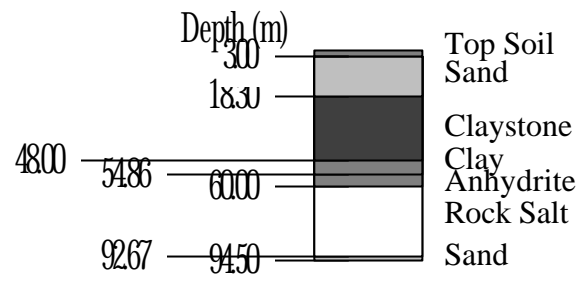


Figure C5 Stratigraphy of potash exploration borehole number K-073.

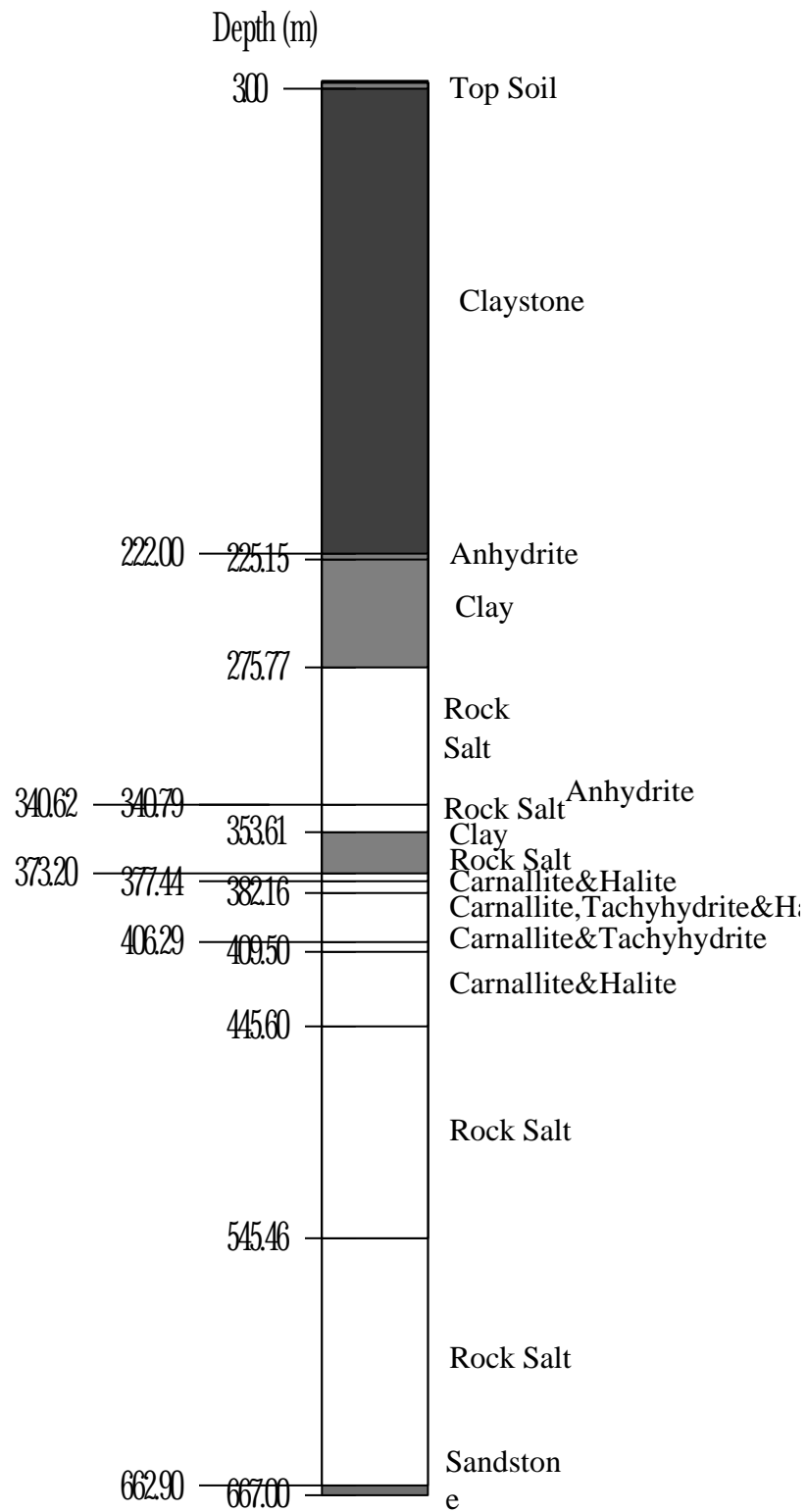


Figure C6 Stratigraphy of potash exploration borehole number K-075.

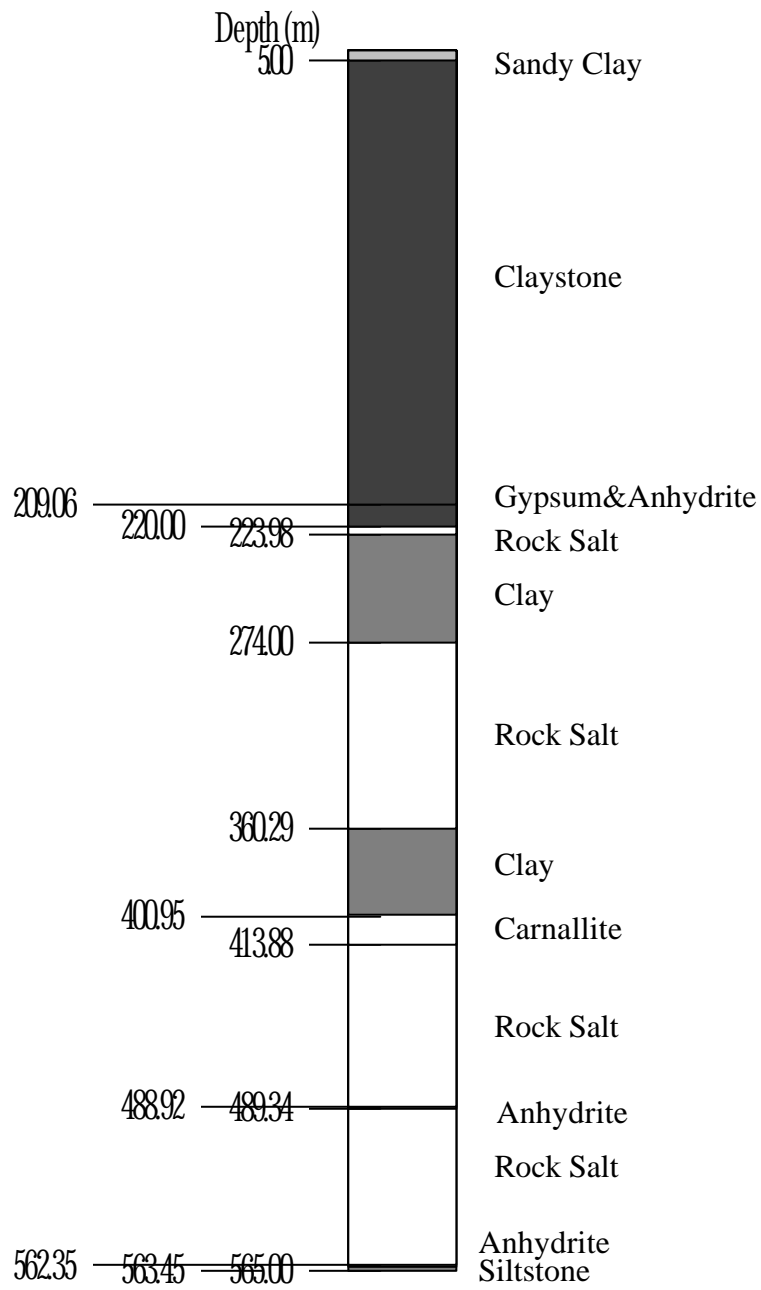


Figure C7 Stratigraphy of potash exploration borehole number K-076.

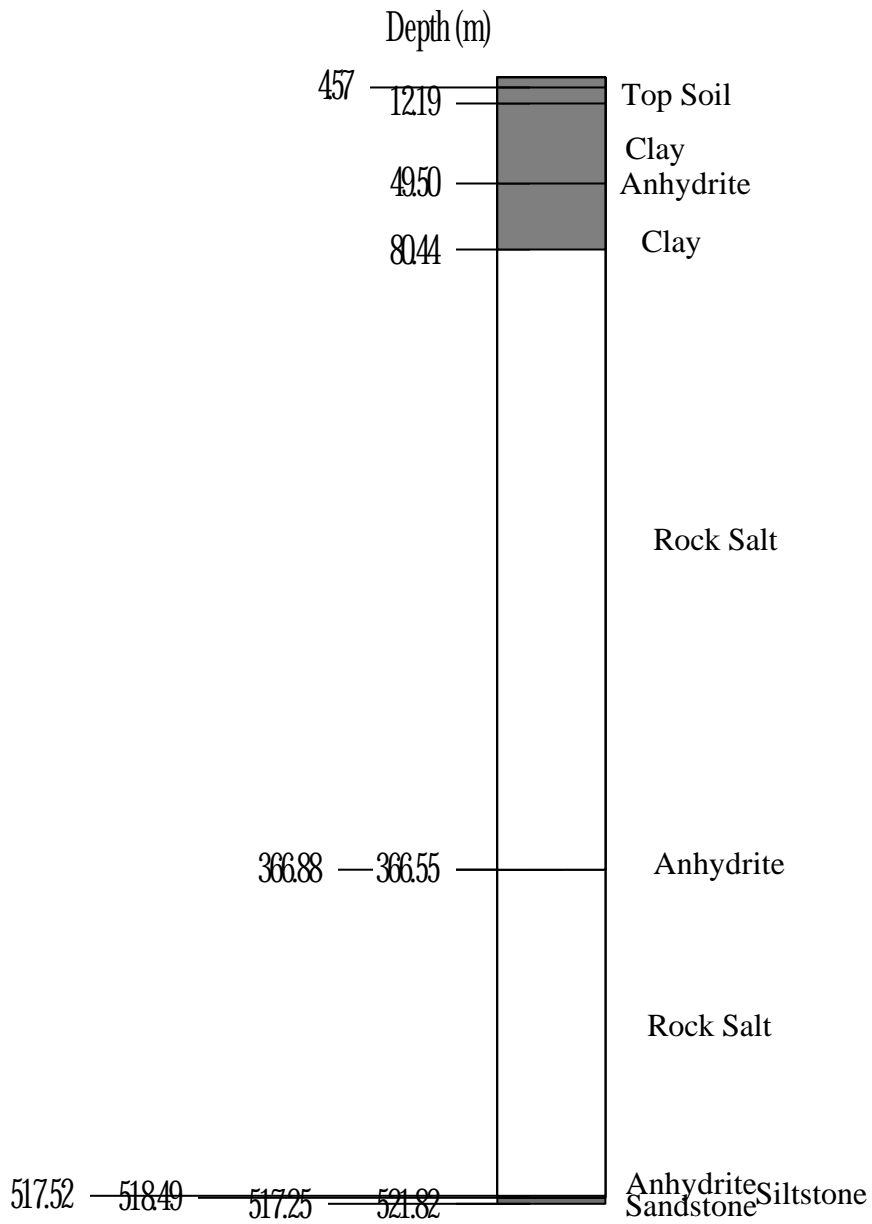


Figure C8 Stratigraphy of potash exploration borehole number K-080.

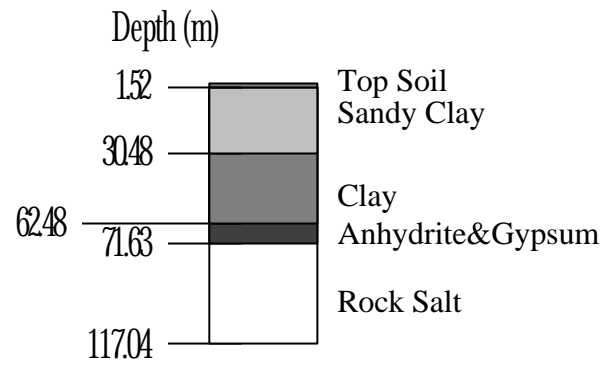


Figure C9 Stratigraphy of potash exploration borehole number K-082.

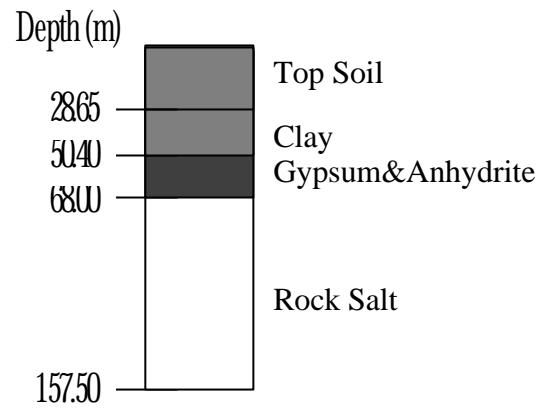


Figure C10 Stratigraphy of potash exploration borehole number K-094.

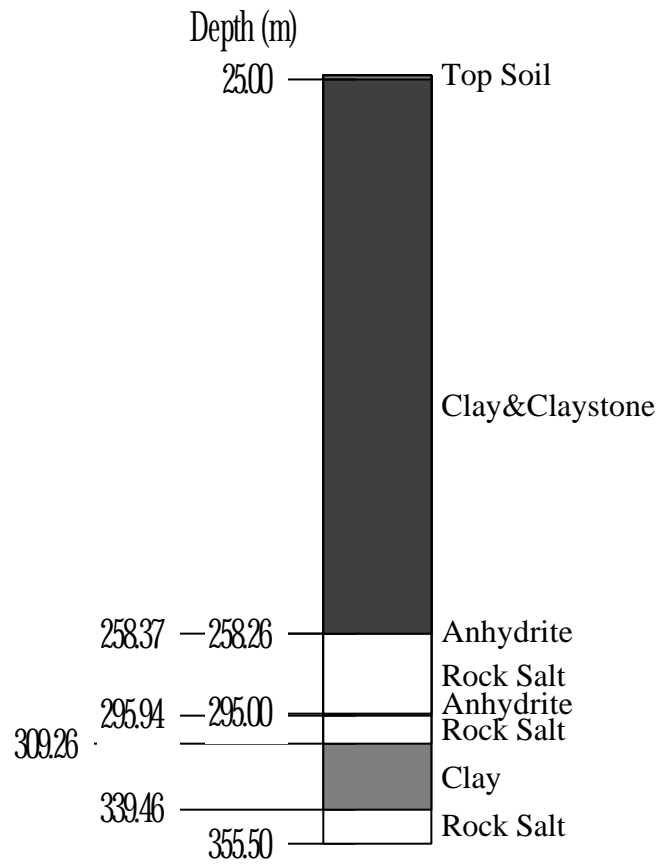


Figure C11 Stratigraphy of potash exploration borehole number K-096.

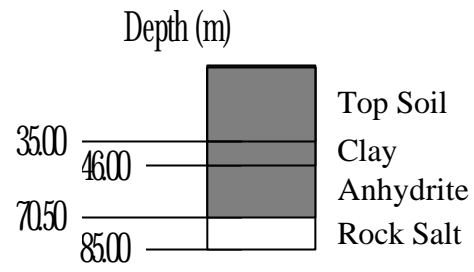


Figure C12 Stratigraphy of potash exploration borehole number K-097.

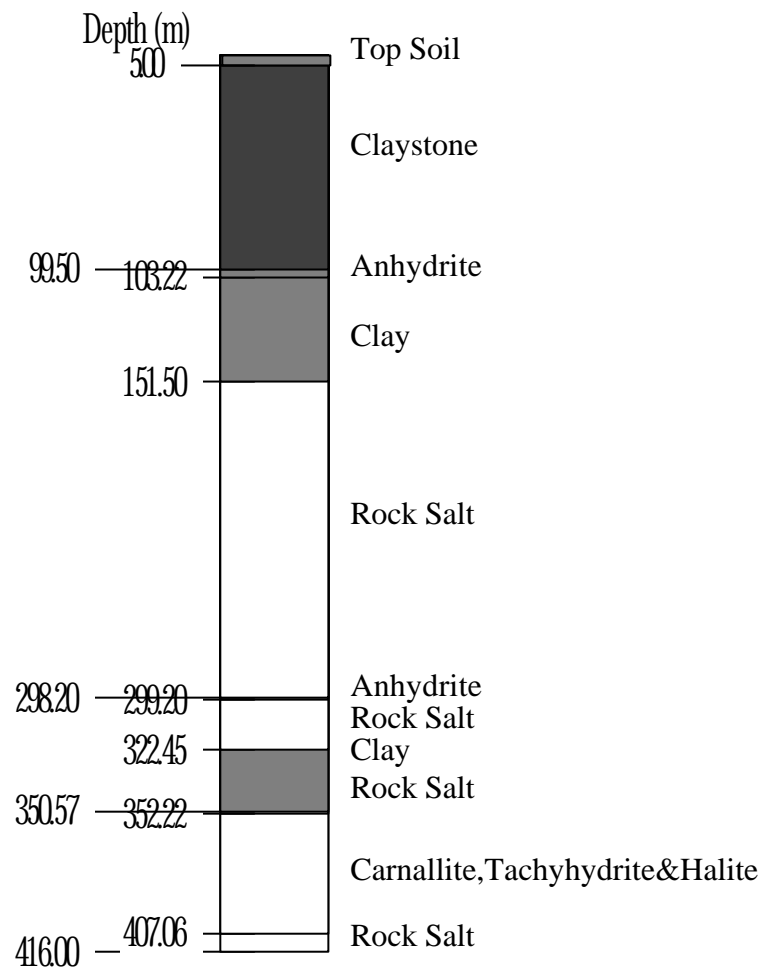


Figure C13 Stratigraphy of potash exploration borehole number K-098.

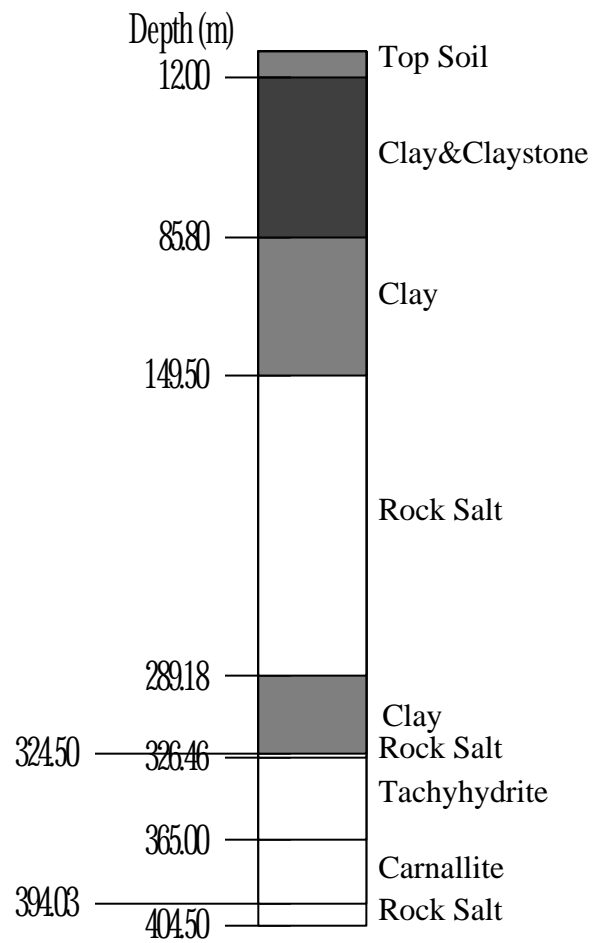


Figure C14 Stratigraphy of potash exploration borehole number K-100.

CURRICULUM VITAE

Mr. Kitsana Malila was born February 3, 1978 in Sukhothai province, Thailand. He received his Bachelor's Degree in Engineering (Geological Engineering Program) from Suranaree University of Technology in 1998. He continued with his graduate studies in the Geological Engineering Program, Institute of Engineering, Suranaree University of Technology.